Genomic Analysis of Divergence and Secondary Contact in Red Foxes (*Vulpes vulpes*) and Gray Foxes (*Urocyon cinereoargenteus*)

By

SOPHIE PRECKLER-QUISQUATER

DISSERTATION

Submitted in partial satisfaction of the requirements for the degree of

DOCTOR OF PHILOSOPHY

in

Ecology

in the

OFFICE OF GRADUATE STUDIES

of the

UNIVERSITY OF CALIFORNIA

DAVIS

Approved:

_____

Benjamin N. Sacks, Chair

_____

Marissa L. Baskett

_____

C. Titus Brown

Committee in Charge

2022

Acknowledgements

I would like to thank my advisor, Dr. Ben Sacks for your patience, encouragement, and guidance. You've always gone above and beyond to support me as I navigate both Ph.D. related endeavors and personal life hurdles. I'm so grateful for feeling like I always have you on my team and couldn't have asked for a better advisor and mentor. I would also like to thank my other committee members, Dr. Marissa Baskett and Dr. Titus Brown for their support and feedback on my dissertation research. Marissa, you have offered constant motivation and inspiration over the years and were always willing to sit down and discuss career paths with me or provide helpful feedback on my grant proposals. Thank you, Titus, for bringing your incredible bioinformatics research lab to UC Davis right as I was preparing to dive into the genomics world. It was through your workshops and instruction, and the help of your amazing graduate students and post-docs, that I developed many of the skills needed to complete my dissertation. I would also like to thank my qualifying exam committee (Dr. Dirk Van Vuren, Dr. Rahel Sollman, Dr. Andrea Schreier, Dr. Marissa Baskett, and Dr. Michael Miller) for your advice and support in refining my research proposal. I am grateful for the early career mentors I had as a UC Davis undergrad, including Dr. Kimberly Vanderwaal, Dr. Nicole Sharpe, and Dr. Tavis Forrester for introducing me to a career in wildlife ecological research and for helping to cultivate my passion for ecology and evolution.

I would like to thank Dr. Tom Batter for being an amazing co-worker, lab mate, and friend. I remember driving around the Sacramento Valley as field technicians talking for hours about our dreams and ambitions for graduate school and beyond and I'm so happy we finally got to do it together at UC Davis. It wouldn't have been the same without you. I also want to thank my lab mate Dr. Cate Quinn. I feel like I would have been lost in the early years of grad school

without your guidance. You are always willing to help troubleshoot an R script or go down a rabbit (fox) hole with me. Chatting with you sparks scientific curiosity without fail and I can't think of anyone I enjoy brainstorming side-projects with more. You simply make science more fun. I want to thank all my other past and present lab mates at the Mammalian Ecology and Conservation Unit (MECU) including Lauren Hennelly, Julia Owen, Cody Aylward, Taylor Davis, Monica Serrano, Carly White, Tali Caspi, Grace Rosburg-Francot, Andrea Broad, Camilo Sanchez, Jennifer Brazeal, Kathleen Miles, Carolyn Whitesell, Joeclyn Akins, Eric Kuo, Preston Alden, Dr. Hira Fatima, Dr. Mark Statham, and Dr. Elizabeth Kierepka, as well as honorary MECU members Dr. Amanda Coen and Dr. Mike Buchalski. I also want to thank the two incredible MECU lab managers Stevi Vanderzwan and Zach Lounsbury for their instruction and guidance over the years. I could not have made it through grad school without the friendship and support of each and every one of you. This research would not have been possible without the many volunteers, field technicians and laboratory interns who also supported it. Thank you all for your incredible effort and commitment over the years.

I want to thank my family for all the incredible camping, hiking, backpacking, and globetrotting I was able to experience growing up. You instilled the values, curiosity, and sense of adventure that motivated me to pursue this career. For that I am eternally grateful. Thank you to my mom and dad for always loving and supporting me. It means the world. And thank you to my big brother for always looking out for me. You were the first person I ever looked up to and chasing you in life fortified my competitive nature and my drive to succeed. I wouldn't have accomplished this without you.

I want to thank my dog Aiden. You were my co-pilot for all of life's best adventures and I couldn't have asked for a better friend and companion. I'm so lucky I got to spend 12 incredible years with you. Thank you for loving me.

Above all, I thank my partner, George. You have supported every one of my intellectual and adventurous pursuits, always leading with patience and kindness. You encourage me to push forward, and more importantly, you help me realize when to take a step back. Whether you're driving out to spend time with me during the remote field jobs, keeping all our house plants alive while I frantically work to meet deadlines, or stopping on the side of the interstate (in formal wedding guest attire) so I can sample that roadkill, you are always there for me. I love you.

Abstract

Speciation results from the accumulation of genetic differences between lineages over time, which initially decreases and eventually eliminates the probability of gene flow between them (i.e., biological species concept). Additionally, the genomes of natural populations are not only shaped by drift and selection, but also by introgression from closely related taxa following secondary contact. Secondary contact between distinct, yet interfertile, lineages may lead to outcomes ranging from complete unification to formation of stable, narrow hybrid zones permitting low levels of genetic exchange. These stable hybrid zones can be maintained either by pre-zygotic (e.g., behavioral) or post-zygotic (e.g., reduced hybrid fitness) reproductive barriers. Additionally, gene flow following long-term isolation provides opportunities for selective introgression between lineages. The process of speciation is therefore a continuum, and there is regular debate as to the classification status of related lineages that have not yet reached complete reproductive isolation and are instead in the "gray zone" of speciation.

Secondary contact between lineages can result from either natural or anthropogenic forces. For example, stable hybrid zones typically arise from the natural expansions and contractions of lineages throughout geologic time due to major climatic fluctuations. Over the past century, however, human translocations have become prevalent, sometimes leading to secondary contact between introduced and native populations of the same species. Here I investigate the dynamics of secondary contact and hybridization between distinct canid lineages, focusing on two different systems, the red fox (*Vulpes vulpes*) and the gray fox (*Urocyon cinereoargenteus*). These vary both in the origins of secondary contact (anthropogenic vs. natural range expansion) and in the level of divergence between lineages (late-Pleistocene vs. mid-

Pleistocene), making them valuable systems to explore the mechanisms maintaining lineage boundaries and the role of selective introgression in their evolution

In Chapter 1, I investigated patterns of human facilitated gene flow between two lineages that are >20,000 years divergent. The native Sacramento Valley red fox (SVRF, *V. v. patwin*) is endemic to the semi-arid region of California's northern Central Valley. In direct contact with the SVRF range is a population of nonnative red foxes, found primarily in the San Joaquin valley to the south of the native population and in the coastal lowland region to the west. This nonnative population was derived from multiple human translocations of fur-farmed foxes in the early 1900s. Most farmed foxes were originally sourced from eastern Canadian and Alaskan lineages in the late 1800s which were phylogenetically divergent (~20–70 kya) from the SVRF. They were bred in fur farms for several decades prior to their release or escape in California in the mid 1900s. I hypothesized that gene flow was restricted, potentially due to post-zygotic genetic mechanisms, and that some genes originating in nonnative foxes would confer higher fitness in the currently human-dominated landscape and would therefore be selectively introgressed into the native fox population. I sequenced 107 red foxes from the native (n = 59) and nonnative (n = 48) ranges at a mitochondrial fragment and >19,000 loci of the nuclear genome.

Observed geographic cline widths were 6.9× (mtDNA) and 14.3× (nuDNA) narrower than expected based on simulations assuming unrestricted gene flow, consistent with the presence of reproductive barriers. Using a Bayesian genomic cline analysis, I identified 10 loci with significantly reduced levels of introgression, several of which were previously associated with reproductive fitness. Consistent with selective introgression, nine loci were identified with significantly elevated levels of gene flow, most of which originated from the nonnative population. Several genes near these outlier regions were potentially associated with adaptation

to human dominated landscapes. It should be noted that pre-zygotic factors, such as assortative mating or natal habitat-biased dispersal, also could have contributed to the maintenance of the hybrid zone. Nevertheless, these findings indicate the presence of some form of reproductive barrier between the native and nonnative red fox populations, which enabled the identification of several exceptional genes that were shared at much higher rates than expected by chance. These genes flowed primarily from the nonnative population, for which ancestors had undergone strong selection for a captive environment, to the native population, which only recently (150 years) experienced the conversion of its historical range to a human-dominated landscape.

In Chapters 2 and 3 I investigated patterns of divergence and gene flow between two lineages that are ~1 million years divergent, where secondary contact was presumed to be a result of natural range expansion. North American gray foxes are composed of two highly divergent, reciprocally monophyletic lineages in the western and eastern portions of their range. They currently hybridize in a relatively a narrow zone of contact in the southern Great Plains. The narrowness of their hybrid zone indicates either that secondary contact was very recent or, if ancient, that reproductive isolating mechanisms prevent their wholesale unification. Given their vagile nature and the lack of clear physical barriers separating them, we hypothesized that one or both lineages occupied smaller ranges removed from the current zone of contact throughout most of the Pleistocene and achieved contact only recently through a massive Holocene expansion. To investigate this hypothesis, we explored their demographic histories and population structure using a combination of whole-genome and reduced-representation sequencing. Additionally, we characterized the timing and extent of gene flow pulses between western and eastern gray foxes using a local ancestry inference-based approach.

In Chapter 2, we used both whole-genome (n = 26) and reduced representation (n = 197) sequencing to contrast the demographic histories of western and eastern gray foxes. Pairwise sequential Markovian coalescent (PSMC) modeling, stairway plots, and summary statistics of eastern and western gray foxes on either side of the contact zone showed contrasting demographic trajectories, with the trajectory of the eastern population declining and the trajectory of the western population increasing for most of their post-divergence history; during the latter portion of the last (Wisconsinan) glacial cycle and most of the Holocene, the eastern trajectory increased and the western trajectory declined. Correspondingly, the eastern lineage exhibited much lower genetic diversity than the western lineage, a cline in diversity consistent with a westward expansion front, and minimal genetic structuring. In contrast, the western lineage exhibited population structure and locally varying demographic histories, reflecting long-term occurrence over a broad region of the continent. The recurrent declines in the eastern population may have kept them both geographically and demographically restricted to the southeast for much of their evolutionary history, resulting in the deep divergence and limited gene flow currently observed between lineages. Additionally, population structure and variable demographic histories within the western lineages may reflect separation in distinct glacial refugia and subsequent gene flow across the western gray fox range.

In Chapter 3, I utilized whole genomes of gray foxes (n = 42) from both the western and eastern lineages as well as from the hybrid zone to investigate (1) the timing of secondary contact and genetic exchange, (2) the width of the hybrid zone in the context of this timing, and (3) signatures of selective introgression between lineages. I inferred the timing of admixture pulses using a local ancestry inference-based approach, which was optimized for low-coverage sequencing data. I tested whether observed patterns of admixture were consistent with

expectations based on a model assuming no reproductive barriers. I then investigated specific genomic regions that were introgressed across the contact zone at unusually high frequencies, consistent with selective introgression. I identified two distinct pulses of late Holocene and historical admixture. The older pulse of admixture (3,500 YBP) reflected unidirectional gene flow from east to west, likely driven by a major demographic expansion of the eastern gray fox. In contrast, the more recent bi-directional pulse of admixture began approximately 200 YBP, coinciding with major anthropogenic landscape changes. Given the recency of genetic interchange, the narrow widths of the geographic clines provided little insight on the question of reproductive isolation but afforded an opportunity to explore selective introgression. Several genomic regions were identified as candidates for selective introgression and may have been associated with behavioral divergence, mate choice, and olfaction.

Contents

Chapter 1: Maintenance of a narrow hybrid zone between native and introduced red foxes (*Vulpes vulpes*) despite conspecificity and high dispersal capabilities

Details of collaboration: In this chapter I (SPQ) present my work on the secondary contact and maintenance of boundaries between native and introduced red fox population in California. I designed the research with input from Dr. Ben Sacks. Dr. Cate Quinn modified the spatially explicit simulations of secondary contact in the program HZAR to include sex-biased dispersal and genetic markers with distinct inheritance patterns. All collaborators contributed to interpretation of the results. I have performed all the analyses presented in this dissertation.

SOPHIE PRECKLER-QUISQUATER,[1] CATE B. QUINN[1], and BENJAMIN N. SACKS[1,2].

[1]Mammalian Ecology and Conservation Unit, Veterinary Genetics Laboratory, School of Veterinary Medicine, University of California, Davis, One Shields Avenue, Davis, CA, 95616, USA
[2]Department of Population Health and Reproduction, School of Veterinary Medicine, University of California, Davis, Davis, CA, USA

Abstract

Human-facilitated introductions of nonnative populations can result in secondary contact between previously allopatric lineages. In such cases, subsequent hybridization can result in homogenization of the lineages or stable hybrid zones, maintained either by pre-zygotic (e.g., behavioral) or post-zygotic (e.g., reduced hybrid fitness) reproductive barriers. We investigated patterns of gene flow between two lineages that were >20,000 years divergent: the native Sacramento Valley red fox (*Vulpes vulpes patwin*) and an introduced conspecific population in the Central Valley region of California that was derived from fur farms. We hypothesized that gene flow was restricted, potentially due to post-zygotic genetic mechanisms, and that some genes originating in nonnative foxes would confer higher fitness in the currently human-dominated landscape and would therefore be selectively introgressed into the native fox population. We sequenced 107 red foxes from the native (n = 59) and nonnative (n = 48) ranges at a mitochondrial fragment and >19,000 loci of the nuclear genome. Observed cline widths were 6.9× (mtDNA) and 14.3× (nuDNA) narrower than expected based on simulations assuming

unrestricted gene flow, consistent with the presence of reproductive barriers. Using a Bayesian genomic cline analysis, we identified 10 loci with significantly reduced levels of introgression, several of which were previously associated with reproductive fitness. Consistent with selective introgression, nine loci were identified with significantly elevated levels of gene flow, most of which originated from the nonnative population. Several genes near these outlier regions were potentially associated with adaptation to human dominated landscapes. We note that pre-zygotic factors, such as assortative mating or natal habitat-biased dispersal, also could have contributed to the maintenance of the hybrid zone. Nevertheless, our findings indicate the presence of some form of reproductive barrier between the native and nonnative red fox populations, which allowed us to identify several exceptional genes that were shared at much higher rates than expected by chance. These genes flowed primarily from the nonnative population, for which ancestors had undergone strong selection for a captive environment, to the native population, which only recently (150 years) experienced the conversion of its historical range to a human-dominated landscape.

Keywords: contact zone, dispersal, introgression, red fox, reproductive barriers, *Vulpes vulpes patwin*

1 | INTRODUCTION

When two previously allopatric populations come into contact, several outcomes are possible, depending in large part on the magnitude of divergence between them. If the populations are related closely enough to interbreed, consequences can range from complete homogenization into a single population to the formation of a stable hybrid zone, whereby hybridization is restricted to a limited zone of overlap with varying degrees of introgression into

the parent populations (Endler, 1977; Barton and Hewitt, 1985). Stable hybrid zones typically arise from the natural expansions and contractions of lineages throughout geologic time, which provide opportunities for evolution of partial reproductive barriers. Over the past century, however, human translocations have become prevalent, sometimes leading to secondary contact between introduced and native populations of the same species (Grant and Grant, 1992; Rhymer and Simberloff, 1996; Larsen, 2010; Seebens, 2017).

The strength of reproductive isolation generally correlates with the time of divergence between lineages due to evolved differences that accumulate while the populations are in allopatry (Edmands, 1999). Thus, hybrid zones that form between recently diverged lineages (e.g., conspecifics), as opposed to more distantly divergent lineages (e.g., sister species), are comparably more likely to result in the swamping of one lineage by the other or the fusion of both lineages (Wilson, 1965; Moore, 1977). Numerous mechanisms can interact to maintain the stability of a hybrid zone, however, including pre-zygotic barriers such as assortative mating and natal habitat-biased dispersal (Davis and Stamps, 2004; Irwin, 2020), which do not necessarily require thousands of generations to evolve, as well as post-zygotic barriers such as reduced hybrid fitness or Dobzhansky-Muller incompatibilities (DMIs), which tend to evolve during longer periods of isolation (Edmands, 1999; Bierne et al., 2011). Regardless of the mechanism impeding gene flow, a second feature of restricted hybrid zones that result from secondary contact is the possibility that advantageous alleles initially unique to one population can be selectively introgressed into the other population (Hedrick 2013). While selective introgression can occur even when overall gene flow is high, detection of selective introgression is facilitated by low overall gene flow, which provides a contrast and the necessary statistical power to detect outliers (Crawford and Nielsen 2013).

Here we investigate a hybrid zone between a native and nonnative populations of red fox (*Vulpes vulpes*) in California. The Sacramento Valley red fox (SVRF, *V. v. patwin*) is endemic to the semi-arid region of California's northern Central Valley (Sacks et al., 2010). In direct contact with the SVRF range is a population of nonnative red foxes, found primarily in the San Joaquin valley to the south of the native population and in the coastal lowland region to the west. This nonnative population was derived from multiple human translocations of fur farmed foxes in the early 1900s (Lewis et al. 1999; Sacks et al. 2016). Most farmed foxes were originally sourced from eastern Canadian and Alaskan lineages in the late 1800s which were phylogenetically divergent (~20–70 kya) from the SVRF. They were bred in fur farms for several decades prior to their release or escape in California in the mid 1900s (Lewis et al., 1999; Sacks et al., 2016).

Despite evidence of secondary contact, a study using mtDNA and microsatellite data indicated that these nonnative and native populations had retained their genetic distinctiveness outside of a limited region where they hybridized (Sacks et al., 2011). Noting their high dispersal distances relative to their range sizes, Sacks et al. (2011) speculated that contact time should have been sufficient for homogenization of these two populations in the absence of any reproductive isolating mechanism. However, this presumption was not quantitatively tested. To determine if one or more reproductive isolating mechanisms is actively reducing gene flow between native and nonnative red foxes, it is necessary to first rule out the possibility that there simply has not been sufficient time for homogenization to occur. Additionally, increased resolution using a genomic method involving thousands of loci can potentially help to clarify the genetic structure and hybrid zone dynamics within this system.

In this study, we developed a null model describing the expected dynamics of homogenization between the two red fox populations in the absence of any reproductive isolating mechanisms. Using genotyping by sequencing (GBS) and mtDNA sequencing of both native and nonnative red foxes, we then clarified the genetic structure in and around the hybrid zone using thousands of loci throughout the genome and compared these empirical data to predictions of our null model to evaluate whether the width of the hybrid zone could be explained without reproductive isolating mechanisms. We then employed a genomic cline approach to identify loci potentially associated with post-zygotic mechanisms for restricted gene flow and investigated whether some genes originating in nonnative foxes potentially conferring higher fitness in the currently human-dominated landscape of the Sacramento Valley would be selectively introgressed into the native fox population.

2 | MATERIALS AND METHODS

2.1 | Sampling

For mitochondrial sequencing, we obtained both scat (n = 195) and tissue (n = 490) samples as well as 4 hair and swab samples from red foxes in the native SVRF (n = 293) and nonnative ranges (n = 396). All samples were collected between 1982–2021 and many of them (n = 472) were first described in previous red fox studies (Table S1.1). Samples were obtained through non-invasive den and transect surveys, roadkill collection, live captures (following American Society of Mammalogy animal care guidelines and with University of California, Davis Animal Care and Use Committee approval, IACUC No.17860), and nonnative species removal programs in the case of the introduced red foxes. We selected a geographically

representative subset of tissue samples from the native SVRF (n = 69) and nonnative ranges (n = 62) for nuclear DNA sequencing.

2.2 | DNA Extraction, Mitochondrial Sequencing, and Sex-Typing

We extracted tissue samples using the Qiagen DNEasy Blood and Tissue Kit and scats using the QiaAmp DNA Stool Mini Kit, in both cases following manufacturer's instructions (Qiagen Inc, Valencia, CA). Using previously published primers, we amplified and sequenced samples new to this study at a 354 bp region of the cytochrome *b* gene (RF14724, RF15149; Perrine et al., 2007; Aubry et al., 2009; Sacks et al., 2010a) and at a 343 bp region of the D-loop (VVDL1, VVDL6; Aubry et al., 2009). We conducted 11 µL polymerase chain reactions (PCR) containing 1X PCR buffer, 2.5 mM $MgCl_2$, 0.2 mM dNTPs, 0.1 µg/µL of bovine serum albumin, 0.5 µM of each primer, and 1 U of Taq DNA polymerase (Applied Biosystems, Foster City, CA, USA). PCR conditions were as follows: 94 °C for 10 min, followed by 40 cycles at 94°C for 45s, 50°C for 45s and 72°C for 45s; followed by a 10-min extension period at 72 °C. We purified PCR products using exonuclease/shrimp alkaline phosphatase and sequencing was conducted on a 3730 DNA Analyzer (Applied Biosystems) and resulting sequences were aligned and called in Sequencher (v5.4.6, Gene Codes Corporation, Inc.). We compared resulting sequences to a large database of reference samples and classified mitochondrial haplotypes as native and nonnative based on previous work (Perrine et al., 2007; Aubry et al., 2009; Sacks et al., 2011; Statham et al. 2012; Sacks et al., 2016).

We determined the sex of individuals by genotyping each sample at a single nuclear microsatellite sex-typing locus (K9-Amelo), which was part of a broader multiplexed assay (Moore et al., 2010). Each 10 µL reaction contained 1 µL or 2 µL of template DNA (for tissue

and scat extracts respectively), 5 μL of Qiagen Multiplex Mastermix, 1 μL of Q-Solution, and 2.5 μL of primer mix. PCR conditions were as follows: denaturing step of 95 °C for 15 min, followed by 33 cycles at 94°C for 30 s, 57°C for 90 s, 72 °C for 60 s, and a final extension step at 58°C for 10 minutes. Products were electrophoresed on an ABI 3730 capillary sequencer (Applied Biosystems, Foster City, CA, USA) and alleles were scored relative to an internal size standard, Genescan 500 LIZ (Applied Biosystems), using STRand software (Locke et al., 2007). Each sample was run in two independent PCRs to ensure confident genotyping calls.

2.3 | Nuclear DNA Library Preparation

We used a genotyping by sequencing (GBS) approach modified from Elshire et al. (2011) to construct reduced representation genomic libraries for red fox. Briefly, all extracts were normalized to 10 ng/μL prior to library preparation and sequencing. We digested 100 ng of DNA per sample at 37°C for 2 hours with a restriction enzyme (NsiI-HF, an equivalent to EcoT22I; New England BioLabs Inc., Ipswich, MA). We then ligated both a common and uniquely barcoded adapter to each DNA sample (95 samples and 1 negative control per run). To minimize unevenness among individual libraries in the final sequencing pool, we pooled ligated samples into 8 separate sub-pools (12 samples each) before purifying via QiaQuick PCR columns (Qiagen Inc.) prior to the PCR reaction. To increase the complexity of our final library, we conducted 4 replicate PCR reactions for each of our 8 library sub-pools, for a total of 36 reactions. Each 50 μL reaction contained 10 μL of purified adapter ligated DNA, 25 μL of NEB 2X Master Mix, 25 pmol of both forward and reverse PCR Primer, and dH_2O. The PCR conditions were as follows: 5 minutes at 72°C, 30 seconds at 98°C, followed by 18 cycles of 10 seconds at 98°C, 30 seconds at 65°C, and 30 seconds at 72°C, with a final extension at 72°C for

five minutes. We purified PCR products with QiaQuick PCR columns, and quantified library concentrations with a Qubit fluorometer (Qiagen Inc.). All libraries were run on 1% agarose gels and a Bioanalyzer (Agilent Technologies, Santa Clara, CA) trace before pooling in equal masses for sequencing (96 libraries/lane) on an Illumina HiSeq4000 (SR100) at the University of California, Davis Genome Center DNA Technologies core.

2.4 | SNP Calling and Data Filtering

We demultiplexed reads and trimmed adapters using GBSX_v1.3.jar (Herten et al., 2015) and then used ngsShort (Chen et al., 2014) to remove any remaining adapters and reads with >50% of bases having a quality score <2 (-methods lqr -lqs 2 -lq_p 50). We then aligned the trimmed reads to the red fox genome (vv2.4; Kukekova et al., 2018) using BWA-MEM (Li and Durbin, 2010, Li 2013). Reads with mapping quality score <10 (-q 10) were removed in SAMTOOLS (Li et al., 2009). We used the 'ref_map.pl' program in Stacks (v2.53) to process the sorted BAM files and call SNPs (Catchen et al., 2011). The 'gstacks' module was run with default SNP model parameters (--model marukilow, --var-alpha 0.05, and --gt-alpha 0.05) for unpaired reads (--unpaired) to create a catalogue of SNPs across our sample set as a single population. We then ran the 'populations' module to filter out monomorphic and low frequency variants (--min_maf 0.01), as well as SNPs with excess heterozygosity likely to reflect paralogs (--max_obs_het 0.60). Additionally, we randomly selected a single SNP per locus (--write_random_snp) to reduce physical linkage across markers. We used a stepwise filtering approach in Plink (v1.90; Purcell et al., 2007) to arrive at a dataset composed of SNPs called in ≥80% of individuals and individuals with ≥80% of SNPs called. First, we removed the lowest quality individuals from the dataset that were missing ≥75% of SNPs (--mind 0.75). We then

removed SNPs present in ≤80% of individuals (--geno 0.2). Finally, we removed individuals with <80% of SNPs called (--mind 0.2).

2.5 | Genetic Inference of Sex-Biased Dispersal Patterns

We estimated dispersal distance of males and females separately by measuring straight line (Euclidean) distance between adult (> 7 months old) same-sex first-order relatives (parent-offspring or full-siblings) (Storm et al., 1976; Walton et al., 2021). To obtain a relatedness (*r*) threshold that would confidently differentiate first-order (parent-offspring, full siblings) from second order (e.g., half-siblings) relatives and unrelated individuals, we simulated genotypes for individuals of known relatedness (*r*; parent-offspring, full-sibling, half-sibling, unrelated) at varying numbers of randomly selected loci (n = 100–500), using the allele frequencies present in our population. We then examined the distributions of *r* using the 'quellergt' estimator (Queller and Goodnight, 1989) in the R package 'Related' (Pew et al. 2015). The simulations demonstrated that a cutoff of r = 0.40 resulted in correctly identifying all pairs of first-order relatives (100% sensitivity) and none of the half-siblings or unrelated individuals (100% specificity) when using a minimum of 400 loci. We therefore calculated estimates of *r* among the individuals in our study using 400 randomly selected loci in our genome-wide SNP (GBS) dataset.

2.6 | Geographic Patterns of Ancestry

To assess population structure and admixture using the genome-wide nuDNA (GBS) dataset, we first generated a multidimensional scaling (MDS) plot in Plink (v1.90; Purcell et al., 2007) to examine the genetic distances among samples in relation to geographic location

(Sacramento Valley vs nonnative range). Then, using the maximum-likelihood program ADMIXTURE (Alexander et al. 2009), we assessed population structure and assignment at K = 1–5 clusters using a 10-fold cross-validation approach to determine K with the highest likelihood. Additionally, we ran 2,000 bootstrapped replicates to obtain 95% confidence intervals around our ancestry assignment point estimates and again explored the relationship between ancestry assignment and geographic location among individuals. For downstream analyses, we conservatively identified "pure" native and nonnative individuals as those with 95% confidence intervals that deviated <0.05 from pure native or nonnative assignment.

2.7 | Geographic Cline Analysis

Expected clinal patterns under a model of neutral diffusion

To assess whether the observed patterns of admixture (nuDNA) or native/nonnative maternal ancestry (mtDNA) across the landscape could reflect neutral diffusion between two populations since the nonnative red fox's introduction, we modeled expectations on the basis of cline position and width. We began by conducting spatially explicit simulations in the R program HZAM (Irwin, 2020), using an informed set of parameters that matched our knowledge of the history and nature of secondary contact. We then characterized the resulting genetic makeup of the simulated populations along a linear cline for both marker types (mtDNA and nuDNA) after multiple generations of random mating, reproduction, survival to adulthood, and dispersal to a new breeding location (with non-overlapping generations).

The spatial boundaries of our simulation were represented by a 1-dimensional transect that spanned the length of the Central Valley, with native SVRF populations occurring within the presumed historical range (Sacramento Valley), and the nonnative population occurring to the

south (San Joaquin Valley). This landmark feature was consistent with historical records and previous genetic analyses, and therefore provided the best estimate for the geographic location of secondary contact (Sacks et al., 2011). To facilitate modeling data as a linear geographic cline, we did not attempt to incorporate the coastal regions into our models, as previous studies identified the coastal mountains as significant barriers to gene flow between nonnative red foxes in the coastal region, and those within the San Joaquin Valley (Sacks et al., 2016).

We assumed a constant population density (one breeding pair/15 km^2) across the entire landscape, which was derived from previous estimates measured within the Sacramento Valley region (Black et al., 2018). We assumed random mating, in which each adult female mates with the male that is geographically closest to her regardless of genetic make-up. The probability of offspring surviving to adulthood was set to 1 across all individuals. We modified the dispersal parameter in the original HZAM simulation to reflect the estimates from our genetic inference of dispersal patterns described above. Specifically, we sampled both the male and female dispersal distances from separate lognormal (as opposed to normal) distributions that fit the estimated mean and standard deviation for both males and females in the population. While nonnative red foxes were documented in the CA lowlands prior to 1975, we conservatively used this date as the initiation of secondary contact based upon the confirmation of their presence adjacent to the SVRF population via systematic survey efforts (Gray et al., 1975). We calculated the average number of years represented by our two genetic datasets, since this date, for both mtDNA (average = 36.5 ± 4.7 years) and nuDNA (average = 35.9 ± 4.5 years). We converted these values to generation times using a previous estimate of 2 years/generation for red fox, again erring on the conservative side (Sacks et al., 2010). We therefore ran our simulations for the

estimated minimum of 18 generations since secondary contact began (Gray, 1975; Lewis et al., 1999; Sacks et al., 2010). We also modified the number of loci and the mode of inheritance for our simulations accordingly, modeling 100 biparentally inherited loci to simulate nuDNA patterns, compared to a single, maternally inherited locus to simulate that of the mtDNA.

We summarized the output of the simulations by assigning individuals, each possessing differing levels of admixture and maternal DNA ancestry, to geographic bins, every 33 km along the length of the cline. We fit classical equilibrium cline models under a likelihood framework using the Metropolis-Hastings Markov chain Monte Carlo algorithm in the program HZAR (Derryberry et al., 2014). For each marker type, we ran 10 model combinations using the default number (100,000 with 10,000 burn-in) of Markov chain Monte Carlo (MCMC) steps for three iterative cycles. We then assessed the best fitting model for each marker type using Akaike information criterion scores corrected for small sample size (AICc). We obtained maximum likelihood estimates for centers, widths, and their corresponding ± 2 log likelihood (LL) intervals (approximately 95% credibility intervals), and we used these to test for concordance of expected cline centers and widths across marker types and to set the expectation for our observed data.

Observed clinal patterns

We summarized the observed data in an identical manner to our simulated data. If the two populations had no reproductive isolating mechanisms, we would expect both nuclear and mitochondrial loci to diffuse across the zone of secondary contact at a rate predicted by dispersal distances. Additionally, because the mitochondrial genome is maternally inherited, we would expect the width of the mtDNA cline to be narrower than that of the nuDNA cline because female dispersal distances are shorter on average than males.

After excluding coastal nonnatives, we re-ran our ADMIXTURE analysis at K = 1–5 using only the subset of individuals found within the Sacramento and San Joaquin Valleys (n = 83). We then measured the Euclidian distance (km) between each sample and the southern edge of the Sacramento Valley. We then summarized the ancestry of individuals across the landscape by grouping samples into 33-km geographic bins and we selected the best-fit cline for each marker type, using the same approach described above for our simulated dataset. We then tested for concordance of cline centers and widths between observed clines as well as be compared the cline widths of our observed data with that expected based on our simulations of neutral diffusion.

2.8 | Genomic Patterns of Ancestry

We aimed to characterize patterns of genetic differentiation across the genome to identify whether specific genomic regions might confer pre or postzygotic barriers that impact rates of gene flow across the hybrid zone. To do this, we conducted a Bayesian genomic cline analysis to quantify the variation in locus specific introgression (Gompert and Buerkle, 2011). Bayesian genomic clines are similar to geographic clines in that they also measure a genome-wide or locus specific cline center (α) and rate (β). However, instead of the transition of ancestry across geographic space, a Bayesian genomic cline estimates these parameters based on the relationship between the relative parental ancestry at each locus (φ) and the hybrid index (h), both of which range between 0 (pure nonnative ancestry) and 1 (pure native ancestry) and are expected to be equivalent under a null model. Loci with positive values of α reflect increased introgression of native ancestry (φ) into nonnative genomic backgrounds relative to the hybrid index (h). In contrast, loci with negative values of α reflect increased introgression of nonnative ancestry (φ)

into native genomic backgrounds. The β parameter measures the slope of the cline, or the rate of transition from one ancestry type to another, relative to the hybrid index (*h)*. Positive β values can reflect selection against hybrid phenotypes and may correspond to reproductive barrier loci, while negative β values may indicate introgression of alleles that have a selective advantage within both populations. We used the same subset of individuals (n = 83) that were described in our geographic cline analysis, excluding those found within the coastal region. To reduce computational time, we selected a subset of 3,572 ancestry informative markers (AIMs) that had allele frequency differences >0.2 between our stringent set of pure parentals. We calculated the allele frequencies across all AIMs within our pure Sacramento Valley (n = 18) and nonnative (n = 21) parental populations. We then generated allele counts for individuals with admixed ancestry (n = 44) to utilize the genotype-likelihood approach within the *bgc* software (v1.04b; Gompert and Buerkle, 2012). We ran five replicate chains, each for 400,000 MCMC iterations with 200,000 burn-in cycles, thinning the data every 40 steps. We assessed convergence by examining the correlation of parameters across independent runs. We classified α and β outliers as loci with 95% credibility intervals for the posterior probability distribution that excluded zero (Gompert and Buerkle, 2011).

As we were specifically interested in putative regions underlying barriers to introgression or those that may be selectively introgressed across the contact zone, we identified genes within 1 Mb of all our positive and negative β outliers by extracting each locus and it's flanking sequence and aligning reads to the dog genome (CanFam 3.1, Lindblad-Toh et al., 2005; UCSC Genome Browser; NCBI *Canis lupus familiaris* Annotation Release 105 [2019-12-10]). We then conducted a gene enrichment analysis using Panther (v16.0), evaluating whether any associated GO terms were overrepresented (Mi et al., 2020). We additionally compared our list of outlier

regions to those that were previously associated with behavioral divergence (e.g., neural crest development, domestication, etc.) or reproductive function (e.g., spermatogenesis, hybrid sterility, etc.) in other studies.

3 | RESULTS

We obtained cytochrome b mitochondrial sequences for 682 individuals. After SNP calling and filtering, our final genotyping by sequencing dataset contained 107 individuals and 19,051 SNPs. The genome-wide coverage for our final sample set averaged 0.4% of the genome (approximately 1 million bases), and mean sequencing depth across loci for all individuals averaged 30×, ranging from 6–133× among individuals.

We identified 18 pairs of same-sex (n = 9) and opposite-sex (n = 9) first-order relatives (Table S2). The average (±SD) pairwise distance between male first-order relatives was 44.9 ± 79.75 km (n = 5), while the average pairwise distance between female first-order relatives was 5.46 ± 3.36 km (n = 4). The average pairwise distance of the opposite sex pairs was 9.78 ± 11.16 km, but we did not include these in our estimates of male and female dispersal. These estimates were similar to previously published dispersal distances for other lowland red fox populations (Table 1.1; Table S1.2).

3.1 | Geographic Patterns of Ancestry

We detected 255 individuals with native SVRF mtDNA haplotypes (D, D2; GenBank Accession Nos: EF064209, GU004541) and 427 individuals with nonnative mtDNA haplotypes (E, F, G, N, O; GenBank Accession Nos: EF064210-EF064212, EF064218, EF064219; Sacks et al. 2011, 2016). All native haplotypes were found within the presumed historical range of the

SVRF. Of those with nonnative haplotypes, 395 (92.5%) were detected south of the historical SVRF range throughout the San Joaquin Valley, and the coastal lowlands (Fig. 1.1).

Based on 19,051 loci in the GBS dataset (n = 107 individuals), the multidimensional scaling plot clearly separated native from nonnative red foxes, yet indicated numerous individuals found within the native SVRF range that were of admixed ancestry (Fig. 1.2). In contrast, we observed little to no native ancestry in individuals found throughout the nonnative range. Additionally, genetic structuring was evident between nonnative red foxes in the San Joaquin Valley and those found in the coastal lowlands. The ADMIXTURE results identified K = 2 with the highest likelihood, followed closely by K = 3 (Fig. S1.1). The ADMIXTURE analysis revealed similar population structuring in the nonnative population at K = 3 to that shown in the MDS plot as well as in previous studies using microsatellite data (Fig. S1.1; Sacks et al., 2016). While no pure nonnative individuals were detected in the Sacramento Valley, there was more nonnative ancestry found within mostly native individuals in the Sacramento Valley region than there was native ancestry in nonnative individuals from the San Joaquin Valley. Instances of discordance between mtDNA haplotypes and nuclear ancestry were rare, occurring in 6.3% of primarily native SVRF and 6.9% of primarily nonnative foxes. Additionally, all individuals with discordant ancestry were found within the Sacramento Valley region (Fig. 1.3).

3.2 | Geographic cline analysis

The empirically measured cline widths for both mtDNA (17 km) and nuDNA (20 km) were 6.9× (mtDNA) and >14.3× (nuDNA) narrower than the expected widths (mtDNA = 117 km; nuDNA = 286 km) derived from our simulated models of neutral diffusion (Table 1.2, Fig.

1.4). Both our expected and observed cline withs were narrower for mtDNA than for nuDNA, as predicted given the male-biased dispersal pattern and the maternal inheritance of the mtDNA.

3.3 | Genomic Patterns of Ancestry

Estimates of genomic cline center (α) and rate (β) parameters were largely concordant across replicate MCMC chains with average r^2 values of 0.997 and 0.985 respectively (Fig. S1.2). We detected similar numbers of positive (n = 253) and negative (n = 263) α outlier loci according to our 95% credibility intervals, and the magnitude was not significantly different ($\bar{\alpha}_{POS}$ = 0.74±0.01, $\bar{\alpha}_{NEG}$ = -0.76±0.01). We also detected similar numbers of positive (n = 10) and negative (n = 9) β outlier regions, supporting some loci as candidates for involvement in maintaining barriers to gene flow or for selective introgression.

We identified 90 genes within 500 kb of the 10 positive β outlier regions (i.e., reduced introgression between populations) that were previously annotated in the dog genome (Table S1.3). We found no evidence of enrichment for specific functional categories dominating these outliers. However, the introgression of several genomic regions were near genes that have been previously associated with reproductive fitness including embryonic development (STIL) and spermatogenesis (TSSK2, SPATA20, MYCBPAP) (David et al., 2014; Li et al., 2011; Furusawa et al., 2001). Additionally, several regions (MYCBPAP, Vulp_V002774, Vulp_V002775) were previously linked to differential expression patterns and high genetic differentiation between red foxes that were selectively bred for tame versus aggressive behavior (Wang et al., 2018, Kukekova et al., 2018).

We identified 37 previously annotated genes within 500 kb of the nine negative β outlier regions (i.e., elevation levels of introgression between lineages) (Table S1.4). We found no

evidence of enrichment for specific functional categories. However, three regions were located within or adjacent to genes that have been previously associated with neural crest function and social behavior, including DLG2, NCAM2, and KIF5C (Reggiani et al., 2017; Winther et al., 2012; Gong et al., 2022). Notably, all three of these regions were introgressed from the nonnative into the native Sacramento Valley population (i.e., negative α -values).

4 | DISCUSSION

We confirmed limited introgression across a zone of secondary contact between the native Sacramento Valley red fox and a recently introduced nonnative red fox population despite recent evolutionary divergence, high dispersal capabilities, and at least 18 generations (and possibly many more) of contact and potential interbreeding. Based on simulated neutral expectations, which assumed random mating, random dispersal, and no selection (i.e., equal probability of survival and reproduction), the expected cline widths for our mtDNA and nuDNA were 117 km and 286 km respectively. In contrast, the observed cline widths for both marker types were significantly narrower (mtDNA = 17 km, nuDNA = 20 km). Additionally, given the small spatial extent of the entire native range, the neutral model of gene flow predicted that we would observe no remaining individuals with pure SVRF ancestry. However, 37% of individuals sampled within the Sacramento Valley retained statistically pure native ancestry, and we found much higher levels of overall native ancestry in the historical range than expected according to the null model, indicating that barriers to gene flow must be operating.

Rather than reflecting two readily interbreeding conspecific populations, our findings are more akin to those describing contact zones in much more evolutionarily divergent populations or species. Previous research comparing observed patterns of cline width relative to dispersal

distances across a diverse set of taxa with those expected under different selection regimes found that most clines align with either neutral expectations or low-to-moderate levels of selection (Barton and Hewitt, 1985). A more recent meta-analysis that examined hybrid zones across 131 pairs of hybridizing taxa drew similar conclusions and additionally found that the median cline width across all systems was 18.6× greater than dispersal length (McEntee et al., 2020). In contrast, the cline widths observed across the red fox secondary contact zone in our study ranged 0.94×–1.1× the average dispersal distance for the mtDNA and nuDNA clines, respectively. When placed within the context of these previously described hybrid zones, the observed red fox cline widths are even narrower than expected under a scenario of moderate selection, and very few systems described in either study had narrower cline widths relative to dispersal distances (Fig. 1.5). While this observation does not provide direct evidence of strong selection acting within the system, it does offer additional support, independent of our simulated neutral models, to the conclusion that some intrinsic or extrinsic mechanism must be limiting gene flow.

To assess whether genomic reproductive barriers were limiting gene flow, we explored the fine-scale variation in clinal patterns for all loci across the genome, specifically addressing a priori hypotheses pertaining to behavioral differentiation or reproductive incompatibilities. We found little evidence from enrichment-based approaches of a single functional category dominating these outliers. However, several regions appeared particularly amenable to adaptive explanations.

The STIL gene plays an important role in embryonic development as well as cellular growth and proliferation, and embryonic lethality was observed in $STIL^{-/-}$ mouse embryos (Davis et al., 2014). The TSSK2 gene is one of the testis-specific serine/threonine kinases which are expressed in spermatids and are essential for male fertility (Li et al., 2011). Additionally, TSSK2

was identified as a candidate sterility gene within a house mouse hybrid zone in Europe (Turner and Harr, 2014). The SPATA20 gene (spermatogenesis associated protein 20) also has a known role in male reproduction and was identified as a candidate gene associated with a sterility hotspot in a study on hybrid dysfunction in the house mouse (Turner et al., 2014). The MYCBPAP gene similarly plays a role in spermatogenesis and an alteration of its expression may therefore have an impact on sperm function (Furusawa et al., 2001).

Additionally, several putative barrier regions were associated with regions that may behaviorally differentiate lineages. For example, the MYCBPAP gene was found to be differentially expressed between red foxes that were selectively bred for tame vs aggressive behavior (Wang et al., 2018). Two other regions (Vulp_V002774, Vulp_V002775) were also differentiated between tame and aggressive foxes in a separate study (Kukekova et al., 2018). These findings support the possibility that selective breeding in captivity of ancestors to the nonnative population caused behavioral or physiological changes that resulted in either pre- or post-zygotic barriers with native red foxes.

We also found support for selective introgression across the contact zone. We were particularly interested in selective introgression from the nonnative into the native population for which several of these putatively introgressed regions were associated with neural crest function and social behavior. Disruption of proper neural crest development has been linked to domestication, and many of the genes identified in this study have been previously linked to the domestication process. It is unclear how such a distinction would relate to fitness in the Sacramento Valley environment, but potentially relates indirectly to association with humans.

An outlier region on red fox chromosome 11p was located within the open reading frame of the DLG2 (Discs Large MAGUK Scaffold Protein 2) gene, which plays an important role in

complex cognitive and learning tasks (Grant, 2016; Nithianantharajah et al., 2013). Additionally, DLG2 and has been linked to neurodevelopmental disorders including global developmental delay and schizophrenia, both of which have characteristics of hyper-domestication (Reggiani et al., 2017; Šimić et al., 2020; Yoo et al., 2020). The DLG2 gene was also found to be under selection in songbirds across Europe and was associated specifically with urbanization (Salmón et al., 2021). Additionally, DLG2 was differentially expressed in red jungle fowl lines bred for either high or low fear of humans (Bélteky et al., 2018). The DLG2 gene was also identified as a candidate gene under selection across European red fox populations, though selection to human-dominated landscapes specifically was not explored in that study (Roberts et al., 2019).

An outlier region on fox chromosome 15p was located within the open reading frame of the NCAM2 (neural cell adhesion molecule 2) gene, which encodes a protein belonging to the immunoglobin superfamily and has been proposed to contribute to neurodevelopmental disorders in humans including autism and schizophrenia (Winther et al., 2012). NCAM2 is mostly expressed in the cerebral cortex, the hippocampus and the olfactory system (Parcerisas et al., 2021). This gene was identified as being under positive selection in domesticated dogs (Wang et al. 2013). The KIF5C (kinesin family member 5C) gene, on red fox chromosome 5pt, was also putatively introgressed from the nonnative into the native population and has been previously linked to behavioral differences between wild and domestic pigs in Europe, specifically the increased vigilance and social sensitivity in wild populations (Gong et al., 2022).

These candidate barrier genes may help maintain the genetic distinctiveness of the native and nonnative red fox populations. However, further research is needed to test whether these genes confer reduced hybrid fitness or contribute to prezygotic behavioral barriers in these populations, specifically. Similarly, while we observed some evidence for selective introgression

of genes linked to social behavior and domestication, additional research investigating the genetic variation of reference fur farm foxes (i.e., the source populations for the present day nonnative red foxes in California) may help to elucidate whether these regions are linked to the nonnative population's long-term history in captive breeding. Additionally, as we used a reduced representation GBS approach, we only captured the variation present at a subset (~0.4%) of the genome, and it is possible that other loci involved in intrinsic reproductive isolation or selective introgression could be more clearly elucidated through whole genome re-sequencing.

The existing behavioral differentiation also could have a learned or cultural component, which could lead to pre-zygotic reproductive barriers and the reduction of gene flow across the contact zone through assortative mating or natal-habitat biased dispersal. Social learning is a key component to the development of cultural behavioral traits (Whitehead et al., 2019), and red foxes are a social canid, with highly flexible social systems. They often exhibit monogamy, with group sizes largely determined by resource availability and population densities (Dorning and Harris, 2019). Both parents are involved in raising litters, and pups typically remain with their parents for approximately 7 months before dispersing (Storm et al., 1976). During this time, they learn what to eat, how to hunt, how to avoid predators, and how to navigate the landscape effectively. It is possible that these two populations have distinct cultural systems, particularly considering the strong selective pressures (increased fecundity, polygyny, tameness, etc.) the nonnative population underwent in captivity, which may have modified their social and cultural systems.

Natal habitat-biased dispersal (when individuals cue on features in their natal habitat to seek as dispersal targets) depends on sufficient habitat heterogeneity (e.g., Sacks et al., 2004). While the landscape throughout the Central Valley is heterogeneous at the landscape scale, the

northern and southern portions are similarly so, making it seem unlikely that landscape cues could explain separation of these populations. However, conspecific scents or other cues can also fuel natal habitat biased dispersal (Stamps, 1991). Therefore, if there are significant cultural difference between these two populations, they may not be recognizing one another as effective conspecifics, which could limit dispersal across the contact zone. Lack of conspecific recognition could also lead to positive assortative mating which would reduce hybridization between the native and nonnative population. Such assortative mating could significantly narrow the width of the observed geographic cline (Irwin, 2020). Additionally, while cultural traits alone may not leave genomic signatures, there is growing evidence of gene-culture coevolution in which culturally learned behaviors impact genetic evolution by relaxing or intensifying selection (Whitehead et al., 2019).

Finally, it is possible that while the Central Valley is largely homogenous at the regional scale, some landscape barrier in or near the contact zone is limiting dispersal, thereby depressing gene flow across the contact zone. The Sacramento-San Joaquin River Delta, along with the city of Sacramento, an urban metropolis with a human population density >5,000 individuals per square mile may act as barriers to gene flow between these two populations. If these landscape features do act as a partial barrier, it is also possible that dispersal is not equally inhibited in both populations due to either genetic or cultural differences. Although both native and nonnative red foxes currently inhabit highly human-altered landscapes, the nonnative foxes may have a higher threshold for human tolerance. Since their establishment in California, nonnative red foxes have expanded to inhabit a wide range of habitat types throughout California's lowlands and appear to do well in both rural and more heavily human-dominated landscapes. It is therefore possible that the nonnative red fox population, with its long history of captive and selective breeding, is more

likely to cross these barriers into the native SVRF range than vice versa, which could potentially account for the asymmetrical introgression of nonnative ancestry into the native range.

5 | CONCLUSION

The observed hybrid zone between the native Sacramento Valley red fox and the introduced nonnative population is significantly narrower than expected given the large dispersal distances of red foxes, the small extent of the native Sacramento Valley red fox range, and many generations since these populations were brought into contact. While the specific mechanism(s) involved are still uncertain, the narrowness of the cline must be explained by some form(s) of reproductive barrier (pre- or post-zygotic) maintaining population boundaries. We turned up several candidate loci potentially reflecting genomic differentiation or incompatibility that could lead to reduced hybrid fitness and a narrow zone of introgression. Additionally, natal habitat-based dispersal and assortative mating resulting from cultural differences could be influencing the observed patterns in ancestry. Regardless of the underlying mechanism, the limited gene flow between two populations with such recent shared evolutionary history is notable and provided an opportunity to investigate selective introgression. The behaviorally linked genes we detected with elevated levels of gene flow from the nonnative to the native population suggest the presence of such selective introgression. If indeed these alleles were beneficial to Sacramento Valley red foxes in the short-term, the long-term consequences are unclear. Taken together, the narrowness of the cline and the asymmetry of the gene flow support the existence of significant differences between the native and nonnative red fox populations, and therefore warrants future monitoring and investigation to better understand the dynamics between these two distinct lineages and the effects of interbreeding on the native Sacramento Valley red fox population.

ACKNOWLEDGMENTS

We thank Mammalian Ecology and Conservation Unit alumni, Dr. Thomas Batter and Dr. Kathleen Black for their contributions to field and lab work, as well as many students, volunteers, state, county, and private wildlife personnel who assisted with sample collection and processing. Critical laboratory support was provided by S. Vanderzwan, Z. Lounsberry, and the University of California, Davis Veterinary Genetics Center Laboratory staff. Funding was provided by the University of California, Davis, Mammalian Ecology and Conservation Unit.

LITERATURE CITED

Alexander, D.H., Novembre, J., Lange, K., 2009. Fast model-based estimation of ancestry in unrelated individuals. Genome Res. 19, 1655–1664.

Aubry, K.B., Statham, M.J., Sacks, B.N., Perrine, J.D., Wisely, S.M., 2009. Phylogeography of the North American red fox: vicariance in Pleistocene forest refugia. Molecular Ecology 18, 2668–2686.

Bailey, R.I., Tesaker, M.R., Trier, C.N., Sætre, G.-P., 2015. Strong selection on male plumage in a hybrid zone between a hybrid bird species and one of its parents. Journal of Evolutionary Biology 28, 1257–1269.

Barton, N.H., Gale, K.S., 1993. Genetic Analysis of Hybrid Zones. Oxford University Press, Oxford.

Barton, N.H., Hewitt, G.M., 1985. Analysis of Hybrid Zones. Annual Review of Ecology and Systematics 1, 113–148.

Bélteky, J., Agnvall, B., Bektic, L., Höglund, A., Jensen, P., & Guerrero-Bosagna, C., 2018. Epigenetics and early domestication: Differences in hypothalamic DNA methylation between red junglefowl divergently selected for high or low fear of humans. *Genetics Selection Evolution, 50*(1), 13.

Bierne, N., Welch, J., Loire, E., Bonhomme, F., David, P., 2011. The coupling hypothesis: why genome scans may fail to map local adaptation genes. Molecular Ecology 20, 2044–2072.

Black, K.M., Preckler-Quisquater, S., Batter, T.J., Anderson, S., Sacks, B.N., 2019. Occupancy, habitat, and abundance of the Sacramento Valley red fox. The Journal of Wildlife Management 83, 158–166.

Catchen, J.M., Amores, A., Hohenlohe, P., Cresko, W., Postlethwait, J.H., 2011. Stacks: Building and Genotyping Loci De Novo from Short-Read Sequences. G3 Genes|Genomes|Genetics 1, 171–182.

Chen, C., Khaleel, S.S., Huang, H., Wu, C.H., 2014. Software for pre-processing Illumina next-generation sequencing short read sequences. Source Code Biol Med 9, 8.

Crawford, J. E., & Nielsen, R. 2013. Detecting adaptive trait loci in nonmodel systems: Divergence or admixture mapping? *Molecular Ecology*, *22*(24), 6131–6148.

David, A., Liu, F., Tibelius, A., Vulprecht, J., Wald, D., Rothermel, U., Ohana, R., Seitel, A., Metzger, J., Ashery-Padan, R., Meinzer, H.-P., Gröne, H.-J., Izraeli, S., & Krämer, A., 2014. Lack of centrioles and primary cilia in STIL−/− mouse embryos. *Cell Cycle*, *13*(18), 2859–2868.

Davis, J., Stamps, J., 2004. The effect of natal experience on habitat preferences. Trends in Ecology & Evolution 19, 411–416.

Demaray, F.M., n.d. Home Range, Home Range Expansion, Dispersal, and Mortality of Juvenile Red Foxes in Southeastern South Dakota 73.

Derryberry, E.P., Derryberry, G.E., Maley, J.M., Brumfield, R.T., 2014. hzar: hybrid zone analysis using an R software package. Molecular Ecology Resources 14, 652–663.

Dorning, J., Harris, S., 2019. Individual and seasonal variation in contact rate, connectivity and centrality in red fox (Vulpes vulpes) social groups. Sci Rep 9, 20095.

Edmands, S., 1999. Heterosis and Outbreeding Depression in Interpopulation Crosses Spanning a Wide Range of Divergence. Evolution 53, 1757–1768.

Elshire, R.J., Glaubitz, J.C., Sun, Q., Poland, J.A., Kawamoto, K., Buckler, E.S., Mitchell, S.E., 2011. A Robust, Simple Genotyping-by-Sequencing (GBS) Approach for High Diversity Species. PLoS ONE 6, e19379.

Endler, J.A., 1977. Geographic Variation, Speciation, and Clines. Princeton University Press.

Furusawa, M., Ohnishi, T., Taira, T., Iguchi-Ariga, S. M. M., & Ariga, H., 2001. AMY-1, a c-Myc-binding Protein, Is Localized in the Mitochondria of Sperm by Association with S-AKAP84, an Anchor Protein of cAMP-dependent Protein Kinase. *Journal of Biological Chemistry*, *276*(39), 36647–36651.

Gompert, Z., Buerkle, C.A., 2011. Bayesian estimation of genomic clines. Molecular Ecology 20, 2111–2127.

Gompert, Z., Buerkle, C.A., 2012. bgc: Software for Bayesian estimation of genomic clines. Molecular Ecology Resources 12, 1168–1176.

Gong, Y., Zhang, H.-Y., Yuan, Y., He, Y., Zhang, W., Han, Y., Na, R., Zeng, Y., Luo, J., Yang, H., Huang, Y., Zhao, Y., Zhao, Z., & E, G.-X., 2022. Genome-Wide Selection Sweep between Wild and Local Pigs from Europe for the Investigation of the Hereditary Characteristics of Domestication in Sus Scrofa. *Animals: An Open Access Journal from MDPI, 12*(8), 1037.

Gosselink, T.E., Piccolo, K.A., Van Deelen, T.R., Warner, R.E., Mankin, P., 2010. Natal Dispersal and Philopatry of Red Foxes in Urban and Agricultural Areas of Illinois. The Journal of Wildlife Management 74, 1204–1217.

Grant, P.R., Grant, B.R., 1992. Hybridization of Bird Species. Science 256, 193–197.

Grant, S. G. N., 2016. The molecular evolution of the vertebrate behavioural repertoire. *Philosophical Transactions of the Royal Society B: Biological Sciences*, *371*(1685), 20150051.

Herten, K., Hestand, M.S., Vermeesch, J.R., Van Houdt, J.K., 2015. GBSX: a toolkit for experimental design and demultiplexing genotyping by sequencing experiments. BMC Bioinformatics 16, 73.

Irwin, D.E., n.d. Assortative Mating in Hybrid Zones Is Remarkably Ineffective in Promoting Speciation 18.

Kent, W.J., 2002. BLAT—The BLAST-Like Alignment Tool. Genome Res. 12, 656–664.

Kukekova, A.V., Johnson, J.L., Xiang, X., Feng, S., Liu, S., Rando, H.M., Kharlamova, A.V., Herbeck, Y., Serdyukova, N.A., Xiong, Z., Beklemischeva, V., Koepfli, K.-P., Gulevich, R.G., Vladimirova, A.V., Hekman, J.P., Perelman, P.L., Graphodatsky, A.S., O'Brien, S.J., Wang, X., Clark, A.G., Acland, G.M., Trut, L.N., Zhang, G., 2018. Red fox genome assembly identifies genomic regions associated with tame and aggressive behaviours. Nat Ecol Evol 2, 1479–1491.

Larsen, P.A., Marchan-Rivadeneira, M.R., Baker, R.J., 2010. Natural hybridization generates mammalian lineage with species characteristics. Proceedings of the National Academy of Sciences 107, 11447–11452.

Lewis, J.C., Sallee, K.L., Golightly, R.T., 1999. Introduction and Range Expansion of Nonnative Red Foxes (Vulpes vulpes) in California. The American Midland Naturalist 142, 372–381.

Li, H., 2013. Aligning sequence reads, clone sequences and assembly contigs with BWA-MEM. arXiv:1303.3997 [q-bio].

Li, H., Durbin, R., 2010. Fast and accurate long-read alignment with Burrows–Wheeler transform. Bioinformatics 26, 589–595.

Li, Y., Sosnik, J., Brassard, L., Reese, M., Spiridonov, N. A., Bates, T. C., Johnson, G. R., Anguita, J., Visconti, P. E., & Salicioni, A. M., 2011. Expression and localization of five members of the testis-specific serine kinase (Tssk) family in mouse and human sperm and testis. *Molecular Human Reproduction, 17*(1), 42–56.

Mayr, E., 1970. Populations, Species, and Evolution: An Abridgment of Animal Species and Evolution. Harvard University Press.

McEntee, J.P., Burleigh, J.G., Singhal, S., 2020. Dispersal Predicts Hybrid Zone Widths across Animal Diversity: Implications for Species Borders under Incomplete Reproductive Isolation. The American Naturalist 196, 9–28.

Moore, W.S., 1977. An Evaluation of Narrow Hybrid Zones in Vertebrates. The Quarterly Review of Biology 52, 263–277.

Moore, M., Brown, S., Sacks, B.N., 2010. Thirty-one short red fox (Vulpes vulpes) microsatellite markers. Mol Ecol Resour 10, 404–408.

Nithianantharajah, J., Komiyama, N. H., McKechanie, A., Johnstone, M., Blackwood, D. H., St Clair, D., Emes, R. D., van de Lagemaat, L. N., Saksida, L. M., Bussey, T. J., & Grant, S. G. N., 2013. Synaptic scaffold evolution generated components of vertebrate cognitive complexity. *Nature Neuroscience, 16*(1), 16–24.

Parcerisas, A., Ortega-Gascó, A., Pujadas, L., & Soriano, E., 2021. The Hidden Side of NCAM Family: NCAM2, a Key Cytoskeleton Organization Molecule Regulating Multiple Neural Functions. *International Journal of Molecular Sciences, 22*(18), 10021.

Perrine, J.D., Pollinger, J.P., Sacks, B.N., Barrett, R.H., Wayne, R.K., 2007. Genetic evidence for the persistence of the critically endangered Sierra Nevada red fox in California. Conserv Genet 8, 1083–1095.

Pew, J., Muir, P.H., Wang, J., Frasier, T.R., 2015. related: an R package for analysing pairwise relatedness from codominant molecular markers. Molecular Ecology Resources 15, 557–561.

Phillips, R.L., Andrews, R.D., Storm, G.L., Bishop, R.A., 1972. Dispersal and Mortality of Red Foxes. The Journal of Wildlife Management 36, 237–248.

Purcell, S., Neale, B., Todd-Brown, K., Thomas, L., Ferreira, M.A.R., Bender, D., Maller, J., Sklar, P., de Bakker, P.I.W., Daly, M.J., Sham, P.C., 2007. PLINK: A Tool Set for

Whole-Genome Association and Population-Based Linkage Analyses. Am J Hum Genet 81, 559–575.

Queller, D.C., Goodnight, K.F., 1989. Estimating relatedness using molecular markers. Evolution 43: 258–275.

Quinn, C.B., Alden, P.B., Sacks, B.N., 2019. Noninvasive Sampling Reveals Short-Term Genetic Rescue in an Insular Red Fox Population. Journal of Heredity 110, 559–576.

Reggiani, C., Coppens, S., Sekhara, T., Dimov, I., Pichon, B., Lufin, N., Addor, M.-C., Belligni, E. F., Digilio, M. C., Faletra, F., Ferrero, G. B., Gerard, M., Isidor, B., Joss, S., Niel-Bütschi, F., Perrone, M. D., Petit, F., Renieri, A., Romana, S., … Smits, G., 2017. Novel promoters and coding first exons in DLG2 linked to developmental disorders and intellectual disability. *Genome Medicine*, *9*(1), 67.

Rhymer, J.M., Simberloff, D., 1996. Extinction by Hybridization and Introgression. Annual Review of Ecology and Systematics 27, 83–109.

Roy, M.S., Geffen, E., Smith, D., Ostrander, E.A., Wayne, Robert K., 1994. Patterns of differentiation and hybridization in North American wolflike canids, revealed by analysis of microsatellite loci. Molecular Biology and Evolution 11:553–570.

Sacks, B.N., Brazeal, J.L., Lewis, J.C., 2016. Landscape genetics of the nonnative red fox of California. Ecology and Evolution 6, 4775–4791.

Sacks, B.N., Moore, M., Statham, M.J., Wittmer, H.U., 2011. A restricted hybrid zone between native and introduced red fox (Vulpes vulpes) populations suggests reproductive barriers and competitive exclusion. Molecular Ecology 20, 326–341.

Sacks, B.N., Statham, M.J., Perrine, J.D., Wisely, S.M., Aubry, K.B., 2010. North American montane red foxes: expansion, fragmentation, and the origin of the Sacramento Valley red fox. Conserv Genet 11, 1523–1539.

Salmón, P., Jacobs, A., Ahrén, D., Biard, C., Dingemanse, N. J., Dominoni, D. M., Helm, B., Lundberg, M., Senar, J. C., Sprau, P., Visser, M. E., & Isaksson, C., 2021. Continent-wide genomic signatures of adaptation to urbanisation in a songbird across Europe. *Nature Communications*, *12*(1), 2983.

Schwartz, M.K., Mills, L.S., McKelvey, K.S., Ruggiero, L.F., Allendorf, F.W., 2002. DNA reveals high dispersal synchronizing the population dynamics of Canada lynx. Nature 415, 520–522.

Seebens, H., Essl, F., Blasius, B., 2017. The intermediate distance hypothesis of biological invasions. Ecology Letters 20, 158–165.

Šimić, G., Vukić, V., Kopić, J., Krsnik, Ž., & Hof, P. R., 2020. Molecules, Mechanisms, and Disorders of Self-Domestication: Keys for Understanding Emotional and Social Communication from an Evolutionary Perspective. *Biomolecules, 11*(1), 2.

Stamps, J.A., 1991. The effect of conspecifics on habitat selection in territorial species. Behav Ecol Sociobiol 28.

Statham, M.J., Sacks, B.N., Aubry, K.B., Perrine, J.D., Wisely, S.M., 2012. The origin of recently established red fox populations in the United States: translocations or natural range expansions? J Mammal 93, 52–65.

Storm, G.L., Andrews, R.D., Phillips, R.L., Bishop, R.A., Siniff, D.B., work(s):, J.R.T.R., 1976. Morphology, Reproduction, Dispersal, and Mortality of Midwestern Red Fox Populations. Wildlife Monographs 3–82.

Turner, L. M., White, M. A., Tautz, D., & Payseur, B. A., 2014. Genomic Networks of Hybrid Sterility. *PLoS Genetics, 10*(2), e1004162.

Turner, L. M., & Harr, B., 2014. Genome-wide mapping in a house mouse hybrid zone reveals hybrid sterility loci and Dobzhansky-Muller interactions. *ELife, 3*, e02504.

Turner, S., 2018. qqman: an R package for visualizing GWAS results using Q-Q and manhattan plots. JOSS 3, 731.

Walton, Z., Hagenlund, M., Østbye, K., Samelius, G., Odden, M., Norman, A., Willebrand, T., Spong, G., 2021. Moving far, staying close: red fox dispersal patterns revealed by SNP genotyping. Conserv Genet 22, 249–257.

Wang, C., Wallerman, O., Arendt, M.-L., Sundström, E., Karlsson, Å., Nordin, J., Mäkeläinen, S., Pielberg, G.R., Hanson, J., Ohlsson, Å., Saellström, S., Rönnberg, H., Ljungvall, I., Häggström, J., Bergström, T.F., Hedhammar, Å., Meadows, J.R.S., Lindblad-Toh, K., 2021. A novel canine reference genome resolves genomic architecture and uncovers transcript complexity. Commun Biol 4, 185.

Wang, X., Pipes, L., Trut, L. N., Herbeck, Y., Vladimirova, A. V., Gulevich, R. G., Kharlamova, A. V., Johnson, J. L., Acland, G. M., Kukekova, A. V., & Clark, A. G., 2018. Genomic responses to selection for tame/aggressive behaviors in the silver fox (*Vulpes vulpes*). *Proceedings of the National Academy of Sciences*, *115*(41), 10398–10403.

Whitehead, H., Laland, K.N., Rendell, L., Thorogood, R., Whiten, A., 2019. The reach of gene–culture coevolution in animals. Nat Commun 10, 2405.

Wilson, E.O., 1965. The challenge from related species. The Genetics of Colonizing Species 7–25.

Winther, M., Berezin, V., & Walmod, P. S., 2012. NCAM2/OCAM/RNCAM: Cell adhesion molecule with a role in neuronal compartmentalization. *The International Journal of Biochemistry & Cell Biology*, *44*(3), 441–446.

Yoo, T., Kim, S.-G., Yang, S. H., Kim, H., Kim, E., & Kim, S. Y., 2020. A DLG2 deficiency in mice leads to reduced sociability and increased repetitive behavior accompanied by aberrant synaptic transmission in the dorsal striatum. *Molecular Autism*, *11*, 19.

Tables and Figures

Table 1.1: Average dispersal distances for both male and female red foxes within the California lowlands as inferred from geographic distances between adult first-order relatives; first-order relatives were inferred from pairwise estimates of relatedness as those >0.4 Relatedness estimates were generated using a subset of 400 randomly selected genomic loci from the larger genotyping-by-sequencing (GBS) dataset (19,051 loci). Dispersal distance estimates were then compared to estimates from other populations obtained using several different approaches including capture/recapture (Philips et al. 1972; Demaray et al. 1981), radio telemetry (Gosselink et al. 2010), and genetic relatedness (Walton et al. 2021). Estimates observed in the present study were within the range of other estimates for male vs. female dispersal patterns.

Estimation method	Geographic location	Reference	Sex	Mean	SD	n
Genetic Relatedness	CA lowland	New to this study	male – male	44.90	79.75	5
Genetic Relatedness	CA lowland	New to this study	female – female	7.84	9.04	4
Genetic Relatedness	CA lowland	New to this study	opposite sex	9.78	11.16	9
Genetic Relatedness	Sweden	Walton et al. (2021)	male – male	37.79	55.54	38
Genetic Relatedness	Sweden	Walton et al. (2021)	female – female	6.17	12.45	64
Genetic Relatedness	Sweden	Walton et al. (2021)	opposite sex	15.85	28.49	22
Capture/Recapture	Iowa/Illinois	Phillips et al. (1972)	male	29.6	-	171
Capture/Recapture	Iowa/Illinois	Phillips et al. (1972)	female	9.98	-	124
Radio Telemetry	Illinois/Indiana	Gosselink et al. (2010)	male	44.6	-	69
Radio Telemetry	Illinois/Indiana	Gosselink et al. (2010)	female	29.8	-	27
Capture/Recapture	South Dakota	Demaray et al. (1981)	male	59.5	66.3	9
Capture/Recapture	South Dakota	Demaray et al. (1981)	female	37.6	19.71	3

Table 1.2: Parameter estimates for the best-fitting cline model for both empirical and simulated geographic clines of mitochondrial and nuclear DNA generated using the program HZAR (Derryberry et al. 2014). Cline width is 1/maximum slope and cline center is measured in distance from the southern tip of the San Joaquin Valley, and ±2 log-likelihood (LL) unit support is presented for both. The shape parameter indicates the tail shape (left, right, both, none, mirrored) of the top model, while p_{min} and p_{max} are the lower and upper bounds of native SVRF ancestry proportion for the top cline model.

	Marker Type	Top Model			Cline Position (km)	± 2 LL		Cline Width (km)	± 2 LL	
		Shape (tail)	pmin	pmax		min (km)	max (km)		min (km)	max (km)
Simulated Cline Models	nuDNA	both	0.0424	0.7729	389.8	389.6	390.0	285.5	284.7	286.5
	mtDNA	left	0.0014	0.9893	428.4	428.1	428.8	117.2	116.4	118.2
Empirical Cline Models	nuDNA	none	0	0.7953	427.2	423.2	437.2	20.0	0.5	39.7
	mtDNA	right	0	1	422.7	418.4	424.9	17.0	2.8	36.9

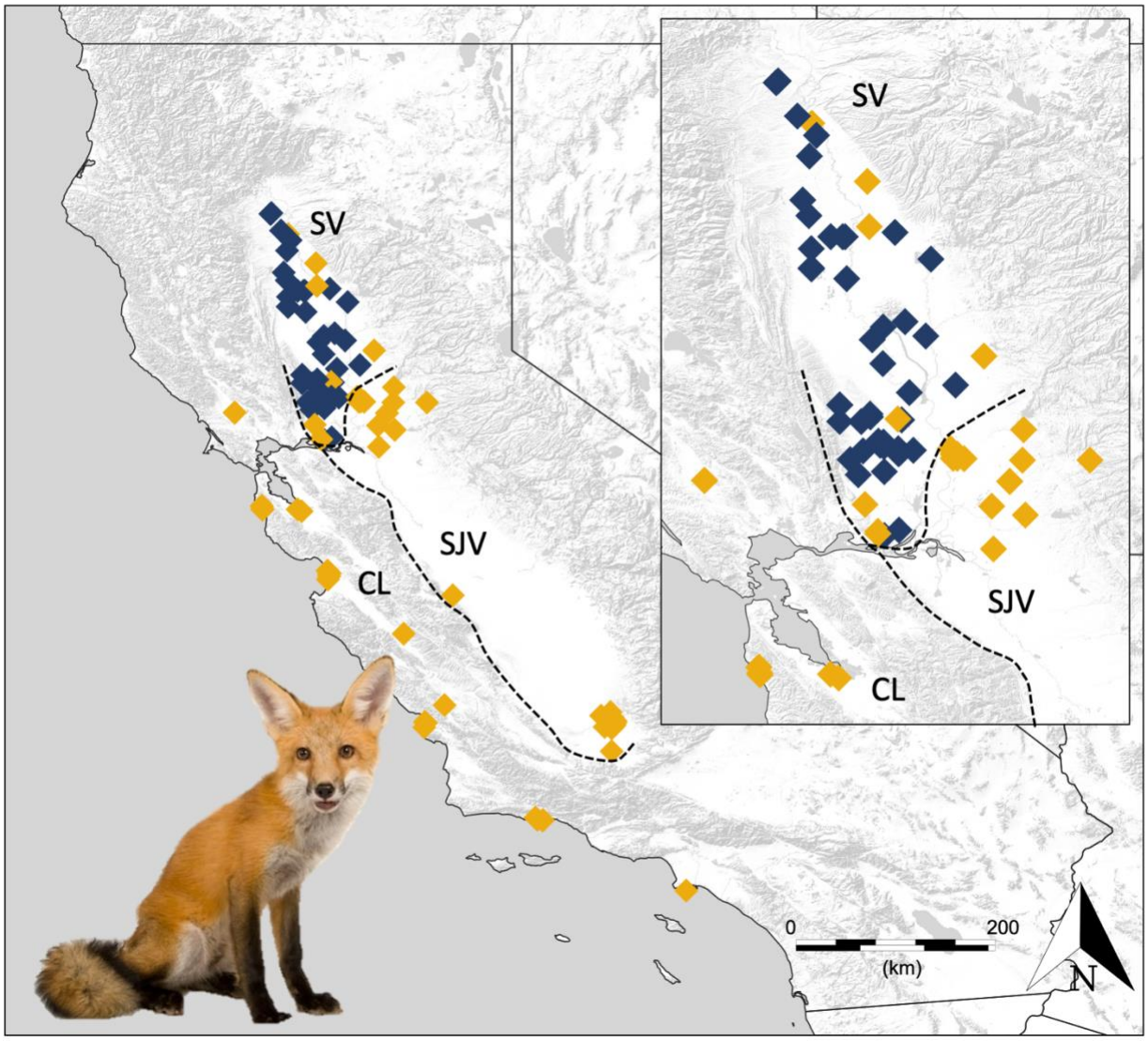

Figure 1.1: Spatial distribution of red fox mitochondrial DNA samples throughout the native Sacramento Valley (SV) range and the nonnative regions of the San Joaquin Valley (SJV) and Coastal Lowlands (CL) . Colored diamonds indicate mtDNA haplotype ancestry (inferred from cytochrome *b* + D-loop), with blue diamonds representing individuals with native SVRF mtDNA, while yellow diamonds represent individuals with nonnative mtDNA. The inset highlights the secondary contact zone which is roughly where the Sacramento Valley, the San Joaquin Valley and the SF-Bay Delta meet.

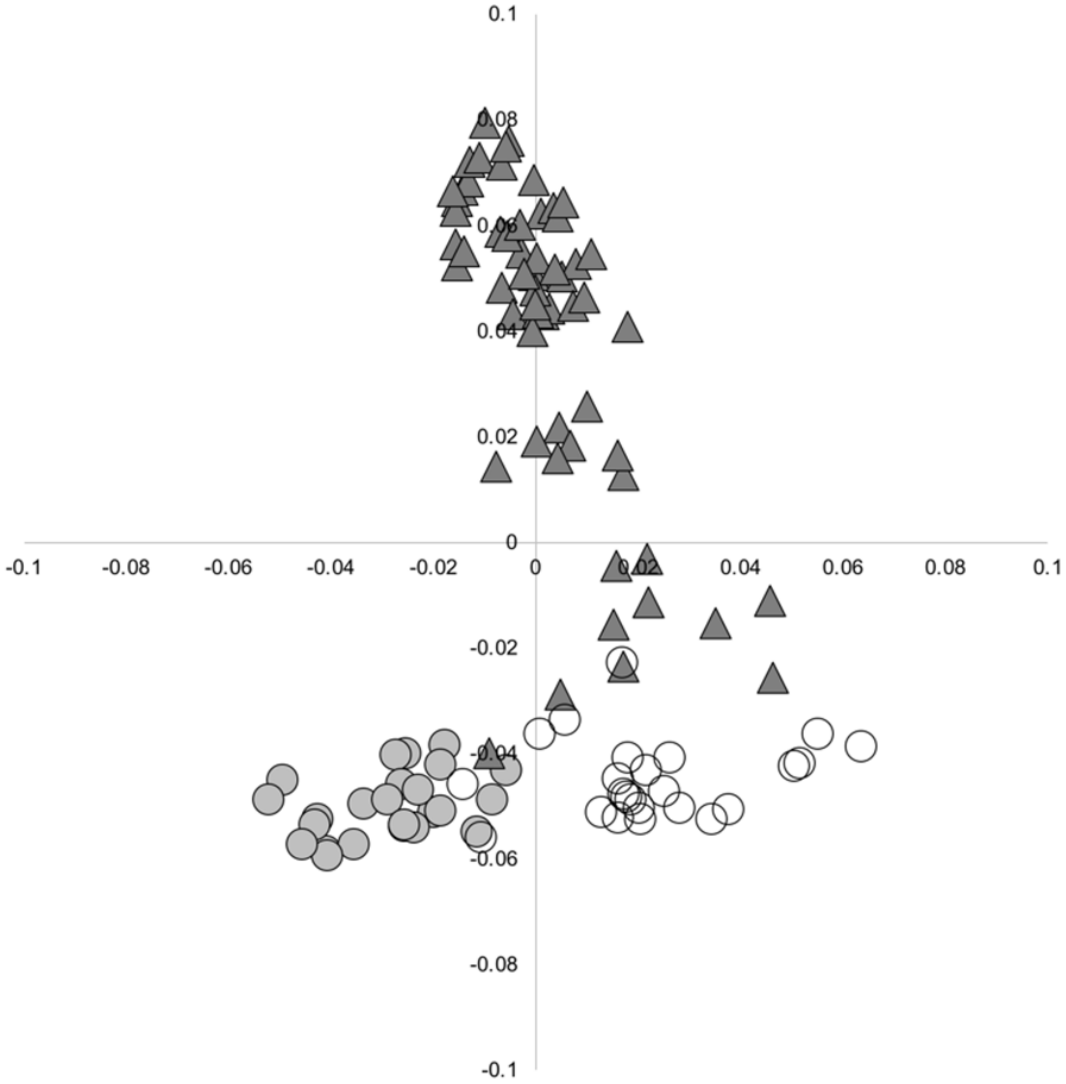

Figure 1.2: Multidimensional scaling plot based on 19,051 autosomal genotyping-by-sequencing (GBS) loci showing the genetic distances between samples found within the presumed historical range of the native Sacramento Valley red fox (triangles), and those found within the nonnative range, including the San Joaquin Valley (open circles) and the coastal lowlands (filled circles. Red foxes found within the Sacramento Valley who varying levels of native and nonnative ancestry, while those found within the nonnative ranges appear to have little to no admixture. Additionally, there is evidence of geographic structuring within the nonnative population, as foxes in the coastal range are genetically differentiated from those found within the San Joaquin Valley.

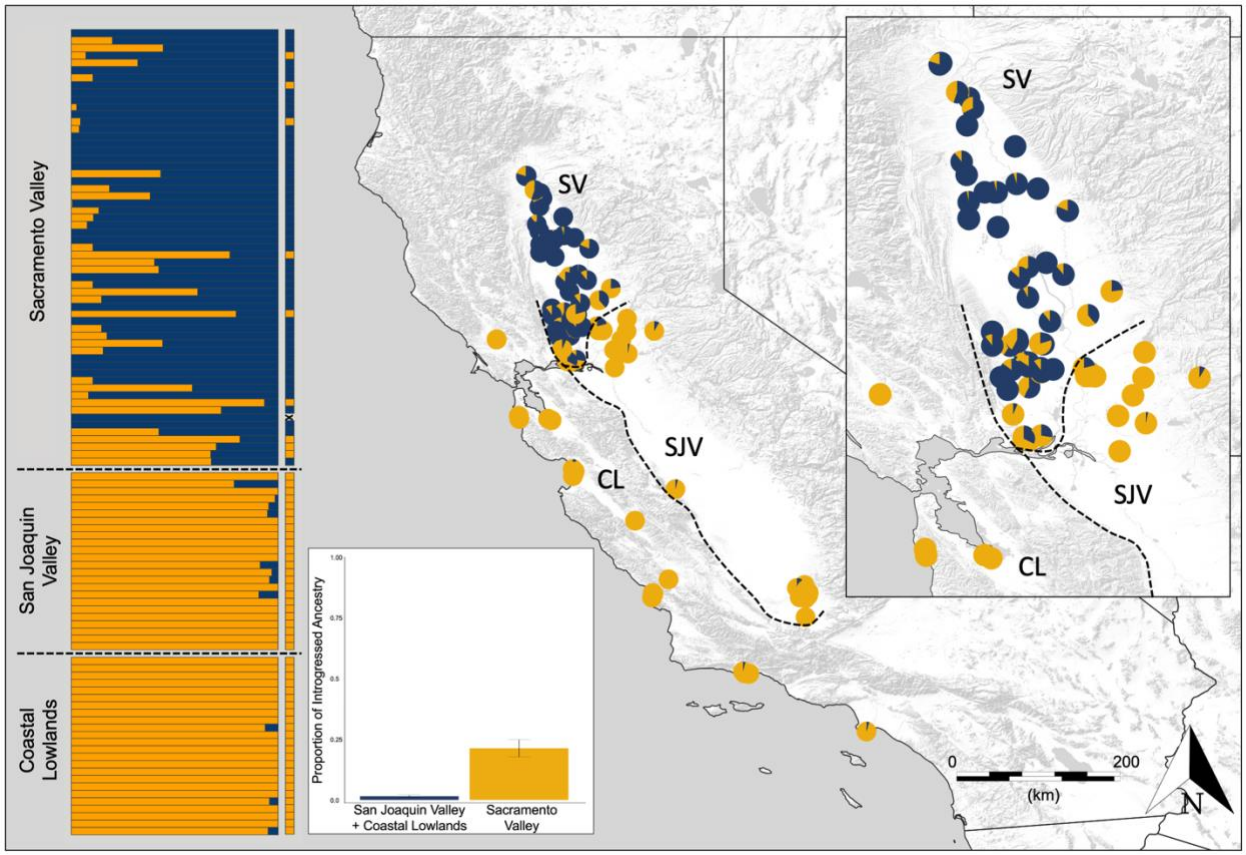

Figure 1.3: Spatial distribution of red fox nuclear DNA samples throughout the native Sacramento Valley (SV) range and the nonnative regions of the San Joaquin Valley (SJV) and Coastal Lowlands (CL) . Relative proportions of blue and yellow within each circle represent the proportion of native SVRF and nonnative ancestry respectively estimated using program ADMIXTURE (K = 2). The inset on the far right highlights the secondary contact zone which is roughly where the Sacramento Valley, the San Joaquin Valley, and the SF-Bay Delta meet. The same information is broken up by region and presented as a bar graph on the far left, with each bar representing the relative ancestry composition of a single individual. Smaller blue and yellow rectangles to the right of each individual bar represent the corresponding mitochondrial haplotype of each individual (blue = native SVRF mtDNA; yellow = nonnative mtDNA). Note that only 6.3% of individuals with majority native SVRF ancestry and 6.9% of individuals with majority non-native ancestry had discordant mitochondrial ancestry. Additionally, the bar graph reflects the mean proportion of introgressed ancestry across the hybrid zone, and indicates asymmetrical introgression, with elevated levels of nonnative ancestry (yellow) found within the Sacramento Valley relative to native ancestry (blue) found within the San Joaquin Valley or Coastal lowland regions.

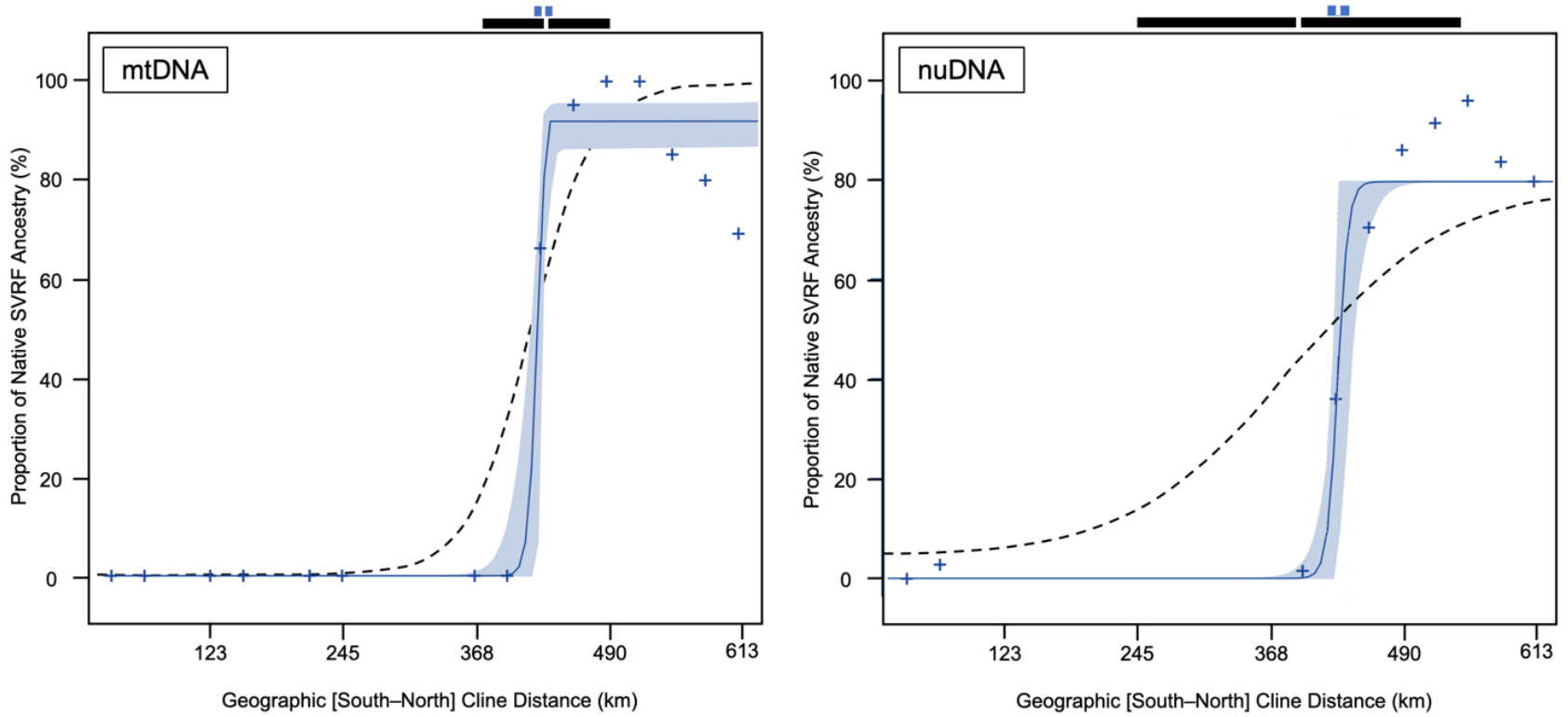

Figure 1.4: Geographic clines show the expected cline shape (black dashed line) for both mtDNA (left) and nuDNA (right) after 18 generations of secondary contact, given our simulated models using biologically informed sex-biased dispersal parameters. The blue crosses indicate the mean proportion of native SVRF ancestry sampled across all individuals within each 33-km geographic region along the cline. Blue lines represent the best fit cline shape for our empirical data with blue shaded region indicating the 95% CI around each cline. Shown above each graph are the empirical (blue bars) and expected (black bars) cline widths and centers. Empirical cline widths for both mtDNA [17 km (2.8 km–36.9 km)] and nuDNA [20 km (0.5 km–39.7 km)] were significantly narrower than the expected cline widths for mtDNA [117.2 km (116.4 km–118.2 km)] or nuDNA [285.5 km (284.7 km–286.5 km)] under our simulated neutral model of gene flow.

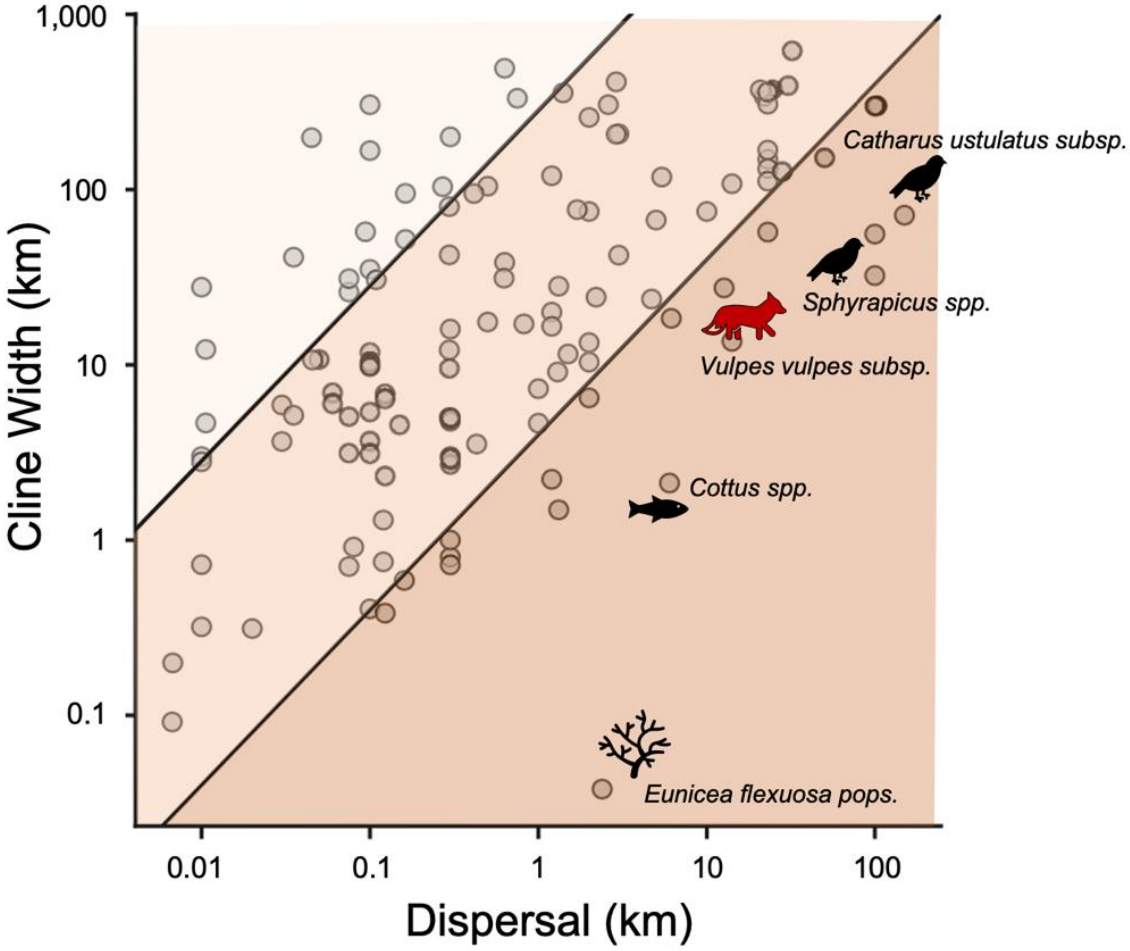

Figure 1.5: Relationship between cline width and average dispersal distance for a diverse set of taxa, modified from McEntee et al. (2020). The region between the upper and lower black lines (medium orange) shows the cline widths that would be maintained by a tension zone model with selection coefficients of 0.0001 and 0.05 respectively. Dots located above the upper diagonal line (light orange) are indicative of neutral clines or clines under extremely low levels of selection (s <0.0001), while those below the lower diagonal line (dark orange) reflect clines widths influenced by stronger selection against hybrids (s >0.05). The average red fox cline width across marker type ($\bar{x}$ = 18.5 km) relative to the average dispersal distance ($\bar{\sigma}$ = 18 km) supports strong selection against hybrids or some other force limiting gene flow and narrowing the cline width. While a few iconic hybrid zones, highlighted by the black animal symbols, have cline widths narrower than red foxes relative to their dispersal distances, the majority indicate moderate to no selection influencing rates of gene flow.

Supplemental Material

Table S1.1: Information for red fox DNA samples from the California Lowlands used in this study, including sample type, spatial coordinates, date collected, markers amplified or sequenced, geographic range delineation, and citations for use in previous studies.

Sample ID	Sample Type	Lat	Long	Collection Year	mtDNA Haplotype	mtDNA Ancestry	Sex Marker (K9Amelo)	GBS Seq	GBS Success	Geographic Range	Studies Used
acvc-98-02	Tissue	35.288	-118.987	1998	N-7	Nonnative	No	No	No	Nonnative	Sacks et al. 2016
DAMIEN	Tissue	37.790	-122.460	2003	O-26	Nonnative	No	No	No	Nonnative	Sacks et al. 2016; Quinn et al. 2019; Quinn et al. 2021
ESRP-5954	Tissue	35.539	-119.186	2002	E-9	Nonnative	Yes	No	No	Nonnative	Sacks et al. 2016; Quinn et al. 2019; Quinn et al. 2021
ESRP-R003	Tissue	35.429	-119.037	2003	E-9	Nonnative	No	No	No	Nonnative	Sacks et al. 2010; Sacks et al. 2016; Quinn et al. 2019; Quinn et al. 2021
ESRP-R004	Tissue	35.375	-118.987	2003	E-9	Nonnative	Yes	Yes	Yes	Nonnative	Sacks et al. 2016; Quinn et al. 2021
ESRP-R005	Tissue	35.462	-119.035	2004	E-9	Nonnative	Yes	Yes	Yes	Nonnative	Sacks et al. 2010; Sacks et al. 2016; Quinn et al. 2019; Quinn et al. 2021
ESRP-R006	Tissue	35.078	-119.024	2004	E-9	Nonnative	Yes	Yes	Yes	Nonnative	Sacks et al. 2016; Quinn et al. 2021
ESRP-R007	Tissue	35.011	-118.979	2004	E-9	Nonnative	Yes	No	No	Nonnative	Sacks et al. 2010; Sacks et al. 2016; Quinn et al. 2019; Quinn et al. 2021
ESRP-R008	Tissue	35.360	-118.987	2004	E-9	Nonnative	Yes	Yes	Yes	Nonnative	Sacks et al. 2010; Sacks et al. 2016; Quinn et al. 2019; Quinn et al. 2021
ESRP-R009	Tissue	35.302	-119.024	2004	E-9	Nonnative	Yes	Yes	Yes	Nonnative	Sacks et al. 2010; Sacks et al. 2016; Quinn et al. 2019; Quinn et al. 2021
ESRP-R010	Tissue	35.443	-118.969	2002	E-9	Nonnative	No	No	No	Nonnative	Sacks et al. 2016
ESRP-R011	Tissue	35.465	-119.018	2002	E-9	Nonnative	No	No	No	Nonnative	Sacks et al. 2016
EV11	Tissue	35.430	-120.867	2002	G-38	Nonnative	No	No	No	Nonnative	Sacks et al. 2016
EV12	Tissue	35.435	-120.867	2002	G-38	Nonnative	No	No	No	Nonnative	Sacks et al. 2016
EV13	Tissue	35.330	-120.860	2002	G-38	Nonnative	No	No	No	Nonnative	Sacks et al. 2016
EV14	Tissue	35.428	-120.867	2002	G-38	Nonnative	No	No	No	Nonnative	Sacks et al. 2016; Quinn et al. 2019; Quinn et al. 2021
EV15	Tissue	35.432	-120.867	2002	G-38	Nonnative	No	No	No	Nonnative	Sacks et al. 2016
EV16	Tissue	36.795	-121.790	2002	G-38	Nonnative	No	No	No	Nonnative	Sacks et al. 2016
EV17	Tissue	36.770	-121.790	2002	G-38	Nonnative	No	No	No	Nonnative	Sacks et al. 2016
EV18	Tissue	36.835	-121.800	2002	F-12	Nonnative	No	No	No	Nonnative	Sacks et al. 2016
EV19	Tissue	36.690	-121.810	2002	G-38	Nonnative	No	No	No	Nonnative	Sacks et al. 2016

EV20	Tissue	36.835	-121.780	2002	G-38	Nonnative	No	No	No	Nonnative	Sacks et al. 2016
EV21	Tissue	36.795	-121.785	2002	G-38	Nonnative	No	No	No	Nonnative	Sacks et al. 2016
EV22	Tissue	36.797	-121.785	2002	G-38	Nonnative	No	No	No	Nonnative	Sacks et al. 2016
EV23	Tissue	36.797	-121.760	2002	G-38	Nonnative	No	No	No	Nonnative	Sacks et al. 2016
EV24	Tissue	36.832	-121.800	2002	G-38	Nonnative	No	No	No	Nonnative	Sacks et al. 2016
EV25	Tissue	36.793	-121.760	2002	G-38	Nonnative	No	No	No	Nonnative	Sacks et al. 2016
EV27	Tissue	37.435	-122.068	2002	N-7	Nonnative	No	No	No	Nonnative	Sacks et al. 2016
EV28	Tissue	37.435	-122.068	2002	F-12	Nonnative	No	No	No	Nonnative	Sacks et al. 2016; Quinn et al. 2019; Quinn et al. 2021
EV29	Tissue	37.435	-122.068	2002	N-7	Nonnative	No	No	No	Nonnative	Sacks et al. 2016
EV31	Tissue	37.467	-122.447	2002	N-7	Nonnative	No	No	No	Nonnative	Sacks et al. 2016; Quinn et al. 2019; Quinn et al. 2021
EV32	Tissue	37.466	-122.447	2002	G-38	Nonnative	No	No	No	Nonnative	Sacks et al. 2016; Quinn et al. 2019; Quinn et al. 2021
EV33	Tissue	37.465	-122.447	2002	O-26	Nonnative	No	No	No	Nonnative	Sacks et al. 2016; Quinn et al. 2019; Quinn et al. 2021
EV34	Tissue	37.468	-122.447	2002	G-38	Nonnative	No	No	No	Nonnative	Sacks et al. 2016
EV36	Tissue	37.467	-122.446	2002	G-38	Nonnative	No	No	No	Nonnative	Sacks et al. 2016
EV37	Tissue	36.965	-120.030	2002	N-7	Nonnative	Yes	No	No	Nonnative	Sacks et al. 2010; Sacks et al. 2016; Quinn et al. 2019; Quinn et al. 2021
EV38	Tissue	36.960	-120.030	2002	N-7	Nonnative	No	No	No	Nonnative	Sacks et al. 2010; Sacks et al. 2016; Quinn et al. 2019; Quinn et al. 2021
EV40	Tissue	37.152	-120.240	2002	N-7	Nonnative	No	No	No	Nonnative	Sacks et al. 2016
EV58	Tissue	35.432	-120.865	2002	G-38	Nonnative	No	No	No	Nonnative	Sacks et al. 2016
EV59	Tissue	36.796	-121.760	2002	G-38	Nonnative	No	No	No	Nonnative	Sacks et al. 2016
EV61	Tissue	36.795	-121.760	2002	G-38	Nonnative	No	No	No	Nonnative	Sacks et al. 2016
EV62	Tissue	36.794	-121.760	2002	G-38	Nonnative	No	No	No	Nonnative	Sacks et al. 2016
EV63	Tissue	36.793	-121.760	2002	G-38	Nonnative	No	No	No	Nonnative	Sacks et al. 2016
EV64	Tissue	36.792	-121.760	2002	G-38	Nonnative	No	No	No	Nonnative	Sacks et al. 2016
EV65	Tissue	36.773	-121.790	2002	G-38	Nonnative	No	No	No	Nonnative	Sacks et al. 2016
EV66	Tissue	36.794	-121.785	2002	N-7	Nonnative	No	No	No	Nonnative	Sacks et al. 2016
EV67	Tissue	36.791	-121.760	2002	G-38	Nonnative	No	No	No	Nonnative	Sacks et al. 2016
EV68	Tissue	36.798	-121.760	2002	G-38	Nonnative	No	No	No	Nonnative	Sacks et al. 2016
EV70	Tissue	36.800	-121.760	2002	G-38	Nonnative	No	No	No	Nonnative	Sacks et al. 2016

EV71	Tissue	36.801	-121.760	2002	G-38	Nonnative	No	No	No	Nonnative	Sacks et al. 2016
FRC-027	Unknown	36.877	-119.793	1997	N-7	Nonnative	No	No	No	Nonnative	Sacks et al. 2016
FRC-061	Unknown	35.264	-119.481	1999	G-38	Nonnative	No	No	No	Nonnative	Sacks et al. 2016
FRC-087	Unknown	36.310	-119.574	2000	G-38	Nonnative	No	No	No	Nonnative	Sacks et al. 2016
FRE	Tissue	37.790	-122.460	2003	G-38	Nonnative	Yes	Yes	No	Nonnative	Sacks et al. 2016; Quinn et al. 2019; Quinn et al. 2021
FRO	Tissue	37.805	-122.452	2003	O-26	Nonnative	No	No	No	Nonnative	Sacks et al. 2016
FUL	Tissue	37.804	-122.461	2003	O-26	Nonnative	No	No	No	Nonnative	Sacks et al. 2016
H-1	Tissue	40.020	-122.120	1986	NA	NA	Yes	No	No	S.Valley	Perrine et al. 2007; Sacks et al. 2010; Statham et al. 2014; Quinn et al. 2019; Quinn et al. 2021
LA1	Tissue	33.750	-118.370	1988	F-12	Nonnative	Yes	Yes	No	Nonnative	Sacks et al. 2016; Quinn et al. 2021
LA4	Tissue	34.147	-118.778	1990	F-9	Nonnative	No	No	No	Nonnative	Sacks et al. 2016
LA5	Tissue	33.715	-118.294	2002	F-12	Nonnative	Yes	Yes	Yes	Nonnative	Sacks et al. 2016; Quinn et al. 2021
LA6	Tissue	33.707	-118.293	1989	F-9	Nonnative	No	No	No	Nonnative	Sacks et al. 2016
LF-42	Tissue	37.880	-122.250	1995	F-12	Nonnative	No	No	No	Nonnative	Sacks et al. 2016
M-2508	Bone	36.324	-121.181	1984	G-38	Nonnative	No	No	No	Nonnative	Sacks et al. 2016
MAM-1937	Tissue	38.410	-121.360	2004	N-7	Nonnative	Yes	No	No	Nonnative	Sacks et al. 2010; Sacks et al. 2016; Quinn et al. 2019; Quinn et al. 2021
MAM-1938	Tissue	38.470	-121.240	2004	N-7	Nonnative	Yes	No	No	Nonnative	Sacks et al. 2010; Sacks et al. 2016; Quinn et al. 2019; Quinn et al. 2021
MAM-1974	Tissue	38.580	-121.260	2004	N-7	Nonnative	No	No	No	Nonnative	Sacks et al. 2016
MAM-2076	Tissue	36.930	-120.060	2004	N-7	Nonnative	No	No	No	Nonnative	Sacks et al. 2016
MAM-2114	Tissue	35.530	-120.660	2004	G-38	Nonnative	No	No	No	Nonnative	Sacks et al. 2016; Quinn et al. 2019; Quinn et al. 2021
MAM-2703	Tissue	38.520	-121.500	2005	F-14	Nonnative	Yes	Yes	Yes	Nonnative	Sacks et al. 2010; Sacks et al. 2016; Quinn et al. 2019; Quinn et al. 2021
MAM-2704	Tissue	38.500	-121.500	2005	F-14	Nonnative	Yes	Yes	Yes	Nonnative	Sacks et al. 2010; Sacks et al. 2016; Quinn et al. 2019; Quinn et al. 2021
MAM-2705	Tissue	38.520	-121.480	2005	F-14	Nonnative	No	Yes	Yes	Nonnative	Sacks et al. 2010; Sacks et al. 2016; Quinn et al. 2019; Quinn et al. 2021
MAM-2706	Tissue	38.500	-121.480	2005	F-14	Nonnative	Yes	Yes	Yes	Nonnative	Sacks et al. 2016; Quinn et al. 2021
MAM-2708	Tissue	35.530	-120.660	2005	G-38	Nonnative	Yes	Yes	Yes	Nonnative	Sacks et al. 2016; Quinn et al. 2019; Quinn et al. 2021
MAM-2709	Tissue	35.530	-120.660	2005	G-38	Nonnative	No	No	No	Nonnative	Sacks et al. 2016; Quinn et al. 2019; Quinn et al. 2021
MAM2736	Tissue	35.356	-120.842	2006	G-38	Nonnative	Yes	Yes	Yes	Nonnative	Sacks et al. 2016; Quinn et al. 2021
MAM2745	Tissue	35.349	-120.830	2006	G-38	Nonnative	Yes	No	No	Nonnative	Sacks et al. 2016; Quinn et al. 2021

MAM2746	Tissue	35.349	-120.808	2006	G-38	Nonnative	No	No	No	Nonnative	Sacks et al. 2016
MAM-2748	Tissue	36.790	-121.790	2005	G-38	Nonnative	Yes	Yes	Yes	Nonnative	Sacks et al. 2016; Quinn et al. 2021
MAM-2749	Tissue	36.790	-121.790	2005	G-38	Nonnative	No	No	No	Nonnative	Sacks et al. 2016; Quinn et al. 2019; Quinn et al. 2021
MAM-2762	Tissue	33.931	-118.429	2005	F-9	Nonnative	No	No	No	Nonnative	Sacks et al. 2016
MAM2773	Tissue	33.931	-118.379	2005	F-9	Nonnative	No	No	No	Nonnative	Sacks et al. 2016
MAM-2774	Tissue	33.931	-118.429	2005	F-9	Nonnative	No	No	No	Nonnative	Sacks et al. 2016
MAM-2793	Tissue	35.408	-119.013	2005	E-9	Nonnative	Yes	Yes	Yes	Nonnative	Sacks et al. 2010; Sacks et al. 2016; Quinn et al. 2019; Quinn et al. 2021
MAM-2794	Tissue	35.614	-119.867	2005	G-38	Nonnative	No	No	No	Nonnative	Sacks et al. 2016
MAM2795	Tissue	35.480	-120.672	2006	G-38	Nonnative	Yes	No	No	Nonnative	Sacks et al. 2016; Quinn et al. 2021
MAM2802	Tissue	35.338	-120.818	2006	G-38	Nonnative	Yes	No	No	Nonnative	Sacks et al. 2016; Quinn et al. 2021
MAM3674	Tissue	37.489	-122.457	2005	O-26	Nonnative	Yes	No	No	Nonnative	Sacks et al. 2016; Quinn et al. 2021
MAM3675	Tissue	37.480	-122.449	2005	G-38	Nonnative	Yes	Yes	Yes	Nonnative	Sacks et al. 2016; Quinn et al. 2021
MAM3676	Tissue	37.472	-122.448	2005	G-38	Nonnative	Yes	No	No	Nonnative	Sacks et al. 2016; Quinn et al. 2021
MAM3677	Tissue	37.464	-122.446	2005	G-38	Nonnative	No	No	No	Nonnative	Sacks et al. 2016
MAM3678	Tissue	37.460	-122.446	2005	O-26	Nonnative	Yes	No	No	Nonnative	Sacks et al. 2016; Quinn et al. 2019; Quinn et al. 2021
MAM3686	Tissue	37.451	-122.445	2005	G-38	Nonnative	Yes	Yes	Yes	Nonnative	Sacks et al. 2016; Quinn et al. 2021
MAM3687	Tissue	37.442	-122.443	2006	G-38	Nonnative	Yes	Yes	Yes	Nonnative	Sacks et al. 2016; Quinn et al. 2021
MAM3688	Tissue	37.429	-122.439	2006	O-26	Nonnative	Yes	No	No	Nonnative	Sacks et al. 2016; Quinn et al. 2021
MG1	Tissue	36.695	-121.809	2005	G-38	Nonnative	No	No	No	Nonnative	Sacks et al. 2016
MVZ-175993	Bone	38.151	-122.938	1982	G-38	Nonnative	No	No	No	Nonnative	Sacks et al. 2016
REJ-1624	Tissue	37.950	-121.290	1997	F-12	Nonnative	Yes	No	No	Nonnative	Perrine et al. 2007; Sacks et al. 2016; Quinn et al. 2019; Quinn et al. 2021
RFA	Tissue	37.061	-121.563	2000	G-38	Nonnative	No	No	No	Nonnative	Sacks et al. 2016
RFB	Tissue	37.061	-121.563	2000	G-38	Nonnative	No	No	No	Nonnative	Sacks et al. 2016
S07-0056	Scat	38.670	-121.780	2007	D-19	Native SVRF	Yes	No	No	S.Valley	Sacks et al. 2011; Quinn et al. 2019; Quinn et al. 2021
S07-0166	Tissue	40.085	-122.230	2007	D2-19	Native SVRF	Yes	No	No	S.Valley	Sacks et al. 2010; Sacks et al. 2011; Statham et al. 2014; Quinn et al. 2019; Quinn et al. 2021
S07-0168	Tissue	38.677	-121.830	2007	D-19	Native SVRF	Yes	Yes	No	S.Valley	Sacks et al. 2011; Quinn et al. 2021
S07-0169	Tissue	38.122	-121.836	2007	D-19	Native SVRF	Yes	Yes	Yes	S.Valley	Sacks et al. 2016; Quinn et al. 2021
S07-0171	Tissue	38.439	-121.836	2007	D-19	Native SVRF	Yes	Yes	No	S.Valley	Sacks et al. 2010; Sacks et al. 2011; Quinn et al. 2019; Quinn et al. 2021

S07-0172	Tissue	38.435	-121.837	2007	D-19	Native SVRF	No	Yes	Yes	S.Valley	
S07-0189	Tissue	38.450	-121.853	2007	D-19	Native SVRF	Yes	No	No	S.Valley	Sacks et al. 2010; Sacks et al. 2011; Quinn et al. 2019; Quinn et al. 2021
S08-0003	Tissue	38.579	-121.841	2007	D-19	Native SVRF	Yes	Yes	Yes	S.Valley	Sacks et al. 2010; Sacks et al. 2011; Quinn et al. 2019; Quinn et al. 2021
S08-0013	Tissue	38.442	-122.716	2008	G-38	Nonnative	Yes	No	No	Nonnative	Sacks et al. 2016; Quinn et al. 2019; Quinn et al. 2021
S08-0019	Scat	38.243	-122.629	2008	G-38	Nonnative	Yes	No	No	Nonnative	Sacks et al. 2016; Quinn et al. 2019; Quinn et al. 2021
S08-0026	Scat	38.745	-121.785	2008	D-19	Native SVRF	Yes	No	No	S.Valley	Sacks et al. 2010; Sacks et al. 2011; Quinn et al. 2019; Quinn et al. 2021
S08-0032	Tissue	38.999	-121.350	2008	G-38	Nonnative	No	Yes	Yes	S.Valley	Sacks et al. 2016; Quinn et al. 2021
S08-0079	Scat	38.806	-121.701	2008	D-19	Native SVRF	Yes	No	No	S.Valley	Sacks et al. 2010; Sacks et al. 2011; Quinn et al. 2019; Quinn et al. 2021
S08-0084	Scat	38.671	-121.871	2008	D-19	Native SVRF	Yes	No	No	S.Valley	Sacks et al. 2011; Quinn et al. 2019; Quinn et al. 2021
S08-0085	Scat	38.815	-121.936	2008	D-19	Native SVRF	Yes	No	No	S.Valley	Sacks et al. 2011; Quinn et al. 2019; Quinn et al. 2021
S08-0086	Scat	38.815	-121.936	2008	D-19	Native SVRF	Yes	No	No	S.Valley	Sacks et al. 2011; Quinn et al. 2019; Quinn et al. 2021
S08-0112	Nobuto	38.678	-121.839	2008	D-19	Native SVRF	Yes	No	No	S.Valley	Sacks et al. 2011; Quinn et al. 2019; Quinn et al. 2021
S08-0162	Scat	38.429	-121.952	2008	D-19	Native SVRF	Yes	No	No	S.Valley	Sacks et al. 2011; Quinn et al. 2019; Quinn et al. 2021
S08-0168	Tissue	38.405	-122.812	2007	G-38	Nonnative	No	Yes	No	Nonnative	Sacks et al. 2016
S08-0199	Scat	38.537	-121.715	2008	D-19	Native SVRF	Yes	No	No	S.Valley	Sacks et al. 2011; Quinn et al. 2019; Quinn et al. 2021
S08-0202	Tissue	38.435	-121.838	2008	D-19	Native SVRF	No	No	No	S.Valley	Sacks et al. 2011; Quinn et al. 2021
S08-0230	Scat	38.663	-121.481	2008	D-19	Native SVRF	Yes	No	No	S.Valley	Sacks et al. 2011; Quinn et al. 2021
S08-0234	Scat	38.381	-121.219	2008	F-12	Nonnative	No	No	No	Nonnative	Sacks et al. 2016
S08-0235	Scat	38.381	-121.219	2008	F-12	Nonnative	No	No	No	Nonnative	Sacks et al. 2016
S08-0239	Scat	38.381	-121.219	2008	F-12	Nonnative	No	No	No	Nonnative	Sacks et al. 2016
S08-0241	Scat	38.451	-121.182	2008	G-38	Nonnative	Yes	No	No	Nonnative	Sacks et al. 2011; Sacks et al. 2016; Quinn et al. 2019; Quinn et al. 2021
S08-0248	Scat	38.539	-121.713	2008	D-19	Native SVRF	Yes	No	No	S.Valley	Sacks et al. 2011; Quinn et al. 2019; Quinn et al. 2021
S08-0253	Scat	38.228	-122.606	2008	G-38	Nonnative	Yes	No	No	Nonnative	Sacks et al. 2016; Quinn et al. 2019; Quinn et al. 2021
S08-0254	Tissue	38.664	-121.860	2008	D-19	Native SVRF	No	No	No	S.Valley	Sacks et al. 2011; Quinn et al. 2021
S08-0255	Tissue	38.664	-121.860	2008	D-19	Native SVRF	Yes	No	No	S.Valley	Quinn et al. 2019; Quinn et al. 2021
S08-0256	Scat	38.664	-121.860	2008	D-19	Native SVRF	Yes	No	No	S.Valley	Quinn et al. 2019; Quinn et al. 2021

S08-0277	Scat	38.683	-122.028	2008	D-19	Native SVRF	Yes	No	No	S.Valley	Sacks et al. 2011; Quinn et al. 2019; Quinn et al. 2021
S08-0301	Tissue	40.367	-122.285	2008	F-12	Nonnative	Yes	No	No	S.Valley	Sacks et al. 2011; Quinn et al. 2019; Quinn et al. 2021
S08-0325	Scat	38.539	-121.712	2008	D-19	Native SVRF	Yes	No	No	S.Valley	Quinn et al. 2019; Quinn et al. 2021
S08-0366	Scat	38.701	-121.907	2008	D-19	Native SVRF	Yes	No	No	S.Valley	Sacks et al. 2011; Quinn et al. 2019; Quinn et al. 2021
S08-0455	Tissue	38.347	-120.773	2008	G-38	Nonnative	Yes	No	No	Nonnative	Sacks et al. 2011; Sacks et al. 2016; Quinn et al. 2019; Quinn et al. 2021
S08-0511	Tissue	38.687	-121.752	2008	D-19	Native SVRF	No	Yes	Yes	S.Valley	Sacks et al. 2011; Quinn et al. 2021
S08-0534	Tissue	38.543	-121.696	2008	D-19	Native SVRF	No	No	No	S.Valley	Sacks et al. 2011; Quinn et al. 2021
S08-0535	Tissue	38.540	-121.695	2008	Fail	NA	Yes	Yes	Yes	S.Valley	Sacks et al. 2011; Quinn et al. 2021
S08-0752	Tissue	38.642	-121.776	2008	D-19	Native SVRF	Yes	No	No	S.Valley	Sacks et al. 2011; Quinn et al. 2019; Quinn et al. 2021
S08-0761	Tissue	38.842	-121.720	2008	D-19	Native SVRF	No	No	No	S.Valley	Sacks et al. 2016
S08-0763	Tissue	39.977	-122.202	2008	D-19	Native SVRF	Yes	Yes	Yes	S.Valley	Sacks et al. 2011; Quinn et al. 2019; Quinn et al. 2021
S08-0765	Tissue	38.493	-122.003	2008	D-19	Native SVRF	Yes	Yes	Yes	S.Valley	Sacks et al. 2011; Quinn et al. 2019; Quinn et al. 2021
S09-0024	Scat	38.449	-121.805	2009	D-19	Native SVRF	Yes	No	No	S.Valley	Sacks et al. 2011; Quinn et al. 2019; Quinn et al. 2021
S09-0032	Tissue	39.187	-121.879	2009		NA	No	No	No	S.Valley	Sacks et al. 2011; Quinn et al. 2021
S09-0034	Tissue	39.157	-121.765	2009	D-19	Native SVRF	Yes	No	No	S.Valley	Sacks et al. 2011; Quinn et al. 2019; Quinn et al. 2021
S09-0042	Scat	38.543	-121.697	2009	D-19	Native SVRF	Yes	No	No	S.Valley	Sacks et al. 2011; Quinn et al. 2019; Quinn et al. 2021
S09-0102	Tissue	39.534	-122.190	2009	D-19	Native SVRF	Yes	No	No	S.Valley	Sacks et al. 2011; Quinn et al. 2019; Quinn et al. 2021
S09-0111	Tissue	39.570	-122.083	2009	D-19	Native SVRF	Yes	No	No	S.Valley	Sacks et al. 2011; Quinn et al. 2019; Quinn et al. 2021
S09-0126	Scat	38.815	-121.936	2009	D-19	Native SVRF	Yes	No	No	S.Valley	Sacks et al. 2011; Quinn et al. 2019; Quinn et al. 2021
S09-0155	Tissue	39.233	-121.679	2009	D-19	Native SVRF	Yes	No	No	S.Valley	Sacks et al. 2011; Quinn et al. 2019; Quinn et al. 2021
s09-0158	Tissue	38.143	-121.868	2009	F-14	Nonnative	Yes	Yes	Yes	S.Valley	Sacks et al. 2016; Quinn et al. 2021
S09-0166	Scat	38.847	-121.728	2009	D-19	Native SVRF	Yes	No	No	S.Valley	Sacks et al. 2011; Quinn et al. 2019; Quinn et al. 2021
S09-0202	Scat	38.926	-122.061	2009	D-19	Native SVRF	Yes	No	No	S.Valley	Quinn et al. 2019; Quinn et al. 2021
S09-0221	Scat	39.070	-121.884	2009	D-19	Native SVRF	Yes	No	No	S.Valley	Sacks et al. 2011; Quinn et al. 2019; Quinn et al. 2021
S09-0232	Scat	39.533	-122.203	2009	D-19	Native SVRF	Yes	No	No	S.Valley	Sacks et al. 2011; Quinn et al. 2019; Quinn et al. 2021
S09-0255	Scat	39.871	-122.172	2009	D-19	Native SVRF	Yes	No	No	S.Valley	Sacks et al. 2011; Quinn et al. 2019; Quinn et al. 2021

S09-0256	Scat	39.871	-122.172	2009	D-19	Native SVRF	Yes	No	No	S.Valley	Sacks et al. 2011; Quinn et al. 2019; Quinn et al. 2021
S09-0261	Scat	40.353	-122.344	2009	D-19	Native SVRF	Yes	No	No	S.Valley	Sacks et al. 2011; Quinn et al. 2021
S09-0268	Tissue	40.344	-122.355	2009	D-19	Native SVRF	Yes	Yes	Yes	S.Valley	Quinn et al. 2019; Quinn et al. 2021
S09-0272	Tissue	38.419	-121.964	2009	D-19	Native SVRF	Yes	Yes	Yes	S.Valley	Sacks et al. 2011; Quinn et al. 2019; Quinn et al. 2021
S09-0273	Tissue	39.546	-122.165	2009	D-19	Native SVRF	Yes	No	No	S.Valley	Sacks et al. 2011; Quinn et al. 2019; Quinn et al. 2021
s09-0274	Tissue	38.005	-122.157	2009	F-12	Nonnative	No	No	No	Nonnative	Sacks et al. 2016; Quinn et al. 2021
s09-0275	Tissue	38.005	-122.157	2009	F-12	Nonnative	No	No	No	Nonnative	Sacks et al. 2016
s09-0276	Tissue	38.005	-122.157	2009	F-12	Nonnative	No	No	No	Nonnative	Sacks et al. 2016
s09-0277	Tissue	38.005	-122.157	2009	F-12	Nonnative	No	No	No	Nonnative	Sacks et al. 2016
s09-0279	Tissue	38.133	-121.838	2007	D-19	Native SVRF	Yes	Yes	No	S.Valley	Sacks et al. 2016; Quinn et al. 2021
s09-0280	Tissue	38.387	-121.224	2009	F-12	Nonnative	Yes	Yes	Yes	Nonnative	Sacks et al. 2016; Quinn et al. 2021
S09-0282	Scat	38.419	-121.816	2009	D-19	Native SVRF	Yes	No	No	S.Valley	Sacks et al. 2011; Quinn et al. 2019; Quinn et al. 2021
S09-0325	Tissue	39.072	-121.889	2009	D-19	Native SVRF	Yes	No	No	S.Valley	Sacks et al. 2011; Quinn et al. 2019; Quinn et al. 2021
S09-0357	Tissue	39.576	-122.093	2009	D-19	Native SVRF	Yes	No	No	S.Valley	Sacks et al. 2011; Quinn et al. 2019; Quinn et al. 2021
S09-0367	Tissue	38.417	-121.817	2009	D-19	Native SVRF	No	No	No	S.Valley	Sacks et al. 2011; Quinn et al. 2021
S09-0375	Scat	40.068	-122.175	2009	D-19	Native SVRF	Yes	No	No	S.Valley	Sacks et al. 2011; Quinn et al. 2019; Quinn et al. 2021
S09-0392	Scat	39.554	-122.084	2009	D-19	Native SVRF	Yes	No	No	S.Valley	Sacks et al. 2011; Quinn et al. 2019; Quinn et al. 2021
S09-0422	Scat	38.420	-121.967	2009	D-19	Native SVRF	Yes	No	No	S.Valley	Quinn et al. 2019; Quinn et al. 2021
S09-0433	Scat	38.381	-121.219	2009	F-12	Nonnative	No	No	No	Nonnative	Sacks et al. 2016
S09-0434	Scat	38.381	-121.219	2009	F-12	Nonnative	No	No	No	Nonnative	Sacks et al. 2016
S09-0436	Scat	38.381	-121.219	2009	F-12	Nonnative	No	No	No	Nonnative	Sacks et al. 2016
S09-0438	Scat	38.451	-121.182	2009	G-38	Nonnative	No	No	No	Nonnative	Sacks et al. 2016
s09-0440	Tissue	38.387	-121.224	2009	F-?	Nonnative	Yes	Yes	Yes	Nonnative	Sacks et al. 2011; Sacks et al. 2016; Quinn et al. 2019; Quinn et al. 2021
S09-0486	Scat	39.554	-122.137	2009	D-19	Native SVRF	Yes	No	No	S.Valley	Sacks et al. 2011; Quinn et al. 2019; Quinn et al. 2021
S09-0498	Scat	38.420	-121.967	2009	D-19	Native SVRF	Yes	No	No	S.Valley	Sacks et al. 2011; Quinn et al. 2019; Quinn et al. 2021
S09-0512	Tissue	38.543	-121.696	2009	D-19	Native SVRF	Yes	No	No	S.Valley	Sacks et al. 2011; Quinn et al. 2019; Quinn et al. 2021
S09-0595	Scat	38.671	-121.871	2009	D-19	Native SVRF	Yes	No	No	S.Valley	Sacks et al. 2011; Quinn et al. 2019; Quinn et al. 2021

S09-0608	Tissue	38.808	-121.940	2009	D-19	Native SVRF	No	No	No	S.Valley	Sacks et al. 2011; Quinn et al. 2021
S09-0614	Scat	39.789	-122.230	2009	D-19	Native SVRF	Yes	No	No	S.Valley	Sacks et al. 2011; Quinn et al. 2019; Quinn et al. 2021
S09-0752	Tissue	38.759	-121.950	2009	D-19	Native SVRF	No	No	No	S.Valley	Sacks et al. 2011; Quinn et al. 2021
S09-0761	Scat	39.150	-122.164	2009	D-19	Native SVRF	Yes	No	No	S.Valley	Sacks et al. 2011; Quinn et al. 2019; Quinn et al. 2021
S09-0776	Tissue	38.577	-121.870	2009	D-19	Native SVRF	No	No	No	S.Valley	Sacks et al. 2011; Quinn et al. 2021
S09-0779	Tissue	40.336	-122.365	2009	D-19	Native SVRF	Yes	Yes	Yes	S.Valley	Sacks et al. 2011; Quinn et al. 2021
S09-0781	Scat	38.333	-121.157	2009	G-38	Nonnative	No	No	No	Nonnative	Sacks et al. 2016
S09-0782	Scat	38.333	-121.157	2009	G-38	Nonnative	No	No	No	Nonnative	Sacks et al. 2016
S09-0785	Scat	38.333	-121.157	2009	G-38	Nonnative	No	No	No	Nonnative	Sacks et al. 2016
S09-0786	Scat	38.333	-121.157	2009	G-38	Nonnative	No	No	No	Nonnative	Sacks et al. 2016
S09-0788	Scat	38.333	-121.157	2009	G-38	Nonnative	No	No	No	Nonnative	Sacks et al. 2016
S09-0789	Scat	38.333	-121.157	2009	G-38	Nonnative	Yes	No	No	Nonnative	Sacks et al. 2011; Sacks et al. 2016; Quinn et al. 2019; Quinn et al. 2021
S09-0790	Scat	38.333	-121.157	2009	G-38	Nonnative	No	No	No	Nonnative	Sacks et al. 2016
S09-0791	Scat	38.333	-121.157	2009	G-38	Nonnative	No	No	No	Nonnative	Sacks et al. 2016
S09-0798	Scat	39.139	-122.146	2009	D-19	Native SVRF	Yes	No	No	S.Valley	Sacks et al. 2011; Quinn et al. 2019; Quinn et al. 2021
S09-0805	Tissue	38.544	-121.768	2009	D-19	Native SVRF	No	Yes	Yes	S.Valley	Sacks et al. 2011; Quinn et al. 2021
S09-0809	Tissue	39.762	-122.235	2009	D-19	Native SVRF	No	Yes	Yes	S.Valley	Sacks et al. 2011; Quinn et al. 2021
S09-0811	Tissue	38.828	-121.719	2009	D-19	Native SVRF	No	No	No	S.Valley	Sacks et al. 2011; Quinn et al. 2021
S09-0816	Tissue	38.583	-121.865	2009	D-19	Native SVRF	No	Yes	Yes	S.Valley	Sacks et al. 2011; Quinn et al. 2021
s09-0912	Tissue	38.858	-121.488	2009	D-19	Native SVRF	No	Yes	Yes	S.Valley	Sacks et al. 2016
S10-0087	Scat	38.536	-121.718	2010	D-19	Native SVRF	No	No	No	S.Valley	New to this study
S10-0110	Scat	40.336	-122.366	2009	D-19	Native SVRF	No	No	No	S.Valley	New to this study
S10-0120	Scat	39.963	-122.161	2009	D-19	Native SVRF	No	No	No	S.Valley	New to this study
S10-0121	Scat	39.963	-122.161	2009	D-19	Native SVRF	No	No	No	S.Valley	New to this study
S10-0166	Tissue	38.761	-122.055	2010	D-19	Native SVRF	No	Yes	No	S.Valley	Quinn et al. 2019; Quinn et al. 2021
S10-0170	Tissue	39.582	-122.040	2010	D-19	Native SVRF	No	Yes	Yes	S.Valley	Quinn et al. 2019; Quinn et al. 2021
S10-0184	Scat	38.543	-121.699	2010	D-19	Native SVRF	No	No	No	S.Valley	New to this study
S10-0188	Tissue	38.761	-122.055	2010	D-19	Native SVRF	No	Yes	Yes	S.Valley	Quinn et al. 2019; Quinn et al. 2021

S10-0191	Tissue	38.760	-122.053	2010	D-19	Native SVRF	No	Yes	Yes	S.Valley	New to this study
S10-0200	Scat	39.811	-121.935	2010	D-19	Native SVRF	No	No	No	S.Valley	New to this study
S10-0201	Scat	39.811	-121.935	2010	D-19	Native SVRF	No	No	No	S.Valley	New to this study
S10-0209	Scat	39.871	-122.172	2010	D-19	Native SVRF	No	No	No	S.Valley	New to this study
S10-0210	Scat	39.871	-122.172	2010	D-19	Native SVRF	No	No	No	S.Valley	New to this study
S10-0251	Scat	38.926	-122.061	2010	D-19	Native SVRF	No	No	No	S.Valley	New to this study
S10-0252	Scat	38.926	-122.061	2010	D-19	Native SVRF	No	No	No	S.Valley	New to this study
S10-0260	Scat	39.070	-121.884	2010	D-19	Native SVRF	No	No	No	S.Valley	New to this study
S10-0261	Scat	39.070	-121.884	2010	D-19	Native SVRF	No	No	No	S.Valley	New to this study
S10-0265	Scat	39.533	-122.203	2010	D-19	Native SVRF	No	No	No	S.Valley	New to this study
S10-0268	Scat	38.672	-121.871	2010	D-19	Native SVRF	No	No	No	S.Valley	New to this study
S10-0270	Scat	38.672	-121.871	2010	D-19	Native SVRF	No	No	No	S.Valley	New to this study
S10-0280	Tissue	38.430	-121.909	2010	D-19	Native SVRF	No	Yes	No	S.Valley	New to this study
S10-0281	Tissue	39.686	-122.205	2010	D-19	Native SVRF	No	Yes	Yes	S.Valley	Quinn et al. 2019; Quinn et al. 2021
S10-0283	Scat	38.530	-121.766	2010	D-19	Native SVRF	No	No	No	S.Valley	New to this study
S10-0291	Scat	38.760	-122.056	2010	D-19	Native SVRF	No	No	No	S.Valley	New to this study
S10-0295	Scat	38.760	-122.053	2010	D-19	Native SVRF	No	No	No	S.Valley	New to this study
S10-0311	Scat	38.457	-121.952	2010	D-19	Native SVRF	No	No	No	S.Valley	New to this study
S10-0312	Scat	38.429	-121.952	2010	D-19	Native SVRF	No	No	No	S.Valley	New to this study
S10-0324	Scat	38.420	-121.965	2010	D-19	Native SVRF	No	No	No	S.Valley	New to this study
S10-0325	Scat	38.420	-121.965	2010	D-19	Native SVRF	No	No	No	S.Valley	New to this study
S10-0334	Tissue	38.963	-121.844	2010	D-19	Native SVRF	No	Yes	Yes	S.Valley	New to this study
S10-0348	Scat	39.769	-122.235	2010	D-19	Native SVRF	No	No	No	S.Valley	New to this study
S10-0349	Scat	39.769	-122.235	2010	D-19	Native SVRF	No	No	No	S.Valley	New to this study
S10-0453	Scat	39.573	-122.085	2010	D-19	Native SVRF	No	No	No	S.Valley	New to this study
S10-0475	Tissue	39.582	-122.027	2010	D-19	Native SVRF	No	Yes	Yes	S.Valley	New to this study
S10-0481	Scat	39.812	-121.962	2010	D-19	Native SVRF	No	No	No	S.Valley	New to this study
S10-0483	Scat	39.812	-121.962	2010	D-19	Native SVRF	No	No	No	S.Valley	New to this study
S10-0509	Scat	38.539	-121.694	2010	D-19	Native SVRF	No	No	No	S.Valley	New to this study

S10-0513	Tissue	38.498	-121.447	2010	F-12	Nonnative	Yes	Yes	Yes	Nonnative	Sacks et al. 2016; Quinn et al. 2021
S10-0514	Tissue	39.559	-122.134	2010		NA	No	No	No	S.Valley	Quinn et al. 2019; Quinn et al. 2021
S10-0515	Tissue	39.624	-122.195	2010		NA	No	No	No	S.Valley	Quinn et al. 2019; Quinn et al. 2021
S10-0561	Tissue	36.811	-121.769	2007	G-38	Nonnative	No	No	No	Nonnative	Sacks et al. 2016; Quinn et al. 2019; Quinn et al. 2021
S10-0562	Tissue	36.818	-121.782	2007	O-26	Nonnative	Yes	Yes	Yes	Nonnative	Sacks et al. 2016; Quinn et al. 2019; Quinn et al. 2021
S10-0563	Tissue	36.850	-121.810	2007	G-38	Nonnative	Yes	No	No	Nonnative	Sacks et al. 2016; Quinn et al. 2019; Quinn et al. 2021
S10-0564	Tissue	36.840	-121.738	2007	G-38	Nonnative	No	No	No	Nonnative	Sacks et al. 2016
S10-0565	Tissue	35.313	-120.859	2007	N-7	Nonnative	No	Yes	Yes	Nonnative	Sacks et al. 2016; Quinn et al. 2019; Quinn et al. 2021
S10-0566	Tissue	36.823	-121.773	2007	N-7	Nonnative	No	No	No	Nonnative	Sacks et al. 2016
S10-0568	Tissue	38.266	-121.312	2001	F-12	Nonnative	No	Yes	Yes	Nonnative	Sacks et al. 2016; Quinn et al. 2019; Quinn et al. 2021
S10-0664	Scat	39.140	-122.144	2010	D-19	Native SVRF	No	No	No	S.Valley	New to this study
S10-0666	Tissue	38.702	-121.904	2010	D-19	Native SVRF	No	Yes	Yes	S.Valley	Quinn et al. 2019; Quinn et al. 2021
S10-0671	Scat	38.527	-121.767	2010	D-19	Native SVRF	No	No	No	S.Valley	New to this study
S10-0672	Scat	38.529	-121.766	2010	D-19	Native SVRF	No	No	No	S.Valley	New to this study
S10-0690	Scat	38.333	-121.156	2010	G-38	Nonnative	No	No	No	Nonnative	Sacks et al. 2016
S10-0697	Scat	38.451	-121.181	2010	G-38	Nonnative	No	No	No	Nonnative	New to this study
S10-0701	Scat	38.333	-121.156	2010	G-38	Nonnative	No	No	No	Nonnative	New to this study
s10-1086	Tissue	39.145	-121.908	2010	D-19	Native SVRF	No	No	No	S.Valley	New to this study
s11-0004	Tissue	38.274	-121.931	2011	G-38	Nonnative	No	Yes	Yes	S.Valley	Sacks et al. 2016; Quinn et al. 2021
s11-0010	Tissue	38.536	-121.940	2011	D-19	Native SVRF	No	Yes	Yes	S.Valley	New to this study
s11-0011	Tissue	38.149	-121.765	2011	D-19	Native SVRF	No	Yes	Yes	S.Valley	Sacks et al. 2016
s11-0012	Tissue	38.525	-121.762	2011	N	Nonnative	No	No	No	S.Valley	New to this study
S11-0222	Scat	38.528	-121.765	2011	D-19	Native SVRF	No	No	No	S.Valley	New to this study
S11-0225	Swab	39.175	-121.939	2011	D-19	Native SVRF	No	No	No	S.Valley	New to this study
S11-0226	Swab	39.175	-121.939	2011	D-19	Native SVRF	No	No	No	S.Valley	New to this study
S11-0227	Swab	38.451	-120.919	2011	G-38	Nonnative	No	No	No	Nonnative	New to this study
S11-0228	Tissue	38.821	-121.714	2011	D-19	Native SVRF	No	Yes	Yes	S.Valley	New to this study
S11-0346	Tissue	38.692	-121.770	2011	N	Nonnative	No	Yes	Yes	S.Valley	New to this study

S11-0347	Tissue	38.679	-121.949	2011	D-19	Native SVRF	No	Yes	Yes	S.Valley	New to this study
S11-0354	Tissue	38.716	-121.906	2011	D-19	Native SVRF	No	Yes	Yes	S.Valley	New to this study
S12-0016	Tissue	38.546	-121.768	2012	D-19	Native SVRF	No	Yes	Yes	S.Valley	New to this study
S12-0188	Tissue	39.168	-121.735	2012	D-19	Native SVRF	No	Yes	Yes	S.Valley	New to this study
S12-0285	Tissue	38.131	-121.868	2012	F-14	Nonnative	Yes	Yes	Yes	S.Valley	Sacks et al. 2016; Quinn et al. 2021
S12-0286	Tissue	38.131	-121.868	2012	F-14	Nonnative	Yes	Yes	Yes	S.Valley	Sacks et al. 2016; Quinn et al. 2021
S12-0677	Tissue	40.169	-122.121	2012	D-19	Native SVRF	No	No	No	S.Valley	New to this study
S12-0817	Scat	40.383	-122.322	2012	D-19	Native SVRF	No	No	No	S.Valley	New to this study
S12-1447	Tissue	38.525	-121.756	2012		NA	No	No	No	S.Valley	New to this study
S13-0062	Tissue	38.522	-121.767	2013	D-19	Native SVRF	No	Yes	Yes	S.Valley	New to this study
S13-0338	Scat	39.070	-121.884	2013	D-19	Native SVRF	No	No	No	S.Valley	New to this study
S13-0612	Tissue	38.640	-121.156	2013	G-38	Nonnative	No	Yes	Yes	Nonnative	Sacks et al. 2016
S13-0807	Hair	38.543	-121.706	2013	G-38	Nonnative	No	No	No	S.Valley	New to this study
S13-0915	Scat	38.543	-121.696	2013	D-19	Native SVRF	No	No	No	S.Valley	New to this study
S13-1297	Scat	38.523	-121.959	2013	D-19	Native SVRF	No	No	No	S.Valley	New to this study
S13-1298	Scat	38.524	-121.958	2013	D-19	Native SVRF	No	No	No	S.Valley	New to this study
S13-1474	Scat	38.530	-121.758	2013	D-19	Native SVRF	No	No	No	S.Valley	New to this study
S13-1687	Scat	38.526	-121.757	2013	D-19	Native SVRF	No	No	No	S.Valley	New to this study
S13-1702	Scat	38.528	-121.758	2013	D-19	Native SVRF	No	No	No	S.Valley	New to this study
S13-1733	Teeth	38.523	-121.960	2013	D-19	Native SVRF	No	No	No	S.Valley	New to this study
S13-1857	Scat	38.432	-121.698	2013	D-19	Native SVRF	No	No	No	S.Valley	New to this study
S13-1866	Scat	38.524	-121.958	2013	D-19	Native SVRF	No	No	No	S.Valley	New to this study
S13-1873	Scat	38.523	-121.960	2013	D-19	Native SVRF	No	No	No	S.Valley	New to this study
S13-1967	Scat	38.452	-121.854	2013	D-19	Native SVRF	No	No	No	S.Valley	New to this study
S13-1971	Tissue	38.539	-121.694	2013	D-19	Native SVRF	No	Yes	Yes	S.Valley	New to this study
S13-2081	Tissue	38.526	-121.761	2013	D-19	Native SVRF	No	Yes	Yes	S.Valley	New to this study
S13-2382	Scat	38.529	-121.757	2013	D-19	Native SVRF	No	No	No	S.Valley	New to this study
S13-2443	Scat	38.523	-121.962	2013	D-19	Native SVRF	No	No	No	S.Valley	New to this study
S13-2444	Scat	38.523	-121.962	2013	D-19	Native SVRF	No	No	No	S.Valley	New to this study

S13-2547	Tissue	39.553	-122.109166	2012	D-19	Native SVRF	No	No	No	S.Valley	New to this study
S13-2578	Scat	38.524	-121.919	2013	G-38	Nonnative	No	No	No	S.Valley	New to this study
S13-2580	Tissue	36.604	-120.579	2012	N-7	Nonnative	Yes	Yes	Yes	Nonnative	Sacks et al. 2016; Quinn et al. 2019; Quinn et al. 2021
S13-2889	Scat	38.457	-121.815	2013	D-19	Native SVRF	No	No	No	S.Valley	New to this study
S13-2903	Scat	38.445	-121.791	2013	G-38	Nonnative	No	No	No	S.Valley	New to this study
S13-3026	Scat	40.390	-122.223	2013	F	Nonnative	No	No	No	S.Valley	New to this study
S13-3555	Scat	39.451	-121.654	2013	D-19	Native SVRF	No	No	No	S.Valley	New to this study
S13-3557	Scat	39.452	-121.649	2013	D-19	Native SVRF	No	No	No	S.Valley	New to this study
S14-0322	Scat	38.543	-121.706	2014	G-38	Nonnative	No	No	No	S.Valley	New to this study
S14-0323	Tissue	39.604	-121.784	2014	D-19	Native SVRF	No	Yes	Yes	S.Valley	New to this study
S14-0838	Tissue	37.435	-122.068	2007	F-9	Nonnative	Yes	Yes	No	Nonnative	Sacks et al. 2016; Sacks et al. 2021; Quinn et al. 2021
S14-0839	Tissue	36.590	-121.879	2006	G-38	Nonnative	Yes	No	No	Nonnative	Sacks et al. 2016; Quinn et al. 2021
S14-0840	Tissue	36.783	-121.795	2006	G-38	Nonnative	Yes	Yes	No	Nonnative	Sacks et al. 2016; Sacks et al. 2021; Quinn et al. 2021
S14-0842	Tissue	38.223	-121.147	2006	G-38	Nonnative	Yes	Yes	Yes	Nonnative	Sacks et al. 2016; Sacks et al. 2021; Quinn et al. 2021
S14-0843	Tissue	38.057	-121.303	2006	N-7	Nonnative	Yes	Yes	Yes	Nonnative	Sacks et al. 2016; Sacks et al. 2021; Quinn et al. 2021
S14-0844	Tissue	35.333	-118.995	2006	E-9	Nonnative	Yes	Yes	Yes	Nonnative	Sacks et al. 2016; Quinn et al. 2019; Quinn et al. 2021
S14-0845	Tissue	35.355	-119.056	2006	E-9	Nonnative	Yes	No	No	Nonnative	Sacks et al. 2016; Quinn et al. 2021
S14-0846	Tissue	36.846	-121.806	2006	G-38	Nonnative	Yes	Yes	Yes	Nonnative	Sacks et al. 2016; Quinn et al. 2021
S14-0847	Tissue	36.845	-121.805	2006	G-38	Nonnative	Yes	No	No	Nonnative	Sacks et al. 2016; Quinn et al. 2019; Quinn et al. 2021
S14-0848	Tissue	35.368	-118.954	2006	E-9	Nonnative	Yes	No	No	Nonnative	Sacks et al. 2016; Sacks et al. 2021; Quinn et al. 2021
S14-0849	Tissue	34.405	-119.696	2006	K-36	Nonnative	No	Yes	Yes	Nonnative	Sacks et al. 2016; Quinn et al. 2021
S14-0850	Tissue	34.402	-119.700	2006	K-36	Nonnative	Yes	Yes	Yes	Nonnative	Sacks et al. 2016; Quinn et al. 2019; Quinn et al. 2021
S14-0851	Tissue	35.426	-119.128	2006	N-7	Nonnative	Yes	Yes	Yes	Nonnative	Sacks et al. 2016; Quinn et al. 2019; Quinn et al. 2021
S14-0852	Tissue	37.493	-122.005	2006	N-7	Nonnative	Yes	Yes	No	Nonnative	Sacks et al. 2016; Quinn et al. 2019; Quinn et al. 2021
S14-0853	Tissue	37.477	-122.450	2006	N-7	Nonnative	Yes	Yes	Yes	Nonnative	Sacks et al. 2016; Quinn et al. 2019; Quinn et al. 2021
S14-0854	Tissue	37.485	-121.978	2006	N-7	Nonnative	Yes	Yes	No	Nonnative	Sacks et al. 2016; Quinn et al. 2019; Quinn et al. 2021
S14-0855	Tissue	37.422	-122.022	2005	N-7	Nonnative	Yes	Yes	No	Nonnative	Sacks et al. 2016; Sacks et al. 2021; Quinn et al. 2021

S14-0856	Tissue	37.440	-121.960	2005	N-7	Nonnative	Yes	Yes	No	Nonnative	Sacks et al. 2016; Sacks et al. 2021; Quinn et al. 2021
S14-0857	Tissue	37.474	-122.448	2006	G-38	Nonnative	Yes	Yes	No	Nonnative	Sacks et al. 2016; Sacks et al. 2021; Quinn et al. 2021
S14-0858	Tissue	37.470	-122.447	2006	O-26	Nonnative	Yes	No	No	Nonnative	Sacks et al. 2016; Sacks et al. 2021; Quinn et al. 2021
S14-0859	Tissue	37.468	-122.447	2006	O-26	Nonnative	Yes	No	No	Nonnative	Sacks et al. 2016; Quinn et al. 2019; Quinn et al. 2021
S14-0860	Tissue	36.827	-121.799	2006	G-38	Nonnative	Yes	No	No	Nonnative	Sacks et al. 2016; Quinn et al. 2019; Quinn et al. 2021
S14-0861	Tissue	37.445	-122.099	2007	N-7	Nonnative	Yes	Yes	Yes	Nonnative	Sacks et al. 2016; Sacks et al. 2021; Quinn et al. 2021
S14-0862	Tissue	36.228	-121.060	2005	G-38	Nonnative	Yes	Yes	Yes	Nonnative	Sacks et al. 2016; Sacks et al. 2021; Quinn et al. 2021
S14-0863	Tissue	35.316	-119.092	2006	E-9	Nonnative	Yes	Yes	Yes	Nonnative	Sacks et al. 2016; Quinn et al. 2019; Quinn et al. 2021
S14-0864	Tissue	34.400	-119.716	2006	K-36	Nonnative	Yes	Yes	No	Nonnative	Sacks et al. 2016; Quinn et al. 2019; Quinn et al. 2021
S14-0865	Tissue	34.422	-119.818	2006	K-36	Nonnative	Yes	No	No	Nonnative	Sacks et al. 2016; Quinn et al. 2019; Quinn et al. 2021
S14-0866	Tissue	34.402	-119.735	2006	K-36	Nonnative	Yes	No	No	Nonnative	Sacks et al. 2016; Quinn et al. 2021
S14-0867	Tissue	34.409	-119.752	2006	K-36	Nonnative	Yes	Yes	Yes	Nonnative	Sacks et al. 2016; Sacks et al. 2021; Quinn et al. 2021
S14-0868	Tissue	36.784	-121.793	2005	G-38	Nonnative	Yes	No	No	Nonnative	Sacks et al. 2016; Quinn et al. 2019; Quinn et al. 2021
S14-0869	Tissue	36.827	-121.799	2005	G-38	Nonnative	No	No	No	Nonnative	Sacks et al. 2016; Quinn et al. 2019; Quinn et al. 2021
S14-0870	Tissue	36.849	-121.807	2005	G-38	Nonnative	Yes	No	No	Nonnative	Sacks et al. 2016; Sacks et al. 2021; Quinn et al. 2021
S14-0871	Tissue	36.848	-121.808	2005	F-12	Nonnative	Yes	No	No	Nonnative	Sacks et al. 2016; Quinn et al. 2019; Quinn et al. 2021
S14-0872	Tissue	37.426	-122.059	2006	N-7	Nonnative	Yes	Yes	Yes	Nonnative	Sacks et al. 2016; Quinn et al. 2021
S14-0873	Tissue	36.815	-121.791	2006	G-38	Nonnative	Yes	Yes	Yes	Nonnative	Sacks et al. 2016; Quinn et al. 2021
S14-0874	Tissue	36.815	-121.791	2006	G-38	Nonnative	Yes	No	No	Nonnative	Sacks et al. 2016; Quinn et al. 2019; Quinn et al. 2021
S14-0875	Tissue	36.805	-121.787	2006	G-38	Nonnative	Yes	No	No	Nonnative	Sacks et al. 2016; Quinn et al. 2021
S14-0876	Tissue	36.818	-121.780	2006	G-38	Nonnative	Yes	No	No	Nonnative	Sacks et al. 2016; Quinn et al. 2021
S14-0877	Tissue	36.759	-121.802	2006	G-38	Nonnative	Yes	No	No	Nonnative	Sacks et al. 2016; Quinn et al. 2019; Quinn et al. 2021
S14-0878	Tissue	34.416	-119.770	2006	K-36	Nonnative	No	No	No	Nonnative	Sacks et al. 2016
S14-0879	Tissue	35.471	-119.261	2006	E-9	Nonnative	Yes	Yes	No	Nonnative	Sacks et al. 2016; Quinn et al. 2021
S14-0880	Tissue	36.887	-121.766	2006	G-38	Nonnative	Yes	No	No	Nonnative	Sacks et al. 2016; Quinn et al. 2019; Quinn et al. 2021
S14-0881	Tissue	35.397	-120.866	2006	G-38	Nonnative	Yes	No	No	Nonnative	Sacks et al. 2016; Quinn et al. 2021

S14-0882	Tissue	35.366	-120.852	2006	G-38	Nonnative	Yes	Yes	Yes	Nonnative	Sacks et al. 2016; Quinn et al. 2019; Quinn et al. 2021
S14-0883	Tissue	36.827	-121.799	2006	G-38	Nonnative	Yes	No	No	Nonnative	Sacks et al. 2016; Quinn et al. 2021
S14-0884	Tissue	36.815	-121.778	2006	G-38	Nonnative	No	No	No	Nonnative	Sacks et al. 2016
S14-0885	Tissue	36.605	-121.865	2006	G-38	Nonnative	No	No	No	Nonnative	Sacks et al. 2016
S14-0886	Tissue	35.392	-120.864	2006	G-38	Nonnative	No	No	No	Nonnative	Sacks et al. 2016
S14-0887	Tissue	36.759	-121.802	2006	G-38	Nonnative	Yes	Yes	Yes	Nonnative	Sacks et al. 2016; Quinn et al. 2021
S14-0888	Tissue	35.381	-120.864	2006	G-38	Nonnative	Yes	No	No	Nonnative	Sacks et al. 2016; Quinn et al. 2019; Quinn et al. 2021
S14-0892	Tissue	39.524	-122.193	2014	D-19	Native SVRF	No	Yes	Yes	S.Valley	New to this study
S14-0894	Scat	38.748	-121.323	2014	D-19	Native SVRF	No	No	No	S.Valley	New to this study
S14-2255	Scat	39.220	-122.017	2014	D-19	Native SVRF	No	No	No	S.Valley	New to this study
S14-2256	Scat	39.220	-122.017	2014	D-19	Native SVRF	No	No	No	S.Valley	New to this study
S14-2257	Scat	39.984	-122.162	2014	F	Nonnative	No	No	No	S.Valley	New to this study
S14-2565	Tissue	37.891	-121.203	2014		NA	Yes	Yes	No	Nonnative	Quinn et al. 2021
S14-2908	Tissue	39.141	-121.842	2014	D-19	Native SVRF	No	Yes	Yes	S.Valley	New to this study
S14-2922	Tissue	39.237	-121.994	2014	D-19	Native SVRF	No	Yes	No	S.Valley	New to this study
S15-0002	Tissue	39.378	-122.020	2014	D-19	Native SVRF	No	Yes	Yes	S.Valley	New to this study
S15-0028	Scat	39.779	-122.063	2015	N	Nonnative	No	No	No	S.Valley	New to this study
S15-0031	Scat	39.983	-122.159	2015	F	Nonnative	No	No	No	S.Valley	New to this study
S15-0033	Tissue	38.235	-120.538	2015	G-38	Nonnative	Yes	No	No	Nonnative	Quinn et al. 2021
S15-0038	Scat	39.882	-122.192	2015	D-19	Native SVRF	No	No	No	S.Valley	New to this study
S15-0197	Scat	40.100	-122.151	2015	D-19	Native SVRF	No	No	No	S.Valley	New to this study
S15-0553	Scat	39.339	-121.686	2015	D-19	Native SVRF	No	No	No	S.Valley	New to this study
S15-0812	Scat	38.543	-121.695	2015	G-38	Nonnative	No	No	No	S.Valley	New to this study
S15-0815	Scat	39.674	-121.780	2015	D-19	Native SVRF	No	No	No	S.Valley	New to this study
S15-0819	Scat	39.734	-122.159	2015	D-19	Native SVRF	No	No	No	S.Valley	New to this study
S15-0823	Scat	39.220	-122.017	2015	D-19	Native SVRF	No	No	No	S.Valley	New to this study
S15-0826	Scat	39.221	-122.017	2015	D-19	Native SVRF	No	No	No	S.Valley	New to this study
S15-0828	Scat	38.543	-121.698	2015	G-38	Nonnative	No	No	No	S.Valley	New to this study

S15-0830	Scat	39.652	-121.790	2015	F	Nonnative	No	No	No	S.Valley	New to this study
S15-0888	Scat	38.971	-122.100	2015	D-19	Native SVRF	No	No	No	S.Valley	New to this study
S15-0889	Scat	38.971	-122.100	2015	D-19	Native SVRF	No	No	No	S.Valley	New to this study
S15-0931	Tissue	39.651	-121.790	2015	F	Nonnative	No	No	No	S.Valley	New to this study
S15-1608	Tissue	39.230	-122.023	2015	D-19	Native SVRF	No	No	No	S.Valley	New to this study
S15-1661	Scat	39.866	-122.078	2015	D-19	Native SVRF	No	No	No	S.Valley	New to this study
S15-1696	Scat	38.810	-121.634	2015	D-19	Native SVRF	No	No	No	S.Valley	New to this study
S15-1966	Scat	38.895	-121.413	2015	D-19	Native SVRF	No	No	No	S.Valley	New to this study
S15-1976	Scat	40.109	-122.163	2015	D-19	Native SVRF	No	No	No	S.Valley	New to this study
S15-1979	Scat	40.005	-122.140	2015	F	Nonnative	No	No	No	S.Valley	New to this study
S15-1981	Scat	40.013	-122.145	2015	F	Nonnative	No	No	No	S.Valley	New to this study
S15-3137	Tissue	39.499	-122.199	2015	D-19	Native SVRF	No	No	No	S.Valley	New to this study
S16-0001	Scat	40.013	-122.145	2015	F	Nonnative	No	No	No	S.Valley	New to this study
S16-0005	Scat	38.812	-121.635	2015	D-19	Native SVRF	No	No	No	S.Valley	New to this study
S16-0007	Scat	39.024	-121.817	2015	D-19	Native SVRF	No	No	No	S.Valley	New to this study
S16-0036	Tissue	39.189	-122.169	2016	D-19	Native SVRF	No	No	No	S.Valley	New to this study
S16-1296	Scat	38.812	-121.635	2016	N	Nonnative	No	No	No	S.Valley	New to this study
S16-1301	Scat	38.491	-120.832	2016	F	Nonnative	Yes	Yes	Yes	Nonnative	Sacks et al. 2016; Quinn et al. 2019; Quinn et al. 2021
S16-1303	Scat	40.137	-122.190	2016	F	Nonnative	No	Yes	Yes	S.Valley	Quinn et al. 2019; Quinn et al. 2021
S16-1309	Scat	39.929	-122.136	2016	D-19	Native SVRF	No	No	No	S.Valley	New to this study
S16-1340	Scat	39.593	-122.193	2016	D-19	Native SVRF	No	No	No	S.Valley	New to this study
S16-1355	Tissue	39.551	-122.035	2014	D-19	Native SVRF	No	Yes	No	S.Valley	New to this study
S16-1356	Scat	38.543	-121.698	2016	G-38	Nonnative	No	No	No	S.Valley	New to this study
S16-1381	Scat	39.647	-121.787	2016	D-19	Native SVRF	No	No	No	S.Valley	New to this study
S16-1382	Scat	39.651	-121.790	2016	D-19	Native SVRF	No	No	No	S.Valley	New to this study
S16-1385	Scat	39.221	-122.017	2016	D-19	Native SVRF	No	No	No	S.Valley	New to this study
S16-1391	Scat	38.814	-121.935	2016	D-19	Native SVRF	No	No	No	S.Valley	New to this study
S16-1392	Scat	38.815	-121.935	2016	D-19	Native SVRF	No	No	No	S.Valley	New to this study
S16-1405	Scat	39.220	-122.017	2016	D-19	Native SVRF	No	No	No	S.Valley	New to this study

S16-1409	Scat	38.543	-121.695	2016	G-38	Nonnative	No	No	No	S.Valley	New to this study
S16-1410	Scat	38.556	-121.839	2016	D-19	Native SVRF	No	No	No	S.Valley	New to this study
S16-1411	Scat	38.671	-121.870	2016	D-19	Native SVRF	No	No	No	S.Valley	New to this study
S16-1412	Scat	38.671	-121.870	2016	D-19	Native SVRF	No	No	No	S.Valley	New to this study
S16-1417	Scat	38.702	-121.467	2016	D-19	Native SVRF	No	No	No	S.Valley	New to this study
S16-1418	Scat	38.702	-121.467	2016	D-19	Native SVRF	No	No	No	S.Valley	New to this study
S16-1429	Scat	38.431	-121.289	2016	G-38	Nonnative	No	No	No	Nonnative	New to this study
S16-1430	Scat	38.431	-121.289	2016	G-38	Nonnative	No	No	No	Nonnative	New to this study
S16-1481	Scat	38.557	-121.839	2016	D-19	Native SVRF	No	No	No	S.Valley	New to this study
S16-1496	Scat	38.971	-122.100	2016	D-19	Native SVRF	No	No	No	S.Valley	New to this study
S16-1497	Scat	38.971	-122.100	2016	D-19	Native SVRF	No	No	No	S.Valley	New to this study
S16-1593	Scat	38.559	-121.840	2016	D-19	Native SVRF	No	No	No	S.Valley	New to this study
S16-1594	Scat	38.559	-121.840	2016	D-19	Native SVRF	No	No	No	S.Valley	New to this study
S16-1603	Scat	38.525	-121.755	2016	D-19	Native SVRF	No	No	No	S.Valley	New to this study
S16-1606	Scat	38.525	-121.755	2016	D-19	Native SVRF	No	No	No	S.Valley	New to this study
S16-1612	Scat	38.531	-121.775	2016	D-19	Native SVRF	No	No	No	S.Valley	New to this study
S16-1613	Scat	38.531	-121.775	2016	D-19	Native SVRF	No	No	No	S.Valley	New to this study
S16-1633	Tissue	39.583	-122.098	2016	D-19	Native SVRF	No	Yes	Yes	S.Valley	New to this study
S16-1645	Scat	39.583	-122.097	2016	D-19	Native SVRF	No	No	No	S.Valley	New to this study
S16-1646	Scat	39.583	-122.097	2016	D-19	Native SVRF	No	No	No	S.Valley	New to this study
S16-1654	Scat	39.233	-121.679	2016	D-19	Native SVRF	No	No	No	S.Valley	New to this study
S16-1655	Scat	39.233	-121.679	2016	D-19	Native SVRF	No	No	No	S.Valley	New to this study
S16-1953	Scat	38.557	-121.839	2016	D-19	Native SVRF	No	Yes	Yes	S.Valley	Quinn et al. 2019; Quinn et al. 2021
S16-1954	Scat	38.557	-121.839	2016	D-19	Native SVRF	No	No	No	S.Valley	Quinn et al. 2019; Quinn et al. 2021
S16-6030	Tissue	38.547	-121.513	2016	N	Nonnative	No	Yes	Yes	Nonnative	New to this study
S16-6031	Tissue	39.168	-122.151	2016	D-19	Native SVRF	No	No	No	S.Valley	New to this study
S17-1465	Scat	38.548	-121.804	2017	D-19	Native SVRF	No	No	No	S.Valley	New to this study
S17-1466	Scat	38.548	-121.804	2017	D-19	Native SVRF	No	No	No	S.Valley	New to this study
S17-1524	Scat	38.564	-121.858	2017	D-19	Native SVRF	No	No	No	S.Valley	New to this study

S17-1530	Tissue	38.562	-121.856	2017	D-19	Native SVRF	No	No	No	S.Valley	New to this study
S17-1551	Tissue	40.078	-122.168	2017	D-19	Native SVRF	No	Yes	Yes	S.Valley	New to this study
S17-2079	Scat	39.140	-122.176	2017	D-19	Native SVRF	No	No	No	S.Valley	New to this study
S17-2080	Scat	39.140	-122.176	2017	D-19	Native SVRF	No	No	No	S.Valley	New to this study
S17-2547	Tissue	39.079	-121.896	2017	D-19	Native SVRF	No	Yes	Yes	S.Valley	New to this study
S17-2548	Tissue	39.632	-121.910	2015	F	Nonnative	No	Yes	Yes	S.Valley	New to this study
S17-2549	Tissue	39.430	-122.193	2017	D-19	Native SVRF	No	Yes	Yes	S.Valley	New to this study
S17-2550	Tissue	39.430	-122.193	2017	D-19	Native SVRF	No	Yes	Yes	S.Valley	New to this study
S17-2573	Scat	39.220	-122.016	2017	D-19	Native SVRF	No	No	No	S.Valley	New to this study
S17-2574	Scat	39.220	-122.017	2017	D-19	Native SVRF	No	No	No	S.Valley	New to this study
S17-7258	Tissue	39.495	-122.193	2017	D-19	Native SVRF	No	No	No	S.Valley	New to this study
S17-7259	Tissue	39.425	-122.192	2017	D-19	Native SVRF	No	Yes	Yes	S.Valley	New to this study
S17-7260	Tissue	38.523	-121.769	2017	D-19	Native SVRF	No	No	No	S.Valley	New to this study
S18-1250	Scat	38.564	-121.857	2018	D-19	Native SVRF	No	No	No	S.Valley	New to this study
S18-1251	Scat	38.564	-121.857	2018	D-19	Native SVRF	No	No	No	S.Valley	New to this study
S18-1284	Scat	38.502	-122.035	2018	D-19	Native SVRF	No	No	No	S.Valley	New to this study
S18-1286	Scat	38.543	-121.698	2018	D-19	Native SVRF	No	No	No	S.Valley	New to this study
S18-1290	Scat	38.543	-121.698	2018	D-19	Native SVRF	No	No	No	S.Valley	New to this study
S18-1388	Scat	40.390	-122.178	2017	D-19	Native SVRF	No	No	No	S.Valley	New to this study
S18-1389	Scat	40.390	-122.179	2017	F	Nonnative	No	No	No	S.Valley	New to this study
S18-1403	Scat	38.529	-121.767	2018	D-19	Native SVRF	No	No	No	S.Valley	New to this study
S18-1404	Scat	38.529	-121.767	2018	D-19	Native SVRF	No	No	No	S.Valley	New to this study
S18-1500	Tissue	38.680	-122.054	2018	D-19	Native SVRF	No	Yes	Yes	S.Valley	New to this study
S18-1501	Tissue	38.677	-122.059	2018	D-19	Native SVRF	No	No	No	S.Valley	New to this study
S18-2042	Tissue	39.473	-121.609	2017	D-19	Native SVRF	No	Yes	Yes	S.Valley	New to this study
S18-2043	Tissue	39.957	-122.197503	2013	D-19	Native SVRF	No	No	No	S.Valley	New to this study
S18-2044	Tissue	39.853	-121.919	2017	F	Nonnative	No	Yes	Yes	S.Valley	New to this study
S18-2045	Tissue	40.172	-122.261	2016	D-19	Native SVRF	No	Yes	Yes	S.Valley	New to this study
S18-2046	Tissue	40.189	-122.197	2015	D-19	Native SVRF	No	No	No	S.Valley	New to this study

S18-2073	Tissue	38.535	-121.768	2018	D-19	Native SVRF	No	Yes	Yes	S.Valley	New to this study
S18-2128	Tissue	38.564	-121.857	2018	D-19	Native SVRF	No	Yes	Yes	S.Valley	New to this study
S18-2174	Scat	38.545	-121.798	2018	D-19	Native SVRF	No	No	No	S.Valley	New to this study
S18-2198	Tissue	39.383	-122.193	2018	D-19	Native SVRF	No	Yes	No	S.Valley	New to this study
S18-2199	Tissue	39.383	-122.193	2018	D-19	Native SVRF	No	No	No	S.Valley	New to this study
S18-2200	Tissue	39.428	-122.193	2018	D-19	Native SVRF	No	Yes	Yes	S.Valley	New to this study
S18-2201	Tissue	39.430	-122.193	2018	D-19	Native SVRF	No	Yes	Yes	S.Valley	New to this study
S18-2202	Tissue	39.460	-121.993	2018	D-19	Native SVRF	No	Yes	No	S.Valley	New to this study
S18-3889	Tissue	38.523	-121.752	2018	D-19	Native SVRF	No	Yes	No	S.Valley	New to this study
S18-3896	Scat	38.502	-122.035	2018	D-19	Native SVRF	No	No	No	S.Valley	New to this study
S18-3899	Tissue	38.491	-121.162	2018	G-38	Nonnative	No	Yes	Yes	Nonnative	New to this study
S18-7596	Tissue	38.204	-121.183	2018	O	Nonnative	No	No	No	Nonnative	New to this study
S18-7763	Tissue	38.562	-121.845	2018	D-19	Native SVRF	No	No	No	S.Valley	New to this study
S19-10392	Scat	38.529	-121.765	2019	D-19	Native SVRF	No	No	No	S.Valley	New to this study
S19-10653	Tissue	38.039	-122.598	2019	F	Nonnative	No	No	No	Nonnative	New to this study
S19-1769	Scat	38.564	-121.857	2019	D-19	Native SVRF	No	No	No	S.Valley	New to this study
S19-1770	Scat	38.564	-121.857	2019	D-19	Native SVRF	No	No	No	S.Valley	New to this study
S19-1797	Blood	38.392	-122.715	2019	N	Nonnative	No	Yes	Yes	Nonnative	New to this study
S19-1798	Blood	38.392	-122.715	2019	N	Nonnative	No	Yes	Yes	Nonnative	New to this study
S19-1799	Blood	39.097	-121.634	2019	D-19	Native SVRF	No	Yes	Yes	S.Valley	New to this study
S19-1800	Blood	38.392	-122.715	2019	N	Nonnative	No	Yes	Yes	Nonnative	New to this study
S19-4934	Tissue	39.006	-121.577	2019	D-19	Native SVRF	No	No	No	S.Valley	New to this study
S19-5730	Scat	38.555	-121.673	2019	G-38	Nonnative	No	No	No	S.Valley	New to this study
S19-5733	Scat	38.555	-121.673	2019	D-19	Native SVRF	No	No	No	S.Valley	New to this study
S19-5762	Tissue	38.672	-121.858	2019	D-19	Native SVRF	No	No	No	S.Valley	New to this study
S19-6908	Tissue	38.753	-121.577	2019	D-19	Native SVRF	No	No	No	S.Valley	New to this study
S19-7478	Tissue	34.738	-120.263	2019	G-38	Nonnative	No	No	No	Nonnative	New to this study
S20-0001	Tissue	38.538	-121.768	2020	D-19	Native SVRF	No	No	No	S.Valley	New to this study
S20-1520	Blood	38.174	-120.837	2020	G-38	Nonnative	No	No	No	Nonnative	New to this study

S20-4941	Tissue	38.553	-121.840	2020	D-19	Native SVRF	No	No	No	S.Valley	New to this study
S21-0001	Tissue	38.540	-121.780	2021	G-38	Nonnative	No	No	No	S.Valley	New to this study
S21-2032	Tissue	38.482	-121.550	2021	N	Nonnative	No	No	No	Nonnative	New to this study
SB1	Tissue	34.430	-119.630	2002	K-36	Nonnative	No	No	No	Nonnative	Sacks et al. 2016
SB2	Tissue	34.430	-119.880	1993	K-36	Nonnative	No	No	No	Nonnative	Sacks et al. 2016
SB3	Tissue	34.430	-119.730	1990	K-36	Nonnative	No	No	No	Nonnative	Sacks et al. 2016
SB4	Tissue	34.460	-119.770	1994	K-36	Nonnative	No	No	No	Nonnative	Sacks et al. 2016
SB5	Tissue	34.430	-119.820	1995	K-36	Nonnative	Yes	Yes	No	Nonnative	Sacks et al. 2016; Quinn et al. 2021
SB6	Tissue	34.430	-119.770	1996	K-36	Nonnative	Yes	Yes	Yes	Nonnative	Sacks et al. 2016; Quinn et al. 2021
V00-0776	Tissue	34.059	-117.609	2000	A-273	Nonnative	No	No	No	Nonnative	Sacks et al. 2016
V00-0779	Tissue	34.059	-117.609	2000	A-273	Nonnative	No	No	No	Nonnative	Sacks et al. 2016
V01-0168	Tissue	37.020	-121.570	2001	G-38	Nonnative	No	No	No	Nonnative	Sacks et al. 2016
V01-0197	Tissue	35.459	-118.974	2001	E-9	Nonnative	Yes	No	No	Nonnative	Sacks et al. 2010; Sacks et al. 2016; Quinn et al. 2019; Quinn et al. 2021
V01-0721	Tissue	37.100	-121.230	2001	G-38	Nonnative	No	No	No	Nonnative	Sacks et al. 2016
V02-1003	Tissue	35.323	-119.004	2002	E-9	Nonnative	Yes	No	No	Nonnative	Sacks et al. 2010; Sacks et al. 2016; Quinn et al. 2019; Quinn et al. 2021
V03-0043	Tissue	37.465	-122.447	2003	G-38	Nonnative	No	No	No	Nonnative	Sacks et al. 2016
V03-0044	Tissue	37.465	-122.447	2003	G-38	Nonnative	No	No	No	Nonnative	Sacks et al. 2016; Quinn et al. 2019; Quinn et al. 2021
V03-0523	Tissue	36.690	-121.810	2003	G-38	Nonnative	No	No	No	Nonnative	Sacks et al. 2016
V03-0601	Tissue	36.790	-121.790	2003	G-38	Nonnative	No	No	No	Nonnative	Sacks et al. 2016
V03-0603	Tissue	36.790	-121.790	2003	F-12	Nonnative	No	No	No	Nonnative	Sacks et al. 2016; Quinn et al. 2019; Quinn et al. 2021
V03-0637	Tissue	37.465	-122.447	2003	O-26	Nonnative	No	No	No	Nonnative	Sacks et al. 2016
V03-0948	Tissue	36.794	-121.785	2003	G-38	Nonnative	No	No	No	Nonnative	Sacks et al. 2016; Quinn et al. 2019; Quinn et al. 2021
V03-0949	Tissue	36.794	-121.785	2003	G-38	Nonnative	No	No	No	Nonnative	Sacks et al. 2016
V03-1267	Tissue	37.465	-122.447	2003	G-38	Nonnative	No	No	No	Nonnative	Sacks et al. 2016
V03-1268	Tissue	37.465	-122.447	2003	G-38	Nonnative	No	No	No	Nonnative	Sacks et al. 2016
V03-1269	Tissue	37.465	-122.447	2003	G-38	Nonnative	No	No	No	Nonnative	Sacks et al. 2016; Quinn et al. 2019; Quinn et al. 2021
V03-1270	Tissue	37.465	-122.447	2003	G-38	Nonnative	No	No	No	Nonnative	Sacks et al. 2016
V04-0102	Tissue	36.790	-121.790	2004	G-38	Nonnative	No	No	No	Nonnative	Sacks et al. 2016

V04-0103	Tissue	36.790	-121.790	2004	G-38	Nonnative	No	No	No	Nonnative	Sacks et al. 2016
V04-0104	Tissue	36.832	-121.800	2004	G-38	Nonnative	No	No	No	Nonnative	Sacks et al. 2016
V04-0106	Tissue	36.832	-121.800	2004	G-38	Nonnative	No	No	No	Nonnative	Sacks et al. 2016; Quinn et al. 2019; Quinn et al. 2021
V04-0292	Tissue	36.801	-121.760	2004	G-38	Nonnative	No	No	No	Nonnative	Sacks et al. 2016; Quinn et al. 2019; Quinn et al. 2021
V04-0293	Tissue	36.750	-121.800	2004	G-38	Nonnative	No	No	No	Nonnative	Sacks et al. 2016
V04-0294	Tissue	36.832	-121.800	2004	G-38	Nonnative	No	No	No	Nonnative	Sacks et al. 2016; Quinn et al. 2019; Quinn et al. 2021
V04-0295	Tissue	36.794	-121.785	2004	G-38	Nonnative	No	No	No	Nonnative	Sacks et al. 2016
V04-0296	Tissue	36.794	-121.785	2004	G-38	Nonnative	No	No	No	Nonnative	Sacks et al. 2016; Quinn et al. 2019; Quinn et al. 2021
V04-0931	Tissue	37.560	-122.060	2004	F-12	Nonnative	No	No	No	Nonnative	Sacks et al. 2016; Quinn et al. 2019; Quinn et al. 2021
V04-0933	Tissue	37.620	-122.160	2004	N-7	Nonnative	No	No	No	Nonnative	Sacks et al. 2016; Quinn et al. 2019; Quinn et al. 2021
VVBNS10	Tissue	36.750	-121.750	1996-2000	G-38	Nonnative	No	No	No	Nonnative	Sacks et al. 2016
VVBNS101	Tissue	36.750	-121.750	2000	G-38	Nonnative	No	No	No	Nonnative	Sacks et al. 2016
VVBNS103	Tissue	36.790	-121.790	1996-2000	G-38	Nonnative	No	No	No	Nonnative	Sacks et al. 2016
VVBNS104	Tissue	37.595	-122.125	2000	G-38	Nonnative	No	No	No	Nonnative	Sacks et al. 2016
VVBNS105	Tissue	37.445	-122.027	1996-2000	N-7	Nonnative	No	No	No	Nonnative	Sacks et al. 2016
VVBNS106	Tissue	37.440	-122.060	1996	F-12	Nonnative	No	No	No	Nonnative	Sacks et al. 2016
VVBNS108	Tissue	36.790	-121.790	1999	F-12	Nonnative	No	No	No	Nonnative	Sacks et al. 2016
VVBNS109	Tissue	37.580	-122.120	1996	N-7	Nonnative	No	No	No	Nonnative	Sacks et al. 2016
VVBNS11	Tissue	37.435	-122.068	1999	F-12	Nonnative	No	No	No	Nonnative	Sacks et al. 2016
VVBNS111	Tissue	37.480	-122.040	1995	F-14	Nonnative	No	No	No	Nonnative	Sacks et al. 2016
VVBNS112	Tissue	37.610	-122.130	1996	N-7	Nonnative	No	No	No	Nonnative	Sacks et al. 2016
VVBNS113	Tissue	37.610	-122.130	1996	N-7	Nonnative	No	No	No	Nonnative	Sacks et al. 2016
VVBNS114	Tissue	37.610	-122.130	1996	N-7	Nonnative	No	No	No	Nonnative	Sacks et al. 2016
VVBNS115	Tissue	37.455	-122.120	1997	F-12	Nonnative	No	No	No	Nonnative	Sacks et al. 2016
VVBNS116	Tissue	37.450	-122.120	1996	F-12	Nonnative	No	No	No	Nonnative	Sacks et al. 2016
VVBNS117	Tissue	37.595	-122.125	1996	N-7	Nonnative	No	No	No	Nonnative	Sacks et al. 2016
VVBNS118	Tissue	37.480	-122.040	1996	F-12	Nonnative	No	No	No	Nonnative	Sacks et al. 2016
VVBNS119	Tissue	37.460	-122.040	1996	F-12	Nonnative	No	No	No	Nonnative	Sacks et al. 2016

VVBNS12	Tissue	37.630	-122.150	1996	N-7	Nonnative	No	No	No	Nonnative	Sacks et al. 2016
VVBNS120	Tissue	37.540	-122.120	1996	N-7	Nonnative	No	No	No	Nonnative	Sacks et al. 2016
VVBNS121	Tissue	37.430	-121.980	1996	F-12	Nonnative	No	No	No	Nonnative	Sacks et al. 2016
VVBNS122	Tissue	37.450	-122.120	1996	F-12	Nonnative	No	No	No	Nonnative	Sacks et al. 2016
VVBNS123	Tissue	37.580	-122.120	1997	N-7	Nonnative	No	No	No	Nonnative	Sacks et al. 2016
VVBNS124	Tissue	37.440	-122.040	1996	N-7	Nonnative	No	No	No	Nonnative	Sacks et al. 2016
VVBNS125	Tissue	37.610	-122.130	1997	N-7	Nonnative	No	No	No	Nonnative	Sacks et al. 2016
VVBNS126	Tissue	37.500	-122.140	1996	F-12	Nonnative	No	No	No	Nonnative	Sacks et al. 2016
VVBNS127	Tissue	37.480	-122.040	1996	F-12	Nonnative	No	No	No	Nonnative	Sacks et al. 2016
VVBNS128	Tissue	37.445	-122.027	1996-2000	N-7	Nonnative	No	No	No	Nonnative	Sacks et al. 2016
VVBNS129	Tissue	37.435	-122.068	1996-2000	F-12	Nonnative	Yes	No	No	Nonnative	Sacks et al. 2016; Quinn et al. 2021
VVBNS13	Tissue	37.430	-122.060	2000	F-12	Nonnative	No	No	No	Nonnative	Sacks et al. 2016
VVBNS130	Tissue	37.450	-122.120	1996	F-12	Nonnative	No	No	No	Nonnative	Sacks et al. 2016
VVBNS132	Tissue	36.790	-121.790	1999	G-38	Nonnative	Yes	No	No	Nonnative	Sacks et al. 2016; Quinn et al. 2021
VVBNS133	Tissue	36.790	-121.790	1999	G-38	Nonnative	No	No	No	Nonnative	Sacks et al. 2016; Quinn et al. 2019; Quinn et al. 2021
VVBNS134	Tissue	37.480	-122.040	1996	F-12	Nonnative	No	No	No	Nonnative	Sacks et al. 2016
VVBNS135	Tissue	36.790	-121.790	1998	G-38	Nonnative	No	No	No	Nonnative	Sacks et al. 2016; Quinn et al. 2019; Quinn et al. 2021
VVBNS136	Tissue	36.801	-121.760	1997	G-38	Nonnative	No	No	No	Nonnative	Sacks et al. 2016
VVBNS137	Tissue	36.790	-121.790	1999	G-38	Nonnative	Yes	No	No	Nonnative	Sacks et al. 2016; Quinn et al. 2021
VVBNS138	Tissue	37.630	-122.160	1996-2000	N-7	Nonnative	No	No	No	Nonnative	Sacks et al. 2016
VVBNS139	Tissue	37.630	-122.160	1996-2000	N-7	Nonnative	No	No	No	Nonnative	Sacks et al. 2016
VVBNS14	Tissue	37.460	-122.040	2000	O-26	Nonnative	No	No	No	Nonnative	Sacks et al. 2016
VVBNS140	Tissue	37.630	-122.160	1996-2000	N-7	Nonnative	No	No	No	Nonnative	Sacks et al. 2016
VVBNS141	Tissue	37.520	-122.220	1997	F-12	Nonnative	No	No	No	Nonnative	Sacks et al. 2016; Quinn et al. 2019; Quinn et al. 2021
VVBNS142	Tissue	37.520	-122.220	1997	F-12	Nonnative	No	No	No	Nonnative	Sacks et al. 2016
VVBNS143	Tissue	37.430	-122.072	1997	F-12	Nonnative	Yes	No	No	Nonnative	Sacks et al. 2016; Quinn et al. 2021
VVBNS144	Tissue	37.450	-122.120	1996	F-12	Nonnative	No	No	No	Nonnative	Sacks et al. 2016
VVBNS145	Tissue	37.610	-122.130	1997	F-12	Nonnative	No	No	No	Nonnative	Sacks et al. 2016

VVBNS146	Tissue	36.750	-121.750	1999	G-38	Nonnative	Yes	No	No	Nonnative	Sacks et al. 2016; Quinn et al. 2021
VVBNS146	Tissue	36.750	-121.750	1999	G-38	Nonnative	No	No	No	Nonnative	Sacks et al. 2016
VVBNS147	Tissue	37.450	-122.120	1996	F-12	Nonnative	No	No	No	Nonnative	Sacks et al. 2016
VVBNS148	Tissue	37.450	-122.120	1996	F-12	Nonnative	No	No	No	Nonnative	Sacks et al. 2016
VVBNS149	Tissue	37.430	-122.068	1997	F-12	Nonnative	No	No	No	Nonnative	Sacks et al. 2016
VVBNS15	Tissue	37.460	-121.940	2000	F-12	Nonnative	No	No	No	Nonnative	Sacks et al. 2016
VVBNS150	Tissue	37.610	-122.130	1996	N-7	Nonnative	No	No	No	Nonnative	Sacks et al. 2016
VVBNS151	Tissue	36.790	-121.790	1999	G-38	Nonnative	No	No	No	Nonnative	Sacks et al. 2016
VVBNS152	Tissue	37.430	-122.068	1997	F-12	Nonnative	No	No	No	Nonnative	Sacks et al. 2016
VVBNS153	Tissue	36.790	-121.790	1999	G-38	Nonnative	No	No	No	Nonnative	Sacks et al. 2016
VVBNS154	Tissue	36.790	-121.790	1998	F-12	Nonnative	No	No	No	Nonnative	Sacks et al. 2016
VVBNS155	Tissue	37.520	-122.220	1997	F-12	Nonnative	No	No	No	Nonnative	Sacks et al. 2016
VVBNS156	Tissue	36.826	-121.738	1997	G-38	Nonnative	No	No	No	Nonnative	Sacks et al. 2016
VVBNS157	Tissue	36.790	-121.790	1997	G-38	Nonnative	No	No	No	Nonnative	Sacks et al. 2016
VVBNS158	Tissue	37.450	-122.125	1997	F-12	Nonnative	No	No	No	Nonnative	Sacks et al. 2016; Quinn et al. 2019; Quinn et al. 2021
VVBNS16	Tissue	37.630	-122.160	1996-2000	F-12	Nonnative	No	No	No	Nonnative	Sacks et al. 2016
VVBNS162	Tissue	36.790	-121.790	1999	G-38	Nonnative	No	No	No	Nonnative	Sacks et al. 2016
VVBNS163	Tissue	36.790	-121.790	1999	G-38	Nonnative	No	No	No	Nonnative	Sacks et al. 2016
VVBNS164	Tissue	36.790	-121.790	1999	G-38	Nonnative	No	No	No	Nonnative	Sacks et al. 2016
VVBNS165	Tissue	36.790	-121.790	1999	G-38	Nonnative	No	No	No	Nonnative	Sacks et al. 2016
VVBNS166	Tissue	36.790	-121.790	1998	G-38	Nonnative	No	No	No	Nonnative	Sacks et al. 2016
VVBNS167	Tissue	36.832	-121.800	1998	G-38	Nonnative	No	No	No	Nonnative	Sacks et al. 2016
VVBNS168	Tissue	36.800	-121.750	1996-2000	G-38	Nonnative	No	No	No	Nonnative	Sacks et al. 2016; Quinn et al. 2019; Quinn et al. 2021
VVBNS169	Tissue	36.790	-121.790	1998	G-38	Nonnative	No	No	No	Nonnative	Sacks et al. 2016
VVBNS170	Tissue	36.832	-121.800	1998	G-38	Nonnative	No	No	No	Nonnative	Sacks et al. 2016
VVBNS171	Tissue	36.800	-121.750	1998	N-7	Nonnative	No	No	No	Nonnative	Sacks et al. 2016
VVBNS172	Tissue	37.610	-122.130	1996	N-7	Nonnative	No	No	No	Nonnative	Sacks et al. 2016
VVBNS173	Tissue	37.610	-122.130	1997	N-7	Nonnative	No	No	No	Nonnative	Sacks et al. 2016

VVBNS174	Tissue	37.455	-122.120	1996	F-12	Nonnative	No	No	No	Nonnative	Sacks et al. 2016
VVBNS175	Tissue	37.435	-122.068	1996-2000	N-7	Nonnative	No	No	No	Nonnative	Sacks et al. 2016
VVBNS176	Tissue	37.430	-122.068	1999	F-12	Nonnative	No	No	No	Nonnative	Sacks et al. 2016
VVBNS177	Tissue	36.800	-121.750	1997	G-38	Nonnative	No	No	No	Nonnative	Sacks et al. 2016
VVBNS178	Tissue	36.750	-121.750	1997	G-38	Nonnative	No	No	No	Nonnative	Sacks et al. 2016
VVBNS179	Tissue	37.435	-122.068	1996	F-12	Nonnative	No	No	No	Nonnative	Sacks et al. 2016
VVBNS18	Tissue	37.630	-122.160	1996	N-7	Nonnative	No	No	No	Nonnative	Sacks et al. 2016
VVBNS180	Tissue	36.790	-121.790	1996-2000	G-38	Nonnative	No	No	No	Nonnative	Sacks et al. 2016
VVBNS181	Tissue	37.610	-122.130	1996	N-7	Nonnative	Yes	No	No	Nonnative	Sacks et al. 2016; Quinn et al. 2021
VVBNS182	Tissue	37.610	-122.130	1996	N-7	Nonnative	No	No	No	Nonnative	Sacks et al. 2016
VVBNS183	Tissue	37.610	-122.130	1996	N-7	Nonnative	No	No	No	Nonnative	Sacks et al. 2016
VVBNS184	Tissue	37.610	-122.130	1996	N-7	Nonnative	Yes	No	No	Nonnative	Sacks et al. 2016; Quinn et al. 2021
VVBNS185	Tissue	36.790	-121.790	1997	F-12	Nonnative	No	No	No	Nonnative	Sacks et al. 2016
VVBNS186	Tissue	37.610	-122.130	1996	N-7	Nonnative	No	No	No	Nonnative	Sacks et al. 2016
VVBNS189	Tissue	37.435	-122.068	1996	F-12	Nonnative	No	No	No	Nonnative	Sacks et al. 2016
VVBNS19	Tissue	37.680	-122.180	1997	N-7	Nonnative	No	No	No	Nonnative	Sacks et al. 2016
VVBNS190	Tissue	37.460	-122.040	1997	G-38	Nonnative	Yes	No	No	Nonnative	Sacks et al. 2016; Quinn et al. 2021
VVBNS191	Tissue	37.550	-122.220	1997	F-12	Nonnative	No	No	No	Nonnative	Sacks et al. 2016
VVBNS192	Tissue	37.520	-122.220	1997	F-12	Nonnative	No	No	No	Nonnative	Sacks et al. 2016
VVBNS21	Tissue	37.460	-121.940	1999	F-12	Nonnative	No	No	No	Nonnative	Sacks et al. 2016
VVBNS22	Tissue	37.630	-122.160	1996-2000	N-7	Nonnative	No	No	No	Nonnative	Sacks et al. 2016
VVBNS24	Tissue	37.630	-122.150	1996	N-7	Nonnative	No	No	No	Nonnative	Sacks et al. 2016
VVBNS25	Tissue	37.560	-122.100	1996	N-7	Nonnative	No	No	No	Nonnative	Sacks et al. 2016
VVBNS26	Tissue	36.790	-121.790	1999	G-38	Nonnative	No	No	No	Nonnative	Sacks et al. 2016
VVBNS27	Tissue	37.630	-122.160	1996	N-7	Nonnative	No	No	No	Nonnative	Sacks et al. 2016
VVBNS28	Tissue	37.680	-122.180	1997	N-7	Nonnative	No	No	No	Nonnative	Sacks et al. 2016
VVBNS29	Tissue	36.800	-121.750	1996-2000	F-12	Nonnative	No	No	No	Nonnative	Sacks et al. 2016
VVBNS30	Tissue	37.630	-122.150	1996	N-7	Nonnative	No	No	No	Nonnative	Sacks et al. 2016
VVBNS31	Tissue	36.790	-121.790	2000	G-38	Nonnative	No	No	No	Nonnative	Sacks et al. 2016

VVBNS32	Tissue	36.790	-121.790	2000	F-12	Nonnative	No	No	No	Nonnative	Sacks et al. 2016
VVBNS33	Tissue	37.460	-122.040	1999	F-12	Nonnative	No	No	No	Nonnative	Sacks et al. 2016
VVBNS34	Tissue	36.790	-121.790	2000	G-38	Nonnative	No	No	No	Nonnative	Sacks et al. 2016
VVBNS35	Tissue	37.435	-122.068	1996	F-12	Nonnative	No	No	No	Nonnative	Sacks et al. 2016
VVBNS36	Tissue	37.580	-122.120	1996	N-7	Nonnative	No	No	No	Nonnative	Sacks et al. 2016
VVBNS40	Tissue	36.832	-121.800	1996-2000	G-38	Nonnative	No	No	No	Nonnative	Sacks et al. 2016
VVBNS43	Tissue	37.595	-122.125	2000	G-38	Nonnative	No	No	No	Nonnative	Sacks et al. 2016
VVBNS45	Tissue	36.800	-121.750	1999	G-38	Nonnative	No	No	No	Nonnative	Sacks et al. 2016
VVBNS46	Tissue	36.630	-121.830	2000	F-12	Nonnative	No	No	No	Nonnative	Sacks et al. 2016
VVBNS47	Tissue	36.790	-121.790	2000	G-38	Nonnative	No	No	No	Nonnative	Sacks et al. 2016
VVBNS48	Tissue	37.435	-122.068	2001	F-12	Nonnative	No	No	No	Nonnative	Sacks et al. 2016
VVBNS49	Tissue	36.800	-121.750	1996-2000	N-7	Nonnative	No	No	No	Nonnative	Sacks et al. 2016
VVBNS50	Tissue	37.435	-122.068	2001	N-7	Nonnative	No	No	No	Nonnative	Sacks et al. 2016
VVBNS51	Tissue	36.832	-121.800	2000	G-38	Nonnative	No	No	No	Nonnative	Sacks et al. 2016
VVBNS52	Tissue	36.800	-121.750	2000	G-38	Nonnative	No	No	No	Nonnative	Sacks et al. 2016
VVBNS54	Tissue	36.790	-121.790	2000	G-38	Nonnative	No	No	No	Nonnative	Sacks et al. 2016
VVBNS55	Tissue	36.790	-121.790	2000	G-38	Nonnative	No	No	No	Nonnative	Sacks et al. 2016
VVBNS56	Tissue	37.440	-122.060	1997	N-7	Nonnative	No	No	No	Nonnative	Sacks et al. 2016
VVBNS57	Tissue	37.440	-122.060	1996	F-12	Nonnative	No	No	No	Nonnative	Sacks et al. 2016
VVBNS58	Tissue	37.440	-122.060	1996	F-12	Nonnative	No	No	No	Nonnative	Sacks et al. 2016
VVBNS59	Tissue	37.440	-122.060	2001	F-12	Nonnative	No	No	No	Nonnative	Sacks et al. 2016
VVBNS60	Tissue	37.610	-122.130	1996	N-7	Nonnative	No	No	No	Nonnative	Sacks et al. 2016
VVBNS61	Tissue	37.610	-122.130	1996	N-7	Nonnative	No	No	No	Nonnative	Sacks et al. 2016
VVBNS62	Tissue	37.610	-122.130	1996	N-7	Nonnative	No	No	No	Nonnative	Sacks et al. 2016
VVBNS63	Tissue	37.580	-122.120	1996	N-7	Nonnative	No	No	No	Nonnative	Sacks et al. 2016
VVBNS65	Tissue	37.580	-122.120	1996	N-7	Nonnative	No	No	No	Nonnative	Sacks et al. 2016
VVBNS67	Tissue	37.480	-122.040	1996	F-12	Nonnative	No	No	No	Nonnative	Sacks et al. 2016
VVBNS69	Tissue	37.450	-121.940	1996	F-12	Nonnative	No	No	No	Nonnative	Sacks et al. 2016
VVBNS70	Tissue	37.480	-122.040	1996	F-12	Nonnative	No	No	No	Nonnative	Sacks et al. 2016

VVBNS72	Tissue	37.500	-122.140	1996	N-7	Nonnative	No	No	No	Nonnative	Sacks et al. 2016
VVBNS73	Tissue	37.595	-122.125	1996	N-7	Nonnative	No	No	No	Nonnative	Sacks et al. 2016
VVBNS74	Tissue	37.440	-122.040	1996	F-12	Nonnative	No	No	No	Nonnative	Sacks et al. 2016
VVBNS75	Tissue	37.610	-122.130	1996	N-7	Nonnative	No	No	No	Nonnative	Sacks et al. 2016
VVBNS76	Tissue	37.595	-122.125	1996	N-7	Nonnative	No	No	No	Nonnative	Sacks et al. 2016
VVBNS77	Tissue	37.630	-122.150	1996	N-7	Nonnative	No	No	No	Nonnative	Sacks et al. 2016
VVBNS78	Tissue	37.595	-122.125	1996	N-7	Nonnative	No	No	No	Nonnative	Sacks et al. 2016
VVBNS8	Tissue	37.595	-122.125	2000	N-7	Nonnative	No	No	No	Nonnative	Sacks et al. 2016
VVBNS81	Tissue	37.630	-122.150	1996	N-7	Nonnative	No	No	No	Nonnative	Sacks et al. 2016
VVBNS82	Tissue	37.595	-122.125	1996	N-7	Nonnative	No	No	No	Nonnative	Sacks et al. 2016
VVBNS83	Tissue	37.630	-122.160	1996	N-7	Nonnative	No	No	No	Nonnative	Sacks et al. 2016
VVBNS84	Tissue	37.630	-122.160	1996	N-7	Nonnative	No	No	No	Nonnative	Sacks et al. 2016
VVBNS85	Tissue	36.832	-121.800	1996-2000	F-12	Nonnative	No	No	No	Nonnative	Sacks et al. 2016
VVBNS86	Tissue	37.460	-121.940	1996	F-12	Nonnative	No	No	No	Nonnative	Sacks et al. 2016
VVBNS88	Tissue	37.430	-122.060	2000	F-12	Nonnative	No	No	No	Nonnative	Sacks et al. 2016
VVBNS89	Tissue	36.790	-121.790	2000	G-38	Nonnative	No	No	No	Nonnative	Sacks et al. 2016
VVBNS9	Tissue	37.435	-122.068	1999	F-12	Nonnative	No	No	No	Nonnative	Sacks et al. 2016
VVBNS90	Tissue	37.440	-122.060	1996	F-12	Nonnative	No	No	No	Nonnative	Sacks et al. 2016
VVBNS92	Tissue	36.790	-121.790	2000	G-38	Nonnative	No	No	No	Nonnative	Sacks et al. 2016
VVBNS93	Tissue	36.790	-121.790	2000	G-38	Nonnative	No	No	No	Nonnative	Sacks et al. 2016
VVBNS94	Tissue	37.580	-122.120	2001	N-7	Nonnative	No	No	No	Nonnative	Sacks et al. 2016
VVBNS95	Tissue	36.750	-121.750	1996-2000	G-38	Nonnative	No	No	No	Nonnative	Sacks et al. 2016
VVBNS96	Tissue	36.790	-121.790	2000	G-38	Nonnative	No	No	No	Nonnative	Sacks et al. 2016
VVBNS97	Tissue	36.832	-121.800	2000	G-38	Nonnative	No	No	No	Nonnative	Sacks et al. 2016
VVBNS98	Tissue	36.750	-121.750	1996-2000	G-38	Nonnative	No	No	No	Nonnative	Sacks et al. 2016

Table S1.2: Measurements of Euclidian distance between first-order relatives (Relatedness >0.4) used to generate estimates of male and female dispersal distances. Genetic relatedness between individuals was determined using the Queller and Goodnight estimator (1989) in the R package 'Related' (Pew et al. 2015) and a random subset (n = 400) of the 19,051 GBS loci.

Ind.1	Ind.1.sex	Ind.2	Ind.2.sex	Distance (km)	quellergt	Used in dispersal Estimation	Reason for exclusion
S14-0843	Unknown	S14-0887	Male	NA	0.949	No	replicate individual?
S19-1797	Unknown	S19-1798	Unkown	NA	0.7161	No	littermates (<6 months)
MAM-2703	Male	MAM-2706	Female	NA	0.6948	No	littermates (<6 months)
S12-0016	Male	S13-1971	Female	6.48	0.6929	Male-Female	
ESRP-R008	Unknown	ESRP-R009	Male	NA	0.6901	No	Undeterined sex
S10-0562	Male	S10-0565	Male	186.60	0.6527	Male-Male	
MAM-3675	Female	MAM-3687	Female	4.28	0.6454	Female-Female	
S14-0856	Female	S14-0872	Female	8.92	0.6018	Female-Female	
S07-0171	Male	S07-0172	Male	NA	0.5992	No	littermates (<6 months)
MAM-2705	Male	MAM-2704	Male	NA	0.5925	No	littermates (<6 months)
S08-0535	Male	S13-1971	Female	0.13	0.5737	Male-Female	
S17-2550	Female	S18-2200	Female	1.33	0.5615	Female-Female	
S09-0779	Female	S09-0268	Male	1.25	0.5447	Male-Female	
S14-0850	Male	S14-0867	Male	4.86	0.541	Male-Male	
MAM-2708	Male	S14-0882	Male	25.16	0.539	Male-Male	
S09-0440	Male	S10-0513	Female	23.05	0.5239	Male-Female	
S09-0280	Male	S09-0440	Unkown	NA	0.5188	No	littermates (<6 months)
S08-0535	Male	S12-0016	Male	6.46	0.5033	Male-Male	
S19-1800	Unknown	S19-1798	Unkown	NA	0.4995	No	littermates (<6 months)
S17-2549	Male	S18-2200	Female	0.22	0.4874	Male-Female	
S10-0188	Male	S10-0191	Male	NA	0.4859	No	littermates (<6 months)
S09-0280	Male	S10-0513	Female	23.05	0.4791	Male-Female	
S17-2549	Male	S17-2550	Female	1.55	0.4554	Male-Female	

MAM-2705	Male	MAM-2706	Female	2.22	0.435	Male-Female	
S19-1800	Unknown	S19-1797	Unkown	NA	0.4338	No	littermates (<6 months)
S14-0855	Female	S14-0861	Female	7.31	0.4291	Female-Female	
S12-0285	Unknown	S12-0286	Unkown	NA	0.4087	No	littermates (<6 months)
ESRP-R006	Female	S14-0863	Male	27.09	0.4019	Male-Female	
MAM-2736	Male	S14-0882	Male	1.43	0.4163	Male-Male	
MAM-3675	Female	MAM-3686	Male	3.25	0.412	Male-Female	
S19-1797	Unknown	S19-1798	Unkown	NA	0.7161	No	littermates (<6 months)

Table S1.3: Location of significant positive beta (*β)* outliers identified in the fox genome using the Bayesian genomic cline analysis and their syntenic position in the dog genome. A list of candidate genes (i.e., putative barrier genes) that were annotated in the dog genome and fell within 500kb of outlier loci were used for gene ontology analysis in Panther (Mi et al. 2013)

Fox Chr/Pos	Dog Chr	Dog Pos	alpha	beta	Genes within 500kb (up or down)
10p 1042020	26	954574 - 954666	-0.0320	0.9544	POLE, PRX2, LRCOL1, FBRSL1, GALNT9, NOC4L, DDX51, EP400, PUS1 †, ULK1, MMP17, SFSWAP, ADGRD1, RAN
10p 29054067	26	30474403 - 30474496	-0.1635	0.9649	CLTCL1, SLC25A1, GSC2, ESS2, TSSK2, DGCR2, ZNF74, SCARF2, KLHL22, MED15, SMPD4, MZT2B, P2RX6, SLC7A4 †, THAP7, LZTR1, AIFM3, CRKL, SNAP29, PI4KA, SERPIND1, TMEM191C, HIC2, UBE2L3, YDJC, CCDC116, SDF2L1, PPIL2, YPEL1
10q 13345183	15	13397607- 13397699	-0.0989	1.0476	TRABD2B, FOXD2, CMPK1, STIL*, TAL1, PDZK1IP1, CYP4X1, CYP4A38, CYP4A11, CYP4B1, EFCAB14, TEX38, ATPAF1, MOB3C, MKNK1
14q 79065499	3	47714986 - 47715078	-0.0367	1.0335	CHD2, FAM174B, ST8SIA2†, SLCO3A1
14q 109943719	3	77969219 - 77969310	-0.0914	1.0644	NA
2pt 26294458	9	26124387 - 26124483	-0.0683	0.9713	NXPH3, SPOP, SLC35B1, FAM117A, KAT7, TAC4, DLX4, ITGA3, PDK2, SAMD14*, SGCA, TMEM92, MRPL27, EME1, LRRC59, ACSF2, CHAD, RSAD1, MYCBPAP, EPN3, SPATA20, CACNA1G, ABCC3, ANKRD40, LUC7L3,
5pt 1057166	19	21227905 - 21227998	-0.2882	0.9584	ARHGEF4, FAM168B, PLEKHB2†,
6p 18141824	22	17956156 - 17956248	0.1116	0.9666	Vulp_V002774¥
6p 18712812	22	18525157 - 18525248	0.0698	1.0087	Vulp_V002775¥
9p 13426646	25	38260535 - 38260628	0.1699	1.0493	CUL3, DOCK10 †, NYAP2,

* Denotes outlier locus is within the open reading frame of a gene

† Denotes closest gene to outlier window

¥ These correspond to genetic regions that differentiated tame and aggressive red foxes (Kukekova et al., 2018)

Table S1.4: Location of significant negative beta (*β)* outliers identified in the fox genome using the Bayesian genomic cline analysis and their syntenic position in the dog genome. A list of candidate genes (i.e., putatively under selective introgression) that were annotated in the dog genome and fell within 500kb of outlier loci were used for gene ontology analysis in Panther (Mi et al. 2013). The directionality of introgression was inferred using the alpha parameter (*α)*, where negative values of alpha indicate excess nonnative ancestry among putative hybrids while positive values indicate excess native Sacramento Valley ref fox (SVRF) ancestry.

Fox Chr/Pos	Dog Chr	Dog Pos	alpha	beta	Genes within 500kb (up or down)	Directionality of Introgression
11p 36468907	21	15161280 - 15161372	-0.2493	-0.8197	DLG2*	Nonnative > SVRF
11q 40766774	23	40518467 - 40518559	-0.0357	-1.2252	-	Nonnative > SVRF
15p 22805225	31	17168312 - 17168404	-0.3435	-0.9341	NCAM2*	Nonnative > SVRF
15q 52114266	28	11511106 - 11511197	-0.1182	-1.1275	GOLGA7B, CRTAC1, R3HCC1L, LOXL4, HPS1†, HPSE2	Nonnative > SVRF
1p 24375627	1	98310009 - 98310102	-0.2644	-1.2298	ZNF169, PTPDC1, BARX1, PHF2, WNK2, NINJ1, SUSD3, FGD3, BICD2, IPPK, CENPP, MIRLET7D, MIRLET7F, MIR8893†	Nonnative > SVRF
2q 30666117	2	30921505 - 30921596	0.3217	-1.0576	CALML5, NET1, TUBAL3, UCN3, AKR1C3†	SVRF > Nonnative
3q 73737915	6	73090796 - 73090888	0.2057	-0.7663	-	SVRF > Nonnative
5pt 30917767	19	51125309 - 51125401	-0.1530	-1.3696	KIF5C, LYPD6B, LYPD6, MMADHC†	Nonnative > SVRF
8p 16531821	27	16333755 - 16333834	0.2810	-0.7870	PKP2, YARS2, DNM1L, FGD4 *, BICD1, KIAA1551	SVRF > Nonnative

* Denotes outlier locus is within the open reading frame of a gene
† Denotes closest gene to outlier window

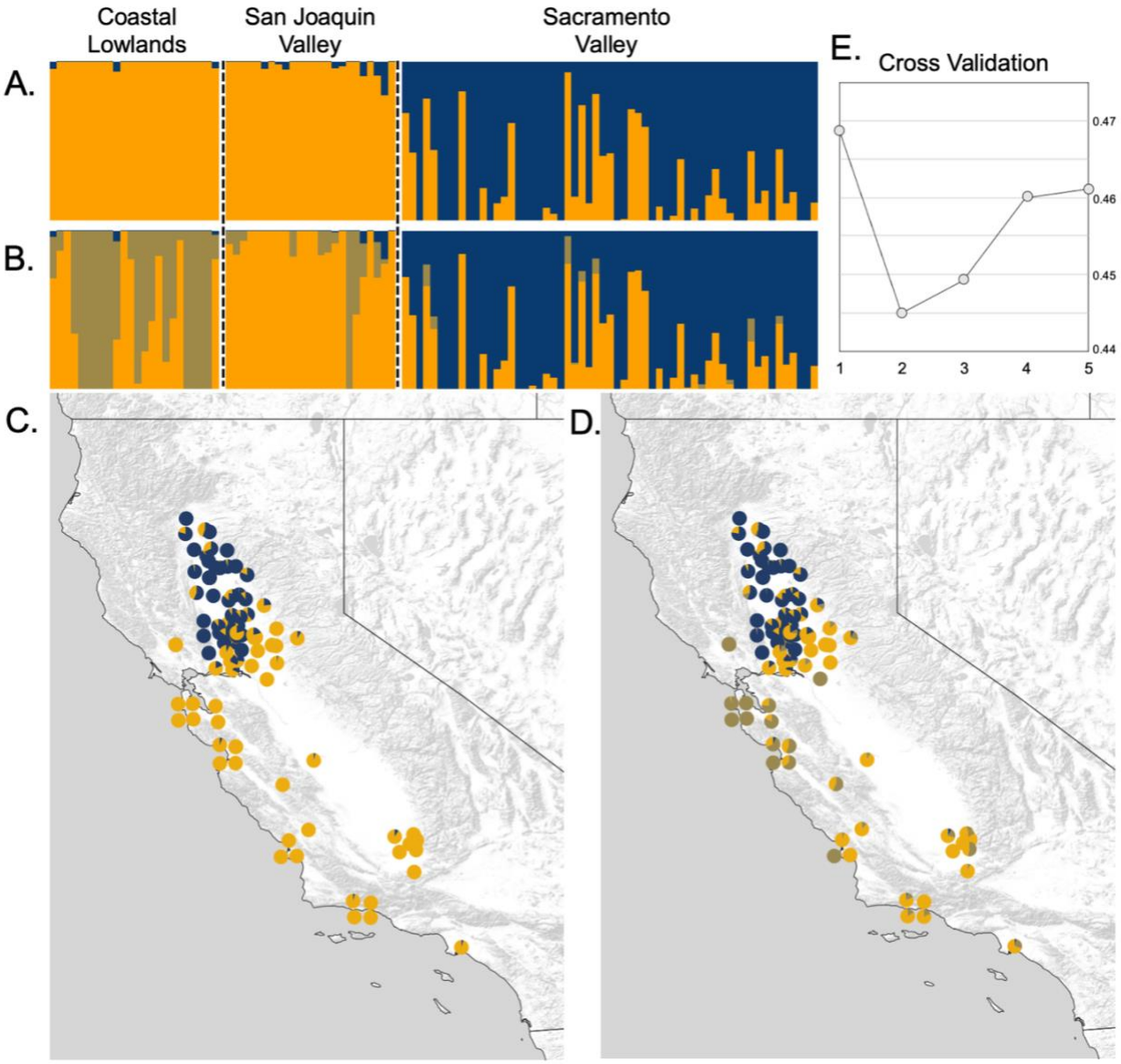

Figure S1.1: Admixture results for (A, C) K = 2 vs (B, D) K = 3 genetic clusters, and (E) cross validation analysis (10-fold) indicating the highest support for K = 2 genetic clusters. At K = 2 genetic clusters, the nonnative population was homogeneous across the San Joaquin valley and coastal lowland regions (A, C). At K = 3 genetic clusters the nonnative population was structured by coastal versus valley regions (B, D).

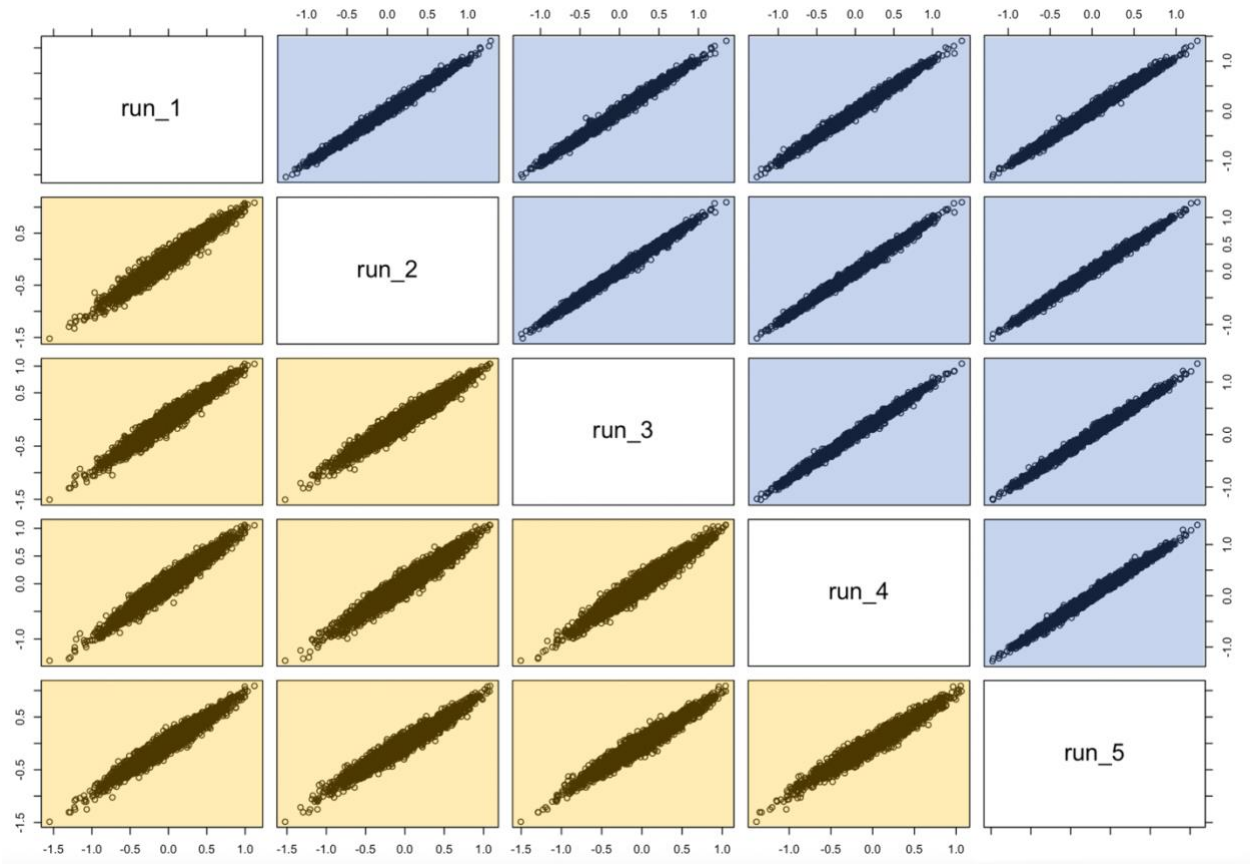

Figure S1.2: Pairwise relationships among 5 replicate runs of Bayesian genomic cline analysis in *bgc* (Gompert & Buerkle, 2012), illustrating that the centers for α (blue rectangles) and *β* (yellow rectangles) loci were highly concordant among five replicate chains for the subset of ancestry informative markers ($AF_{DIFF} > 0.2$) used in the analysis. On average values of alpha and beta were strongly correlated between loci across independent runs (alpha-$r^2 = 0.997$; beta-$r^2 = 0.985$)

Chapter 2: Population genomics reveals distinct demographic histories among extant gray fox (*Urocyon*) lineages in North America

Details of collaboration: In this chapter I present my work on the demographic histories of extant members of the gray fox lineage. I designed the research with input from Dr. Ben Sacks. The collaborators listed below provided samples, offered laboratory support, and contributed to interpretation of the results. I have performed all the analyses presented in this dissertation.

SOPHIE PRECKLER-QUISQUATER,[1] ELIZABETH M. KIEREPKA[2], DAWN M. REDING[3], ANTOINETTE J. PIAGGIO[4] and BENJAMIN N. SACKS[1,5].

[1]Mammalian Ecology and Conservation Unit, Veterinary Genetics Laboratory, School of Veterinary Medicine, University of California, Davis, One Shields Avenue, Davis, CA, 95616, USA
[2]North Carolina Museum of Natural Sciences, Department of Forestry and Environmental Resources, North Carolina State University, Raleigh, NC, USA
[3]Department of Biology, Luther College, Decorah, IA, USA
[4]USDA, Wildlife Services, National Wildlife Research Center, Wildlife Genetics Lab, Fort Collins, CO, USA
[5]Department of Population Health and Reproduction, School of Veterinary Medicine, University of California, Davis, Davis, CA, USA

Abstract

North American gray foxes (*Urocyon cinereoargenteus*) are composed of two highly divergent, reciprocally monophyletic lineages. Although they currently interbreed along a narrow contact zone in the Great Plains, their phylogenomic divergence suggests that for most of the past million years, these populations must have been reproductively isolated from one another. Given their vagile nature and the lack of clear physical barriers separating them, we hypothesized that one or both lineages occupied smaller ranges removed from the current zone of contact throughout most of the Pleistocene and achieved contact only recently through a massive Holocene expansion. To investigate this hypothesis, we explored their demographic history and population structure using a combination of whole-genome and reduced-representation sequencing. Pairwise sequential Markovian coalescent (PSMC) modeling, stairway plots, and summary statistics of eastern and western gray foxes on either side of the contact zone showed

contrasting demographic trajectories, with the trajectory of the eastern population declining and the trajectory of the western population increasing for most of their post-divergence history; during the latter portion of the last (Wisconsinan) glacial cycle and most of the Holocene, the eastern trajectory increased, and the western trajectory declined. Correspondingly, the eastern lineage exhibited much lower genetic diversity than the western lineage, a cline in diversity consistent with a westward expansion front, and minimal genetic structuring. In contrast, the western lineage exhibited population structure and locally varying demographic histories, reflecting long-term occurrence over a broad region of the continent. The recurrent declines in the eastern population may have kept them both geographically and demographically restricted to the southeast for much of their evolutionary history, resulting in the deep divergence and limited gene flow currently observed between lineages. Additionally, population structure and variable demographic histories within the western lineages may reflect separation in distinct glacial refugia and subsequent gene flow across the western gray fox range.

Keywords: demographic history, divergence, glacial refugia, gray fox, pairwise sequentially Markovian coalescent, stairway plot, *Urocyon cinereoargenteus*

1 | INTRODUCTION

Climatic fluctuations over the Quaternary Period (i.e., the past 2.6 million years) have been a major driver of lineage differentiation and have shaped species distributions and patterns of diversity across the landscape (Hewitt, 1996; Hewitt, 2000; Hewitt, 2004). Cycles of glacial expansion and retreat resulted in shifts in habitat and food resources causing both the distributions and sizes of many populations to contract and expand. These geographic and demographic shifts have often resulted in variable selection, drift, and admixture between

previously separated lineages during interglacial periods, leaving unique signatures in the genomes of present-day individuals (Lessa et al., 2003; Hewitt, 2004). Here, we investigate such signatures of historical demography and range dynamics in a North American carnivore to understand an unusually deep divergence between lineages in the absence of an apparent physical barrier.

The gray fox (*Urocyon cinereoargenteus*) and its diminutive relative, the island fox (*Urocyon littoralis*), are the only extant members of the genus Urocyon, which represents the earliest extant genus to branch off the canid family tree. Within the gray fox, previous studies have identified deep divergence (approximately 1 MYA) and reciprocal monophyly between lineages east and west of the Great Plains in North America (Goddard et al., 2015; Reding et al., 2021; Kierepka et al., in review). This divergence corresponds to the Early-Middle Pleistocene Transition (1.4–0.4 MYA; Head and Gibbard 2015) in the Irvingtonian land mammal age, which is substantially earlier than those typically describing intraspecific divisions for most North American carnivores (e.g., Aubry et al. 2009; Reding et al. 2012; Puckett et al. 2015). The reciprocal monophyly of eastern and western gray foxes further suggests that the two lineages have been reproductively isolated for most of their post-divergence history, although admixed individuals occur today along a narrow contact zone (Kierepka et al., in review).

Whether (incomplete) post-zygotic barriers operate currently to minimize gene flow and maintain a narrow contact zone is unknown. Regardless, a pre-zygotic explanation would be needed to explain their initial divergence. One possibility is that eastern and western refugia initially became isolated from one another in distinct refugia by the emergence of inhospitable habitat between them and remained allopatric until later Pleistocene or Holocene environments favored expansion, bringing them back into secondary contact. As a step in assessing such a

scenario, we sought to reconstruct demographic histories and characterize population structure to better understand how population expansions and contractions may have contributed to contemporary distributions, patterns of diversity, and observed secondary contact between lineages.

Based on observations in other North American mesocarnivores with similar levels of divergence, each gray fox lineage could potentially reflect multiple evolutionarily distinct populations (Harding and Dragoo, 2012; Ferguson et al., 2017; McDonough 2022). Although it seems clear that populations within each gray fox lineage are currently connected by gene flow, our interest was whether multiple independent refugia potentially sustained contracting lineages during glacial periods (Goddard et al. 2015; Reding et al. 2021; Kierepka et al., in review). Second, we were interested in the relationship of the island fox to California gray foxes. Previous mitochondrial studies found that the mitochondrial haplotypes present on the islands were most closely related to those of gray foxes from northern California, despite the proximity of the southern gray fox population to the Channel Islands (Goddard et al. 2015; Hofman et al. 2015). We therefore sought to use nuclear genetic markers to investigate genetic connectivity of island foxes to gray foxes of northern and southern California.

Here we use a combination of whole genome and reduced representation sequencing data from the eastern and western gray fox lineages as well as from the Channel Islands to compare demographic histories of the eastern and western lineages and to investigate population structuring and heterogeneity of demographic histories within each of these and the island fox lineages. We synthesize these results with previous findings to more fully describe the evolutionary dynamics of these foxes in the context of past climatic cycles.

2 | MATERIALS AND METHODS

2.1 | Sampling and laboratory methods

For whole genome sequencing (WGS), we selected 26 gray foxes from both the eastern (n = 14) and western (n = 12) sampled ranges, as well as a single island fox (Table S1). We selected these individuals from a larger GBS dataset of foxes from throughout North America, ensuring that they were geographically representative and did not show any admixture between the eastern and western lineages (Kierepka et al. in review). In addition, we used the raw WGS reads downloaded from GenBank of two California gray foxes (18–21x) and six island foxes, one from each of the Channel Islands (Robinson et al. 2016; Robinson et al. 2018). We also used the GBS data from the 197 non-admixed samples from the east (n = 83) and west (n = 114) that were used in the study by Kierepka et al. (in review).

For WGS libraries, we fragmented 200 ng of each DNA sample with a Covaris E220 sonicator (Covaris, Woburn, Massachusetts) and prepared genomic libraries using a NEBNext® Ultra™ II DNA Library Prep kit for Illumina, following manufacturer's instructions, except that we used half reactions (San Diego, CA, USA). We targeted insert sizes of 300–400 bps using AMPure XP magnetic beads (Beckman Coulter, Pasadena, CA). We then PCR-amplified the DNA using unique forward- and reverse-indexed custom, Illumina-compatible primers for each sample. The PCR conditions were as follows: Initial denaturation at 98 °C for 30 sec; 7 cycles of 98 °C for 10 sec and 65 °C for 75s, followed by a 65 °C extension step for 5 min. We quantified the individual libraries using a Qubit fluorometer (Qiagen Inc, Valencia, CA), pooled them in equal concentrations, and submitted the final library to the University of California, Davis Genome Center for paired end 150 bp sequencing on an Illumina Novaseq S4 lane.

Detailed methods regarding extraction and library preparation can be found in Kierepka et al. (in review). Briefly, tissue samples were extracted using Qiagen DNEasy Blood and Tissue kits (Qiagen Inc, Valencia, CA), and normalized to 10 ng/uL prior to library preparation. A GBS approach modified from Elshire et al. (2011) was used to construct reduced representation libraries with the high-fidelity restriction enzyme, *Nsil-HF* (an equivalent to *EcoT22I*: New England Biolabs Inc.). Resulting libraries were sent to the University of California, Davis Genome Center DNA Technologies core for 100-bp single-end sequencing on an Illumina HiSeq4000.

2.2 | Alignment and SNP Calling

For the WGS dataset, we trimmed raw reads using bbduk (B. Bushnell, https://sourceforge.net/projects/bbmap) and mapped trimmed reads to the dog genome (CanFam3.1), along with the Y chromosome (Oetjens et al., 2018), using BWA-MEM. We then marked duplicate reads with PICARD (Broad Institute, http://broadinstitute.github.io/picard), and used SAMtools to remove them (-F 1024), along with non-primary reads (-F 256). We used a relaxed mapping quality filter (-q 10) in SAMTOOLS v1.9 (Li et al., 2009) to account for increased levels of divergence between our target species and the reference genome.

The GBS library was first demultiplexed and adapters were trimmed using GBSX v1.3.jar (Herten et al 2015). Resulting reads were similarly aligned to the dog genome (CanFam3.1) using BWA-MEM (Li and Durbin 2010; Li 2013) and a relaxed mapping quality filter (-q 10). SNP calling was conducted using the reference genome "ref_map.pl" pipeline in Stacks (v2.53, Catchen et al. 2011) and the 'populations' module was used to filter out low frequency variants (--min_maf 0.02) and SNPs with excess heterozygosity (--max_obs_het 0.6)

that could reflect paralogs. We removed the lowest quality individuals that were missing >90% of SNPs (--mind 0.9). We then filtered out SNPs that were called in <80% of the remaining individuals (--geno 0.2) and identified a final maximum SNP missingness cutoff of 32% (---mind 0.32). Additionally, we filtered out SNPs to only include autosomes.

2.3 | Variable post-divergence demography between eastern and western gray fox lineages

We used a pairwise sequentially Markovian coalescent (PSMC) approach to assess the role of variable demography between eastern and western gray fox lineages in facilitating long-term divergence (Li and Durbin 2011). For this analysis, we used the low coverage (4–7x each) WGS diploid consensus sequences (in fasta format) of 14 gray foxes from the east and 4 from West Texas. We first subsetted the aligned WGS sequences to include only the autosomes using bedtools (v2.27.1; Quinlan et al. 2010). We then converted the bam files to fastq files using 'vcfutils.pl vcf2fq' filtering sites that had low base (-q30) and mapping (-Q30) quality scores. To minimize the impact of allelic dropout and paralogs, we excluded all sites for which read depth was less than one-third of (–d minDP) or more than twice the average depth (–D maxDP) across the genome for each sample using the samtools mpileup command and the bcftools call command. Lastly, we used the program 'fq2psmcfa' within the PSMC software to transform the consensus sequence into the fasta-like format files for downstream analysis.

Low-coverage data can limit resolution and introduce biases through the misinterpretation of heterozygous sites as homozygous sites. While broader demographic trends (e.g., expansions and contractions) are typically preserved, samples with >18x coverage are recommended to accurately recreate demographic trajectories (Nadachowska-Brzyska et al., 2016). Alternatively, a false negative rate (FNR) can be applied within the PSMC program to

correct for these biases (Nadachowska-Brzyska et al., 2016; Hawkins et al., 2018; Sarabia et al., 2021). To determine appropriate FNR corrections for low coverage samples, we first down sampled one of the high coverage western gray foxes (18x) at a range of corresponding low coverage depths [4x, 5x, 6x, 7x, 8x] using a combination of samtools (v1.9) and bcftools (v1.10.2). We then tested different FNR corrections until we were able to recover the original high coverage PSMC trajectory. From here, we fit a log-transformed linear model to the data, which allowed us to select an appropriate FNR correction for each low coverage sample. As an independent validation, we compared the demographic reconstructions of two low coverage samples (Northern California = 7.7x; Santa Cruz Island = 4.9x), after applying FNR corrections, to the trajectories of high coverage samples from these same populations (Northern California = 21x; Santa Cruz Island = 23x).

Demographic histories were then reconstructed using 64 atomic time intervals (-p "4 + 25 × 2 + 4 + 6") as in previous studies of other canids (Wang et al. 2020). Additionally, the upper limit of the TMRCA was set to 15 (-t 15) and the theta/rho value was set to 5 (-r 5). We ensured that sufficient (>20) recombination events occurred within each atomic interval and removed intervals that did not have enough resolution. To convert from coalescent units to absolute units of both population size and time, we assumed a generation time of 2 years (Goddard et al., 2015) and a mutation rate of 4.5×10^{-9} (Koch et al., 2019) per site per generation. We then used the program psmc_plot.pl to visualize the trajectory of demographic history across time for all the eastern and western (Texas) individuals, applying an appropriate FNR correction where applicable.

2.4 | Population structure and patterns of genetic diversity

We examined population structure within the eastern and western regions using the GBS dataset. We first examined ancestry assignment using the Bayesian program Admixture (Alexander et al. 2009) assuming 1–5 genetic clusters (K = 1–5) over five independent runs for the eastern and western gray foxes separately. We then reported the K values that minimized the cross-validation error and best explain the structure within each lineage. We also performed a multi-dimensional scaling analysis (MDS) in Plink (Purcell et al. 2007) to assess whether geographic location was correlated with the positioning of western and eastern gray foxes in the MDS plots.

We calculated the genome-wide heterozygosity for each individual to assess differences between eastern and western lineages as well as to explore spatial trends in diversity within the eastern and western lineages**.** We first created a consensus ancestral fasta file by merging the bam files of three *Vulpes* foxes (kit fox, *V. macrotis*; red fox, *V. vulpes*; arctic fox, *V. lagopus*) and three *Canis* species (golden jackal, *C. aureus*; coyote, *C. latrans*; gray wolf, *C. lupus*). This collection was then used to estimate the site allele frequency likelihood (-dosaf 1) using a genotype likelihood estimation (-gl 1) in ANGSD (Nielsen et al., 2012), removing sites with low read (-minQ 20) or mapping (-minMapQ 20) quality as well as sites with an overall depth <0.5x or >2.5x the individual mean. Using the ANGSD-based program realSFS, we then generated the 1D-SFS for each individual. To infer levels of heterozygosity we extracted the individual SFS and divided the number of observed heterozygous sites by the total number of sites (i.e., homozygous ancestral, heterozygous, and homozygous derived). We explored fine-scale patterns across the landscape using an interpolated, inverse distance weighted surface in QGIS (v3.22.8).

2.5 | Comparison of demographic histories within the eastern and western lineages

Using multiple analyses that each highlight demographic changes at different temporal scales, we then compared demographic trajectories of distinct populations within the eastern and western lineages as determined based on the population structure analyses above. We first reconstructed the deeper time-scale demographic histories using the PSMC for the remaining western gray foxes from New Mexico (n = 3), Nevada (n = 2) and California (n = 3) as well as for the island foxes (n = 7). We followed the same procedure as described above.

More recent demographic history was reconstructed using a stairway plot analysis (v2.1.1, Liu et al., 2020), which provides a flexible approach to infer fluctuations in effective population size (N_e) over time separately for each population (Liu et al., 2015). Briefly, this approach maximizes the composite likelihood of the observed site frequency spectrum (SFS) and, as with the PSMC analysis, does not rely on a priori hypotheses of demographic history, as is typically required for most SFS based approaches (Gutenkunst et al., 2009). We utilized the GBS dataset for this analysis as we expected the greater number of individuals to result in a more accurate representation of the true SFS. We generated an independent SFS for each geographic region that indicated distinct genetic structuring based on previous analyses (section 2.4).

To generate the 1D-SFS for each of our focal populations, we used the same ancestral fasta file described above (section 2.4). This was then used to estimate the site allele frequency likelihood (-dosaf 1) using a genotype likelihood estimation (-gl 1) in ANGSD (Nielsen et al., 2012), removing sites with low read (-minQ 20) or mapping quality (-minMapQ 20) as well as sites with an overall depth <0.5x or >2.5x the global mean. Additionally, we excluded a site if it was not covered in 80% of individuals within a population. The exception to this being in northern California where we only included sites that were called in 100% of individuals as the sample size was low (n = 5). Using the ANGSD based program realSFS, we then generated the

1D-SFS for each population and used this to parameterize the input file for the stairway plot analysis. To convert coalescent units to absolute units of population size and time we used the same parameters for generation time and mutation rate as those described for the PSMC analysis above. Additionally, changes in effective population sizes across time were estimated using the median of 200 bootstrap replicates and we generated 95% confidence intervals to evaluate precision of the estimations.

To investigate whether the recent demographic trajectories within the eastern and western lineages supported a stable, increasing, or decreasing population, we also we used two different measures of genetic diversity, Tajima's θ (θπ) and Watterson's theta (θs), both of which are affected by demographic history (Tajima 1983; Watterson 1975; Tajima 1989; Wakeley and Sargsyan 2009). When diversity has been stable, these two estimators should be equal. However, if a population has been increasing, there will be an excess of rare variants, and $\theta s > \theta \pi$. In contrast, if the population has been decreasing, rare variants will be lost, leaving an excess of intermediate frequency variants where $\theta s < \theta \pi$. A scaled parameter $\Delta\theta$ ($[\theta\pi - \theta s]/([\theta\pi + \theta s]/2)$ can be used to compare recent changes in diversity, where positive values indicate a demographic contraction and negative values indicate an expansion (Peek et al. 2021). To generate estimates of Tajima's and Watterson's theta, we again generated the 1D-SFS for each of our distinct populations. We then computed the values of theta (-doThetas 1) along each chromosome, with the population-based SFS as a prior (-pest) and extracted these using the thetaStat function in ANGSD. We used a one sample t-test to determine whether $\Delta\theta$ values deviated significantly from zero for each population, supporting either expansion or contraction.

Lastly, we compared patterns of linkage disequilibrium (LD) between the eastern and western lineages as these can offer insights into the contemporary effective population sizes

(Sved, 1971; Hill, 1981; Waples et al. 2016). We used the whole genome data and inferred LD between loci separately within the eastern and western lineage from genotype likelihoods using the program ngsLD (Fox et al., 2019). We ran the analysis on a heavily thinned dataset (0.1%) to reduce computational intensity, and only calculated LD between sites within 2 Mb of one another along the same chromosome. We then generated LD decay curves using the internal plotting script in R (fit_LDdecay.R).

3 | RESULTS

We generated 27 whole genome sequences, which had an average coverage of 5.6x (SD = 0.8x; Table S1) (Fig. 1). Additionally, we incorporated previously sequenced high-coverage gray fox genomes from California (n = 2) and island foxes (n = 6), which had average coverages of 22x (SD = 2.2x) (Robinson et al., 2016; Robinson et al., 2018). The GBS samples had an average coverage of 34x (SD = 21x), and the final GBS dataset contained 29,233 variable sites.

3.1 | Variable demography between geographically proximate eastern and western gray fox lineages

We systematically applied FNR corrections (Fig. S1) to all PSMC plots generated from lower coverage whole genome sequences and determined these to be sufficient based on comparisons of high and low coverage samples that originated from the same populations (Fig. S2). The PSMC plots derived from eastern gray foxes were consistent with a history of recurrent genetic bottlenecks throughout much of their evolutionary history since their divergence from the western lineage, with no evidence of large expansions. In contrast, the plots derived from

western gray foxes from Texas had strong signatures of expansion after their divergence from the eastern lineage with peaks in population size occurring during the last glacial period (Fig. 2).

3.2 | Population structure and patterns of genetic diversity

Within the eastern lineage, the MDS analysis indicated limited genetic structuring with no clear evidence of geographic structure (Fig. 3A). The admixture analysis indicated the strongest support (i.e. lowest cross-validation error) for a single (K = 1; CVE = 0.211) or two (K = 2; CVE = 0.213) genetic clusters and also showed limited regional structure and minimal differentiation (F_{ST} = 0.06) between clusters (Fig. 3C; Fig. S3)). In contrast, the MDS analysis indicated significant genetic structuring by region within the western lineage (Fig. 3B). The admixture analysis in the west found the highest support for two (K = 2; CVE = 0.389) or three (K = 3; CVE = 0.394) genetic clusters with higher average levels of genetic differentiation (F_{ST} = 0.114 – 0.118) between clusters (Fig. 3D; Fig. S3).

We identified significantly lower overall heterozygosity in the eastern (M = 6.0 x 10^{-4}, SE = 5.4 x 10^{-6}) relative to the western (M = 9.8 x 10^{-4}, SE = 1.3 x 10^{-5}) population ($p << 0.001$). In the eastern lineage, we identified a bias in the data where coverage was negatively correlated with heterozygosity ($r^2 = 0.29$, $p << 0.001$), possibly due to an overcompensation of heterozygous call rates at lower coverage levels. We therefore corrected for this in downstream analyses when assessing the spatial patterns of diversity. This relationship between coverage and heterozygosity was not detected in the western lineage, likely due to higher average sequencing depth. Using multiple regression, we identified a significant decrease in heterozygosity along a northwest gradient in the eastern lineage ($r^2 = 0.46$, $p << 0.001$), which was visualized using inverse distance weighting (Fig. 4). In the west, there was a significant decrease in heterozygosity along

a western gradient from Texas to California ($r^2 = 0.71$, $p << 0.001$; Fig. 4). In California, diversity was significantly higher in southern than northern samples ($p<<0.001$).

3.3 | Distinct demographic trajectories within the eastern and western gray fox lineages

The PSMC results indicated that the eastern demographic trajectories were closely aligned (Fig. 2). In the western population however, the gray fox individuals from California had distinct demographic trajectories when compared to those generated from Texas gray foxes (Fig. S4). Additionally, there were notable differences between PSMC trajectories of the gray foxes from northern California and that of the gray fox from southern California, where the northern individuals showed a stronger signal of decline throughout their demographic histories when compared with the southern individuals. This difference was particularly evident during the last glacial period when the northern California gray foxes showed continued declines while the trajectory of the southern California individual indicated a demographic increase. Demographic reconstruction using gray foxes sampled between Texas and California showed intermediate PSMC trajectories, which was likely a result of their intermediate ancestry that was identified above and highlights the sensitivity of the PSMC analysis to population structure (Fig. S4).

The island foxes also showed variation in the resolution of their demographic trajectories, despite high coverage levels (>20x) (Fig. S5), which could be a result of the distortion of coalescent patterns due to extremely low heterozygosity levels reported in the island fox populations (Li and Durbin, 2012; Armstrong et al., 2020; Robinson et al. 2016). This interpretation is further supported by the correlation between increased temporal resolution of the PSMC trajectories and the greater reported heterozygosity levels across the islands (Fig. S5). Using the individual with the highest heterozygosity from the island fox lineage (Santa Catalina

Island), we identified a very close match between PSMC trajectories of the island fox and the southern California gray fox until approximately 50,000 YBP, after which their trajectories differed substantially (Fig. 5). This timeframe is much older than the oldest-known faunal remains found on the islands, which were 7,100 YBP based on radiocarbon dating (Rick et al., 2009).

Based on stairway plots, the demographic pattern in the east showed a strong signature of expansion after the end of the Wisconsinan glaciation (Fig. 6A). The Texas population indicated a sharp decline after the end of the last glacial period that was followed by a period of stability and a small increase approximately 1,500 years ago (Fig. 6B). The northern California population underwent a decline that began around the start of the last glacial period and persisted throughout the Holocene (Fig. 6C). In contrast, the population size in southern California reached a peak during the last glacial period but showed persistent declines throughout the Holocene, similar to the trend observed in northern California (Fig. 6D).

Within the eastern population, we identified a significant signature of recent population expansion based on the scaled delta theta parameter ($\Delta\theta = -0.20$, $p<<0.001$). The population in Texas also exhibited an expansion signature ($\Delta\theta = -0.06$, $p<<0.001$), but it was smaller than that in the eastern population. In contrast, both the northern ($\Delta\theta = 0.045$, $p<<0.001$) and southern ($\Delta\theta = 0.016$, $p<0.05$) California populations showed significantly positive values of $\Delta\theta$, with the signal of diversity loss in northern California stronger than that in southern California (Fig. 7). Observed patterns of linkage disequilibrium also supported the general trend of stronger expansion signals in the eastern population relative to the west. In the eastern population, LD decays to an $r^2 < 0.2$ within 35kb while within the western population $r^2 < 0.2$ within 150kb supporting faster rates of decay in the eastern relative to the western gray fox population.

Additionally, the western population had a higher intercept, consistent with a smaller effective population size (Rogers, 2014). We also found that the asymptote was higher within the western population, which could be potentially attributed to population structure (Fig. 8) (Fox et al. 2019).

4 | DISCUSSION

The primary objective of this study was to compare the demographic histories of eastern and western gray foxes to identify how variable demographic patterns played a role in driving ancient divergence and maintaining long-term differentiation between lineages. Additionally, we sought to assess population structure and geographic patterns of diversity within the eastern and western ranges, and to synthesize these patterns with demographic histories to characterize population dynamics in space and time relative to climatic cycles.

4.1 | Demography as a driver of long-term divergence between eastern and western gray fox lineages

The results of the PSMC and stairway plot analyses suggest that after its divergence from the western gray fox the eastern gray fox population underwent recurrent demographic declines coinciding with major glaciation events. Additionally, the eastern population had significantly reduced levels of genetic diversity compared with the western population, which is consistent with the steady decline in effective population size over time. Thus, it seems plausible that for most of the late Pleistocene, the eastern gray fox was restricted to a southeastern portion of the continent far from the eastern extent of the western gray fox range. This scenario also accords with previous interpretations based on the fossil record and mitochondrial data (Bozarth et al., 2011).

In contrast to the eastern lineage, the PCMS plots for western gray foxes from Texas supported a major demographic expansion well into the Wisconsinan glacial period. Gray foxes from southwestern Texas also had significantly greater genetic diversity than those from the eastern US or from other parts of the western gray fox range. Although we did not sample from further south, it seems likely that our Texas samples reflected a larger refugium including northern Mexico and possibly further south. Regardless of the extent, the high heterozygosity and population size indicated by the PSMC suggested that this population likely reflected one of the primary refugia for the western lineage. Despite evidence that supports increasing demographic trajectories of western gray foxes in Texas, there is little to no evidence in the fossil record of expansion into eastern Texas or farther since the end of the last glacial maximum (Graham and Lundelius, 2010). Thus, we hypothesize that prior to the last glacial maximum, the lineages were kept apart primarily through the small size and restricted distribution of the eastern lineage.

4.2 | Holocene expansion as a driver of secondary contact between eastern and western gray fox lineages

In contrast to the long-term decline of the eastern gray fox trajectory ending near the last glacial maximum, several lines of evidence indicate that this lineage experienced a significant demographic expansion during the Holocene, including (1) a rapid increase in effective population size approximately 7,000 YBP, as observed in the stairway plot analysis, (2) a significantly negative scaled $\Delta\theta$ value, (3) a high rate of linkage disequilibrium decay, (4) reduced levels of heterozygosity along the presumed expansion front, and (5) limited genetic structuring across the population. Although we did not sample gray foxes from the northeast,

studies using mitochondrial DNA also found evidence of an eastern expansion that continued into recent time at more northerly latitudes (Bozarth et al., 2011; Reding et al., 2021). These studies included foxes as far north as Vermont and New Hampshire with an overall latitudinal sampling range nearly double that in our study (Bozarth et al. 2011, Reding et al 2021). Additionally, the fossil record supports a clear pattern of post-Pleistocene expansion, from a presumed southeastern refugia, both to the north and to the west (Graham and Lundelius, 2010).

While we also observed recent expansion signatures in the Texas population as evidenced by the stairway plots and the negative scaled $\Delta\theta$ value, these were not nearly as strong as those in the eastern US. This set of findings suggests that the primary driver of secondary contact was an expansion of eastern gray foxes westward. While introgressive gene flow has been previously identified in the southern Great Plains, the directionality and timing of this gene flow remains unknown. Based on the findings in our study, we would predict that gene flow could be asymmetrical, specifically dominated by that from eastern into western gray foxes. Analyses of WGS data from within the hybrid zone could be used to assess directionality, as well as timing, of gene flow.

4.3 | Demographic patterns of western gray and Island foxes

Overall, PSMC plots indicated net demographic declines in both the northern and southern California populations until the Sangamonian interglacial period (approximately 100,000 years ago), at which time the southern California trajectory began to increase. This increase contrasted both with trajectories of northern California gray foxes and island foxes, which experienced only slowed (northern) or halted (island) population declines during the same period. Given that island foxes diverged from the western gray fox lineage only approximately 10,000 years ago,

this difference was unexpected. It is possible that the trajectory represented by southern California gray foxes was distorted by admixture that occurred after divergence from island foxes. Such a scenario would be consistent with the large signal of expansion from the Texas foxes observed in the stairway plot. Mitochondrial data further support such a scenario, showing connectivity of southern California to Nevada that is not shared with northern California (Goddard et al. 2015).

Goddard et al. (2015) identified a similar pattern using demographic reconstructions from mitochondrial DNA. The historical demographic trajectory of the gray fox sampled from southern California is largely similar to that of the northern California individual, however we identified higher effective population sizes at deeper time scales in the south. Additionally, we identified an increase in effective population size of the southern CA population during the Wisconsin glaciation (85,000 – 11,000 YBP), while the demographic trajectory in the north showed sharp declines.

CONCLUSION

We identified unique demographic histories between eastern and western gray fox lineages that may have contributed to their ancient divergence and continued differentiation. Specifically, the recurrent demographic declines in the east may have limited any major geographic expansions, ultimately maintaining allopatry between lineages for much of their evolutionary history. In contrast, the western gray fox lineage has maintained much higher levels of genetic diversity and complex population structure. Future analysis including genomes from foxes in the admixture zone between eastern and western gray foxes can further elucidate the directionality and timing of secondary contact, as well as other evolutionary dynamics, such as potential role of

selective introgression or post-zygotic reproductive barriers associated with genomic incompatibilities.

ACKNOWLEDGEMENTS

We thank the landowners, fur trappers, USDA Wildlife Services personnel, and S. Riley (NPS), J.Beasley (Savannah River Ecology Laboratory, University of Georgia) and E. Boydston (USGS) for providing tissue samples and extracted DNA for this study. Funding was provided by the University of California, Davis, Mammalian Ecology and Conservation Unit.

REFERENCES

Alexander, D.H., Novembre J., & Lange, K. (2009). Fast model-based estimation of ancestry in unrelated individuals. *Genome Research*, 19(9), 1655–1644.

Armstrong, E. E., Taylor, R. W., Miller, D. E., Kaelin, C. B., Barsh, G. S., Hadly, E. A., & Petrov, D. (2020). Long live the king: Chromosome-level assembly of the lion (Panthera leo) using linked-read, Hi-C, and long-read data. *BMC Biology*, *18*(1), 3.

Aubry, K. B., Statham, M. J., Sacks, B. N., Perrine, J. D., & Wisely, S. M. (2009). Phylogeography of the North American red fox: Vicariance in Pleistocene forest refugia. *Molecular Ecology*, *18*(12), 2668–2686.

Catchen, J. M., Amores, A., Hohenlohe, P., Cresko, W., & Postlethwait, J. H. (2011). Stacks: Building and Genotyping Loci De Novo From Short-Read Sequences. *G3 Genes|Genomes|Genetics*, *1*(3), 171–182.

Elshire, R. J., Glaubitz, J. C., Sun, Q., Poland, J. A., Kawamoto, K., Buckler, E. S., & Mitchell, S. E. (2011). A Robust, Simple Genotyping-by-Sequencing (GBS) Approach for High Diversity Species. *PLoS ONE*, *6*(5), e19379.

Ferguson, A. W., McDonough, M. M., Guerra, G. I., Rheude, M., Dragoo, J. W., Ammerman, L. K., & Dowler, R. C. (2017). Phylogeography of a widespread small carnivore, the western spotted skunk (Spilogale gracilis) reveals temporally variable signatures of isolation across western North America. *Ecology and Evolution*, *7*(12), 4229–4240.

Fox, E. A., Wright, A. E., Fumagalli, M., & Vieira, F. G. (2019). ngsLD: Evaluating linkage disequilibrium using genotype likelihoods. *3856*.

Goddard, N. S., Statham, M. J., & Sacks, B. N. (2015). Mitochondrial Analysis of the Most Basal Canid Reveals Deep Divergence between Eastern and Western North American Gray Foxes (Urocyon spp.) and Ancient Roots in Pleistocene California. *PLOS ONE*, *10*(8), e0136329.

Graham, R. W., Lundelius Jr. E. L. (2010). FAUNMAP II: New data for North America with a temporal extension for the Blancan, Irvingtonian and early Rancholabrean. FAUNMAP II Database, version 1.0; 2010. http://www.ucmp.berkeley.edu/faunmap.

Harding, L. E., & Dragoo, J. W. (2012). Out of the tropics: A phylogeographic history of the long-tailed weasel, *Mustela frenata*. *Journal of Mammalogy*, *93*(4), 1178–1194.

Hawkins, M. T. R., Culligan, R. R., Frasier, C. L., Dikow, R. B., Hagenson, R., Lei, R., & Louis, E. E. (2018). Genome sequence and population declines in the critically endangered greater bamboo lemur (Prolemur simus) and implications for conservation. *BMC Genomics*, *19*(1), 445.

Head, M. J., & Gibbard, P. L. (2015). Early–Middle Pleistocene transitions: Linking terrestrial and marine realms. *Quaternary International*, *389*, 7–46.

Hewitt, G. (2000). The genetic legacy of the Quaternary ice ages. *Nature*, *405*(6789), 907–913.

Hewitt, G. M. (n.d.). *Some genetic consequences of ice ages, and their role in divergence and speciation*. 30.

Hewitt, G. M. (2004). Genetic Consequences of Climatic Oscillations in the Quaternary. *Philosophical Transactions: Biological Sciences*, *359*(1442), 183–195.

Hill, W. G. (1981). Estimation of effective population size from data on linkage disequilibrium. *Genetical Research*, *38*(3), 209–216.

Hofman, C. A., Rick, T. C., Hawkins, M. T. R., Funk, W. C., Ralls, K., Boser, C. L., Collins, P. W., Coonan, T., King, J. L., Morrison, S. A., Newsome, S. D., Sillett, T. S., Fleischer, R. C., & Maldonado, J. E. (2015). Mitochondrial Genomes Suggest Rapid Evolution of Dwarf California Channel Islands Foxes (Urocyon littoralis). *PLOS ONE*, *10*(2), e0118240.

Koch, E. M., Schweizer, R. M., Schweizer, T. M., Stahler, D. R., Smith, D. W., Wayne, R. K., & Novembre, J. (2019). De Novo Mutation Rate Estimation in Wolves of Known Pedigree. *Molecular Biology and Evolution*, *36*(11), 2536–2547.

Lessa, E. P., Cook, J. A., & Patton, J. L. (2003). Genetic footprints of demographic expansion in North America, but not Amazonia, during the Late Quaternary. *Proceedings of the National Academy of Sciences*, *100*(18), 10331–10334.

Li, H. (2013). Aligning sequence reads, clone sequences and assembly contigs with BWA-MEM. *ArXiv:1303.3997 [q-Bio]*.

Li, H., & Durbin, R. (2010). Fast and accurate long-read alignment with Burrows–Wheeler transform. *Bioinformatics*, *26*(5), 589–595.

Li, H., & Durbin, R. (2011). Inference of Human Population History From Whole Genome Sequence of A Single Individual. *Nature*, *475*(7357), 493–496.

Liu, X. (2020). *Stairway Plot 2: Demographic history inference with folded SNP frequency spectra*. 9.

Mather, N., Traves, S. M., & Ho, S. Y. W. (2020). A practical introduction to sequentially Markovian coalescent methods for estimating demographic history from genomic data. *Ecology and Evolution*, *10*(1), 579–589.

McDonough, M. M., Ferguson, A. W., Dowler, R. C., Gompper, M. E., & Maldonado, J. E. (2022). Phylogenomic systematics of the spotted skunks (Carnivora, Mephitidae, Spilogale): Additional species diversity and Pleistocene climate change as a major driver of diversification. *Molecular Phylogenetics and Evolution*, *167*, 107266.

Mercure, A., Ralls, K., Koepfli, K. P., & Wayne, R. K. (1993). Genetic Subdivisions Among Small Canids: Mitochondrial Dna Differentiation of Swift, Kit, and Arctic Foxes. *Evolution*, *47*(5), 1313–1328.

Nadachowska-Brzyska, K., Burri, R., Smeds, L., & Ellegren, H. (2016). PSMC analysis of effective population sizes in molecular ecology and its application to black-and-white Ficedula flycatchers. *Molecular Ecology*, *25*(5), 1058–1072.

Nielsen, R., Korneliussen, T., Albrechtsen, A., Li, Y., & Wang, J. (2012). SNP Calling, Genotype Calling, and Sample Allele Frequency Estimation from New-Generation Sequencing Data. *PLoS ONE*, *7*(7), e37558.

Obbard, M. E. (1987). Fur grading and pelt identification. In *Wild Furbearer Management and Conservation in North America* (pp. 717–826). Ontario Ministry of Natural Resources.

Oetjens, M. T., Martin, A., Veeramah, K. R., & Kidd, J. M. (2018). Analysis of the canid Y-chromosome phylogeny using short-read sequencing data reveals the presence of distinct haplogroups among Neolithic European dogs. *BMC Genomics*, *19*(1), 350.

Peek, R. A., O'Rourke, S. M., & Miller, M. R. (2021). Flow modification associated with reduced genetic health of a river-breeding frog, Rana boylii. *Ecosphere*, *12*(5), e03496.

Puckett, E. E., Etter, P. D., Johnson, E. A., & Eggert, L. S. (2015). Phylogeographic Analyses of American Black Bears (*Ursus americanus*) Suggest Four Glacial Refugia and Complex Patterns of Postglacial Admixture. *Molecular Biology and Evolution*, *32*(9), 2338–2350.

Purcell, S., Neale, B., Todd-Brown, K., Thomas, L., Ferreira, M. A. R., Bender, D., Maller, J., Sklar, P., de Bakker, P. I. W., Daly, M. J., & Sham, P. C. (2007). PLINK: A Tool Set for Whole-Genome Association and Population-Based Linkage Analyses. *American Journal of Human Genetics*, *81*(3), 559–575.

Quinlan, A. R., & Hall, I. M. (2010). BEDTools: A flexible suite of utilities for comparing genomic features. *Bioinformatics*, *26*(6), 841–842.

Raj, A., Stephens, M., & Pritchard, J. K. (2014). fastSTRUCTURE: Variational Inference of Population Structure in Large SNP Data Sets. *Genetics*, *197*(2), 573–589.

Reding, D. M., Castañeda-Rico, S., Shirazi, S., Hofman, C. A., Cancellare, I. A., Lance, S. L., Beringer, J., Clark, W. R., & Maldonado, J. E. (2021). Mitochondrial Genomes of the United States Distribution of Gray Fox (Urocyon cinereoargenteus) Reveal a Major Phylogeographic Break at the Great Plains Suture Zone. *Frontiers in Ecology and Evolution*, *9*, 666800.

Rick, T. C., Erlandson, J. M., Vellanoweth, R. L., Braje, T. J., Collins, P. W., Guthrie, D. A., & Stafford, T. W. (2009). Origins and antiquity of the island fox (*Urocyon littoralis*) on California's Channel Islands. *Quaternary Research*, *71*(2), 93–98.

Robinson, J. A., Brown, C., Kim, B. Y., Lohmueller, K. E., & Wayne, R. K. (2018). Purging of strongly deleterious mutations explains long-term persistence and absence of inbreeding depression in island foxes. *Current Biology : CB*, *28*(21), 3487-3494.e4.

Robinson, J. A., Ortega-Del Vecchyo, D., Fan, Z., Kim, B. Y., vonHoldt, B. M., Marsden, C. D., Lohmueller, K. E., & Wayne, R. K. (2016). Genomic Flatlining in the Endangered Island Fox. *Current Biology*, *26*(9), 1183–1189.

Rogers, A. R. (2014). How Population Growth Affects Linkage Disequilibrium. *Genetics*, *197*(4), 1329–1341.

Sarabia, C., vonHoldt, B., Larrasoaña, J. C., Uríos, V., & Leonard, J. A. (2021). Pleistocene climate fluctuations drove demographic history of African golden wolves (*Ca nis lupaster*). *Molecular Ecology*, *30*(23), 6101–6120.

Sved, J. A. (1971). Linkage disequilibrium and homozygosity of chromosome segments in finite populations. *Theoretical Population Biology*, *2*(2), 125–141.

Tajima, F. (1983). Evolutionary Relationship of DNA Sequences in Finite Populations. *Genetics*, *105*(2), 437–460.

Tajima, F. (1989). Statistical Method for Testing the Neutral Mutation Hypothesis by DNA Polymorphism. *Genetics*, *123*(3), 585–595.

Wakeley, J., & Sargsyan, O. (2009). Extensions of the Coalescent Effective Population Size. *Genetics*, *181*(1), 341–345.

Wang, M.-S., Wang, S., Li, Y., Jhala, Y., Thakur, M., Otecko, N. O., Si, J.-F., Chen, H.-M., Shapiro, B., Nielsen, R., Zhang, Y.-P., & Wu, D.-D. (2020). Ancient Hybridization with an Unknown Population Facilitated High-Altitude Adaptation of Canids. *Molecular Biology and Evolution*, *37*(9), 2616–2629.

Waples, R. K., Larson, W. A., & Waples, R. S. (2016). Estimating contemporary effective population size in non-model species using linkage disequilibrium across thousands of loci. *Heredity*, *117*(4), 233–240.

Watterson, G. A. (1975). On the number of segregating sites in genetical models without recombination. *Theoretical Population Biology*, *7*(2), 256–276.

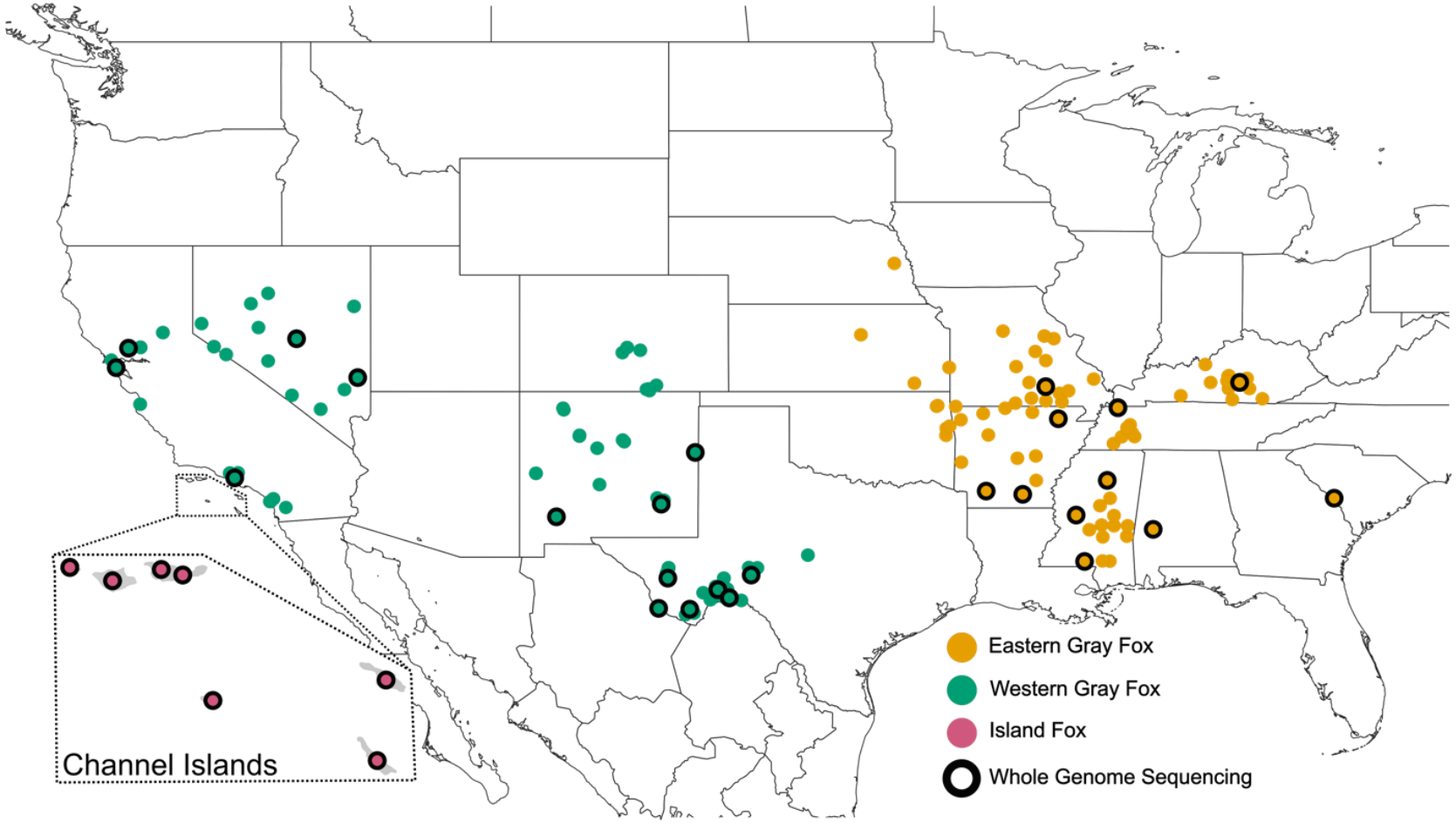

Figure 2.1: Sampling distribution of eastern (n = 83; yellow) and western (n = 114; green) gray foxes (*Urocyon cinereoargenteus*) sequenced at 29,233 loci using genotyping-by-sequencing (GBS), including a subset (black outline) of eastern (n = 14) and western (n = 12) gray foxes for which we conducted whole genome shotgun sequencing (WGS) to a depth of 4–8x. We also included previously published WGS sequences of 10 island foxes and two mainland gray foxes. Additional sampling data are included in Table S1

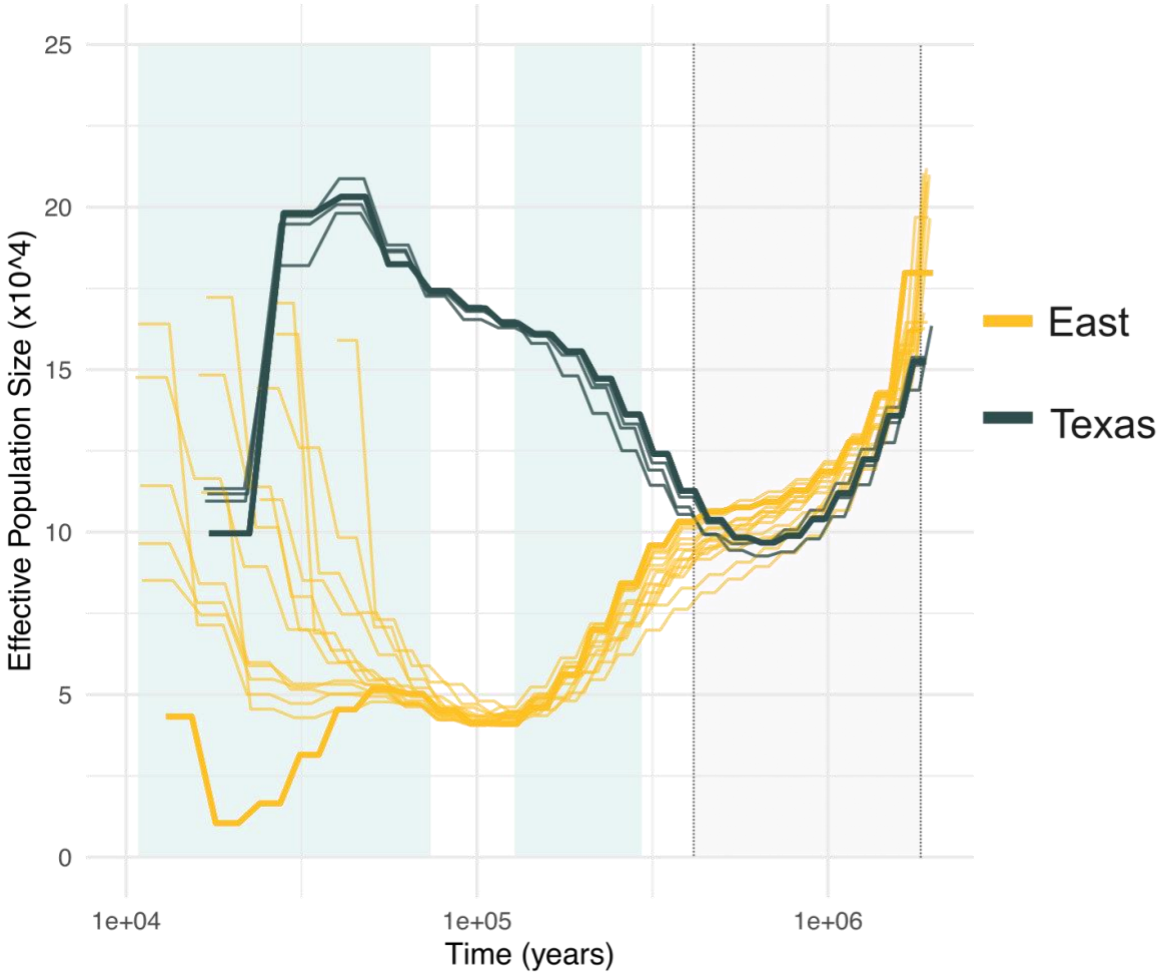

Figure 2.2: Pairwise sequentially Markovian coalescent (PSMC) demographic reconstructions for eastern gray foxes (n = 14; yellow) and western gray foxes from Texas (n = 4; dark green). The demographic trajectories show changes in effective population size throughout deeper historical time periods. Coalescence time was converted to years assuming a mutation rate of 4.5 x 10^{-9} (Koch et al., 2019) and generation time of 2 years. Blue highlighted regions correspond to the Wisconsinan (85,000 – 11,000 YBP) and Illinoian (190 – 130 KYA) glaciation periods. Coverage ranged from 4–7x with the highest coverage sample from the east (7.2x) and west (6.4x) indicated by the bolded PSMC trajectories. The gray shaded region corresponds to the previously inferred estimate of divergence time between eastern and western gray foxes [0.87 MYA (0.41 MYA – 1.86 MYA)] which was derived from GBS markers (Kierepka et al. in review).

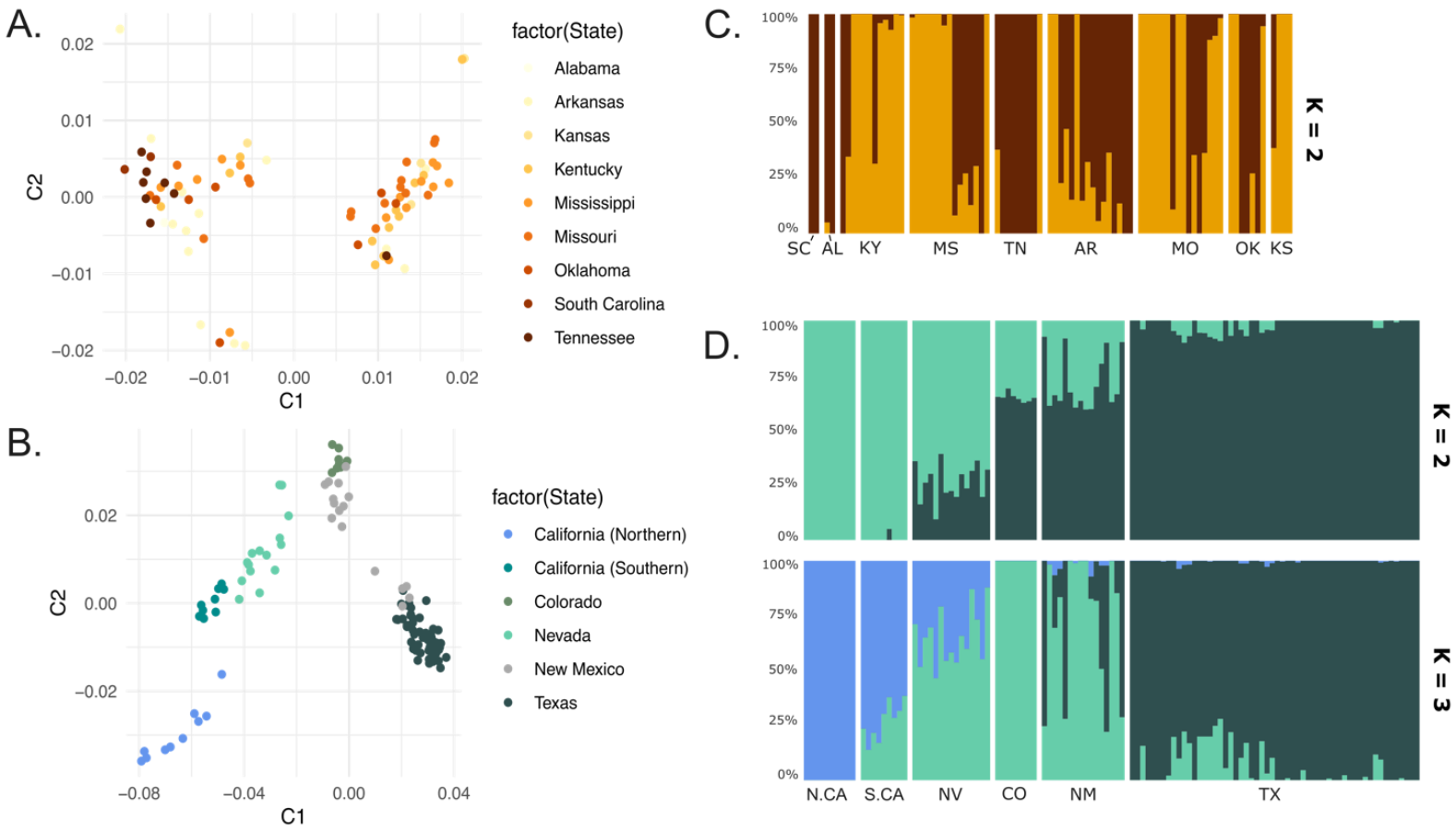

Figure 2.3: Multidimensional scaling (MDS) analysis showing geographic genetic structuring for the (A) eastern and (B) western gray fox populations based on 29,233 single nucleotide polymorphisms. Each circle represents an individual fox colored by its finer-scale geographic origin (state). Genetic clustering analyses using Admixture identified limited genetic structuring within the East with the strongest support (i.e., lowest cross validation error) for a K = 1 (CVE = 0.211) or K = 2 (CVE = 0.213). Alternatively, the western population had clear evidence of genetic structuring by region in the MDS analysis (B), and a cline in ancestry from California to Texas was evident in the Admixture model with the highest support for K = 2 (CVE = 0.389) or three (CVE = 0.394) genetic clusters. Average genetic differentiation between clusters in the western population was higher (K2 F_{ST} = 0.114; K3 F_{ST} = 0.118) than in the eastern population (K2 F_{ST} = 0.06).

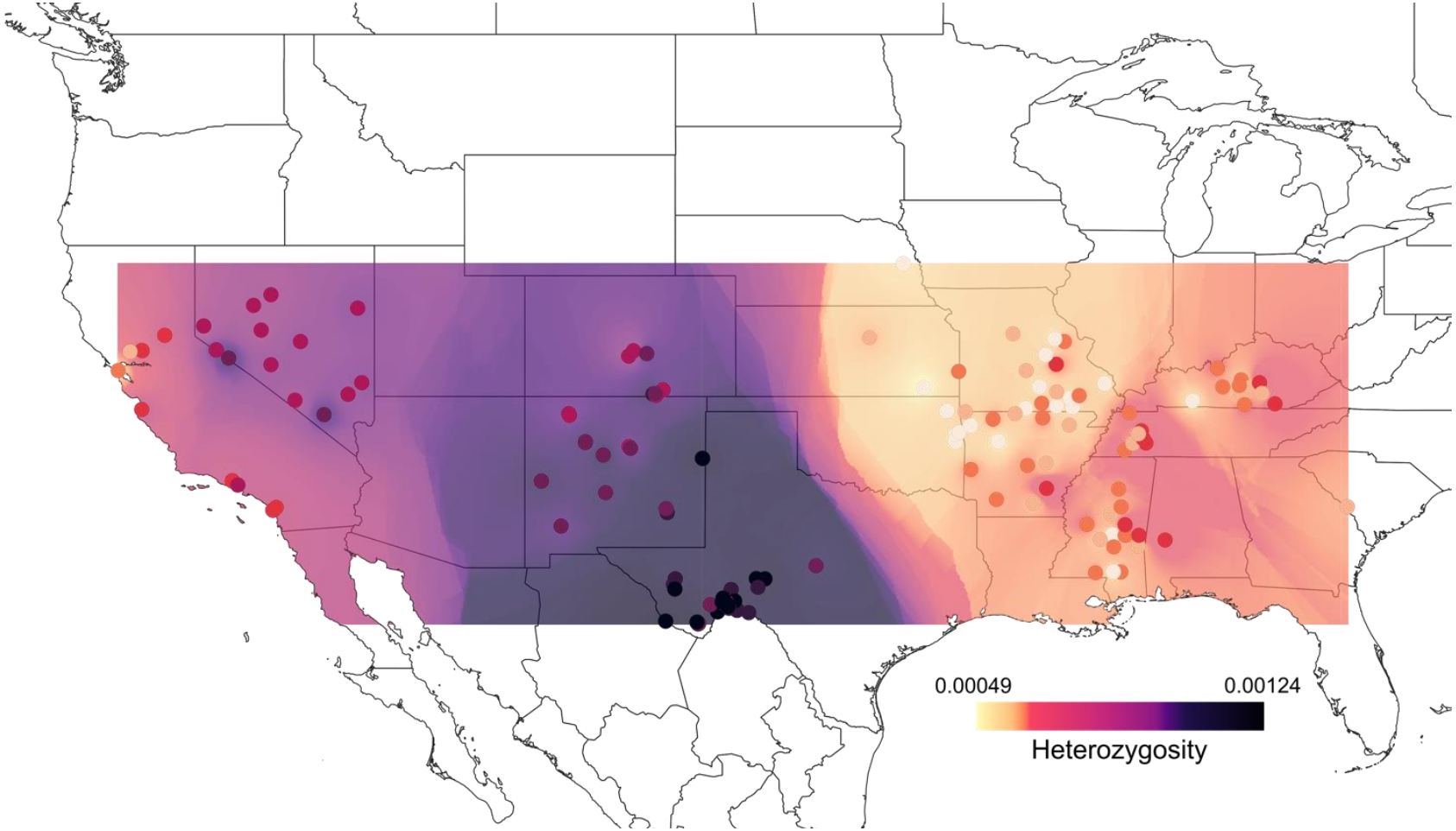

Figure 2.4: Spatial patterns of heterozygosity generated using the individual site frequency spectrum. The dots represent point estimates of heterozygosity for all eastern (n = 83) and western (n = 114) individuals for which we had GBS sequencing data. The inverse distance weighted surface was generated using a quantile-based scale to highlight fine-scale diversity changes across the landscape. Low levels of individual and regional heterozygosity are represented by lighter/yellower colors and higher heterozygosity individuals and regions are indicated by darker/purple shades.

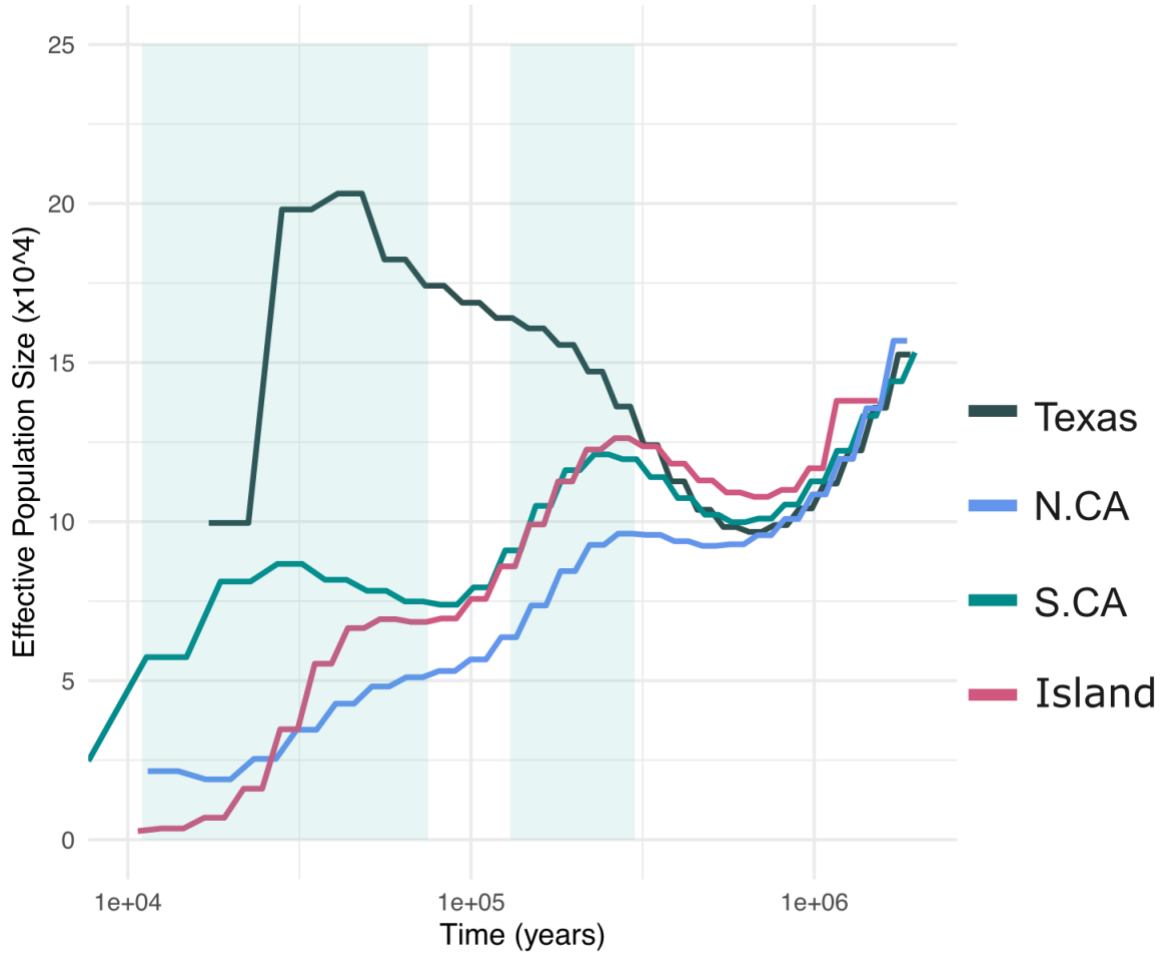

Figure 2.5: Reconstructed pairwise sequentially Markovian coalescent (PSMC) trajectories of the highest-coverage samples representative of each western gray fox population an island fox from Santa Catalina Island. The demographic trajectories show changes in effective population size throughout deeper historical time periods. Coalescence time was converted to years assuming a mutation rate of 4.5 x 10^{-9} (Koch et al., 2019) and generation time of 2 years. Blue highlighted regions correspond to the Wisconsin (85,000 – 11,000 YBP) and Illinoian (190 – 130 KYA) glaciation periods. Average read depths were 21x and 18x for the northern and southern California samples respectively and 24x for the Channel Island fox. Average read depth was lowest for the Texas individual (6x) but had an appropriate false negative rate applied.

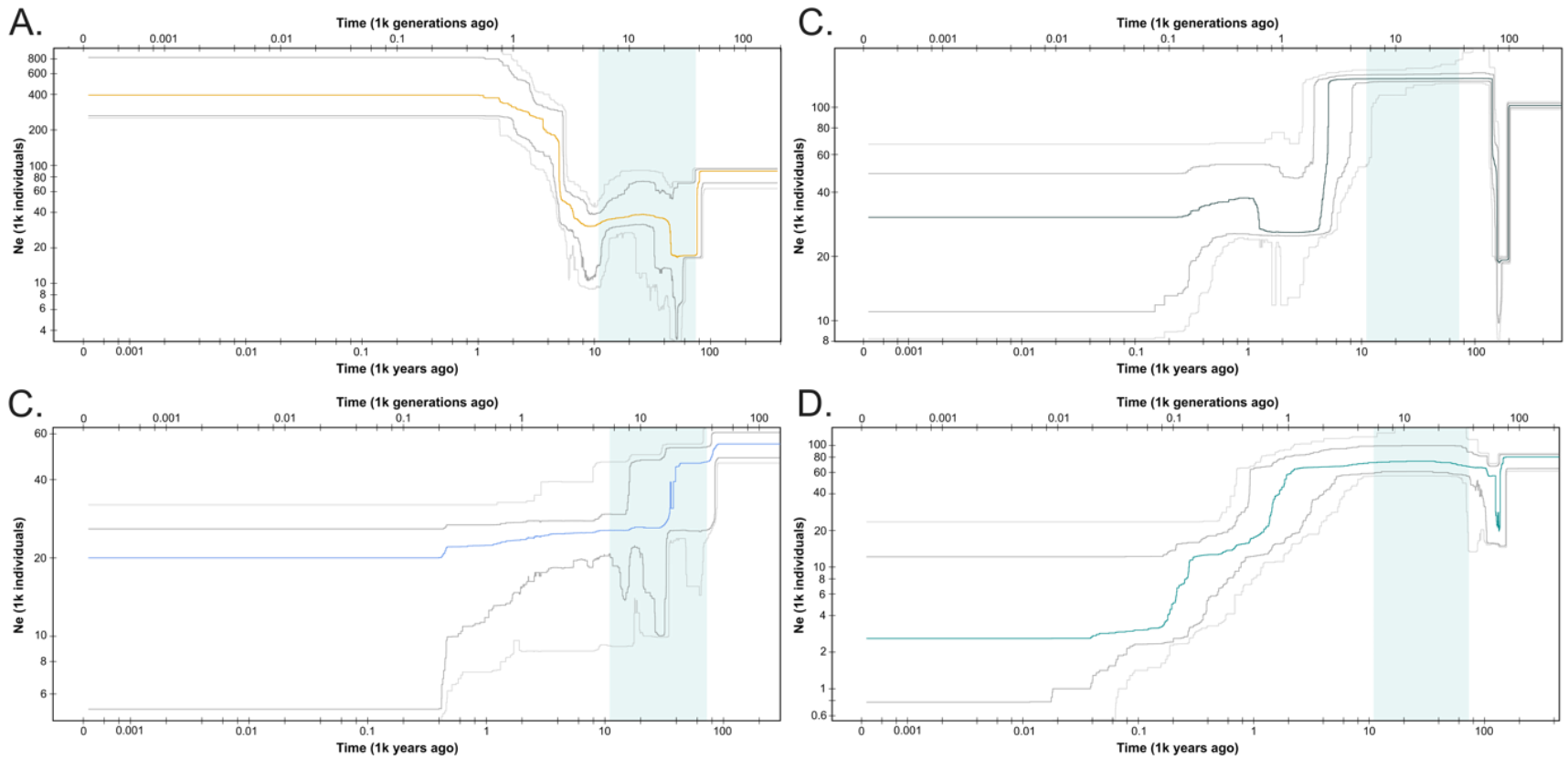

Figure 2.6: Stairway plots generated using the site frequency spectrum of the (A) eastern, (B) Texas, (C) northern California, and (D) southern California gray fox populations. The demographic trajectories show changes in effective population size. Coalescence time was converted to years assuming a mutation rate of 4.5×10^{-9} (Koch et al., 2019) and generation time of 2 years (Goddard et al., 2015). The blue highlighted region corresponds to the Wisconsin (85,000 – 11,000 YBP) glaciation period. Data show median estimates from 200 bootstrap replicates (colored line), 95% confidence intervals (dark gray line), and 75% confidence intervals (light gray line).

Supplemental Material

Table S2.1: Information for gray fox DNA samples used in this study, including geographic range delineations, spatial coordinates, information on sequencing type and associated coverage levels and citations for use in previous studies.

Sample ID	Species	Region	State	Lat	Long	GBS Cov. (x)	WGS Cov. (x)	Source	Seq. Type
NPS_GF030	U. cinereoargenteus	West	California (Northern)	NA	NA	NA	20.96	Robinson et al. (2018)	WGS
NPS_GF041	U. cinereoargenteus	West	California (Southern)	NA	NA	NA	18.25	Robinson et al. (2016)	WGS
S13-2845	U. cinereoargenteus	West	California (Northern)	38.526	-121.757	10	NA	Kierepka et al. in review	GBS
S13-2846	U. cinereoargenteus	West	California (Northern)	38.516	-121.749	12	NA	Kierepka et al. in review	GBS
S13-2949	U. cinereoargenteus	West	California (Northern)	38.490	-122.152	25	8	Kierepka et al. in review	GBS + WGS
S13-2950	U. cinereoargenteus	West	California (Northern)	38.490	-122.152	16	NA	Kierepka et al. in review	GBS
S13-2953	U. cinereoargenteus	West	California (Northern)	38.490	-122.152	25	NA	Kierepka et al. in review	GBS
S14-0369	U. cinereoargenteus	West	California (Northern)	39.026	-121.002	9	NA	Kierepka et al. in review	GBS
S14-0371	U. cinereoargenteus	West	California (Southern)	36.569	-121.765	13	NA	Kierepka et al. in review	GBS
S14-0889	U. cinereoargenteus	West	California (Northern)	38.485	-122.150	10	NA	Kierepka et al. in review	GBS
S14-1425	U. cinereoargenteus	West	California (Northern)	37.863	-122.532	55	NA	Kierepka et al. in review	GBS
S14-1440	U. cinereoargenteus	West	California (Northern)	37.859	-122.545	58	NA	Kierepka et al. in review	GBS
S14-1441	U. cinereoargenteus	West	California (Northern)	37.858	-122.544	67	NA	Kierepka et al. in review	GBS
S14-1451	U. cinereoargenteus	West	California (Southern)	34.203	-118.755	91	NA	Kierepka et al. in review	GBS
S14-1455	U. cinereoargenteus	West	California (Southern)	34.211	-118.756	90	NA	Kierepka et al. in review	GBS
S14-1458	U. cinereoargenteus	West	California (Southern)	34.200	-118.761	70	NA	Kierepka et al. in review	GBS
S14-1461	U. cinereoargenteus	West	California (Southern)	34.067	-118.574	60	NA	Kierepka et al. in review	GBS
S16-1457	U. cinereoargenteus	West	California (Southern)	33.233	-117.405	95	NA	Kierepka et al. in review	GBS
S16-1458	U. cinereoargenteus	West	California (Southern)	33.236	-117.414	28	NA	Kierepka et al. in review	GBS
S16-1459	U. cinereoargenteus	West	California (Southern)	33.328	-117.299	34	NA	Kierepka et al. in review	GBS
S16-1460	U. cinereoargenteus	West	California (Southern)	33.237	-117.393	61	NA	Kierepka et al. in review	GBS

S19-2913	U. cinereoargenteus	West	Texas	30.960	-101.076	23	NA	Kierepka et al. in review	GBS
S19-2916	U. cinereoargenteus	West	Texas	30.098	-102.228	69	NA	Kierepka et al. in review	GBS
S19-2918	U. cinereoargenteus	West	Texas	31.395	-99.381	50	NA	Kierepka et al. in review	GBS
S19-2923	U. cinereoargenteus	West	Texas	30.969	-101.361	53	NA	Kierepka et al. in review	GBS
S19-2924	U. cinereoargenteus	West	Texas	29.918	-102.002	47	NA	Kierepka et al. in review	GBS
S19-2925	U. cinereoargenteus	West	Texas	29.924	-101.992	59	6	Kierepka et al. in review	GBS + WGS
S19-2926	U. cinereoargenteus	West	Texas	30.606	-102.198	26	NA	Kierepka et al. in review	GBS
S19-2927	U. cinereoargenteus	West	Texas	30.606	-102.198	77	NA	Kierepka et al. in review	GBS
S19-2959	U. cinereoargenteus	West	Texas	30.778	-104.112	13	NA	Kierepka et al. in review	GBS
S19-2960	U. cinereoargenteus	West	Texas	30.778	-104.112	8	NA	Kierepka et al. in review	GBS
S19-2962	U. cinereoargenteus	West	Texas	30.961	-104.051	66	NA	Kierepka et al. in review	GBS
S19-2963	U. cinereoargenteus	West	Texas	30.961	-104.051	26	NA	Kierepka et al. in review	GBS
S19-2964	U. cinereoargenteus	West	Texas	30.961	-104.051	20	NA	Kierepka et al. in review	GBS
S19-2968	U. cinereoargenteus	West	Texas	30.961	-104.051	48	NA	Kierepka et al. in review	GBS
S19-2969	U. cinereoargenteus	West	Texas	30.961	-104.051	45	NA	Kierepka et al. in review	GBS
S19-2970	U. cinereoargenteus	West	Texas	30.961	-104.051	77	NA	Kierepka et al. in review	GBS
S19-2971	U. cinereoargenteus	West	Texas	30.961	-104.051	86	NA	Kierepka et al. in review	GBS
S19-2972	U. cinereoargenteus	West	Texas	30.961	-104.051	96	NA	Kierepka et al. in review	GBS
S19-2973	U. cinereoargenteus	West	Texas	30.961	-104.051	99	NA	Kierepka et al. in review	GBS
S19-2974	U. cinereoargenteus	West	Texas	30.625	-104.067	45	6	Kierepka et al. in review	GBS + WGS
S19-2988	U. cinereoargenteus	West	Texas	29.843	-101.613	12	NA	Kierepka et al. in review	GBS
S19-3056	U. cinereoargenteus	West	Texas	29.869	-102.647	9	NA	Kierepka et al. in review	GBS
S19-3064	U. cinereoargenteus	West	Texas	29.561	-104.372	10	6	Kierepka et al. in review	GBS + WGS
S19-3066	U. cinereoargenteus	West	Texas	30.684	-101.308	78	6	Kierepka et al. in review	GBS + WGS
S19-3096	U. cinereoargenteus	West	Texas	30.229	-102.082	9	NA	Kierepka et al. in review	GBS
S19-3099	U. cinereoargenteus	West	Texas	29.467	-103.293	79	NA	Kierepka et al. in review	GBS
S19-3104	U. cinereoargenteus	West	Texas	29.484	-103.272	7	NA	Kierepka et al. in review	GBS

S19-3108	U. cinereoargenteus	West	Texas	30.162	-102.333	22	NA	Kierepka et al. in review	GBS
S19-3110	U. cinereoargenteus	West	Texas	30.127	-102.340	8	NA	Kierepka et al. in review	GBS
S19-3111	U. cinereoargenteus	West	Texas	30.114	-102.362	28	NA	Kierepka et al. in review	GBS
S19-3112	U. cinereoargenteus	West	Texas	30.098	-102.304	23	NA	Kierepka et al. in review	GBS
S19-3113	U. cinereoargenteus	West	Texas	30.127	-102.316	39	NA	Kierepka et al. in review	GBS
S19-3114	U. cinereoargenteus	West	Texas	30.183	-102.347	21	NA	Kierepka et al. in review	GBS
S19-3115	U. cinereoargenteus	West	Texas	30.168	-102.409	39	NA	Kierepka et al. in review	GBS
S19-3116	U. cinereoargenteus	West	Texas	30.193	-102.356	24	NA	Kierepka et al. in review	GBS
S19-3117	U. cinereoargenteus	West	Texas	30.046	-102.298	21	NA	Kierepka et al. in review	GBS
S19-3118	U. cinereoargenteus	West	Texas	30.150	-102.386	20	NA	Kierepka et al. in review	GBS
S19-3121	U. cinereoargenteus	West	Texas	30.060	-102.326	37	NA	Kierepka et al. in review	GBS
S19-3122	U. cinereoargenteus	West	Texas	30.144	-102.438	47	NA	Kierepka et al. in review	GBS
S19-3123	U. cinereoargenteus	West	Texas	30.059	-102.312	58	NA	Kierepka et al. in review	GBS
S19-3124	U. cinereoargenteus	West	Texas	30.093	-102.291	53	NA	Kierepka et al. in review	GBS
S19-3125	U. cinereoargenteus	West	Texas	30.115	-102.359	27	NA	Kierepka et al. in review	GBS
S19-3126	U. cinereoargenteus	West	Texas	30.182	-102.405	21	NA	Kierepka et al. in review	GBS
S19-3127	U. cinereoargenteus	West	Texas	30.026	-102.292	13	NA	Kierepka et al. in review	GBS
S19-3128	U. cinereoargenteus	West	Texas	30.188	-102.432	10	NA	Kierepka et al. in review	GBS
S19-3129	U. cinereoargenteus	West	Texas	30.036	-102.302	20	NA	Kierepka et al. in review	GBS
S19-3132	U. cinereoargenteus	West	Texas	30.320	-102.469	12	NA	Kierepka et al. in review	GBS
S19-3133	U. cinereoargenteus	West	Texas	29.508	-103.328	27	5	Kierepka et al. in review	GBS + WGS
S19-3134	U. cinereoargenteus	West	Texas	29.529	-103.329	10	NA	Kierepka et al. in review	GBS
S19-3149	U. cinereoargenteus	West	Texas	30.323	-102.467	11	NA	Kierepka et al. in review	GBS
S19-3152	U. cinereoargenteus	West	Texas	30.213	-102.430	19	6	Kierepka et al. in review	GBS + WGS
S19-3154	U. cinereoargenteus	West	Texas	29.989	-102.268	49	NA	Kierepka et al. in review	GBS
S19-3157	U. cinereoargenteus	West	Texas	30.106	-102.890	77	NA	Kierepka et al. in review	GBS
S19-3162	U. cinereoargenteus	West	Texas	30.198	-102.496	12	NA	Kierepka et al. in review	GBS
S19-3163	U. cinereoargenteus	West	Texas	30.041	-102.301	41	NA	Kierepka et al. in review	GBS

S19-3167	U. cinereoargenteus	West	Texas	30.219	-102.424	14	NA	Kierepka et al. in review	GBS
S19-4604	U. cinereoargenteus	East	Kentucky	37.106	-85.281	49	NA	Kierepka et al. in review	GBS
S19-4605	U. cinereoargenteus	East	Kentucky	36.729	-85.153	32	NA	Kierepka et al. in review	GBS
S19-4606	U. cinereoargenteus	East	Kentucky	37.534	-85.293	46	NA	Kierepka et al. in review	GBS
S19-4607	U. cinereoargenteus	East	Kansas	38.951	-97.603	49	NA	Kierepka et al. in review	GBS
S19-4609	U. cinereoargenteus	West	Colorado	37.221	-104.458	34	NA	Kierepka et al. in review	GBS
S19-4610	U. cinereoargenteus	West	Colorado	37.079	-104.790	34	NA	Kierepka et al. in review	GBS
S19-4611	U. cinereoargenteus	West	Colorado	37.035	-104.693	46	NA	Kierepka et al. in review	GBS
S19-4612	U. cinereoargenteus	West	Colorado	37.098	-104.722	39	NA	Kierepka et al. in review	GBS
S19-4614	U. cinereoargenteus	West	Colorado	38.514	-105.440	21	NA	Kierepka et al. in review	GBS
S19-4615	U. cinereoargenteus	West	Colorado	38.339	-105.599	38	NA	Kierepka et al. in review	GBS
S19-4616	U. cinereoargenteus	West	Colorado	38.514	-105.440	42	NA	Kierepka et al. in review	GBS
S19-4617	U. cinereoargenteus	West	Colorado	38.421	-105.000	22	NA	Kierepka et al. in review	GBS
S19-4618	U. cinereoargenteus	East	Missouri	36.685	-91.402	50	NA	Kierepka et al. in review	GBS
S19-4619	U. cinereoargenteus	East	Missouri	36.606	-92.425	29	NA	Kierepka et al. in review	GBS
S19-4620	U. cinereoargenteus	East	Missouri	36.649	-90.867	66	NA	Kierepka et al. in review	GBS
S19-4621	U. cinereoargenteus	East	Missouri	37.314	-91.964	41	NA	Kierepka et al. in review	GBS
S19-4622	U. cinereoargenteus	East	Missouri	36.945	-90.946	54	NA	Kierepka et al. in review	GBS
S19-4623	U. cinereoargenteus	East	Missouri	37.152	-91.391	31	6	Kierepka et al. in review	GBS + WGS
S19-4624	U. cinereoargenteus	East	Mississippi	32.267	-89.946	25	NA	Kierepka et al. in review	GBS
S19-4625	U. cinereoargenteus	East	Mississippi	33.937	-89.337	32	5	Kierepka et al. in review	GBS + WGS
S19-4626	U. cinereoargenteus	East	Mississippi	32.766	-90.388	24	5	Kierepka et al. in review	GBS + WGS
S19-4627	U. cinereoargenteus	East	Mississippi	31.189	-89.259	21	NA	Kierepka et al. in review	GBS
S19-4628	U. cinereoargenteus	East	Mississippi	31.164	-90.103	35	4	Kierepka et al. in review	GBS + WGS
S19-4629	U. cinereoargenteus	East	Mississippi	31.198	-89.506	70	NA	Kierepka et al. in review	GBS
S19-4630	U. cinereoargenteus	East	Mississippi	32.427	-89.533	51	NA	Kierepka et al. in review	GBS
S19-4631	U. cinereoargenteus	East	Mississippi	32.267	-89.946	42	NA	Kierepka et al. in review	GBS

S19-4632	U. cinereoargenteus	East	Mississippi	32.402	-89.118	22	NA	Kierepka et al. in review	GBS
S19-4633	U. cinereoargenteus	East	Mississippi	32.045	-88.688	32	NA	Kierepka et al. in review	GBS
S19-4634	U. cinereoargenteus	East	Mississippi	32.404	-88.660	12	NA	Kierepka et al. in review	GBS
S19-4635	U. cinereoargenteus	East	Mississippi	32.019	-89.495	29	NA	Kierepka et al. in review	GBS
S19-4636	U. cinereoargenteus	East	Mississippi	33.090	-89.589	15	NA	Kierepka et al. in review	GBS
S19-4637	U. cinereoargenteus	East	Mississippi	33.346	-89.251	26	NA	Kierepka et al. in review	GBS
S19-4638	U. cinereoargenteus	East	Mississippi	32.753	-89.119	27	NA	Kierepka et al. in review	GBS
S19-4639	U. cinereoargenteus	East	Tennessee	36.457	-88.984	29	4	Kierepka et al. in review	GBS + WGS
S19-4640	U. cinereoargenteus	East	Tennessee	35.865	-88.580	10	NA	Kierepka et al. in review	GBS
S19-4641	U. cinereoargenteus	East	Tennessee	35.222	-89.134	14	NA	Kierepka et al. in review	GBS
S19_4642	U. cinereoargenteus	East	Tennessee	35.543	-88.856	30	6	Kierepka et al. in review	GBS + WGS
S19-4643	U. cinereoargenteus	East	Tennessee	35.460	-88.429	11	NA	Kierepka et al. in review	GBS
S19-4644	U. cinereoargenteus	East	Tennessee	35.452	-88.863	26	NA	Kierepka et al. in review	GBS
S19-4646	U. cinereoargenteus	East	Tennessee	35.767	-88.677	28	NA	Kierepka et al. in review	GBS
S19-4647	U. cinereoargenteus	East	Tennessee	35.591	-88.513	24	NA	Kierepka et al. in review	GBS
S19-4648	U. cinereoargenteus	East	Tennessee	35.767	-88.677	40	NA	Kierepka et al. in review	GBS
S19-4649	U. cinereoargenteus	East	Missouri	38.067	-91.406	15	NA	Kierepka et al. in review	GBS
S19-4650	U. cinereoargenteus	East	Missouri	38.377	-91.756	37	NA	Kierepka et al. in review	GBS
S19-4652	U. cinereoargenteus	East	Missouri	38.908	-91.455	32	NA	Kierepka et al. in review	GBS
S19-4653	U. cinereoargenteus	East	Missouri	37.029	-90.645	24	NA	Kierepka et al. in review	GBS
S19-4654	U. cinereoargenteus	East	Missouri	38.819	-91.135	16	NA	Kierepka et al. in review	GBS
S19-4656	U. cinereoargenteus	East	Missouri	37.433	-89.800	37	NA	Kierepka et al. in review	GBS
S19-4657	U. cinereoargenteus	East	Missouri	37.861	-92.400	31	NA	Kierepka et al. in review	GBS
S19-4659	U. cinereoargenteus	East	Missouri	36.774	-91.887	12	NA	Kierepka et al. in review	GBS
S19-4661	U. cinereoargenteus	East	Missouri	39.077	-92.842	31	NA	Kierepka et al. in review	GBS
S19-4662	U. cinereoargenteus	East	Missouri	38.908	-91.455	28	NA	Kierepka et al. in review	GBS
S19-4663	U. cinereoargenteus	East	Alabama	32.248	-87.791	31	5	Kierepka et al. in review	GBS + WGS

S19-4664	U. cinereoargenteus	East	Alabama	32.248	-87.791	12	NA	Kierepka et al. in review	GBS
S19-4665	U. cinereoargenteus	East	Kansas	37.831	-94.645	47	NA	Kierepka et al. in review	GBS
S19-4666	U. cinereoargenteus	East	Kansas	37.831	-94.645	17	NA	Kierepka et al. in review	GBS
S19-4667	U. cinereoargenteus	East	Arkansas	34.718	-92.358	19	NA	Kierepka et al. in review	GBS
S19-4670	U. cinereoargenteus	West	Nevada	36.399	-115.713	28	NA	Kierepka et al. in review	GBS
S19-4671	U. cinereoargenteus	West	Nevada	39.335	-119.707	35	NA	Kierepka et al. in review	GBS
S19-4672	U. cinereoargenteus	West	Nevada	39.199	-117.799	32	NA	Kierepka et al. in review	GBS
S19-4673	U. cinereoargenteus	West	Nevada	40.017	-118.052	17	NA	Kierepka et al. in review	GBS
S19-4674	U. cinereoargenteus	West	Nevada	38.274	-118.881	24	NA	Kierepka et al. in review	GBS
S19-4675	U. cinereoargenteus	West	Nevada	37.459	-114.460	45	5	Kierepka et al. in review	GBS + WGS
S19-4676	U. cinereoargenteus	West	Nevada	36.877	-116.677	32	NA	Kierepka et al. in review	GBS
S19-4677	U. cinereoargenteus	West	Nevada	40.372	-117.475	38	NA	Kierepka et al. in review	GBS
S19-4678	U. cinereoargenteus	West	Nevada	38.544	-119.291	19	NA	Kierepka et al. in review	GBS
S19-4679	U. cinereoargenteus	West	Nevada	38.821	-116.494	46	6	Kierepka et al. in review	GBS + WGS
S19-4680	U. cinereoargenteus	West	Nevada	38.053	-117.475	69	NA	Kierepka et al. in review	GBS
S19-4681	U. cinereoargenteus	West	Nevada	39.926	-114.596	37	NA	Kierepka et al. in review	GBS
S19-4682	U. cinereoargenteus	West	Nevada	37.073	-114.916	44	NA	Kierepka et al. in review	GBS
S19-4683	U. cinereoargenteus	West	Nevada	38.544	-119.291	29	NA	Kierepka et al. in review	GBS
S19-4684	U. cinereoargenteus	West	Nevada	39.926	-114.596	33	NA	Kierepka et al. in review	GBS
S19-4686	U. cinereoargenteus	East	Oklahoma	36.500	-95.064	32	NA	Kierepka et al. in review	GBS
S19-4687	U. cinereoargenteus	East	Oklahoma	35.502	-94.751	41	NA	Kierepka et al. in review	GBS
S19-4688	U. cinereoargenteus	East	Oklahoma	35.741	-94.741	46	NA	Kierepka et al. in review	GBS
S19-4689	U. cinereoargenteus	East	Oklahoma	36.524	-95.032	14	NA	Kierepka et al. in review	GBS
S19-4691	U. cinereoargenteus	East	Oklahoma	35.815	-94.631	34	NA	Kierepka et al. in review	GBS
S19-4693	U. cinereoargenteus	East	Oklahoma	36.524	-95.032	40	NA	Kierepka et al. in review	GBS
S19-4696	U. cinereoargenteus	East	Oklahoma	35.815	-94.631	30	NA	Kierepka et al. in review	GBS
S19-4697	U. cinereoargenteus	East	Arkansas	41.399	-96.483	39	NA	Kierepka et al. in review	GBS

S19-4699	U. cinereoargenteus	East	Arkansas	36.052	-90.973	23	6	Kierepka et al. in review	GBS + WGS
S19-4700	U. cinereoargenteus	East	Arkansas	34.581	-94.237	31	NA	Kierepka et al. in review	GBS
S19-4701	U. cinereoargenteus	East	Arkansas	33.467	-92.169	26	6	Kierepka et al. in review	GBS + WGS
S19_4703	U. cinereoargenteus	East	Arkansas	35.708	-92.519	30	7	Kierepka et al. in review	GBS + WGS
S19-4704	U. cinereoargenteus	East	Arkansas	36.291	-91.855	6	NA	Kierepka et al. in review	GBS
S19-4706	U. cinereoargenteus	East	Arkansas	36.250	-93.505	12	NA	Kierepka et al. in review	GBS
S19-4707	U. cinereoargenteus	East	Arkansas	33.958	-91.728	13	NA	Kierepka et al. in review	GBS
S19-4708	U. cinereoargenteus	East	Arkansas	36.037	-94.252	17	NA	Kierepka et al. in review	GBS
S19-4709	U. cinereoargenteus	East	Arkansas	36.494	-94.426	23	NA	Kierepka et al. in review	GBS
S19_4710	U. cinereoargenteus	East	Arkansas	34.287	-91.338	30	6	Kierepka et al. in review	GBS + WGS
S19-4711	U. cinereoargenteus	East	Arkansas	35.515	-93.332	40	NA	Kierepka et al. in review	GBS
S19-4712	U. cinereoargenteus	East	Arkansas	34.795	-91.740	26	NA	Kierepka et al. in review	GBS
S19-4713	U. cinereoargenteus	East	Arkansas	36.432	-92.769	31	NA	Kierepka et al. in review	GBS
S19-4714	U. cinereoargenteus	East	Arkansas	33.588	-93.391	61	5	Kierepka et al. in review	GBS + WGS
S19-4715	U. cinereoargenteus	West	New Mexico	34.956	-103.157	55	5	Kierepka et al. in review	GBS + WGS
S19-4716	U. cinereoargenteus	West	New Mexico	33.816	-106.367	42	NA	Kierepka et al. in review	GBS
S19-4717	U. cinereoargenteus	West	New Mexico	32.711	-107.845	94	5	Kierepka et al. in review	GBS + WGS
S19-4718	U. cinereoargenteus	West	New Mexico	34.198	-108.497	60	NA	Kierepka et al. in review	GBS
S19-4719	U. cinereoargenteus	West	New Mexico	33.282	-104.357	23	NA	Kierepka et al. in review	GBS
S19-4720	U. cinereoargenteus	West	New Mexico	35.342	-105.590	73	NA	Kierepka et al. in review	GBS
S19-4721	U. cinereoargenteus	West	New Mexico	35.475	-107.040	77	NA	Kierepka et al. in review	GBS
S19-4722	U. cinereoargenteus	West	New Mexico	35.505	-107.036	86	NA	Kierepka et al. in review	GBS
S19-4723	U. cinereoargenteus	West	New Mexico	36.434	-107.587	30	NA	Kierepka et al. in review	GBS
S19-4724	U. cinereoargenteus	West	New Mexico	34.202	-108.497	22	NA	Kierepka et al. in review	GBS
S19-4725	U. cinereoargenteus	West	New Mexico	35.062	-106.442	36	NA	Kierepka et al. in review	GBS
S19-4726	U. cinereoargenteus	West	New Mexico	34.949	-103.144	7	NA	Kierepka et al. in review	GBS

S19-4728	U. cinereoargenteus	West	New Mexico	33.156	-104.321	53	6	Kierepka et al. in review	GBS + WGS
S19-4729	U. cinereoargenteus	West	New Mexico	36.377	-107.564	18	NA	Kierepka et al. in review	GBS
S19-4730	U. cinereoargenteus	West	New Mexico	35.284	-105.538	19	NA	Kierepka et al. in review	GBS
S19-4731	U. cinereoargenteus	West	New Mexico	33.282	-104.358	36	NA	Kierepka et al. in review	GBS
S19-4732	U. cinereoargenteus	East	Kansas	37.291	-95.811	21	NA	Kierepka et al. in review	GBS
S19-4734	U. cinereoargenteus	East	Kentucky	37.553	-85.269	25	NA	Kierepka et al. in review	GBS
S19-4735	U. cinereoargenteus	East	Kentucky	36.758	-84.145	15	NA	Kierepka et al. in review	GBS
S19-4736	U. cinereoargenteus	East	Kentucky	37.316	-85.879	29	NA	Kierepka et al. in review	GBS
S19-4737	U. cinereoargenteus	East	Kentucky	37.322	-84.928	50	6	Kierepka et al. in review	GBS + WGS
S19-4738	U. cinereoargenteus	East	Kentucky	37.457	-84.658	9	NA	Kierepka et al. in review	GBS
S19-4739	U. cinereoargenteus	East	Kentucky	36.860	-86.881	35	NA	Kierepka et al. in review	GBS
S19-4740	U. cinereoargenteus	East	Kentucky	37.934	-86.057	16	NA	Kierepka et al. in review	GBS
S19-4741	U. cinereoargenteus	East	Kentucky	37.366	-85.328	20	NA	Kierepka et al. in review	GBS
S19-4742	U. cinereoargenteus	East	Kentucky	37.108	-84.580	27	NA	Kierepka et al. in review	GBS
S19-6655	U. cinereoargenteus	East	South Carolina	33.346	-81.743	44	6	Kierepka et al. in review	GBS + WGS
S19-6656	U. cinereoargenteus	East	South Carolina	33.344	-81.746	24	NA	Kierepka et al. in review	GBS
RKW11697	U. littoralis	Channel Islands	Santa Catalina	NA	NA	NA	24	Robinson et al. (2018)	WGS
RKW12297	U. littoralis	Channel Islands	San Nicolas	NA	NA	NA	23	Robinson et al. (2018)	WGS
RKW12355	U. littoralis	Channel Islands	Santa Rosa	NA	NA	NA	22	Robinson et al. (2018)	WGS
RKW8695	U. littoralis	Channel Islands	Santa Cruz	NA	NA	NA	23	Robinson et al. (2018)	WGS
SCLV4F	U. littoralis	Channel Islands	San Clemente	NA	NA	NA	20	Robinson et al. (2016)	WGS
SMI15F	U. littoralis	Channel Islands	San Miguel	NA	NA	NA	25	Robinson et al. (2016)	WGS
Z01_0174	U. littoralis	Channel Islands	Santa Cruz			NA	5	This Study	WGS

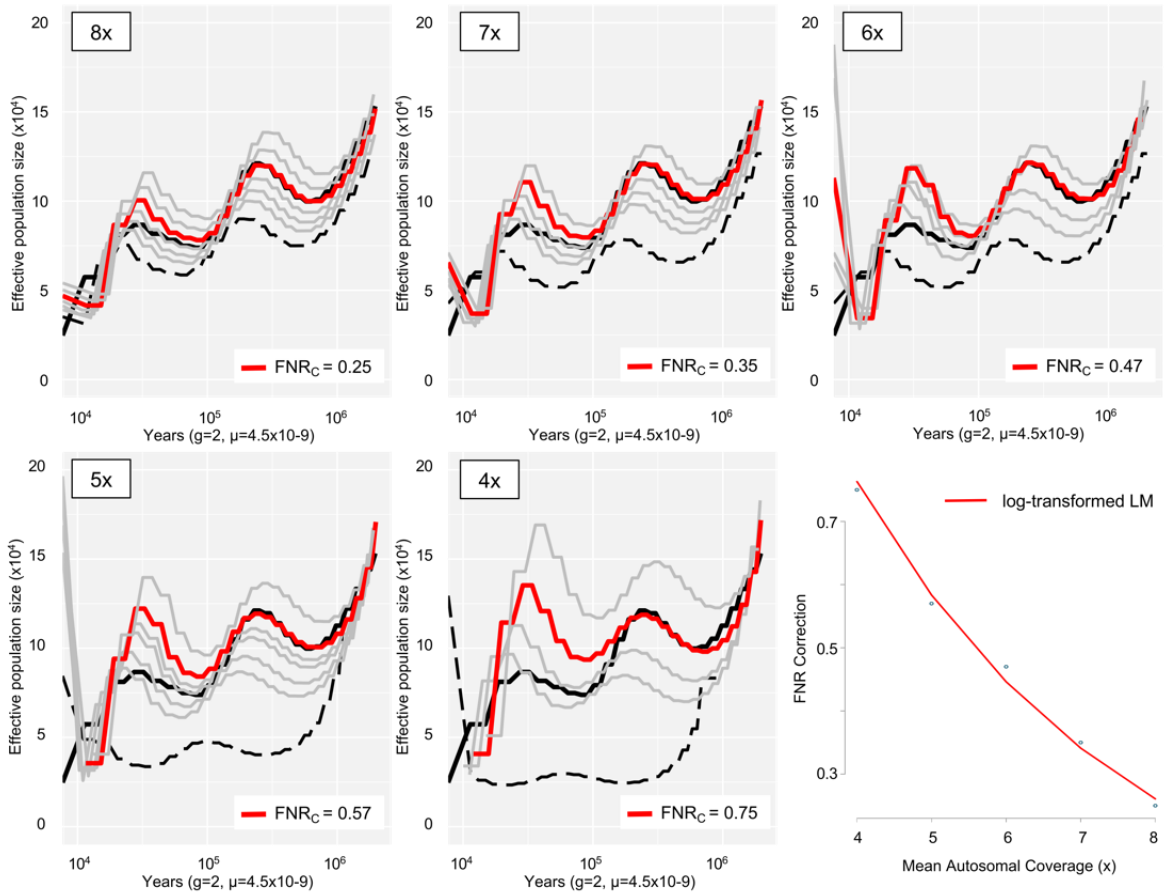

Figure S2.1: Reconstructed pairwise sequentially Markovian coalescent (PSMC) trajectories of a high coverage (18x) sample from southern California (solid black line) that was systematically down sampled to average read depths of 4x, 5x, 6x, 7x, and 8x (dashed black line). A range of false negative rate corrections were systematically applied to each down sampled genome (gray lines) until the 'true' demographic trajectory was recovered (red line). A log-transformed linear model [$y = 2.3051e^{-0.274x}$] was then fit to the data, allowing for the selection of appropriate FNR corrections for the full range of low coverages samples. Note the demographic trajectories show changes in effective population size throughout deeper historical time periods. Coalescence time was converted to years assuming a mutation rate of 4.5×10^{-9} (Koch et al., 2019) and generation time of 2 years. (Goddard et al., 2015)

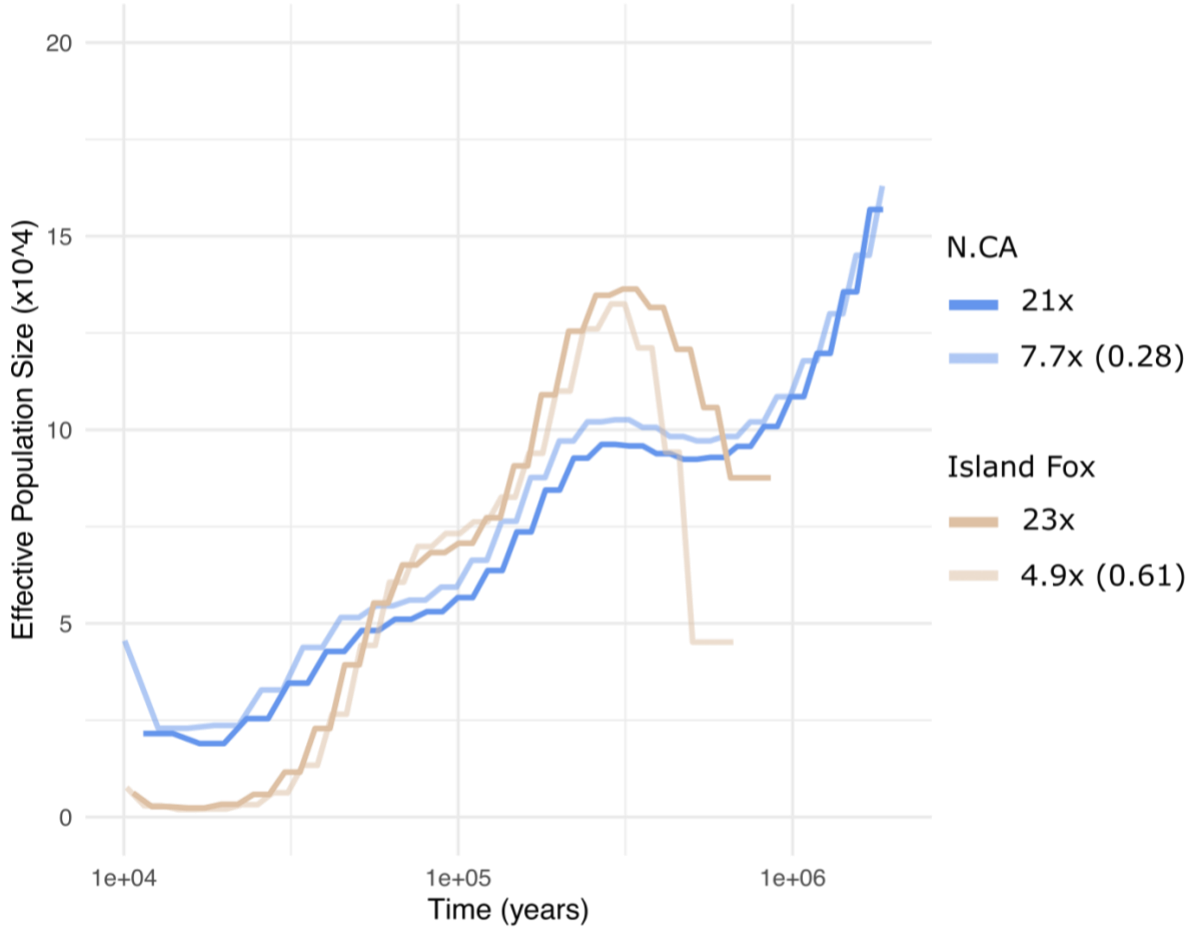

Figure S2.2: Reconstructed pairwise sequentially Markovian coalescent (PSMC) trajectories of two high coverage (darker solid lines) samples from northern California (blue; 21x) and the Channel Islands (beige; 23x) were compared with two independent lower coverage samples (lighter/transparent lines) from the same populations that had a false negative rate (FNR; $y = 2.3051e^{-0.274x}$) applied where y is equal to the FNR, and x is equal to the average read depth of the sample. Note the demographic trajectories show changes in effective population size throughout deeper historical time periods. Coalescence time was converted to years assuming a mutation rate of 4.5×10^{-9} (Koch et al., 2019) and generation time of 2 years. (Goddard et al., 2015)

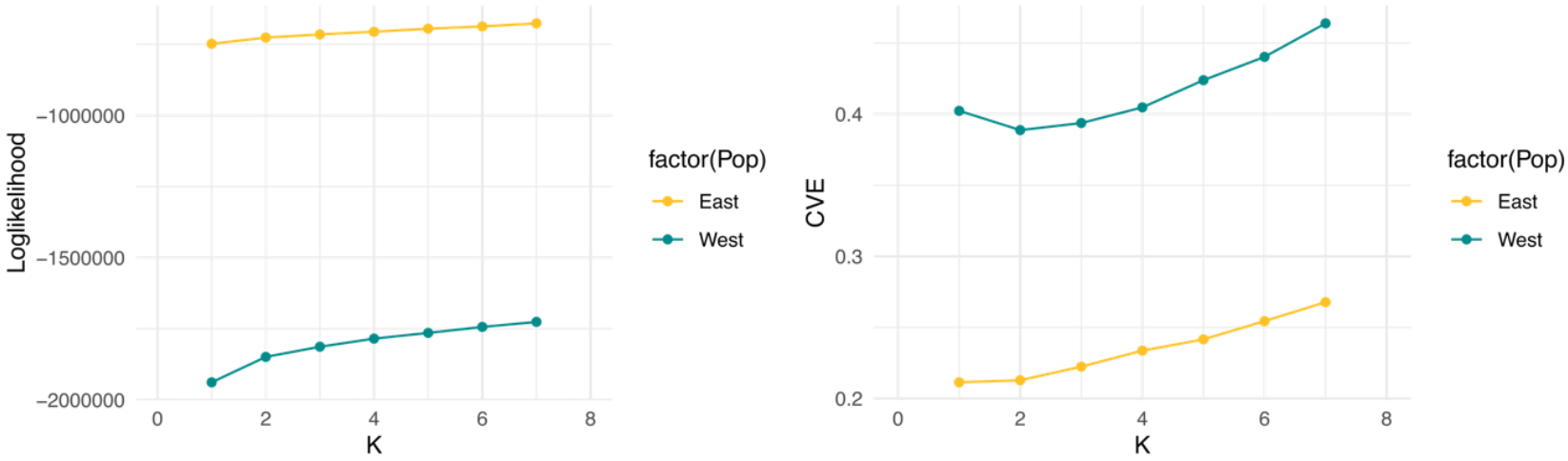

Figure S2.3: Log likelihood scores and cross validation error (CVE) rates of the admixture models testing different numbers of genetic clusters within the eastern (yellow) and western (green) gray fox lineages. Models supported the lowest CVE rates at K = 1 and K = 2 in the eastern gray fox population while K = 2 and K = 3 were more likely in the western population.

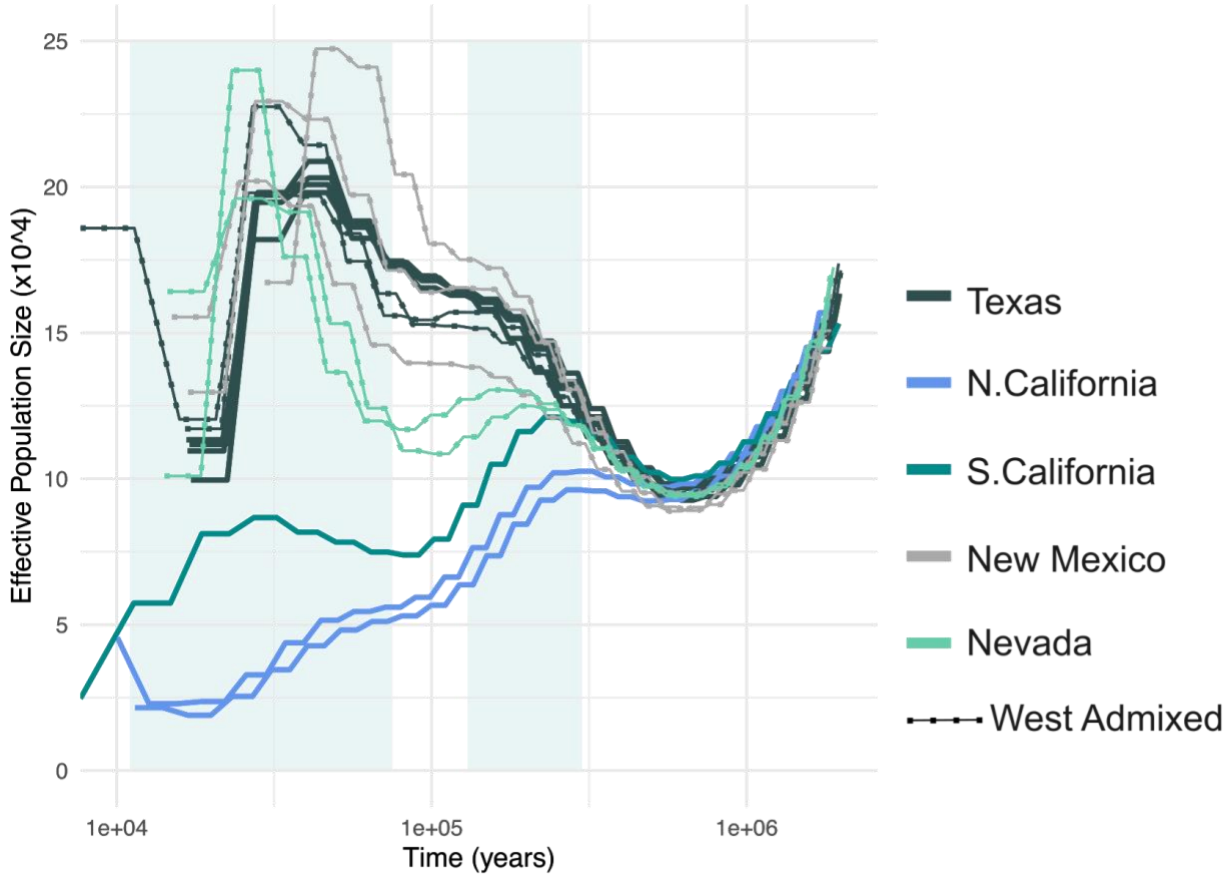

Figure S2.4: Reconstructed pairwise sequentially Markovian coalescent (PSMC) trajectories of western gray foxes from Texas (n = 9), New Mexico (n = 3), Nevada (n = 2), southern California (n = 1), and northern California (n = 2). Coverage levels varied and a false negative rate was applied to any sample with a mean read depth <18x. Additionally, samples that showed evidence of incomplete assignment to one the 2-3 genetic clusters identified in the admixture analysis are highlighted with an additional dotted line. The demographic trajectories show changes in effective population size throughout deeper historical time periods. Coalescence time was converted to years assuming a mutation rate of 4.5×10^{-9} (Koch et al., 2019) and generation time of 2 years. (Goddard et al., 2015). Blue highlighted regions correspond to the Wisconsin (85,000 – 11,000 YBP) and Illinoian (190 – 130 KYA) glaciation periods.

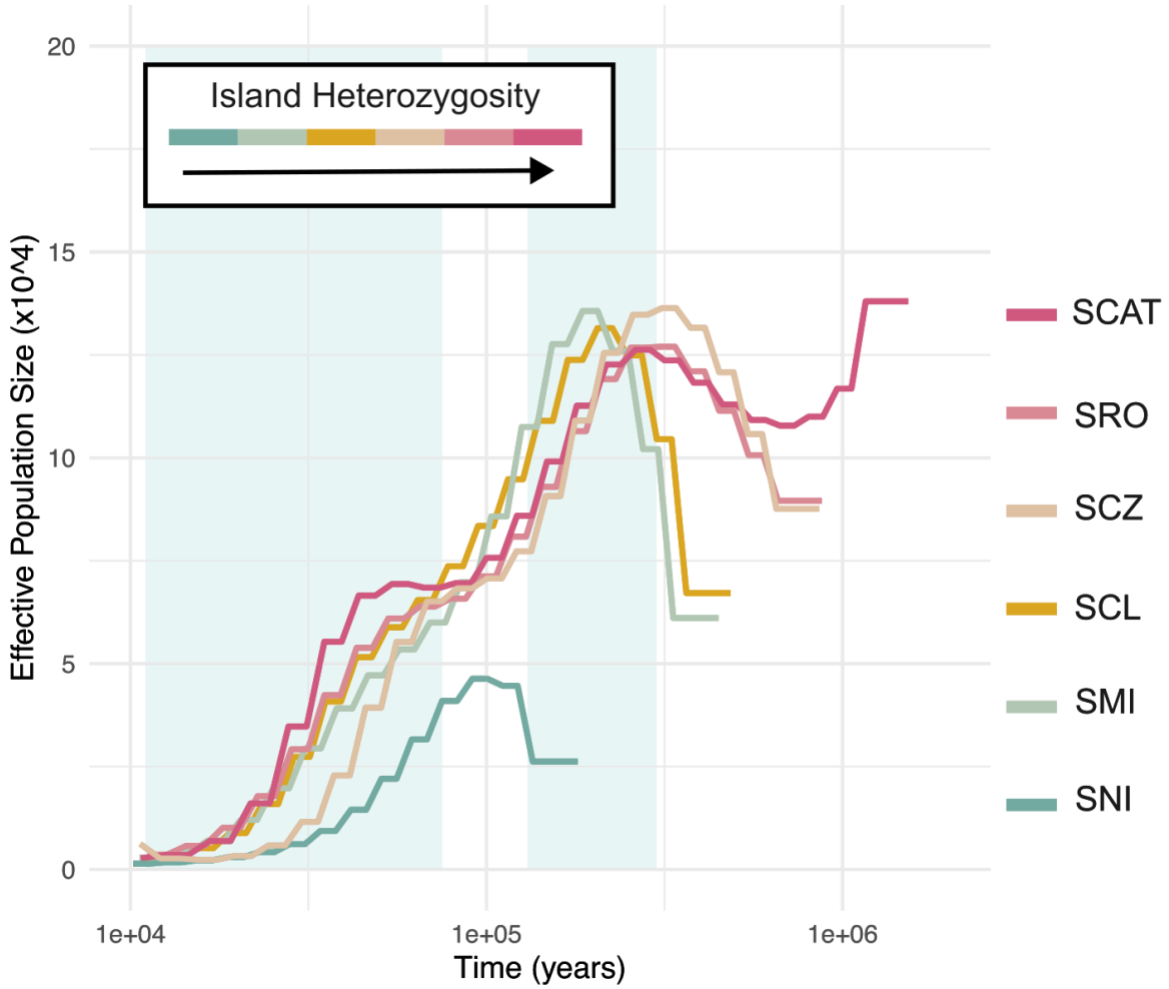

Figure S2.5: Reconstructed pairwise sequentially Markovian coalescent (PSMC) trajectories of Island foxes from Santa Catalina (SCAT, n = 1), Santa Rosa (SRO, n = 1), Santa Cruz (SCZ, n = 1), San Clemente (SCL, n = 1), San Miguel (SMI, n = 1), San Nicolaus (SNI, n = 1). Coverage levels ranged from 20–25x. Heterozygosity (H_e) levels varied across the islands with cooler colors representing the lowest H_e and warmer colors representing the highest H_e. The demographic trajectories show changes in effective population size throughout deeper historical time periods. Coalescence time was converted to years assuming a mutation rate of 4.5×10^{-9} (Koch et al., 2019) and generation time of 2 years. (Goddard et al., 2015). Blue highlighted regions correspond to the Wisconsin (85,000 – 11,000 YBP) and Illinoian (190 – 130 KYA) glaciation periods.

Chapter 3: Evidence for multiple pulses of asymmetric admixture and selective introgression between highly divergent gray fox (*Urocyon cinereoargenteus*) lineages

Details of collaboration: In this chapter I present my work on the characterization of the timing and extent of secondary contact between eastern and western lineages of gray fox (*Urocyon cinereoargenteus*). I designed the research with input from Dr. Ben Sacks. The collaborators listed below provided samples, offered laboratory support, and contributed to interpretation of the results. I have performed all the analyses presented in this dissertation.

SOPHIE PRECKLER-QUISQUATER,[1] ELIZABETH M. KIEREPKA[2], DAWN M. REDING[3], ANTOINETTE J. PIAGGIO[4] and BENJAMIN N. SACKS[1,5].

[1]Mammalian Ecology and Conservation Unit, Veterinary Genetics Laboratory, School of Veterinary Medicine, University of California, Davis, One Shields Avenue, Davis, CA, 95616, USA
[2]North Carolina Museum of Natural Sciences, Department of Forestry and Environmental Resources, North Carolina State University, Raleigh, NC, USA
[3]Department of Biology, Luther College, Decorah, IA, USA
[4]USDA, Wildlife Services, National Wildlife Research Center, Wildlife Genetics Lab, Fort Collins, CO, USA
[5]Department of Population Health and Reproduction, School of Veterinary Medicine, University of California, Davis, Davis, CA, USA

Abstract

Secondary contact between distinct, yet interfertile, lineages may lead to outcomes ranging from complete unification to formation of stable, narrow hybrid zones permitting low levels of genetic exchange. In either case, gene flow following long-term isolation provides opportunities for selective introgression. North American gray foxes (*Urocyon cinereoargenteus*) are divided into western and eastern lineages that diverged during the mid-Pleistocene, similarly to some sister species. They currently hybridize in a relatively a narrow zone of contact in the southern Great Plains. The narrowness of their hybrid zone indicates either that secondary contact was very recent or, if ancient, that reproductive isolating mechanisms prevent their wholesale unification. We sequenced whole genomes of gray foxes (n = 42) from each lineage and in the hybrid zone to investigate the timing of secondary contact and genetic exchange, the width of the hybrid zone in the context of this timing, and signatures of selective introgression between lineages. We

inferred the timing of admixture pulses using a local ancestry inference-based approach, optimized for low-coverage sequencing data. We tested whether observed patterns of admixture were consistent with expectations based on a model assuming no reproductive barriers. We then investigated specific genomic regions that introgressed across the contact zone at unusually high frequencies, consistent with selective introgression. We identified two distinct pulses of late Holocene and historical admixture. The older pulse of admixture (3,500 YBP) reflected unidirectional gene flow from east to west, likely driven by a major demographic expansion of the eastern gray fox. In contrast, the more recent bi-directional pulse of admixture began approximately 200 YBP, coinciding with major anthropogenic landscape changes. Given the recency of genetic interchange, the narrow widths of the geographic clines provided little insight on the question of reproductive isolation but afforded an opportunity to explore selective introgression. We identified several genomic regions potentially associated with behavioral divergence, mate choice, and olfaction.

Keywords: gray fox, local ancestry deconvolution, secondary contact, selective introgression, *Urocyon cinereoargenteus*

1 | INTRODUCTION

Hybridization often occurs via natural expansion and secondary contact of distinct lineages that have accumulated genetic differences while in allopatry but have not yet evolved complete reproductive isolation (Coyne and Orr, 2004; Roux et al., 2016). Such gene flow can introduce novel variation that selection can act upon (Hedrick, 2013; Arnold and Martin, 2009). Under scenarios where allopatric populations are isolated for long periods of time (e.g., multiple glacial and interglacial cycles) or experience high drift or selection, reproductive barriers (e.g.,

behavioral or genomic incompatibilities) between lineages can form, limiting hybridization and introgressive gene flow upon secondary contact (Harrison and Larson, 2014). Thus, secondary contact zones can offer valuable windows into the speciation process, allowing the investigation of both reproductive barriers that maintain lineage boundaries as well as genomic regions under selection across populations.

Here, we explore a relatively narrow hybrid zone between two divergent lineages of gray fox (*Urocyon cinereoargenteus*). The gray fox is currently recognized as a single species, including 16 named subspecies distributed throughout North America, Central America, and the northern tip of South America. Within the United States are seven recognized subspecies, including three in the west and four in the east (Fritzell and Haroldson, 1982). Several studies, using both mitochondrial and reduced representation nuclear DNA sequencing, identified deep, mid-Pleistocene divergence and a narrow zone of hybridization between western and eastern lineages (Goddard et al., 2015; Reding et al., 2021; Kierepka et al., in review), both similar to that between other fox sister species, such as swift foxes (*Vulpes velox*) and kit foxes (*V. macrotis*; Mercure et al., 1993). The contact zone between western and eastern gray fox lineages coincides with the Great Plains Suture Zone (Reding et al., 2021; Kierepka et al., in review).

The narrow hybrid zone observed between gray fox lineages suggests either that secondary contact was relatively recent or, if contact has been longstanding, that reproductive barriers restrict gene flow (Kierepka et al., in review). If the former case was true (high, but recent, gene flow), this implies that some demographic or physical barrier must have kept these lineages separate for the vast majority of their million or so years divergence. Alternatively, given such a long-term isolation between them, post-zygotic reproductive barriers could have evolved between western and eastern lineages through accumulation of genomic differentiation

via natural selection or drift (e.g., Dobzhanski-Muller incompatibilities; Delph and Demuth, 2016; Kuo et al., 2019; Schumer et al., 2017). Pre-zygotic barriers, such as those related to natal habitat biased dispersal, also could serve to restrict gene flow (Davis and Stamps, 2004; Sacks et al., 2004).

To clarify the timing of hybridization, as well as to explore the possibility of reproductive barriers and selective introgression, we re-sequenced whole genomes of 42 gray foxes from throughout their range. We inferred patterns of local ancestry across the genomes of admixed western and eastern gray foxes to estimate the timing and number of admixture pulses across the secondary contact zone. We then incorporated these timing estimates, along with previously described estimates of dispersal distances for gray foxes, into a null model to predict the width of the geographic ancestry cline assuming no reproductive barriers and assessed concordance of this model with empirical estimates of cline width. Lastly, we scanned the genomes of both lineages for evidence of selective introgression and explored the functional significance of candidate gene regions.

2 | MATERIALS AND METHODS

2.1 | Sample collection

We selected 42 representative gray fox samples distributed across North America for whole genome shotgun sequencing (WGS) (Table S1). These samples were chosen based on their geographic locations and ancestry as determined from a previous genotyping by sequencing (GBS) study of 259 gray foxes (Fig. 1). We selected 27 individuals from reference (i.e., non-admixed) western (n = 13) and eastern (n = 14) lineages as well as 15 admixed individuals from western (n = 9) and eastern (n = 6) populations near the contact zone.

2.2 | DNA sequencing

The DNA samples were extracted using Qiagen DNEasy Blood and Tissue kits following the manufacturer's instructions (Qiagen Inc, Valencia, CA). We fragmented 200 ng of each DNA sample with a Covaris E220 sonicator (Covaris, Woburn, Massachusetts) to produce fragments averaging approximately 400 bp and prepared genomic libraries using a NEBNext® Ultra™ II DNA Library Prep kit for Illumina, following manufacturer's instructions, except that we used half reactions (San Diego, CA, USA). We conducted a size selection using AMPure XP magnetic beads (Beckman Coulter, Pasadena, CA), targeting insert sizes of 300–400 bps. We then PCR-amplified the DNA using unique forward- and reverse-indexed custom, Illumina-compatible primers for each sample. The PCR conditions were as follows: Initial denaturation at 98 °C for 30 sec; 7 cycles of 98 °C for 10 sec and 65 °C for 75s, followed by a 65 °C extension step for 5 min. We quantified the individual libraries using a Qubit fluorometer (Qiagen Inc, Valencia, CA), pooled them in equal concentrations, and submitted the final library to the University of California, Davis Genome Center for paired-end 150 bp sequencing on an Illumina Novaseq S4 lane.

2.3 | Alignment and SNP calling

In addition to the sequences generated for this study, we included the raw reads of two previously published high coverage (18–21x) western gray foxes from California (Table S1, Robinson et al., 2016; Robinson et al., 2018). We trimmed raw reads using bbduk (B. Bushnell, https://sourceforge.net/projects/bbmap). We mapped trimmed reads to the CanFam3.1 (domestic dog) reference genome (Lindblad-Toh et al., 2005), along with the Y chromosome (Oetjens et

al., 2018), using bwa mem, and removed reads with low mapping quality (-q 10) (Li and Durbin, 2010; Li, 2013). We then marked duplicate reads with PICARD (Broad Institute, http://broadinstitute.github.io/picard), and used SAMtools to remove them (-F 1024), along with non-primary reads (-F 256) and those with a mapping quality below 10 (-q 10). We used ANGSD to generate a full SNP dataset, removing bad reads (-remove_bads 1) and those that aligned to multiple regions in the genome (-uniqueOnly 1). We estimated allele frequencies directly from allele counts (-doMajorMinor 2 -doCounts 1 -doMaf 8) as opposed to inferred genotypes or genotype likelihoods, both of which may exhibit significant biases when depths of coverage are low (<10x) (Li et al., 2010; Kim et al., 2011; Korneliussen et al., 2014; Han et al., 2014; Maruki and Lynch, 2017). We additionally filtered SNPs to include those with a minor allele frequency ≥5% (-minMaf 0.05), and we applied standard quality filters including base and mapping quality scores ≥30 (-minQ 30, -minMapQ 30). Based on distributions of read depths, we retained sites with a combined global read depth between 110x (0.5x the sample mean) and 450x (2x the sample mean), and those with genotypes present in approximately 80% of individuals or more (-minInd 34). In addition to the full SNP dataset, which was composed of genotype likelihoods for all individuals, we also generated a dataset with called genotypes that we used to estimate the major and minor allele counts for the western and eastern reference populations. To do this, we inferred genotypes for each pure parental individual at all sites with ≥1x coverage (-geno_minDepth 1). Although this lax coverage requirement was expected to result in higher allelic dropout, it should not have biased allele frequency estimates of the reference populations, which we aimed to base on the largest number of chromosomes possible.

2.4 | Local ancestry inference and admixture timing

We used a hidden Markov model to infer local ancestry across the genome as well as the timing of admixture based on the resulting distribution of ancestry block sizes, which are predicted to become smaller over time due to recombination (Leitwein et al., 2020; Gravel, 2012; Pool and Nielsen, 2009; Chimusa et al., 2018). While several approaches exist to model these two parameters separately, Ancestry_HMM models them jointly and uses genotype likelihoods, making it well suited to low coverage data (Ancestry_HMM v0.94, Corbett-Detig and Nielson, 2017).

We thinned the data set to include only ancestry informative markers (AIMs) SNPs for which ≥12 individuals from each reference population had confidently called genotypes in our full SNP dataset. After removing SNPs without sufficient call rates in reference populations, we retained only those SNPs with allele frequency differences ≥0.6 between reference populations. Background linkage disequilibrium (LD) (i.e., the LD present in the non-admixed reference populations) can bias the inference of admixture timing, resulting in estimates that are older than the true initiation of gene flow (Medina et al., 2018). Therefore, to remove the effects of background LD, we selected a single AIM from each 50-kb window for downstream analysis, which resulted in keeping LD between markers lower than the observed background LD threshold in the western and eastern reference populations ($r^2 < 0.25$; Preckler-Quisquater, Chapter 2).

We used the called genotypes of the western and eastern reference individuals to infer allele frequencies for the two reference populations in Ancestry_HMM. For the admixed populations however, we used raw read counts of the major and minor allele for each admixed individual, which allowed the hidden Markov model to incorporate genotype likelihoods into the local ancestry inference. To incorporate varying recombination rates along the genome into the

model, we approximated the genetic position (cM) for each SNP using a 200-kb scale recombination map for the dog genome and a linear interpolation approach in R (Campbell et al., 2016). Additionally, we utilized estimates of global ancestry proportions generated using fastStructure (Raj et al., 2014) from the GBS dataset (Kierepka et al., in review) as a prior for Ancestry_HMM. We inferred the local ancestry and timing of admixture separately for each admixed individual because individuals displayed a range of global ancestry proportions that would have been poorly characterized by a single input parameter.

We modeled admixture scenarios involving a single pulse and two pulses of gene flow and compared the resulting likelihoods. Assuming a generation time of 2 years (Goddard et al., 2015), we allowed admixture timing to range from 2–10,000 generations (approximately 20,000 years), extending approximately to the end of the last glacial maximum of the Pleistocene, when western and eastern gray foxes were believed to be separated in distinct refugia (Goddard et al., 2015; Reding et al., 2021; Kierepka et al., in review).

2.5 | Geographic cline analysis

A geographic cline in ancestry generated from secondary contact and unobstructed gene flow (i.e., random dispersal and interbreeding) is expected to become wider over time as a function of dispersal distance. To assess whether the cline width between divergent lineages of gray fox was consistent with unobstructed gene flow since secondary contact (i.e., no reproductive barriers), we modeled the expected width (w) as seen in Equation (1):

$$w = \sigma\sqrt{2\pi T}, \quad (1)$$

where σ was the average lifetime dispersal distance of the organism and T represented the number of generations since secondary contact (Endler, 1977; Gay et al., 2008). We assumed an average dispersal distance for gray fox of $\sigma = 8.5$ km (Nicholson et al., 1985) and used as the time (T) since the onset of gene flow that inferred from the Ancestry_HMM analysis described above.

We tested the model against the observed cline width which we estimated by fitting classical equilibrium cline models to our empirical data under a likelihood framework using the Metropolis-Hastings Markov chain Monte Carlo algorithm in the program HZAR (Derryberry et al., 2014). The shape of the observed cline (i.e., location of the cline center, sigmoidal curve, and two exponential decay curves) can be modeled by estimating changes in trait frequencies (i.e., ancestry proportion) along geographic transects, and the cline width can then be modeled as 1/maximum slope (Szymura and Barton, 1986; Szymura and Barton, 1991; Endler, 1977). To obtain the most precise estimate possible, we used the GBS dataset, including previously estimated ancestry proportions (Kierepka et al., in review), because the sample size was larger than the subset used for whole genome sequencing. To estimate the location of the cline center, we first generated a 2-dimensional ancestry surface by interpolating the western and eastern proportions using an empirical Bayesian Kriging approach in ArcGIS 10 (ESRI, Redlands, CA, United States). We then defined the cline center as a spline, which corresponded to the geographic location at which 50% western and 50% eastern ancestry was projected. To convert the dataset into a single dimension, we then measured the Euclidean distance (km) between each sample and the nearest point on the cline center (i.e., spline) and recorded whether samples occurred on the western or eastern side of the contact zone (Fig. S1). Because we inferred

admixture timing estimates separately for the western and eastern populations, we also took a similar approach for modeling the cline widths independently. To do this, we generated two additional datasets in which we mirrored population-specific samples across the cline center. We ran 5 model combinations in which we allowed the shape of the tails to vary and used the default number of Markov chain Monte Carlo (MCMC) steps (100,000 with 10,000 burn-in) for three iterative cycles. We determined the best fitting model using Akaike information criterion scores corrected for small sample size (AICc).

2.6 | Selective introgression across the contact zone

We used two different approaches to identify regions potentially under selection across the contact zone in each of the recipient populations. For the first approach, we averaged the proportion of introgressed ancestry at each locus across all admixed individuals. The second approach utilized Ancestry_HMM-S, which uses a hidden Markov model to detect genomic regions consistent with adaptive introgression and quantifies the strength of putative selection acting on them (Svedberg et al., 2021). As in previous analyses, we ran the Ancestry_HMM-S analysis on the western and eastern gray foxes separately. We used the same input files as for the Ancestry_HMM analyses described above, except that we specified priors for the timing of admixture based on the results of previous analysis. To identify candidate regions for selective introgression, we then ranked loci for western and eastern admixed populations separately according to both methods and considered as candidates only those loci within the top 1% for both approaches in a given population. A genomic region, as opposed to a single locus, was classified as an outlier region if all loci within the region were above this outlier threshold.

2.7 | Gene ontology analyses of outlier regions

We identified all genes located within outlier regions using the NCBI RefSeq curated and predicted gene tracks annotated within the CanFam3.1 reference genome **(**UCSC Genome Browser; NCBI Canis lupus familiaris Annotation Release 105 [2019-12-10**])**. We considered all genes within or overlapping a given chromosomal region (i.e., even if only a part of the reading frame was located within that block). We then classified the gene ontology of these regions and conducted an enrichment analysis using Panther (v16.0) to assess whether specific biological processes or molecular functions were overrepresented among outlier regions in the western or eastern lineages (Mi et al., 2020).

3 | RESULTS

We retained sequences for 41 of the samples sequenced for this study, which had coverage levels ranging 4–8x (Table S1). One sample from California had an average coverage <1x and was therefore removed from downstream analyses. Additionally, we included the two previously published western gray fox genomes, which had average coverage levels of 18x and 21x. The full dataset for 43 gray foxes contained 19.7 million SNPs.

3.1 | Local ancestry inference and admixture timing

The proportions of western and eastern ancestry inferred for each individual using the posterior estimates of local ancestry across the genome in Ancestry_HMM were concordant (Pearson's r ≥0.994) with ancestry estimates obtained in fastStructure (Kierepka et al., in review) (Fig. S2). The distribution of block sizes in the western admixed population conformed best to a model of two distinct pulses of gene flow (Fig. S3), with the more recent pulse occurring at

approximately 34–98 generations ago while the estimate for the older pulse was 233–1,740 generations ago (Table S2). In contrast, ancestry blocks in the eastern admixed population conformed best to a single pulse model of gene flow (Fig. S3) that began at approximately the same time (36–68 generations ago) as the more recent pulse in the west (Table S2). The timing of admixture inferred across individuals from both the western and eastern admixed populations increased as distance from the inferred cline center increased, indicating that gene flow was likely continuous for a protracted period, as opposed to having occurred over one to several generations (Fig. 2). However, positive correlations between timing and distance from cline center were only significant in the older ($r^2 = 0.46$, $p < 0.05$), and in the more recent pulse ($r^2 = 0.81$, $p < 0.001$) of eastern gene flow into the western admixed population. The lack of significance between timing of gene flow and distance from cline center ($r^2 = 0.27$, $p > 0.25$) in the eastern admixed population is possibly due to the lower sample.

3.2 | Geographic cline analysis

Assuming gene flow from the eastern into the western population began 1,740 generations ago, while gene flow from the western into eastern population began 68 generations ago, we used two approaches to estimate the expected cline width as a function of dispersal distance assuming no reproductive barriers. First, we averaged these two time periods ($T = 904$ generations) to generate a total expected cline width (w) of 641 km. Next, we used the population-specific timing estimates ($T_{WEST} = 1{,}740$ generations, $T_{EAST} = 68$ generations) to estimate expected cline widths for the western and eastern sides of the cline, separately, as 445 km (889 km/2) and 88 km (176 km/2) respectively, which sum to 533 km (Table S3). Thus, the timing estimates predict a cline width somewhere between 533 and 641 km if gene flow is random.

The empirical estimate of cline width agreed closely with these predictions. The strongest support was for a model with no exponential tails regardless of whether we modeled the east and west data together or separately (Table S3). The estimated cline width for the jointly modeled data was 524 km (2 LL intervals: 376–712 km). When modeled separately (i.e., mirrored and then halved), the western half of the cline (328 km, 266–404 km) was significantly wider than the eastern half (188 km, 112–292 km), as expected based on the older admixture pulses into the western population relative to the eastern population (Fig. 3B; Table S3). Thus, both estimates were similar and neither differed significantly from the null expectation based on admixture timing above (Fig. 3A).

3.3 | Selective introgression across the contact zone

We identified several regions of the genome that displayed elevated levels of introgression following secondary contact between the western and eastern gray fox lineages. In the western admixed population 40 genomic regions spanning 50 genes exceeded the 99% outlier threshold for introgression fraction, selection coefficient, and log likelihood, with selection coefficients ranging from 0.0367 to 0.0504 (Table S4; Fig. 4A). In the eastern admixed population 15 genomic regions spanning 58 genes were identified as outliers, with selection coefficients ranging from 0.0910 to 0.1072 (Table S2; Fig. 4B). None of these outliers was implicated in both populations. The sizes of these regions were significantly smaller on average in the western admixed group (M = 169 kb, SD = 150 kb) than in the eastern admixed group (M = 622 kb, SD = 534 kb), consistent with the older estimated timing since the admixture began in the western relative to eastern lineage.

3.4 | Gene ontology analyses of outlier regions

In the western admixed population, 71% of ontological terms associated with outlier regions across the contact zone were classified as biological processes compared with 51% of terms in the eastern admixed population. Most associated biological processes were similar between the two populations (Table S6). Additionally, 48% (western) and 52% (eastern) of terms were linked to molecular functions that were identified in both populations (Table S7). However, cytoskeletal motor activity (GO:0003774) was linked to a single putatively introgressed genomic region in the western admixed population.

While there was no indication of over-representation or enrichment of specific biological processes or molecular functions within each admixed population, several regions that showed the strongest outlier signals were notable based upon their links to behavioral divergence, mate choice, olfaction, and immune response. For example, the region with the strongest signature of selective introgression into the western gray fox population encompassed a large, maternally imprinted domain (*NDN*, *MAGEL2*), and all putatively admixed western gray foxes possessed at least one copy of eastern ancestry in this region (Jay et al., 1997; Lorenc et al., 2014). While imprinted genes are known to play a strong role in early development, they have been shown to influence adult behavior as well (Curley, 2011). This region specifically has been identified as a candidate for population-specific mate choice decisions in mice, with strong paternal expression patterns in the hypothalamus and vomeronasal organ (Lorenc et al., 2014).

Several regions associated with both primary and motile cilium function also showed signatures of selective introgression and were overrepresented among the candidate regions in both the western and eastern admixed populations, making up 10.4% and 5.7 % respectively (Table S8), while only 2.2 % of genes in the genome are associated with cilium function (Reiter

and Leroux, 2017). Primary cilia are immotile organelles known for their roles in development as well as cell and immune signaling (Hua and Ferland, 2018), while motile cilia are found within the respiratory tract, the middle ear, the ventricles of the central nervous system and the reproductive tracts (Mitchison and Valente, 2017). Many of the cilia genes that appeared to be selectively introgressed across the contact zone were linked to olfaction.

The melanin-concentrating hormone gene (*MCHR1*), an axoneme ciliary signaling gene primarily expressed in the brain, has been implicated in the control of motivated behaviors including feeding, drinking, mating and maternal behavior (Berman et al., 2009; Diniz and Bittencourt, 2017; Hervieu, 2003). In mice and rats, ciliary *MCHR1* were found to be extremely dense in several areas that are important for olfactory processing (e.g., olfactory bulb, piriform cortex, etc.) (Diniz et al., 2020). Additionally, normal expression of the intraflagellar transport gene (*IFT88*) is necessary for the maintenance of olfactory cilia (McIntyre et al., 2012; Green et al., 2018), and the smoothened gene (*SMO*), a member of the hedgehog signaling pathway, plays a role in the transport of odorant receptors (Maurya et al., 2017).

4 | DISCUSSION

Although gray foxes have historically been considered a single species, our awareness of deep divergence between western and eastern lineages is relatively new (Goddard et al., 2015; Reding et al., 2021; Kierepka et al., in review). Other North American carnivores with similarly deep divergence between western and eastern lineages tend to compose sister species (Mercure et al., 1993; Stone and Cook, 2002; McDonough et al., 2022). Consequently, the possibility that these morphologically similar lineages of gray fox reflect cryptic sister or incipient species was of interest. Indeed, the relatively narrow hybrid zone that had been identified prior to this study,

similar to that observed between kit and swift foxes, was consistent with a longstanding contact between lineages separated by permeable reproductive barriers (Mercure et al., 1993; Reding et al., 2021; Kierepka et al., in review). On the other hand, without knowledge of how long western and eastern lineages have had the opportunity for genetic exchange (i.e., been parapatric), it was impossible to rule out recency as an explanation for the narrow cline width. Thus, our most fundamental question in this study pertained to the antiquity of gene flow between western and eastern lineages of gray fox and whether it was consistent with seamless gene flow. Regardless of the answer to this question, the long-term divergence between lineages presented an opportunity for each lineage to obtain potentially novel adaptive mutations from the other (Hedrick et al., 2013). Thus, we also explored evidence for selective introgression, and finally discuss implications for speciation between lineages.

4. 1 | Evolutionary timeline of divergence and secondary contact

Somewhat unexpectedly and despite their mid-Pleistocene divergence, the earliest evidence of gene flow we found between these lineages was late Holocene and that was only in one direction. Our results suggest bi-directional gene flow did not occur until the past century or two. Below, we consider explanations for how these two lineages might have remained allopatric for so long and discuss the events that only recently enabled their secondary contact and subsequent gene flow.

Shortly after their divergence approximately 1 million years ago, genomic data suggest that the eastern and western lineages experienced distinct and opposing demographic trajectories, with the western population in Texas showing a broad signature of expansion while the eastern population underwent a demographic decline (Preckler-Quisquater, Chapter 2). Although PSMC

analysis suggested that the eastern population increased slightly during the Sangamon interglacial period (125,000–85,000 YBP), it is possible that this expansion was insufficient in size or geographic extent to result in secondary contact with the western lineage. Based on several lines of evidence, the eastern population experienced a protracted decline throughout most of the Wisconsin glaciation (85,000–11,000 YBP), potentially occurring in a restricted distribution in the extreme southeast (Bozarth et al., 2011; Preckler-Quisquater, Chapter 2). On more recent timescales however, the eastern population shows a clear signature of population expansion that began shortly after the end of the last glacial period and has persisted throughout much of the Holocene, coinciding with the inferred onset of unidirectional gene flow (approximately 3,500 YBP) from the eastern into the western population (Fig. S4, Preckler-Quisquater, Chapter 2).

Additionally, the fossil record supports a clear pattern of a post-Pleistocene expansion from the presumed southeastern refugia, both to the north and to the west, towards the secondary contact zone (Graham and Lundelius, 2010). Gray foxes had reached approximately 300 km east of the present cline center 1,500–4,500 YBP, which aligns with the older pulse of gene flow from the eastern into the western population estimated to have begun approximately 1,700 generations ago (1,740–3,500 YBP). In contrast, central and western Texas south into Mexico, likely reflected one of the primary refugial locations for the western lineage as gray foxes were documented there throughout the Pleistocene. While the fossil record supports a northward population expansion from Texas, the recent demographic history may be more complex. Based on analysis of frequency spectra, the eastern expansion coincided with a decline in the Texas population (Fig. S4, Preckler-Quisquater, Chapter 2), potentially explaining the unidirectional (east-to-west) gene flow during the initial pulse approximately 3,500 YBP.

The estimated timing of the recent bi-directional gene flow between eastern and western lineages coincides with a signature of very recent population expansion in both the eastern and the Texas populations (Tajima's D; Preckler-Quisquater, Chapter 2), as well as significant landscape changes, and an increase in gray fox sightings in eastern Texas that began in the early 1900s (Bailey, 1905). Shifting range dynamics and hybridization between distinct lineages or species is often associated with the colonization of new or disturbed habitats (Detwiler et al., 2005; Nolte et al., 2005). This transition region in the southern Great Plains has undergone substantial anthropogenic landscape changes in the last 100–200 years, including extensive lumber harvesting within much of the eastern forest, conversion of natural landscapes to agriculture, primarily for cotton and cattle, and the expansion of towns and cities (Barr, accessed June 2022). Gray foxes often adapt to areas in or adjacent to human development (Lombardi et al., 2017), and they have been shown to utilize these areas as a refuge from coyotes (Gosselink et al., 2003; Riley, 2006).

4. 1 | Selective introgression of behavioral and olfactory genes

Among the 15 to 50 or so outlier regions we identified in each of the lineages, potentially reflective of selective introgression, we found little evidence from enrichment approaches of a single functional category of gene dominating these outliers. However, some of the strongest outliers appeared particularly amenable to adaptive explanations. The strongest evidence of selective introgression into the western gray fox population encompassed a large, maternally imprinted domain (*NDN*, *MAGEL2*) that has been implicated in mate choice decisions (Curley, 2011; Lorenc, 2014). While differences in mate-recognition between divergent lineages may be predicted to act as a barrier to gene flow during secondary contact, many of the hybrids were

heterozygous for ancestry types at this locus, possibly indicating that this region is under balancing selection in the western admixed population. For example, increased diversity at genomic regions associated with mate-recognition could conceivably increase mating opportunities for individuals in and around the contact zone.

Notably, many of the other outlier regions were associated with primary and motile cilium function. Genomic regions associated with primary cilia function, specifically axoneme signaling, have previously been shown to be under diversifying selection between domestic and free-ranging dogs (Pilot et al., 2016). Additionally, these regions have been identified as targets of selective introgression from Eurasian wolves into free-ranging dogs (Pilot et al., 2021). Taken together, these findings support the role of primary cilia function in the improvement of fitness among free-living canid populations.

Several other cilia related genes were associated with the olfactory system which has adapted this organelle (cilia) for its unique sensory function and optimized it for the detection of external stimuli (McEwan et al., 2008). Olfaction is important in animals for detecting a diverse array of volatile chemicals or odorants in the external environment including food quality, reproductive status, and potential dangers including toxins or predators (Green et al., 2018). Selective introgression of olfactory genes has been documented across other, well studied mammalian hybrid zones (Staubach et al., 2012; Teeter et al., 2008). These regions are plausible targets of selection as they play important roles in survival and reproduction. In a scenario where the genomic composition of mate availability is altered due to secondary contact (i.e., has become more heterogeneous), these regions may be under some form of balancing selection whereby individuals that are heterozygous for both forms of ancestry have a selective advantage

due to increased accessibility to mates of both ancestry types, particularly closest to and in the zone of contact.

4. 3 | Inconclusive evidence for speciation

Although consistent with predictions of a model assuming unobstructed gene flow, our estimates of cline width alone did not necessarily imply a lack of reproductive barriers. Given the recency of time since secondary contact, particularly that inferred for bi-directional gene flow, we doubt that a model of partial reproductive isolation could be rejected either. We also lacked the resolution to assess regions of the genome that are refractory to introgression (i.e., barrier genes) as our hybrid samples essentially fell into two discrete types: those mostly eastern with a little western introgression and those mostly western with a little eastern introgression. Assessing barrier genes, such as using a genomic cline approach (Gompert and Buerkle, 2011), would require sampling of a more continuous range of ancestry fractions such as would be expected nearer to the cline center. Other approaches that could help clarify the presence and magnitude of any reproductive barriers include more direct observations of behavior (e.g., assortative mating patterns, habitat-biased dispersal, etc.) and fitness of different crosses, both in the wild and through captive experimentation (Mech et al., 2014; Sanz-Perez et al., 2018; vonHoldt et al., 2017).

5 | CONCLUSION

Despite ancient divergence and a history of cyclic population expansion and retreat during glacial cycling in North America, we found evidence of only recent (mid-late Holocene) admixture between the western and eastern gray fox lineages. This timing can be explained by a

long-term decline of the eastern lineage since divergence, presumably maintaining allopatry, followed by a widespread Holocene expansion, initiating consequential contact for the first time since their divergence approximately 1 million years earlier. The more recent (approximately century-old) bi-directional pulse in gene flow may have been driven by more localized demographic expansions in both populations owing to anthropogenic landscape changes near the zone of secondary contact. Populations are highly dynamic over time and can be influenced by a range of factors including climatic fluctuations, anthropogenic forces, selection to the local environment, and hybridization with other related populations. Though our study sheds light on the timing and consequences of secondary contact between these two divergent lineages of gray fox, reproductive isolation and speciation remain questions in need of future investigation.

ACKNOWLEDGEMENTS

We thank the landowners, fur trappers, USDA Wildlife Services personnel, and S. Riley (NPS), J.Beasley (Savannah River Ecology Laboratory, University of Georgia) and E. Boydston (USGS) for providing tissue samples and extracted DNA for this study. Funding was provided by the University of California, Davis, Mammalian Ecology and Conservation Unit.

REFERENCES

Alwyn, B. (accessed June 10, 2022). Late Nineteenth-Century Texas. *Handbook of Texas Online.* https://www.tshaonline.org/handbook/entries/late-nineteenth-century-texas.

Bailey, V. (1905). Biological survey of Texas. U.S. Department of Agriculture Biological Survey-*North American Fauna*. 25: 89-92.

Arnold, M. L., & Martin, N. H. (2009). Adaptation by introgression. *Journal of Biology*, *8*(9), 82.

Berman, J. R., Skariah, G., Maro, G. S., Mignot, E., & Mourrain, P. (2009). Characterization of Two Melanin-Concentrating Hormone Genes in Zebrafish Reveals Evolutionary and

Physiological Links with the Mammalian MCH System. *The Journal of Comparative Neurology*, *517*(5), 695–710.

Bozarth, C. A., Lance, S. L., Civitello, D. J., Glenn, J. L., & Maldonado, J. E. (2011). Phylogeography of the gray fox (Urocyon cinereoargenteus) in the eastern United States. *Journal of Mammalogy*, *92*(2), 283–294.

Campbell, C. L., Bhérer, C., Morrow, B. E., Boyko, A. R., & Auton, A. (2016). A Pedigree-Based Map of Recombination in the Domestic Dog Genome. *G3: Genes|Genomes|Genetics*, *6*(11), 3517–3524.

Chimusa, E. R., Defo, J., Thami, P. K., Awany, D., Mulisa, D. D., Allali, I., Ghazal, H., Moussa, A., & Mazandu, G. K. (2018). Dating admixture events is unsolved problem in multi-way admixed populations. *Briefings in Bioinformatics*.

Corbett-Detig, R., & Nielsen, R. (2017). A Hidden Markov Model Approach for Simultaneously Estimating Local Ancestry and Admixture Time Using Next Generation Sequence Data in Samples of Arbitrary Ploidy. *PLOS Genetics*, *13*(1), e1006529.

Coyne, J. A., & Orr, A. H. (2004). *Speciation*. Sinauer Associates.

Curley, J. P. (2011). Is there a genomically imprinted social brain? *BioEssays*, *33*(9), 662–668.

Davis, J., & Stamps, J. (2004). The effect of natal experience on habitat preferences. *Trends in Ecology & Evolution*, *19*(8), 411–416.

Delph, L. F., & Demuth, J. P. (2016). Haldane's Rule: Genetic Bases and Their Empirical Support. *Journal of Heredity*, *107*(5), 383–391.

Derryberry, E. P., Derryberry, G. E., Maley, J. M., & Brumfield, R. T. (2014). hzar: Hybrid zone analysis using an R software package. *Molecular Ecology Resources*, *14*(3), 652–663.

Detwiler, K. M., Burrell, A. S., & Jolly, C. J. (2005). Conservation Implications of Hybridization in African Cercopithecine Monkeys. *International Journal of Primatology*, *26*(3), 661–684.

Diniz, G. B., Battagello, D. S., Klein, M. O., Bono, B. S. M., Ferreira, J. G. P., Motta-Teixeira, L. C., Duarte, J. C. G., Presse, F., Nahon, J., Adamantidis, A., Chee, M. J., Sita, L. V., & Bittencourt, J. C. (2020). Ciliary melanin-concentrating hormone receptor 1 (MCHR1) is widely distributed in the murine CNS in a sex-independent manner. *Journal of Neuroscience Research*, *98*(10), 2045–2071.

Diniz, G. B., & Bittencourt, J. C. (2017). The Melanin-Concentrating Hormone as an Integrative Peptide Driving Motivated Behaviors. *Frontiers in Systems Neuroscience*, *11*.

Endler, J. A. (1977). *Geographic Variation, Speciation, and Clines*. Princeton University Press.

Fritzell, E. K., & Haroldson, K. J. (1982). *Urocyon cinereoargenteus*. *189*, 1–8.

Gay, L., Crochet, P.-A., Bell, D. A., & Lenormand, T. (2008). Comparing Clines on Molecular and Phenotypic Traits in Hybrid Zones: A Window on Tension Zone Models. *Evolution*, *62*(11), 2789–2806.

Goddard, N. S., Statham, M. J., & Sacks, B. N. (2015). Mitochondrial Analysis of the Most Basal Canid Reveals Deep Divergence between Eastern and Western North American Gray Foxes (Urocyon spp.) and Ancient Roots in Pleistocene California. *PLOS ONE*, *10*(8), e0136329.

Gompert, Z., & Buerkle, C. A. (2011). Bayesian estimation of genomic clines. *Molecular Ecology*, *20*(10), 2111–2127.

Gosselink, T. E., Van Deelen, T. R., Warner, R. E., & Joselyn, M. G. (2003). Temporal Habitat Partitioning and Spatial Use of Coyotes and Red Foxes in East-Central Illinois. *The Journal of Wildlife Management*, *67*(1), 90–103.

Graham, R. W., Lundelius Jr. E. L. (2010). FAUNMAP II: New data for North America with a temporal extension for the Blancan, Irvingtonian and early Rancholabrean. FAUNMAP II Database, version 1.0; 2010. http://www.ucmp.berkeley.edu/faunmap.

Gravel, S. (2012). Population Genetics Models of Local Ancestry. *Genetics*, *191*(2), 607–619.

Green, W. W., Uytingco, C. R., Ukhanov, K., Kolb, Z., Moretta, J., McIntyre, J. C., & Martens, J. R. (2018). Peripheral Gene Therapeutic Rescue of an Olfactory Ciliopathy Restores Sensory Input, Axonal Pathfinding, and Odor-Guided Behavior. *The Journal of Neuroscience*, *38*(34), 7462–7475.

Hall, E. R. (1981). *The Mammals of North America* (2nd ed.). John Wiley and Sons.

Han, E., Sinsheimer, J. S., & Novembre, J. (2014). Characterizing Bias in Population Genetic Inferences from Low-Coverage Sequencing Data. *Molecular Biology and Evolution*, *31*(3), 723–735.

Harrison, R. G., & Larson, E. L. (2014). Hybridization, Introgression, and the Nature of Species Boundaries. *Journal of Heredity*, *105*(S1), 795–809.

Hedrick, P. W. (2013). Adaptive introgression in animals: Examples and comparison to new mutation and standing variation as sources of adaptive variation. *Molecular Ecology*, *22*(18), 4606–4618.

Hervieu, G. (2003). Melanin-concentrating hormone functions in the nervous system: Food intake and stress. *Expert Opinion on Therapeutic Targets*, *7*(4), 495–511.

Hua, K., & Ferland, R. J. (2018). Primary cilia proteins: Ciliary and extraciliary sites and functions. *Cellular and Molecular Life Sciences : CMLS*, *75*(9), 1521–1540.

Ignatieva, E. V., Levitsky, V. G., Yudin, N. S., Moshkin, M. P., & Kolchanov, N. A. (2014). Genetic basis of olfactory cognition: Extremely high level of DNA sequence polymorphism in promoter regions of the human olfactory receptor genes revealed using the 1000 Genomes Project dataset. *Frontiers in Psychology*, *5*.

James, G., Key, B., & Beverdam, A. (2014). The E3 ubiquitin ligase Mycbp2 genetically interacts with Robo2 to modulate axon guidance in the mouse olfactory system. *Brain Structure and Function*, *219*(3), 861–874.

Jay, P., Rougeulle, C., Massacrier, A., Moncla, A., Mattel, M.-G., Malzac, P., Roëckel, N., Taviaux, S., Bergé Lefranc, J.-L., Cau, P., Berta, P., Lalande, M., & Muscatelli, F. (1997). The human necdin gene, NDN, is maternally imprinted and located in the Prader-Willi syndrome chromosomal region. *Nature Genetics*, *17*(3), 357–361.

Kent WJ, Sugnet CW, Furey TS, Roskin KM, Pringle TH, Zahler AM, Haussler D. The human genome browser at UCSC. *Genome Res.* 2002 Jun;12(6):996-1006.

Kierepka, E. M., Preckler-Quisquater S., Reding, D. M., Piaggio A. J., Riley, S. P. D., Sacks, B. N. (**in review**). Genomic analyses of gray fox lineages suggest ancient divergence and secondary contact in the Southern Great Plains. *Journal of Heredity*. In Review.

Kim, S. Y., Lohmueller, K. E., Albrechtsen, A., Li, Y., Korneliussen, T., Tian, G., Grarup, N., Jiang, T., Andersen, G., Witte, D., Jorgensen, T., Hansen, T., Pedersen, O., Wang, J., & Nielsen, R. (2011a). Estimation of allele frequency and association mapping using next-generation sequencing data. *BMC Bioinformatics*, *12*(1), 231.

Korneliussen, T. S., Albrechtsen, A., & Nielsen, R. (2014). ANGSD: Analysis of Next Generation Sequencing Data. *BMC Bioinformatics*, *15*(1), 356.

Kuo, Y. H., Vanderzwan, S. L., Kasprowicz, A. E., & Sacks, B. N. (2019). Using Ancestry-Informative SNPs to Quantify Introgression of European Alleles into North American Red Foxes. *Journal of Heredity*, *110*(7), 782–792.

Leitwein, M., Duranton, M., Rougemont, Q., Gagnaire, P.-A., & Bernatchez, L. (2020). Using Haplotype Information for Conservation Genomics. *Trends in Ecology & Evolution*, *35*(3), 245–258.

Li, Y., Vinckenbosch, N., Tian, G., Huerta-Sanchez, E., Jiang, T., Jiang, H., Albrechtsen, A., Andersen, G., Cao, H., Korneliussen, T., Grarup, N., Guo, Y., Hellman, I., Jin, X., Li, Q., Liu, J., Liu, X., Sparsø, T., Tang, M., … Wang, J. (2010). Resequencing of 200 human exomes identifies an excess of low-frequency non-synonymous coding variants. *Nature Genetics*, *42*(11), 969–972.

Li, H., & Durbin, R. (2010). Fast and accurate long-read alignment with Burrows–Wheeler transform. *Bioinformatics*, *26*(5), 589–595.

Lindblad-Toh et al., Lindblad-Toh, K., Wade, C. M., Mikkelsen, T. S., Karlsson, E. K., Jaffe, D. B., Kamal, M., Clamp, M., Chang, J. L., Kulbokas, E. J., Zody, M. C., Mauceli, E., Xie, X., Breen, M., Wayne, R. K., Ostrander, E. A., Ponting, C. P., Galibert, F., Smith, D. R., … Lander, E. S. (2005). Genome sequence, comparative analysis and haplotype structure of the domestic dog. *Nature*, *438*(7069), 803–819.

Lombardi, J. V., Comer, C. E., Scognamillo, D. G., & Conway, W. C. (2017). Coyote, fox, and bobcat response to anthropogenic and natural landscape features in a small urban area. *Urban Ecosystems*, *20*(6), 1239–1248.

Lorenc, A., Linnenbrink, M., Montero, I., Schilhabel, M. B., & Tautz, D. (2014). Genetic Differentiation of Hypothalamus Parentally Biased Transcripts in Populations of the House Mouse Implicate the Prader–Willi Syndrome Imprinted Region as a Possible Source of Behavioral Divergence. *Molecular Biology and Evolution*, *31*(12), 3240–3249.

Maruki, T., & Lynch, M. (2017a). Genotype Calling from Population-Genomic Sequencing Data. *G3: Genes|Genomes|Genetics*, *7*(5), 1393–1404.

Maruki, T., & Lynch, M. (2017b). Genotype Calling from Population-Genomic Sequencing Data. *G3 Genes|Genomes|Genetics*, *7*(5), 1393–1404.

Maurya, D. K., Bohm, S., & Alenius, M. (2017). Hedgehog signaling regulates ciliary localization of mouse odorant receptors. *Proceedings of the National Academy of Sciences*, *114*(44).

McEwen, D. P., Jenkins, P. M., & Martens, J. R. (2008). Chapter 12 Olfactory Cilia: Our Direct Neuronal Connection to the External World. In *Current Topics in Developmental Biology* (Vol. 85, pp. 333–370). Elsevier.

McIntyre, J. C., Davis, E. E., Joiner, A., Williams, C. L., Tsai, I.-C., Jenkins, P. M., McEwen, D. P., Zhang, L., Escobado, J., Thomas, S., Szymanska, K., Johnson, C. A., Beales, P. L., Green, E. D., Mullikin, J. C., Sabo, A., Muzny, D. M., Gibbs, R. A., Attié-Bitach, T., … Martens, J. R. (2012). Gene therapy rescues cilia defects and restores olfactory function in a mammalian ciliopathy model. *Nature Medicine*, *18*(9), 1423–1428.

Mech, L. D., Christensen, B. W., Asa, C. S., Callahan, M., & Young, J. K. (2014). Production of Hybrids between Western Gray Wolves and Western Coyotes. *PLoS ONE*, *9*(2), e88861.

Medina, P., Nielsen, R., Thronlow, B., & Corbett-Detig, R. (2018). *Supplemental Material for Medina et al., 2018*. 605152 Bytes.

Meisner, J., & Albrechtsen, A. (n.d.). *Inferring Population Structure and Admixture Proportions in Low-Depth NGS Data*. 13.

Mercure, A., Ralls, K., Koepfli, K. P., & Wayne, R. K. (1993). Genetic Subdivisions Among Small Canids: Mitochondrial Dna Differentiation of Swift, Kit, and Arctic Foxes. *Evolution*, *47*(5), 1313–1328.

Mi, H., Ebert, D., Muruganujan, A., Mills, C., Albou, L.-P., Mushayamaha, T., & Thomas, P. D. (2021). PANTHER version 16: A revised family classification, tree-based classification tool, enhancer regions and extensive API. *Nucleic Acids Research*, *49*(D1), D394–D403.

Nicholson, W. S., Hill, E. P., & Briggs, D. (1985). Denning, Pup-Rearing, and Dispersal in the Gray Fox in East-Central Alabama. *The Journal of Wildlife Management*, *49*(1), 33.

Nolte, A. W., Freyhof, J., Stemshorn, K. C., & Tautz, D. (2005). An invasive lineage of sculpins, *Cottus* sp. (Pisces, Teleostei) in the Rhine with new habitat adaptations has originated from hybridization between old phylogeographic groups. *Proceedings of the Royal Society B: Biological Sciences*, *272*(1579), 2379–2387.

Oetjens, M. T., Martin, A., Veeramah, K. R., & Kidd, J. M. (2018). Analysis of the canid Y-chromosome phylogeny using short-read sequencing data reveals the presence of distinct haplogroups among Neolithic European dogs. *BMC Genomics*, *19*(1), 350.

Pilot, M., Malewski, T., Moura, A. E., Grzybowski, T., Oleński, K., Kamiński, S., Fadel, F. R., Alagaili, A. N., Mohammed, O. B., & Bogdanowicz, W. (2016). Diversifying Selection Between Pure-Breed and Free-Breeding Dogs Inferred from Genome-Wide SNP Analysis. *G3: Genes|Genomes|Genetics*, *6*(8), 2285–2298.

Pilot, M., Moura, A. E., Okhlopkov, I. M., Mamaev, N. V., Manaseryan, N. H., Hayrapetyan, V., Kopaliani, N., Tsingarska, E., Alagaili, A. N., Mohammed, O. B., Ostrander, E. A., & Bogdanowicz, W. (2021). Human-modified canids in human-modified landscapes: The evolutionary consequences of hybridization for grey wolves and free-ranging domestic dogs. *Evolutionary Applications*, *14*(10), 2433–2456.

Pool, J. E., & Nielsen, R. (2009). Inference of Historical Changes in Migration Rate From the Lengths of Migrant Tracts. *Genetics*, *181*(2), 711–719.

Raj, A., Stephens, M., & Pritchard, J. K. (2014). fastSTRUCTURE: Variational Inference of Population Structure in Large SNP Data Sets. *Genetics*, *197*(2), 573–589.

Reding, D. M., Castañeda-Rico, S., Shirazi, S., Hofman, C. A., Cancellare, I. A., Lance, S. L., Beringer, J., Clark, W. R., & Maldonado, J. E. (2021). Mitochondrial Genomes of the United States Distribution of Gray Fox (Urocyon cinereoargenteus) Reveal a Major Phylogeographic Break at the Great Plains Suture Zone. *Frontiers in Ecology and Evolution*, *9*, 666800.

Reiter, J. F., & Leroux, M. R. (2017). Genes and molecular pathways underpinning ciliopathies. *Nature Reviews. Molecular Cell Biology*, *18*(9), 533–547.

Riley, S. P. D. (2006). Spatial Ecology of Bobcats and Gray Foxes in Urban and Rural Zones of a National Park. *The Journal of Wildlife Management*, *70*(5), 1425–1435.

Robinson, J. A., Brown, C., Kim, B. Y., Lohmueller, K. E., & Wayne, R. K. (2018). Purging of strongly deleterious mutations explains long-term persistence and absence of inbreeding depression in island foxes. *Current Biology : CB*, *28*(21), 3487-3494.e4.

Robinson, J. A., Ortega-Del Vecchyo, D., Fan, Z., Kim, B. Y., vonHoldt, B. M., Marsden, C. D., Lohmueller, K. E., & Wayne, R. K. (2016). Genomic Flatlining in the Endangered Island Fox. *Current Biology*, *26*(9), 1183–1189.

Roux, C., Fraïsse, C., Romiguier, J., Anciaux, Y., Galtier, N., & Bierne, N. (2016). Shedding Light on the Grey Zone of Speciation along a Continuum of Genomic Divergence. *PLOS Biology*, *14*(12), e2000234.

Sacks, B. N., Brown, S. K., & Ernest, H. B. (2004). Population structure of California coyotes corresponds to habitat-specific breaks and illuminates species history: Coyote population structure tracks habitat. *Molecular Ecology*, *13*(5), 1265–1275.

Sanz-Pérez, A., Ordiz, A., Sand, H., Swenson, J. E., Wabakken, P., Wikenros, C., Zimmermann, B., Åkesson, M., & Milleret, C. (2018). No place like home? A test of the natal habitat-biased dispersal hypothesis in Scandinavian wolves. *Royal Society Open Science*, *5*(12), 181379.

Schumer, M., Powell, D. L., Delclós, P. J., Squire, M., Cui, R., Andolfatto, P., & Rosenthal, G. G. (2017). Assortative mating and persistent reproductive isolation in hybrids. *Proceedings of the National Academy of Sciences*, *114*(41), 10936–10941.

Skotte, L., Korneliussen, T. S., & Albrechtsen, A. (2013). Estimating Individual Admixture Proportions from Next Generation Sequencing Data. *Genetics*, *195*(3), 693–702.

Staubach, F., Lorenc, A., Messer, P. W., Tang, K., Petrov, D. A., & Tautz, D. (2012). Genome Patterns of Selection and Introgression of Haplotypes in Natural Populations of the House Mouse (Mus musculus). *PLoS Genetics*, *8*(8), e1002891.

Stone, K. D., Flynn, R. W., & Cook, J. A. (2002). Post-glacial colonization of northwestern North America by the forest-associated American marten (Martes americana, Mammalia: Carnivora: Mustelidae). *Molecular Ecology*, *11*(10), 2049–2063.

Svedberg, J., Shchur, V., Reinman, S., Nielsen, R., & Corbett-Detig, R. (2021). Inferring Adaptive Introgression Using Hidden Markov Models. *Molecular Biology and Evolution*, *38*(5), 2152–2165.

Szymura, J. M., & Barton, N. H. (1986). Genetic Analysis of a Hybrid Zone Between the Fire-Bellied Toads, Bombina Bombina and B. Variegata, Near Cracow in Southern Poland. *Evolution*, *40*(6), 1141–1159.

Szymura, J. M., & Barton, N. H. (1991). The Genetic Structure of the Hybrid Zone Between the Fire-Bellied Toads Bombina Bombina and B. Variegata: Comparisons Between Transects and Between Loci. *Evolution*, *45*(2), 237–261.

Teeter, K. C., Payseur, B. A., Harris, L. W., Bakewell, M. A., Thibodeau, L. M., O'Brien, J. E., Krenz, J. G., Sans-Fuentes, M. A., Nachman, M. W., & Tucker, P. K. (2008). Genome-wide patterns of gene flow across a house mouse hybrid zone. *Genome Research*, *18*(1), 67–76.

vonHoldt, B., Heppenheimer, E., Petrenko, V., Croonquist, P., & Rutledge, L. Y. (2017). Ancestry-Specific Methylation Patterns in Admixed Offspring from an Experimental Coyote and Gray Wolf Cross. *Journal of Heredity*, *108*(4), 341–348.

Tables and Figures

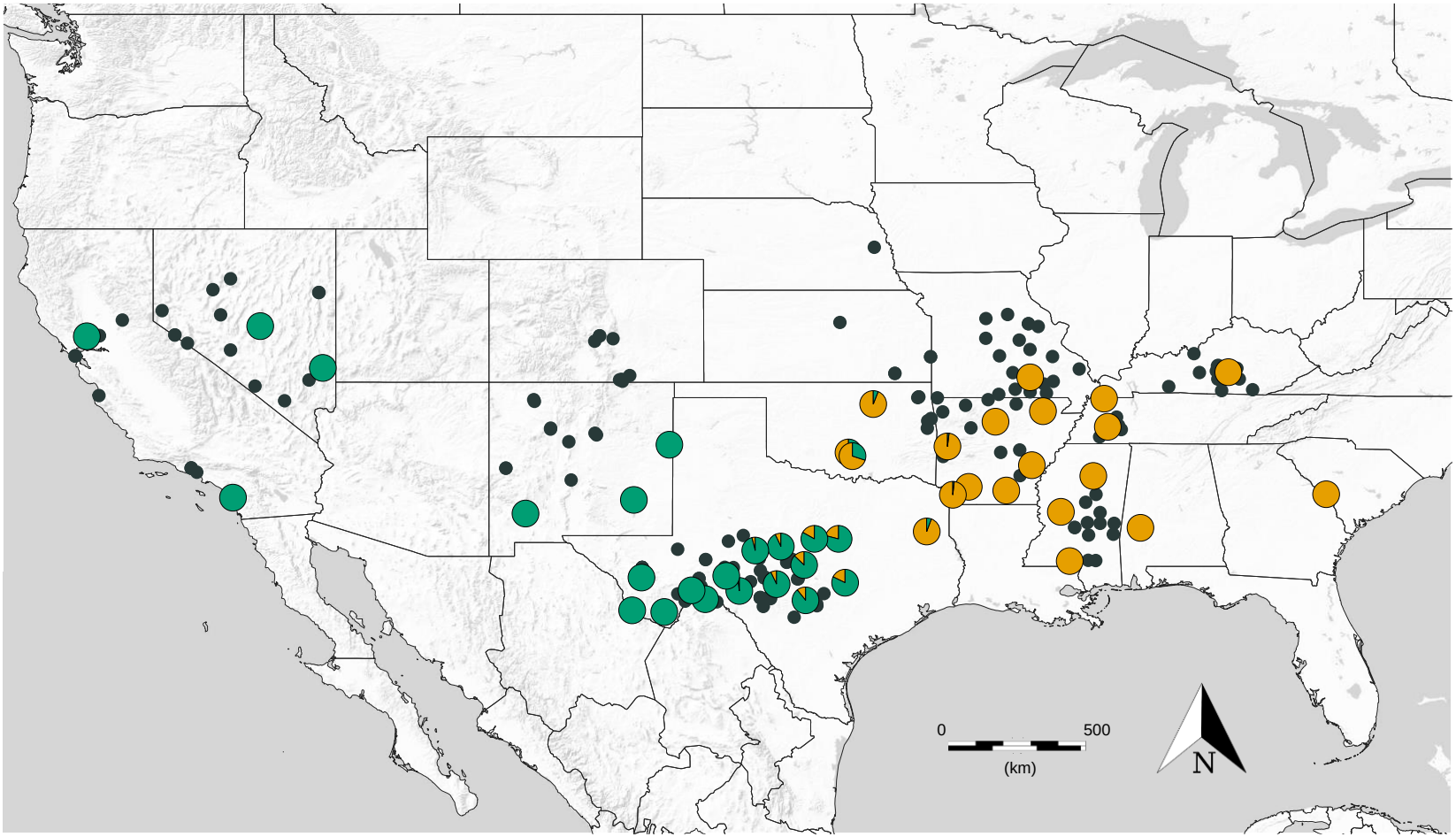

Figure 3.1: Geographic distribution of gray fox samples used in this study (large circles) in relation to the full sample set (all circles) used previously for genotyping-by-sequencing (GBS; Kierepka et al. in review). Pie charts indicate composition of western (green) and eastern (yellow) ancestry in foxes based on previous fastStructure analysis of GBS data (Kierepka et al. in review). Samples used in the current study include 13 pure western, 14 pure eastern, and 15 hybrid samples. Hybrid samples include 9 primarily western gray foxes with eastern introgression and 6 primarily eastern gray foxes with western introgression.

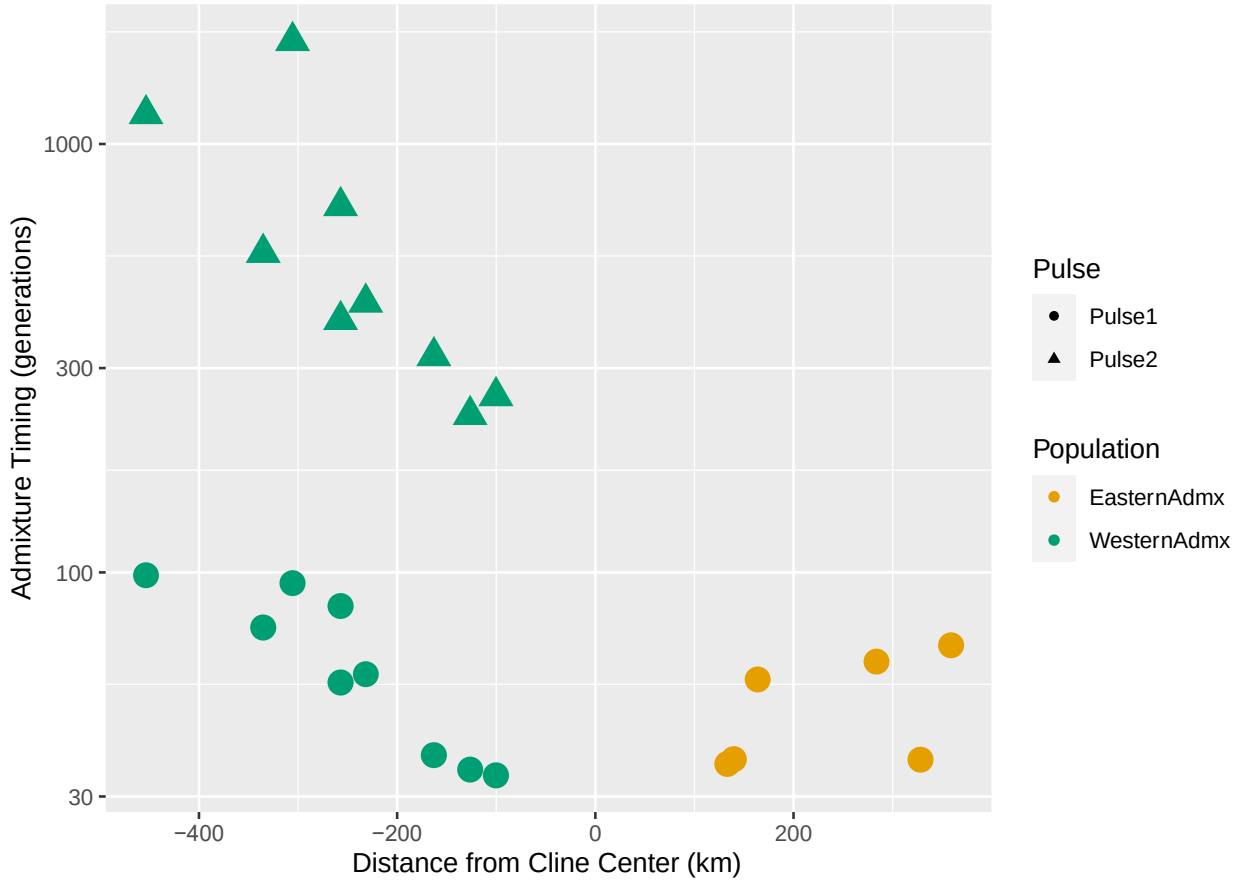

Figure 3.2: Estimated admixture timing (generations) in relation to distance from cline center (km) for 15 admixed gray foxes, including 9 sampled west of the cline center and 6 sampled east of the cline center. Numbers of admixture pulses (2 in the west, 1 in the east) and timing were estimated based on ancestry block sizes inferred in Ancestry_HMM. Estimates of admixture timing increased significantly with distance from cline center across both the older ($r^2 = 0.46$, $p < 0.05$) and more recent ($r^2 = 0.81$, $p < 0.001$) pulses of gene flow into the western population, indicating that gene flow was likely continuous for a protracted period. In the eastern admixed population, the admixture timing was also positively correlated with distance from cline center, but the relationship was not significant ($r^2 = 0.27$, $p > 0.25$)

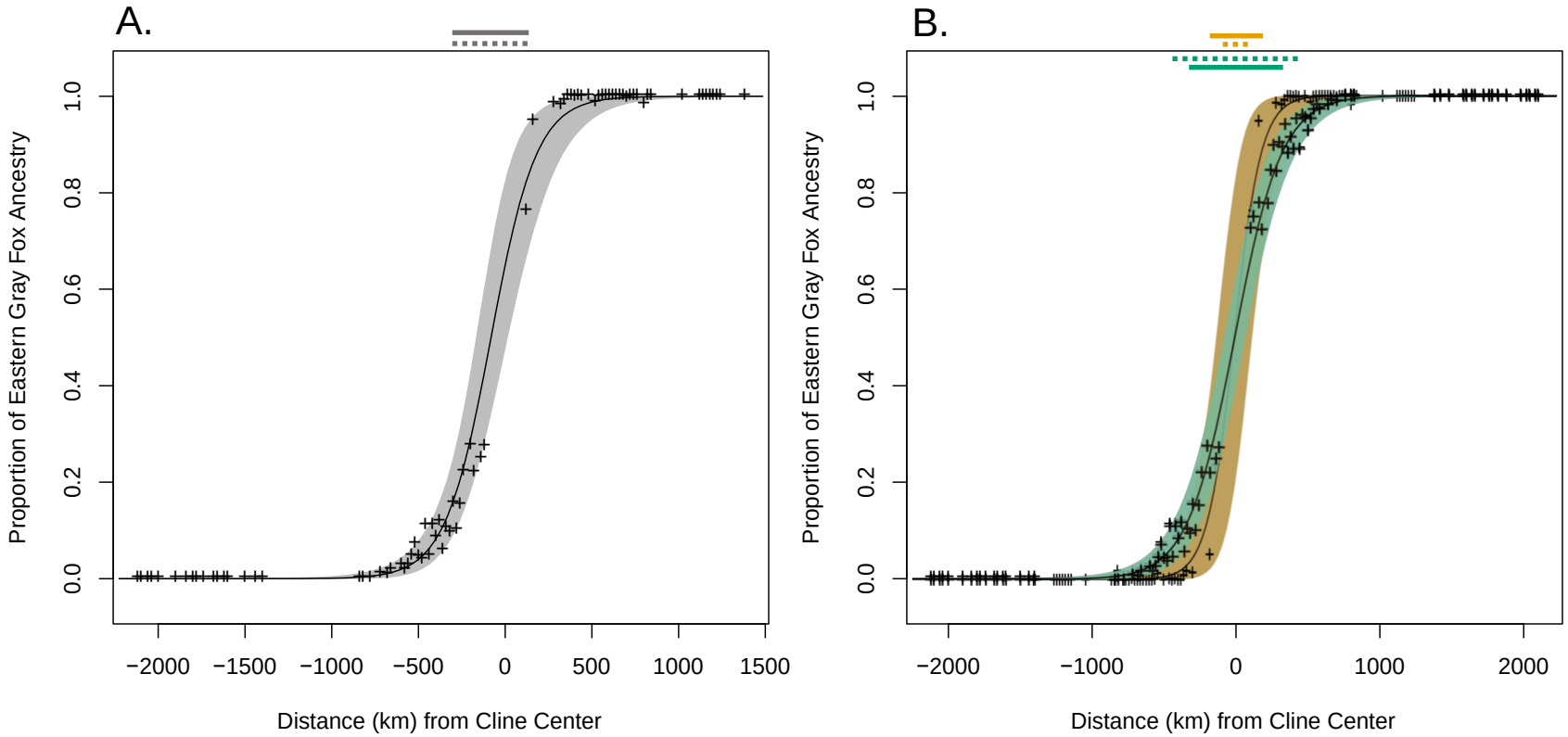

Figure 3.3: Clines with 95% confidence regions in gray fox ancestry described in terms of the admixture fraction as a function of distance from the inferred contact line between eastern and western gray fox lineages (cline center). Clines were estimated in HZAR (A) assuming a symmetrical function or (B) by mirroring western (green) and eastern (yellow) sides of the cline and estimating separately. The cline widths are defined as 1/slope at the steepest point, are shown above the plots as solid bars, and are estimated at (A) 524 km (95% CI = 376–712 km), (B) 328 km (266–404 km) for the west-mirrored, and 188 km (112–292 km) for the east-mirrored clines. Also shown for reference are the predicted cline widths (dashed lines on top of graphs) based on admixture timing under a model assuming random dispersal and interbreeding (see text for details).

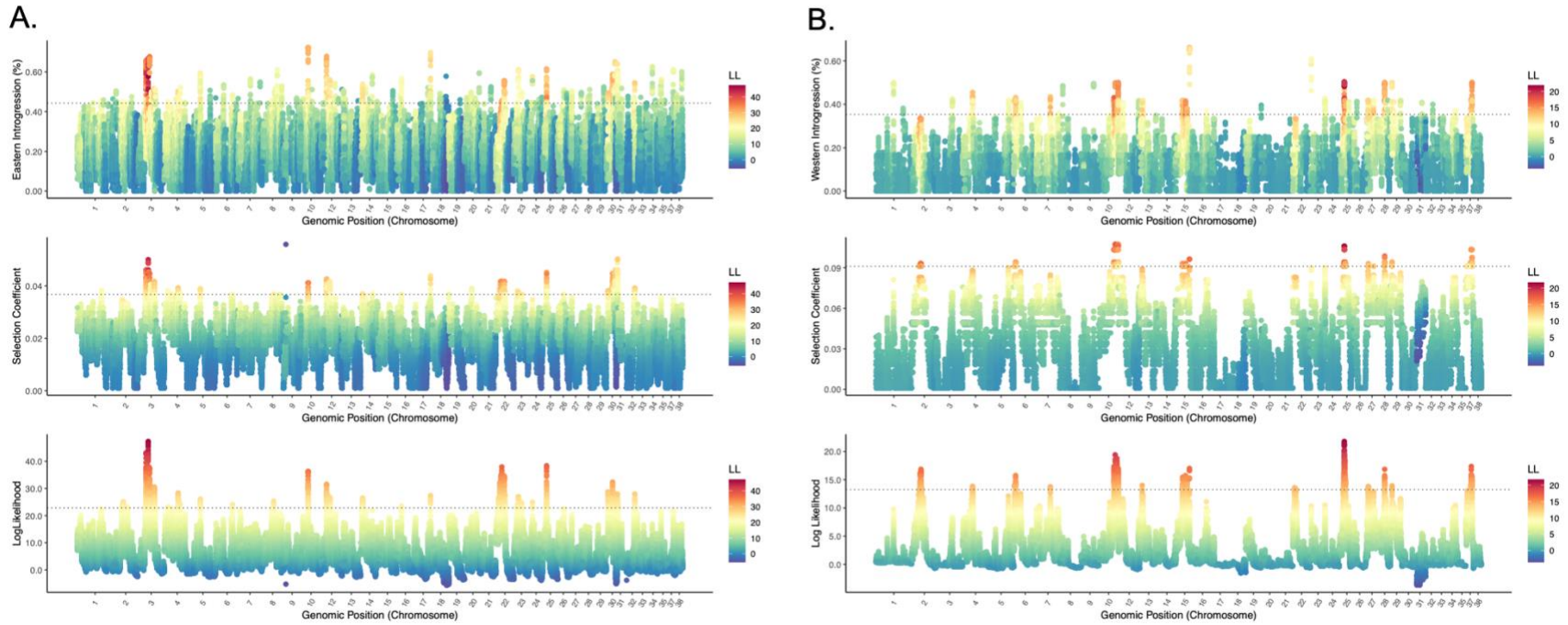

Figure 3.4: Estimates of introgression (top), selection coefficients (middle), and log-likelihoods (bottom) across the genomes of western (A) and eastern (B) gray fox populations. The frequency of introgressed ancestry across the genome was estimated from admixed individuals based on local ancestry estimation using ancestry informative markers (AIMS) in Ancestry_HMM. Selection coefficient and corresponding log-likelihood ratios were based on Ancestry_HMM-S, which uses a modified transition probability to generate expectations for the increased frequency of a locus under varying levels of selection relative to background levels. Loci are colored in all panels according to log-likelihood ratios, with warmer colors indicating higher likelihoods. In the western population, 40 genomic regions spanning 50 different genes fell above the 99% outlier threshold. In the eastern population, 15 genomic regions spanning 58 different genes fell above the 99% outlier threshold.

Supplemental Material

Table S3.1: Sample information for all gray foxes included in this study including a representative subset of gray foxes selected from Kierepka et al. (in review) for whole genome-sequencing as well as two previously published western gray fox genomes (Robinson et al. 2016; Robinson et al. 2018). All raw sequences from this study will be available for download from the NCBI Sequence Read Archive upon publication of the manuscript. Raw sequence reads from the Robinson et al. (2016) and Robinson et al. (2018) publications can be found under the BioProjects PRJNA312115 and PRJNA478450 respectively.

Sample ID	Population	Mean Coverage Autosomes	Mean Coverage Xchr	Mean Coverage Ychr	Sex	Source	BioProject	Accession ID
S19_4623	East	6.23	5.72	0.45	Female	This Study	-	-
S19_4625	East	5.12	4.74	0.37	Female	This Study	-	-
S19_4626	East	4.79	4.45	0.36	Female	This Study	-	-
S19_4628	East	4.39	2.22	3.32	Male	This Study	-	-
S19_4639	East	4.18	3.88	0.39	Female	This Study	-	-
S19_4642	East	5.74	2.83	4.19	Male	This Study	-	-
S19_4663	East	4.78	2.37	3.76	Male	This Study	-	-
S19_4699	East	5.58	5.18	0.6	Female	This Study	-	-
S19_4701	East	6.23	3.1	5.31	Male	This Study	-	-
S19_4703	East	7.16	6.58	0.64	Female	This Study	-	-
S19_4710	East	6.44	3.2	5.1	Male	This Study	-	-
S19_4714	East	4.89	4.5	0.35	Female	This Study	-	-
S19_4737	East	6.28	3.08	5.56	Male	This Study	-	-
S19_6655	East	6.00	2.88	4.15	Male	This Study	-	-
S19_3074	East_Admixed	5.84	2.76	4.07	Male	This Study	-	-
S19_4685	East_Admixed	5.22	2.6	4.38	Male	This Study	-	-
S19_4692	East_Admixed	5.56	2.76	4.88	Male	This Study	-	-
S19_4695	East_Admixed	5.45	4.97	0.47	Female	This Study	-	-
S19_4698	East_Admixed	4.96	4.57	0.58	Female	This Study	-	-

S19_4702	East_Admixed	5.89	5.48	0.37	Female	This Study	-	-
S13_2949	West	7.74	3.72	4.85	Male	This Study	-	-
S16_1460	West	<1x	<1x	<1x	Unk	This Study	-	-
S19_2925	West	6.42	3.12	4.49	Male	This Study	-	-
S19_2974	West	5.50	2.71	4.41	Male	This Study	-	-
S19_3064	West	5.52	2.67	4.28	Male	This Study	-	-
S19_3066	West	6.05	5.32	0.27	Female	This Study	-	-
S19_3133	West	5.36	2.58	3.83	Male	This Study	-	-
S19_3152	West	6.12	2.99	4.57	Male	This Study	-	-
S19_4675	West	5.04	4.65	0.32	Female	This Study	-	-
S19_4679	West	5.82	2.88	4.53	Male	This Study	-	-
S19_4715	West	5.01	2.46	4.35	Male	This Study	-	-
S19_4717	West	4.94	2.44	4.23	Male	This Study	-	-
S19_4728	West	5.54	5.06	0.35	Female	This Study	-	-
GF041F	West	18.25	16.65	1.42	Female	Robinson et al. (2016)	PRJNA312115	SRR5198019, SRR5198020, SRR5198021
GOGANRA.NPS.GF30	West	20.96	10.26	17.63	Male	Robinson et al. (2018)	PRJNA478450	SRR7458270
S19_2940	West_Admixed	4.84	4.46	0.39	Female	This Study	-	-
S19_2977	West_Admixed	6.00	5.26	0.33	Female	This Study	-	-
S19_2992	West_Admixed	6.75	3.3	5.2	Male	This Study	-	-
S19_3050	West_Admixed	5.99	5.34	0.21	Female	This Study	-	-
S19_3061	West_Admixed	5.11	2.5	4.27	Male	This Study	-	-
S19_3072	West_Admixed	6.93	6.31	0.45	Female	This Study	-	-
S19_3075	West_Admixed	5.86	2.81	4.27	Male	This Study	-	-
S19_3084	West_Admixed	6.20	2.99	4.67	Male	This Study	-	-
S19_3098	West_Admixed	6.26	5.54	0.23	Female	This Study	-	-

Table S3.2: Timing estimates of admixture pulses inferred for each putatively admixed individual using AHMM. Likelihood scores and associated inferences of admixture time are shown for both single pulse and two-pulse models of gene. All individuals from the eastern admixed population show stronger support for a single pulse of admixture that occurred 36-68 generations ago. Alternatively, the western admixed population shows stronger support for two pulses of admixture, a more recent pulse that occurred 34-99 generation ago which coincides with the pulse in the east, and an older pulse that occurred 233-1740 generations ago.

SampleID	Admixed Population	Single Pulse Model		Multi-Pulse Model		
		Admixture Timing (generations)	Likelihood	Admixture Timing (generations; Pulse 1)	Admixture Timing (generations; Pulse 2)	Likelihood
S19_3074	East_Admixed	56.2467	-882452	82.1877	31.3466	-882472
S19_4685	East_Admixed	36.5589	-878197	58.1238	20.1665	-878218
S19_4692	East_Admixed	35.7165	-895379	51.5938	15.5572	-895382
S19_4695	East_Admixed	36.6483	-891294	58.7884	13.9215	-891300
S19_4698	East_Admixed	67.6089	-865996	104.215	43.0933	-866018
S19_4702	East_Admixed	61.9129	-881516	113.935	33.8748	-881535
S19_2940	West_Admixed	160.915	-885960	1174.69	98.5155	-885929
S19_2977	West_Admixed	119.297	-905919	388.508	55.3355	-905874
S19_2992	West_Admixed	144.651	-908945	557.255	74.3797	-908899
S19_3050	West_Admixed	107.34	-907111	320.016	37.4516	-907027
S19_3061	West_Admixed	143.262	-893838	1740.09	94.4144	-893794
S19_3072	West_Admixed	96.9881	-916830	257.99	33.6021	-916761
S19_3075	West_Admixed	126.542	-904135	426.5	57.8633	-904096
S19_3084	West_Admixed	168.768	-904856	716.806	83.454	-904792
S19_3098	West_Admixed	92.8849	-909749	233.122	34.6592	-909705

Table S3.3: Parameter estimates for the best-fitting cline model for empirical geographic clines of based on admixture proportions generated from 44k nuclear GBS SNPs (Kierepka et al. (in prep). Clines were generated using the program HZAR (Derryberry et al. 2014). Cline width is 1/maximum slope, and the cline center was measured as the 50% ancestry transition spline based on empirical Bayesian Kriging in ArcMap. Additionally, clines widths are presented for the data modeled together (All Gray Foxes) and with the eastern and western gray foxes modeled separately. The ±2 log-likelihood (LL) unit support is presented for both. The shape parameter indicates the tail shape (left, right, both, none, mirrored) of the top model, while pmin and pmax are the lower and upper bounds of ancestry proportion for the top cline model.

	AHMM Predicted Cline Width [$w = \sigma \sqrt{2\pi T}$]	Top Model			Cline Position (km)	± 2 LL		Cline Width (km)	± 2 LL	
		Shape (tails)	pmin	pmax		min (km)	max (km)		min (km)	max (km)
All Gray Foxes	641	none	0	1	-82.57	-174.51	28.53	524.10	376.21	712.44
Western Gray Fox Only	889 (445)	none	0	1	-9.32	-89.82	69.93	655.16 (327.58)	532.89 (266.45)	807.5 (403.75)
Eastern Gray Fox Only	176 (88)	none	0	1	-9.93	-150.16	130.82	376.94 (188.47)	223.52 (111.76)	583.28 (291.64)

Table S3.4: Genes identified within candidate regions for selective introgression from the eastern gray fox population into the western gray fox population. Chromosome (Chr) and region (chromosomal block position) refer to position in the CanFam 3.1 genome and were classified as outliers if all loci within the region were in the top 1% of sites putatively under selection using AHMM-S approach as well as those that showed an excess proportion of introgressed ancestry across all admixed individuals. We considered all genes located within a chromosomal region if either the entire open reading frame or only a part of the reading frame was located within that block and included only the genes that were described using the NCBI RefSeq curated and predicted gene tracks annotated within the canFam3.1 reference genome (UCSC Genome Browser; NCBI Canis lupus familiaris Annotation Release 105 (2019-12-10)).

Population	Chr	Chromosomal block position (bp)	Block Size (bp)	No. of Genes	Gene(s)
Western Gray Fox	3	28517048-28709197	192149	1	AP3B1
Western Gray Fox	3	28902567-29323654	421087	4	TBCA, OTP, WDR41, PDE8B
Western Gray Fox	3	29620187-29682687	62500	1	AGGF1
Western Gray Fox	3	36142267-36427011	284744	3	NDN, MAGEL2, MKRN3
Western Gray Fox	3	37306907-37342931	36024	0	
Western Gray Fox	3	37913933-37978308	64375	2	TRPM1, MTMR10
Western Gray Fox	3	41011892-41160546	148654	1	MEF2A
Western Gray Fox	3	56543609-56662741	119132	2	IL16, CFAP161
Western Gray Fox	3	56937328-57705920	768592	4	ARNT2, ZFAND6, BCL2A1, MTHFS
Western Gray Fox	4	47510064-47617640	107576	0	
Western Gray Fox	4	47943748-48093961	150213	0	
Western Gray Fox	5	35745864-35834163	88299	1	DNAH9
Western Gray Fox	8	41111184	1	1	GPHN
Western Gray Fox	10	24555446-24811589	256143	3	MCHR1, MKL1, SGSM3
Western Gray Fox	12	18702848-18976827	273979	0	
Western Gray Fox	12	19468777-19690759	221982	1	PKHD1
Western Gray Fox	12	25424126-25664804	240678	1	KHDRBS2
Western Gray Fox	12	30759460-30922233	162773	0	
Western Gray Fox	14	7243784-7605051	361267	5	SMKR1, STRIP2, AHCYL2, SMO, TSPAN33
Western Gray Fox	16	16009678-16020219	10541	1	KMT2C
Western Gray Fox	17	56862106-56946432	84326	1	NOTCH2
Western Gray Fox	22	19830630-20076168	245538	0	
Western Gray Fox	22	27441546-27516270	74724	0	
Western Gray Fox	22	28389899-28839288	449389	0	
Western Gray Fox	22	30709913-30789614	79701	1	MYCBP2
Western Gray Fox	23	12792322-12874296	81974	1	OSPBL10
Western Gray Fox	23	15964801-15985941	21140	1	CMC1

Western Gray Fox	23	26916340-26937588	21248	1	ANKRD28
Western Gray Fox	25	12454254-12567041	112787	1	USP12
Western Gray Fox	25	12949705-13191127	241422	1	CDK8
Western Gray Fox	25	13259302-13342155	82853	0	
Western Gray Fox	25	13410115-13705402	295287	1	ATP8A2
Western Gray Fox	30	5614816-5713627	98811	1	SPRED1
Western Gray Fox	30	19115191-19236386	121195	1	WDR72
Western Gray Fox	30	21265795-21390829	125034	1	RFX7
Western Gray Fox	30	29708105-29800644	92539	2	IGDCC3, IGDCC4
Western Gray Fox	30	30072728-30124973	52245	1	DENND4A
Western Gray Fox	30	38547348-38900666	353318	2	LINGO1, HMG20A
Western Gray Fox	30	39827424-39902494	75070	1	ETFA
Western Gray Fox	32	28121902-28192924	71022	1	USP3

Table S3.5: Genes identified within candidate regions for selective introgression from the western gray fox population into the eastern gray fox population. Chromosome (Chr) and region (chromosomal block position) refer to position in the CanFam 3.1 genome and were classified as outliers if all loci within the region were in the top 1% of sites putatively under selection using AHMM-S approach as well as those that showed an excess proportion of introgressed ancestry across all admixed individuals. We considered all genes located within a chromosomal region if either the entire open reading frame or only a part of the reading frame was located within that block and included only the genes that were described using the NCBI RefSeq curated and predicted gene tracks annotated within the canFam3.1 reference genome (UCSC Genome Browser; NCBI *Canis lupus familiaris* Annotation Release 105 (2019-12-10)).

Population	Chr	Chromosomal block position (bp)	Block Size (bp)	No. of Genes	Gene(s)
Eastern Gray Fox	6	2860489-4550845	1690356	1	AUTS2
Eastern Gray Fox	6	5981436-6262685	281249	4	GTF2IRD1, CLIP2, RFC2, LAT2
Eastern Gray Fox	10	57119347-57398833	279486	1	CCDC85A
Eastern Gray Fox	10	62842495-64194857	1352362	6	WDPCP, UGP2, VPS54, PELI1, LGALSL, AFTPH
Eastern Gray Fox	10	66983231-68220230	1236999	16	C1D, WDR92, WDR92, PNO1, PPP3R1, CNRIP1, FBXO48, APLF, APLF, PROKR1, ARHGAP25, BMP10, BMP10, GKN2, GKN1, ANTXR1, GFPT1, NFU1, AAK1
Eastern Gray Fox	15	24722917-24917063	194146	1	TMTC2
Eastern Gray Fox	15	39872429-40712694	840265	9	ANO4, SLC5A8, UTP20, ARL1, SPIC, MYBPC1, CHPT1, SYCP3, GNPTAB
Eastern Gray Fox	15	48762895-48805440	42545	1	LRBA
Eastern Gray Fox	25	17399264-17994478	595214	3	IFT88, CRYL1, GJB6
Eastern Gray Fox	25	18225064-19525868	1300804	9	ZMYM5, PSPC1, MPHOSPH8, CENPJ, FRNF17, PTPN18, CCDC115, PALLD, CBR4
Eastern Gray Fox	27	10054433-10213730	159297	1	TMEM117
Eastern Gray Fox	29	5402571-5436728	34157	1	ATP6V1H
Eastern Gray Fox	37	19251033-19800342	549309	1	ERBB4
Eastern Gray Fox	37	20147005-20572130	425125	1	IKZF2
Eastern Gray Fox	37	21816053-22158783	342730	3	VWC2L, BARD1, ABCA12

Table S3.6: Gene ontology of candidate regions under selective introgression that were linked to biological processes identified using Panther (Mi. et al 2013).

				Biological Processes										
Introgressed From>To	**Ensemble Gene ID**	**Mapped Gene ID**	**Gene Name**	**biological adhesion (GO:0022610)**	**biological regulation (GO:0065007)**	**cellular process (GO:0009987)**	**developmental process (GO:0032502)**	**immune system process (GO:0002376)**	**localization (GO:0051179)**	**locomotion (GO:0040011**	**metabolic process (GO:0008152)**	**multicellular organismal process (GO:0032501)**	**response to stimulus (GO:0050896)**	**signaling (GO:0023052)**
East>West	ENSCAFG00000016029	RFX7	Regulatory factor X7		X	X					X			
East>West	ENSCAFG00000013922	ARNT2	Aryl hydrocarbon receptor nuclear translocator 2		X	X					X			
East>West	ENSCAFG00000016993	USP3	Ubiquitin carboxyl-terminal hydrolase											
East>West	ENSCAFG00000016305	GPHN	Domain E			X					X			
East>West	ENSCAFG00000013972	ZFAND6	Uncharacterized protein			X			X					
East>West	ENSCAFG00000009227	WDR41	WD repeat domain 41											
East>West	ENSCAFG00000008643	SPRED1	Sprouty related EVH1 domain containing 1		X	X							X	X
East>West	ENSCAFG00000038351	SMKR1	Uncharacterized protein											
East>West	ENSCAFG00000010775	MEF2A	Myocyte enhancer factor 2A		X	X	X				X	X		

East>West	ENSCAFG00000001524	AHCYL2	Adenosylhomocysteinase like 2		X				X			
East>West	ENSCAFG00000001533	TSPAN33	Tetraspanin									
East>West	ENSCAFG00000013849	CFAP161	Cilia and flagella associated protein 161		X			X				
East>West	ENSCAFG00000001515	STRIP2	Striatin interacting protein 2		X							
East>West	ENSCAFG00000006870	CDK8	Cyclin dependent kinase 8		X				X			
East>West	ENSCAFG00000013833	IL16	Pro-interleukin-16	X	X		X	X	X			X
East>West	ENSCAFG00000017769	DNAH9	Dynein axonemal heavy chain 9		X							
East>West	ENSCAFG00000018057	LINGO1	Leucine rich repeat and Ig domain containing 1									
East>West	ENSCAFG00000001172	SGSM3	RUN and TBC1 domain-containing protein 3	X								
East>West	ENSCAFG00000028682	TBCA	Tubulin-specific chaperone A		X							
East>West	ENSCAFG00000015875	WDR72	WD repeat domain 72		X			X				
East>West	Gene=AP3B1	AP3B1	AP-3 complex subunit beta-1		X			X				
East>West	ENSCAFG00000010476	NOTCH2	Uncharacterized protein									
East>West	ENSCAFG00000005916	ANKRD28	Ankyrin repeat domain 28									
East>West	ENSCAFG00000007007	ATP8A2	Phospholipid-transporting ATPase	X	X	X		X			X	
East>West	ENSCAFG00000010141	MKRN3	Makorin ring finger protein 3									
East>West	ENSCAFG00000009253	PDE8B	Phosphodiesterase 8B									
East>West	ENSCAFG00000002165	PKHD1	Fibrocystin									
East>West	ENSCAFG00000005105	MYCBP2	RCR-type E3 ubiquitin transferase									
East>West	ENSCAFG00000009215	OTP	Orthopedia homeobox		X	X					X	
East>West	ENSCAFG00000010306	TRPM1	Transient receptor potential cation channel subfamily M member 1	X	X			X				
East>West	ENSCAFG00000004955	KMT2C	[Histone H3]-lysine(4) N-trimethyltransferase	X	X				X			

East>West	ENSCAFG00000013986	MTHFS	5-formyltetrahydrofolate cyclo-ligase			X				X				
East>West	ENSCAFG00000010336	MTMR10	Myotubularin related protein 10											
East>West	ENSCAFG00000006816	USP12	Ubiquitin carboxyl-terminal hydrolase			X				X				
East>West	ENSCAFG00000010136	MAGEL2	MAGE family member L2		X	X				X				
East>West	ENSCAFG00000017149	IGDCC3	Immunoglobulin superfamily DCC subclass member 3	X	X	X	X		X		X	X		
East>West	ENSCAFG00000002470	KHDRBS2	KH RNA binding domain containing, signal transduction associated 2		X	X				X				
East>West	ENSCAFG00000009207	AP3B1	AP-3 complex subunit beta			X		X						
East>West	ENSCAFG00000005492	CMC1	C-X9-C motif containing 1											
East>West	ENSCAFG00000018061	HMG20A	High mobility group 20A		X					X				
East>West	ENSCAFG00000017160	IGDCC4	Immunoglobulin superfamily DCC subclass member 4	X	X	X	X		X		X	X		
East>West	ENSCAFG00000017250	DENND4A	DENN domain containing 4A		X	X						X	X	
East>West	ENSCAFG00000001531	SMO	Smoothened, frizzled class receptor		X	X	X		X		X	X	X	
East>West	ENSCAFG00000001143	MCHR1	G-protein coupled receptor 24		X	X						X	X	
East>West	ENSCAFG00000018143	ETFA	Electron transfer flavoprotein subunit alpha			X								
East>West	ENSCAFG00000010134	NDN	Necdin, MAGE family member		X					X				
East>West	ENSCAFG00000013979	BCL2A1	BCL2 related protein A1		X							X	X	
East>West	ENSCAFG00000009268	AGGF1	Angiogenic factor with G-patch and FHA domains 1											
West>East	ENSCAFG00000031832	CCDC115	Coiled-coil domain containing 115											
West>East	ENSCAFG00000003256	PNO1	RNA-binding protein PNO1											
West>East	ENSCAFG00000003271	BMP10	Bone morphogenetic protein 10		X	X				X		X	X	

West>East	ENSCAFG00000045568	MPHOSPH8	Uncharacterized protein									
West>East	ENSCAFG00000003273	GKN2	Gastrokine 2		X	X						
West>East	ENSCAFG00000006992	ARL1	ADP ribosylation factor like GTPase 1			X		X				
West>East	ENSCAFG00000003137	UGP2	UTP--glucose-1-phosphate uridylyltransferase									
West>East	ENSCAFG00000007391	CENPJ	Centromere protein J			X		X				
West>East	ENSCAFG00000005914	TMTC2	Dolichyl-phosphate-mannose--protein mannosyltransferase									
West>East	ENSCAFG00000006947	ATP6V1H	ATPase H+ transporting V1 subunit H									
West>East	ENSCAFG00000003153	VPS54	Vacuolar protein sorting-associated protein 54			X		X				
West>East	ENSCAFG00000003119	WDPCP	WD repeat containing planar cell polarity effector									
West>East	ENSCAFG00000007288	CRYL1	Crystallin lambda 1									
West>East	ENSCAFG00000003309	AAK1	AP2 associated kinase 1									
West>East	ENSCAFG00000029460	VWC2L	von Willebrand factor C domain containing 2 like		X	X					X	X
West>East	ENSCAFG00000014278	ABCA12	ATP binding cassette subfamily A member 12					X				
West>East	ENSCAFG00000007907	LRBA	LPS responsive beige-like anchor protein					X				
West>East	ENSCAFG00000007492	PALLD	Palladin, cytoskeletal associated protein			X	X		X		X	X
West>East	ENSCAFG00000003261	FBXO48	F-box protein 48	X								
West>East	ENSCAFG00000003276	ANTXR1	ANTXR cell adhesion molecule 1									
West>East	ENSCAFG00000014224	IKZF2	IKAROS family zinc finger 2		X	X				X		
West>East	ENSCAFG00000011916	CLIP2	CAP-Gly domain containing linker protein 2			X						
West>East	ENSCAFG00000009609	TMEM117	Transmembrane protein 117		X	X					X	X
West>East	ENSCAFG00000003162	PELI1	E3 ubiquitin-protein ligase pellino homolog			X				X		

West>East	ENSCAFG00000007134	MYBPC1	Myosin binding protein C1									
West>East	ENSCAFG00000003175	AFTPH	Aftiphilin		X		X					
West>East	ENSCAFG00000031669	CNRIP1	CB1 cannabinoid receptor-interacting protein 1	X	X						X	X
West>East	ENSCAFG00000002927	CCDC85A	Coiled-coil domain containing 85A									
West>East	ENSCAFG00000031586	LGALSL	Galectin									
West>East	ENSCAFG00000007359	ZMYM5	Uncharacterized protein									
West>East	ENSCAFG00000003262	APLF	Aprataxin and PNKP like factor		X				X		X	
West>East	ENSCAFG00000003296	GFPT1	Glutamine--fructose-6-phosphate transaminase (isomerizing)		X				X			
West>East	ENSCAFG00000043712	PSPC1	RRM domain-containing protein	X	X				X			
West>East	ENSCAFG00000006942	SLC5A8	Electrogenic sodium monocarboxylate cotransporter				X					
West>East	ENSCAFG00000023258	ERBB4	Receptor protein-tyrosine kinase	X	X	X			X	X	X	X
West>East	ENSCAFG00000011763	GTF2IRD1	GTF2I repeat domain containing 1									
West>East	ENSCAFG00000006964	UTP20	UTP20 small subunit processome component									
West>East	ENSCAFG00000011962	RFC2	Replication factor C subunit 2		X				X		X	
West>East	ENSCAFG00000029145	PROKR1	Prokineticin receptor 1	X	X						X	X
West>East	ENSCAFG00000006923	ANO4	Anoctamin		X		X					
West>East	ENSCAFG00000003275	GKN1	Gastrokine 1	X	X							
West>East	ENSCAFG00000007250	IFT88	Intraflagellar transport 88		X		X					
West>East	ENSCAFG00000003248	WDR92	WD_REPEATS_REGION domain-containing protein									
West>East	ENSCAFG00000007316	GJB6	Gap junction protein									
West>East	ENSCAFG00000007248	GNPTAB	N-acetylglucosamine-1-phosphate transferase subunits alpha and beta									

West>East	ENSCAFG00000048035	PPP3R1	Uncharacterized protein									
West>East	ENSCAFG00000007012	SPIC	Spi-C transcription factor	X	X	X			X			
West>East	ENSCAFG00000011229	AUTS2	Activator of transcription and developmental regulator AUTS2									
West>East	ENSCAFG00000012003	LAT2	Linker for activation of T cells family member 2	X	X		X				X	X
West>East	ENSCAFG00000030099	C1D	Nuclear nucleic acid-binding protein C1D	X	X				X			
West>East	ENSCAFG00000007520	CBR4	Carbonyl reductase 4									
West>East	ENSCAFG00000014264	BARD1	BRCA1 associated RING domain 1									

Table S3.7: Gene ontology of candidate regions under selective introgression that were linked to molecular functions identified using Panther (Mi. et al 2013)

Introgressed From>To	Ensemble Gene ID	Mapped Gene ID	Gene Name	Molecular Function: binding (GO:0005488)	ATP-dependent activity (GO:0140657)	catalytic activity (GO:0003824)	cytoskeletal motor activity (GO:0003774)	molecular function regulator (GO:0098772)	molecular transducer activity (GO:0060089)	transcription regulator activity (GO:0140110)	transporter activity (GO:0005215)
East>West	ENSCAFG00000016029	RFX7	Regulatory factor X7	X						X	
East>West	ENSCAFG00000013922	ARNT2	Aryl hydrocarbon receptor nuclear translocator 2	X						X	
East>West	ENSCAFG00000016993	USP3	Ubiquitin carboxyl-terminal hydrolase								
East>West	ENSCAFG00000016305	GPHN	Domain E			X					
East>West	ENSCAFG00000013972	ZFAND6	Uncharacterized protein	X							
East>West	ENSCAFG00000009227	WDR41	WD repeat domain 41								
East>West	ENSCAFG00000008643	SPRED1	Sprouty related EVH1 domain containing 1	X							
East>West	ENSCAFG00000038351	SMKR1	Uncharacterized protein								
East>West	ENSCAFG00000010775	MEF2A	Myocyte enhancer factor 2A	X						X	
East>West	ENSCAFG00000001524	AHCYL2	Adenosylhomocysteinase like 2			X					
East>West	ENSCAFG00000001533	TSPAN33	Tetraspanin								
East>West	ENSCAFG00000013849	CFAP161	Cilia and flagella associated protein 161								
East>West	ENSCAFG00000001515	STRIP2	Striatin interacting protein 2								

East>West	ENSCAFG00000006870	CDK8	Cyclin dependent kinase 8	X		X					
East>West	ENSCAFG00000013833	IL16	Pro-interleukin-16	X				X	X		
East>West	ENSCAFG00000017769	DNAH9	Dynein axonemal heavy chain 9	X	X	X	X				
East>West	ENSCAFG00000018057	LINGO1	Leucine rich repeat and Ig domain containing 1								
East>West	ENSCAFG00000001172	SGSM3	RUN and TBC1 domain-containing protein 3	X		X		X			
East>West	ENSCAFG00000028682	TBCA	Tubulin-specific chaperone A	X							
East>West	ENSCAFG00000015875	WDR72	WD repeat domain 72								
East>West	Gene=AP3B1	AP3B1	AP-3 complex subunit beta-1								
East>West	ENSCAFG00000010476	NOTCH2	Uncharacterized protein								
East>West	ENSCAFG00000005916	ANKRD28	Ankyrin repeat domain 28								
East>West	ENSCAFG00000007007	ATP8A2	Phospholipid-transporting ATPase		X	X					X
East>West	ENSCAFG00000010141	MKRN3	Makorin ring finger protein 3								
East>West	ENSCAFG00000009253	PDE8B	Phosphodiesterase 8B			X					
East>West	ENSCAFG00000002165	PKHD1	Fibrocystin								
East>West	ENSCAFG00000005105	MYCBP2	RCR-type E3 ubiquitin transferase								
East>West	ENSCAFG00000009215	OTP	Orthopedia homeobox	X							
East>West	ENSCAFG00000010306	TRPM1	Transient receptor potential cation channel subfamily M member 1								X
East>West	ENSCAFG00000004955	KMT2C	[Histone H3]-lysine(4) N-trimethyltransferase	X		X				X	
East>West	ENSCAFG00000013986	MTHFS	5-formyltetrahydrofolate cyclo-ligase			X					
East>West	ENSCAFG00000010336	MTMR10	Myotubularin related protein 10								
East>West	ENSCAFG00000006816	USP12	Ubiquitin carboxyl-terminal hydrolase			X					
East>West	ENSCAFG00000010136	MAGEL2	MAGE family member L2								
East>West	ENSCAFG00000017149	IGDCC3	Immunoglobulin superfamily DCC subclass member 3								
East>West	ENSCAFG00000002470	KHDRBS2	KH RNA binding domain containing, signal transduction associated 2	X							
East>West	ENSCAFG00000009207	AP3B1	AP-3 complex subunit beta								
East>West	ENSCAFG00000005492	CMC1	C-X9-C motif containing 1								
East>West	ENSCAFG00000018061	HMG20A	High mobility group 20A								

East>West	ENSCAFG00000017160	IGDCC4	Immunoglobulin superfamily DCC subclass member 4						
East>West	ENSCAFG00000017250	DENND4A	DENN domain containing 4A						
East>West	ENSCAFG00000001531	SMO	Smoothened, frizzled class receptor	X				X	
East>West	ENSCAFG00000001143	MCHR1	G-protein coupled receptor 24	X				X	
East>West	ENSCAFG00000018143	ETFA	Electron transfer flavoprotein subunit alpha						
East>West	ENSCAFG00000010134	NDN	Necdin, MAGE family member						
East>West	ENSCAFG00000013979	BCL2A1	BCL2 related protein A1	X					X
East>West	ENSCAFG00000009268	AGGF1	Angiogenic factor with G-patch and FHA domains 1						
West>East	ENSCAFG00000031832	CCDC115	Coiled-coil domain containing 115	X					
West>East	ENSCAFG00000003256	PNO1	RNA-binding protein PNO1						
West>East	ENSCAFG00000003271	BMP10	Bone morphogenetic protein 10	X			X	X	
West>East	ENSCAFG00000045568	MPHOSPH8	Uncharacterized protein						
West>East	ENSCAFG00000003273	GKN2	Gastrokine 2						
West>East	ENSCAFG00000006992	ARL1	ADP ribosylation factor like GTPase 1	X					
West>East	ENSCAFG00000003137	UGP2	UTP--glucose-1-phosphate uridylyltransferase						
West>East	ENSCAFG00000007391	CENPJ	Centromere protein J	X					
West>East	ENSCAFG00000005914	TMTC2	Dolichyl-phosphate-mannose--protein mannosyltransferase						
West>East	ENSCAFG00000006947	ATP6V1H	ATPase H+ transporting V1 subunit H						
West>East	ENSCAFG00000003153	VPS54	Vacuolar protein sorting-associated protein 54	X					
West>East	ENSCAFG00000003119	WDPCP	WD repeat containing planar cell polarity effector						
West>East	ENSCAFG00000007288	CRYL1	Crystallin lambda 1			X			
West>East	ENSCAFG00000003309	AAK1	AP2 associated kinase 1						
West>East	ENSCAFG00000029460	VWC2L	von Willebrand factor C domain containing 2 like						
West>East	ENSCAFG00000014278	ABCA12	ATP binding cassette subfamily A member 12	X	X	X			X
West>East	ENSCAFG00000007907	LRBA	LPS responsive beige-like anchor protein	X					
West>East	ENSCAFG00000007492	PALLD	Palladin, cytoskeletal associated protein	X					
West>East	ENSCAFG00000003261	FBXO48	F-box protein 48						

West>East	ENSCAFG00000003276	ANTXR1	ANTXR cell adhesion molecule 1							
West>East	ENSCAFG00000014224	IKZF2	IKAROS family zinc finger 2	X				X		
West>East	ENSCAFG00000011916	CLIP2	CAP-Gly domain containing linker protein 2	X						
West>East	ENSCAFG00000009609	TMEM117	Transmembrane protein 117							
West>East	ENSCAFG00000003162	PELI1	E3 ubiquitin-protein ligase pellino homolog			X				
West>East	ENSCAFG00000007134	MYBPC1	Myosin binding protein C1							
West>East	ENSCAFG00000003175	AFTPH	Aftiphilin	X						
West>East	ENSCAFG00000031669	CNRIP1	CB1 cannabinoid receptor-interacting protein 1	X						
West>East	ENSCAFG00000002927	CCDC85A	Coiled-coil domain containing 85A							
West>East	ENSCAFG00000031586	LGALSL	Galectin							
West>East	ENSCAFG00000007359	ZMYM5	Uncharacterized protein							
West>East	ENSCAFG00000003262	APLF	Aprataxin and PNKP like factor			X				
West>East	ENSCAFG00000003296	GFPT1	Glutamine--fructose-6-phosphate transaminase (isomerizing)			X				
West>East	ENSCAFG00000043712	PSPC1	RRM domain-containing protein							
West>East	ENSCAFG00000006942	SLC5A8	Electrogenic sodium monocarboxylate cotransporter							X
West>East	ENSCAFG00000023258	ERBB4	Receptor protein-tyrosine kinase	X		X		X		
West>East	ENSCAFG00000011763	GTF2IRD1	GTF2I repeat domain containing 1	X					X	
West>East	ENSCAFG00000006964	UTP20	UTP20 small subunit processome component							
West>East	ENSCAFG00000011962	RFC2	Replication factor C subunit 2	X	X	X				
West>East	ENSCAFG00000029145	PROKR1	Prokineticin receptor 1					X		
West>East	ENSCAFG00000006923	ANO4	Anoctamin							X
West>East	ENSCAFG00000003275	GKN1	Gastrokine 1							
West>East	ENSCAFG00000007250	IFT88	Intraflagellar transport 88	X						
West>East	ENSCAFG00000003248	WDR92	WD_REPEATS_REGION domain-containing protein	X						
West>East	ENSCAFG00000007316	GJB6	Gap junction protein							
West>East	ENSCAFG00000007248	GNPTAB	N-acetylglucosamine-1-phosphate transferase subunits alpha and beta							
West>East	ENSCAFG00000048035	PPP3R1	Uncharacterized protein							

West>East	ENSCAFG00000007012	SPIC	Spi-C transcription factor	X		X
West>East	ENSCAFG00000011229	AUTS2	Activator of transcription and developmental regulator AUTS2			
West>East	ENSCAFG00000012003	LAT2	Linker for activation of T cells family member 2			
West>East	ENSCAFG00000030099	C1D	Nuclear nucleic acid-binding protein C1D	X		
West>East	ENSCAFG00000007520	CBR4	Carbonyl reductase 4		X	
West>East	ENSCAFG00000014264	BARD1	BRCA1 associated RING domain 1			

Table S3.8: Candidate regions under selective introgression that have been previously linked to proper cilia function. Table was modified from Reiter and Leroux 2017 with additional information denoting the genes that have established links to olfactory sensing.

Gene name	Description	Localization / functional category	Disease association	Other Names	Human ENSEMBL ID	Link to Olfaction?	Citation
CFAP161	cilia and flagella associated protein 161	Chlamydomonas flagellar protein	no disease	C15ORF26	ENSG00000156206		
DNAH9	dynein, axonemal, heavy chain 9	axonemal dynein	no disease (mislocalisation in PCD patients)	DNAH17L; Dnahc9; DNEL1; HL20; DYH9; HL-20	ENSG00000007174		
PKHD1	polycystic kidney and hepatic disease 1 (autosomal recessive)	axoneme - signalling	ARPKD	TIGM1; FCYT; ARPKD	ENSG00000170927		
SMO	smoothened, frizzled class receptor	axoneme - ciliary signalling	Curry-Jones syndrome; basal cell carcinoma; Medulloblastoma	SMOH	ENSG00000128602	YES	Maurya et al. 2017
MCHR1	melanin concentrating hormone receptor 1	axoneme ciliary signalling	no disease	SLC1; GPR24; MCH-1R; MCH1R; SLC-1	ENSG00000128285	YES	Diniz et al 2020
CENPJ	centromere protein J	BB	Seckel syndrome; Microcephaly	MCPH6; BM032; LIP1; Sas-4; CENP-J; LAP; SASS4; SCKL4; CPAP	ENSG00000151849		
WDPCP	WD repeat containing planar cell polarity effector	BBS; BB; axoneme	BBS (1 patient); OFD; Heart defect-tongue hamartoma-polysyndactyly syndrome	FRTZ; BBS15; C2ORF86; CHDTHP; FRITZ	ENSG00000143951	YES	Khan et al. 2016
IFT88	intraflagellar transport 88	IFT-B	no disease; PKD, situs inversus in mouse model	D13S1056E; DAF19; TG737; TTC10; hTg737	ENSG00000032742	YES	McIntyre et al. 2012, Green et al. 2018